Metatech

Meta-R-321

The Late-Time (E3) High-Altitude Electromagnetic Pulse (HEMP) and Its Impact on the U.S. Power Grid

James Gilbert
John Kappenman
William Radasky
Edward Savage

Metatech Corporation
358 S. Fairview Ave., Suite E
Goleta, CA 93117

January 2010

Prepared for

Oak Ridge National Laboratory
Attn: Dr. Ben McConnell
1 Bethel Valley Road
P.O. Box 2008
Oak Ridge, Tennessee 37831
Subcontract 6400009137

FOREWORD

This report introduces in Section 1 the threat of the late-time (E3) high-altitude electromagnetic pulse (HEMP) produced by nuclear explosions above an altitude of ~30 km. The report describes the mechanisms that create the E3 HEMP, including the two portions known as the Blast Wave and Heave. In addition to the basic physics models, the conversion of the B-fields into electric fields in the Earth are discussed in Section 2, as this is the mechanism for coupling to the high voltage power grid.

Section 3 presents a series of threat calculations for the U.S. power grid for bursts over different cities or regions. These identify the levels of the induced threat to the transmission power grid. Section 4 follows with a discussion of potential impacts on circuit breakers, while Section 5 emphasizes the possible damage impacts to transformers and the restoration aspects due to the loss of a large number of transformers. Section 6 provides a bibliography for those who wish to delve in more detail concerning the E3 HEMP.

Table of Contents

Section **Page**

Appendices

List of Figures

Appendices

List of Tables

Section 1
Introduction

The detonation of nuclear weapons at altitudes above 20 km produces electromagnetic environments called High-Altitude EMP or HEMP through a number of physical processes. The HEMP environment is generally described in three phases – E1, or early time HEMP, from sub-nanosecond times to one microsecond; E2, or intermediate-time EMP, ranging from one microsecond to one second; and E3, or late-time EMP covering environments later than one second.

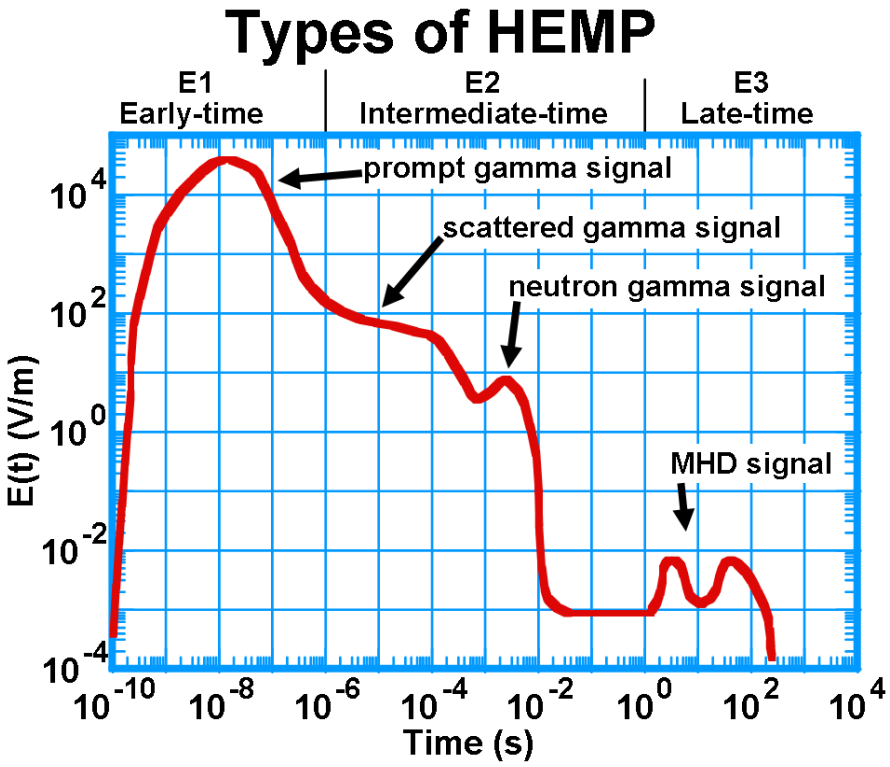

Figure 1-1. Schematic of various phases of HEMP

Figure 1-1 shows the various forms of HEMP arising from a high altitude burst. The E1 prompt gamma signal is driven by the Compton currents generated by the first scatter of gamma rays directly from the burst, which represent only about 0.1% of the total energy released. The scattered gamma signal, much lower in amplitude but more persistent, arises from the gammas which have been previously Compton scattered. Both of these fields reach the ground as plane waves, and they are specified as freely propagating fields with a specified polarization. For most threat devices, the fields at the ground are largest for bursts between 50 and 100 km altitude. The neutron gamma signal is caused by the inelastic scattering in air of high energy neutrons generated in thermonuclear reactions, and the fields at the ground are greatest for low altitude bursts between 20 and 50 km. For this time scale, the ground reflections are of great importance, and the field shown in Figure 1-1 is the vertical electric field; the horizontal electric fields that couple to conductors are substantially less.

The last phase is the E3 MHD signal, which is driven by the hydrodynamic motion of the weapons debris and the ionized atmosphere across the geomagnetic field lines. This is driven by the approximately 25% of the weapon energy that shows up at the kinetic energy of the debris. The remaining approximately 75% of the energy is emitted as x-rays, which modifies the E3 MHD HEMP, greatly lowering the early time portion of the electric field. The fields shown schematically for E3 HEMP are the horizontal components. The E3 HEMP fields are maximized for burst altitudes between 130 and 500 km altitude, much higher than the burst heights that optimize the E1 HEMP.

The E1 early time phase of EMP produces the greatest electric field, and generally the greatest peak coupled current on long conductors, but the E3, the longest phase, can dominate the time integral of the electric field, and produce system malfunction and damage through different mechanisms than the earlier phases. The time scale of E3, which ranges from a second to minutes, has much overlap with the time scale of geomagnetic storm threats, which are the subject of a companion report, and the methods used to analyze the E3 coupling are nearly identical – the principal differences are that, for E3, somewhat higher frequencies must be considered in developing models relating the horizontal electric field to the horizontal magnetic field at the surface of the earth, and the fact that the horizontal electric field associated with E3 HEMP can be substantially greater than that associated with geomagnetic storms.

Section 2 of this report will describe the generation of the E3A Blast Wave and the E3B Heave, describe the stratified soil models used to calculate the associated electric fields, and describe the U.S. power grid models of the lines and transformers to which the E3 HEMP fields will be applied. Section 3 presents a subset of the coupling results that were performed for the EMP Commission for E3B Heave and E3A Blast Wave, and shows the regions of likely collapse due to the generation of reactive demand. Section 4 analyzes the potential damage to circuit breakers due to the high levels of common mode currents flowing in the grid from E3A Blast Wave and E3B Heave scenarios. Section 5 deals with the potential damage to transformers from E3 HEMP.

Two appendices deal with the details of collapse and damage models – Appendix 1 covers the threat to system operation from the common mode currents driven by E3 MHD and Appendix 2 deals with transformer heating models.

Section 2
E3 HEMP Description and the U.S. Power Grid Model

2.1 The E3 HEMP Environment

E3 HEMP is also called Magneto-hydrodynamic or MHD EMP as it arises from the motion of the ionized bomb debris and atmosphere relative to the geomagnetic field. It was first noticed in 1958 in the Teak and Orange exoatmospheric nuclear weapons tests in the Pacific and Operation Argus in the Atlantic the same year, and additional information was obtained in the later exoatmospheric tests of the Fishbowl series, especially the Starfish Prime test in 1962.

Analysis of these tests has shown that the E3 electromagnetic environments are produced by two basically different physical mechanisms for bursts, both producing significant threats to electrical systems.

1. The 1-10 second time period is known as the “Blast Wave”

2. The 10-300 second time period is known as the “Heave”

The first of these, designated E3A or Blast Wave, is the expansion of the fireball, expelling the geomagnetic field and creating a magnetic bubble. At later times, the debris in the bubble flows along geomagnetic field lines and heats and ionizes the upper atmosphere, causing it to expand buoyantly and rise. The rising, conducting patch crosses the geomagnetic field lines, causing currents to flow in the patch and producing magnetic fields on the surface of the earth beneath the patch. This is designated E3B or Heave. The two processes occur in different time regimes and have different geographical distributions of the electrical field at the surface of the earth.

The qualitative understanding developed from examination of the nuclear test data, as well as theoretical and numerical modeling in the 1970s and 1980s of the physical mechanisms responsible for E3 HEMP, coupled with the growing awareness that such low level fields could pose significant risks to extended commercial and military electrical networks associated with power and communications, lead to E3 being considered a significant threat.

We will describe the physical mechanisms associated with E3A and E3B in turn.

2.1.1 E3A Blast Wave

About 75% of the energy of an exoatmospheric nuclear explosion is emitted as x-rays. Those x-rays emitted downward are absorbed in the atmosphere, generally between 80 and 110 km altitude. The vast majority of the 25% remaining of the energy is in the kinetic energy, or energy of motion, of the weapon debris, which has become highly

ionized and therefore has a high electrical conductivity. The debris expands outward, pushing the geomagnetic field ahead of the conducting region, and this forms a "magnetic bubble." The initial expansion of the bubble is determined by the velocity of the debris, which is greater than 1000 km/s; the later expansion of the bubble depends on the altitude at which the detonation occurs. For altitudes less than 300 km, the dominant effect slowing the expansion is the density of the atmosphere outside of the bubble, and the bubble becomes asymmetric as it expands more easily upward into more rarefied air than downward into denser air. For higher altitudes, the expansion is slowed by magnetic pressure, which is anisotropic, and the kinetic energy of the debris is converted into magnetic energy of distorted field lines. The anisotropy of the magnetic pressure is such that the bubble expands more rapidly along the field lines and less rapidly perpendicular to the magnetic field lines. For observers at large distances from the burst, the perturbation of the magnetic field is that of a dipole aligned with the geomagnetic field at the burst point. This mechanism for generating electromagnetic signals was postulated by Karzas and Latter in 1962. The resulting fields are quite low, but they can exist over long time periods and large areas. Thus, there is concern with coupling to very long communication lines (such as the copper power conductors in seafloor fiber optics cables), as well as commercial power lines.

For the early time nearly spherical expansion of the magnetic bubble, the perturbed magnetic fields at the surface of the ground would be nearly those of a magnetic dipole whose magnitude is given by

$$M(t) = -\frac{B_0 R(t)^3}{2}$$

where $R(t)$ is the time dependent bubble radius and B_0 is the magnitude of the geomagnetic field. Typically, the magnetic bubble attains its maximum size in less than a second after the burst, and then collapses in a few seconds. For night-time bursts occurring near the minimum of the solar cycle, the perturbed magnetic field propagates to the ground through the ionosphere in a time scale short compared to the bubble dynamics, so that using a magnetostatic field approximation is valid. However, nighttime bursts during periods of heightened solar activity and all daytime bursts produce much smaller magnetic perturbations (and electric fields) at the ground because the time for the magnetic disturbances to diffuse through the ionosphere to ground level become much longer that the time scale of bubble growth and collapse.

The electric fields resulting from this perturbation to the geomagnetic fields could be calculated in a straightforward manner except for complications introduced by the x-rays produced by the device. About 75% of the total yield of the threat device is released in the form of x-rays with quantum energies of a few kilo electron volts (keV). For burst heights above about 100 km, the downward going x-rays are stopped in the upper atmosphere by the photoelectric process at altitudes between 80 and 110 kilometers; and in the first few microseconds, these photoelectrons deposit their energy creating additional secondary electrons, substantially ionizing this region, and creating a high electrical conductivity within it. This region, which extends out somewhat beyond the

horizon at 110 km altitude as seen from the burst, acts to shield the ground from direct electromagnetic signals generated in the burst region. The extension beyond the 110 km altitude horizon is due to the more energetic portion of the x-ray spectrum.

Figure 2-1 shows this basic physical mechanism, with a fireball growing in size preferentially upward and along the geomagnetic field, inducing perturbations in the geomagnetic field. The lines are tightly anchored in the conducting x-ray patch, and loosely anchored in the ground – in the ground they can diffuse sideways, but only with the skin depth, which increases as a function of time.

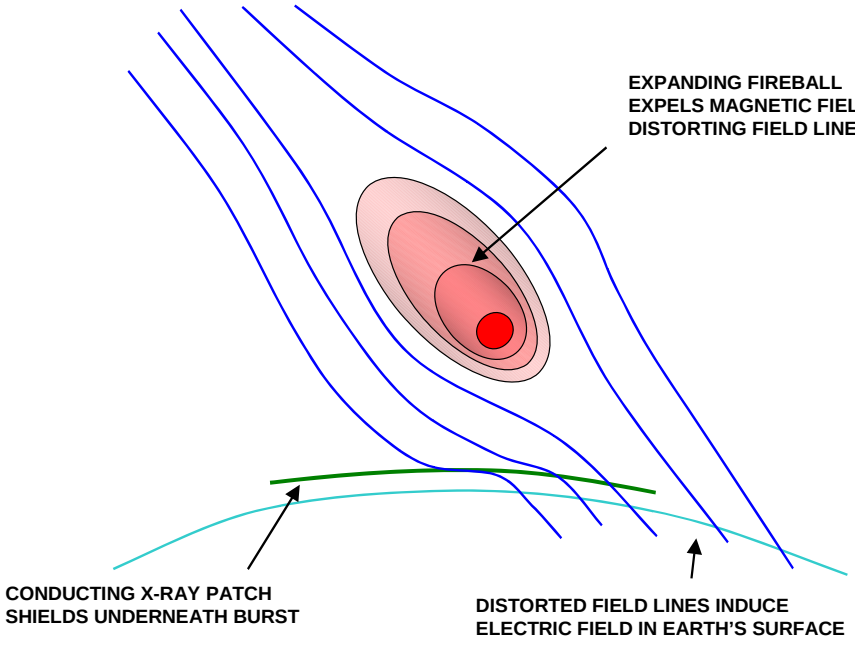

Figure 2-1. Schematic of E3A Blast Wave phenomenology. The x-ray patch is shown at less that its actual radius for illustrative purposes.

Because of the x-ray patch shield effect, the largest fields for the E3A or Blast Wave signal are seen beyond the edge of the patch. Fields are developed beneath the patch by the perturbed magnetic fields at the edge of the patch "sliding" under the edge horizontally rather than penetrating vertically. The sliding fields can be calculated by calculating a magnetic scalar potential that, using

$$\Delta\vec{B} = -\vec{\nabla}\phi_M$$

fits the perturbed magnetic field at the edge of the patch for a perfectly conducting earth, and then finding the interior sourceless solution beneath the patch. The dipole term, which has a uniform horizontal magnetic field pointed northward dominates, and produces east-west electric fields. Figure 2-2 shows the spatial variation of the relative magnitude of the magnetic perturbations associated with the blast wave for a burst at an altitude of 400 km over Mexico and Figure 2-3 shows the same figure with arrows showing the direction of the horizontal component of the perturbed magnetic field.

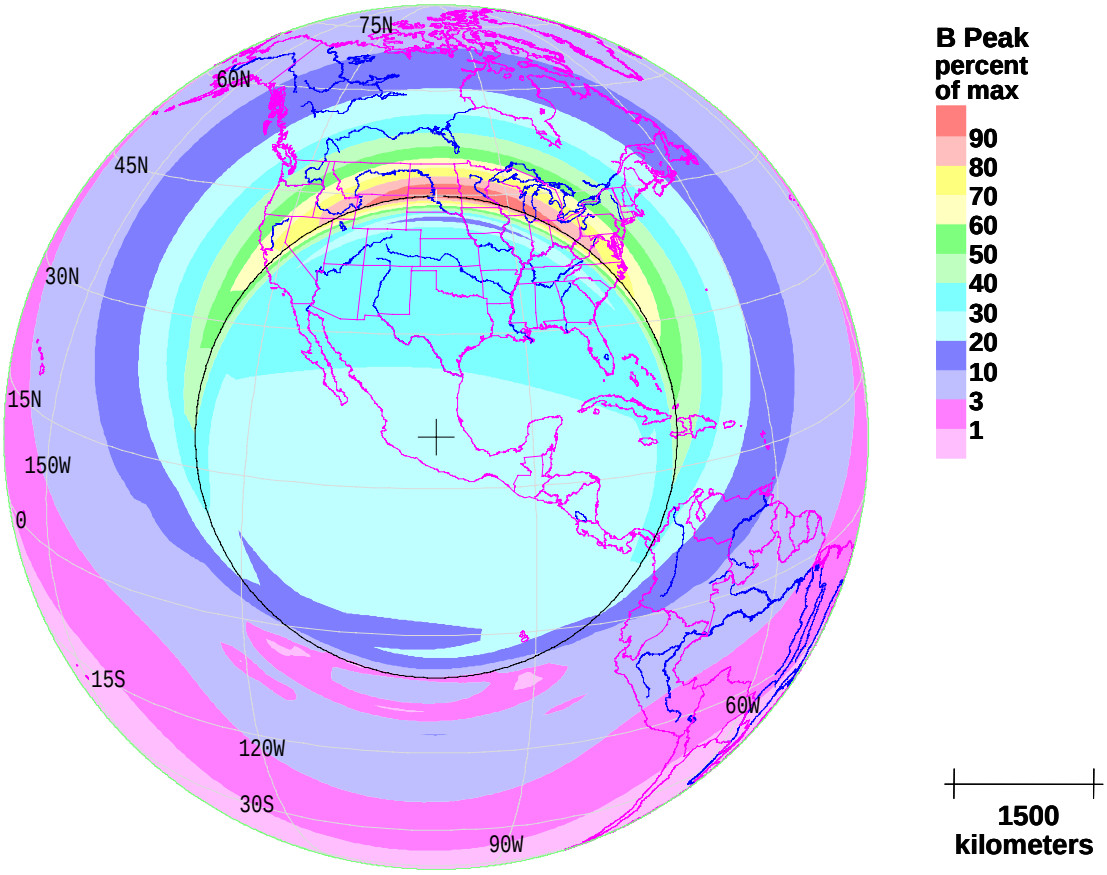

Figure 2-2. Spatial distribution of the perturbed magnetic field for E3A Blast Wave, showing the effect of the shielding by the x-ray patch.

In Figure 2-2, the effective edge of the x-ray patch is indicated with a thin black circle – the fields within the circle are primarily those that have slid sideways underneath the patch. For low yield weapons and high burst altitudes, the x-ray patch may only be slightly ionized, and then the field has considerable variation in that region. But this situation has electric fields so small that they are of little concern for damage to systems. With the x-ray patch shown, the fields are relatively uniform under the patch.

In Figure 2-3, where we have superimposed vectors indicating the direction of the perturbed magnetic field, the length of the arrows are all the same on the surface of the earth and they only show the direction of the perturbed magnetic field.

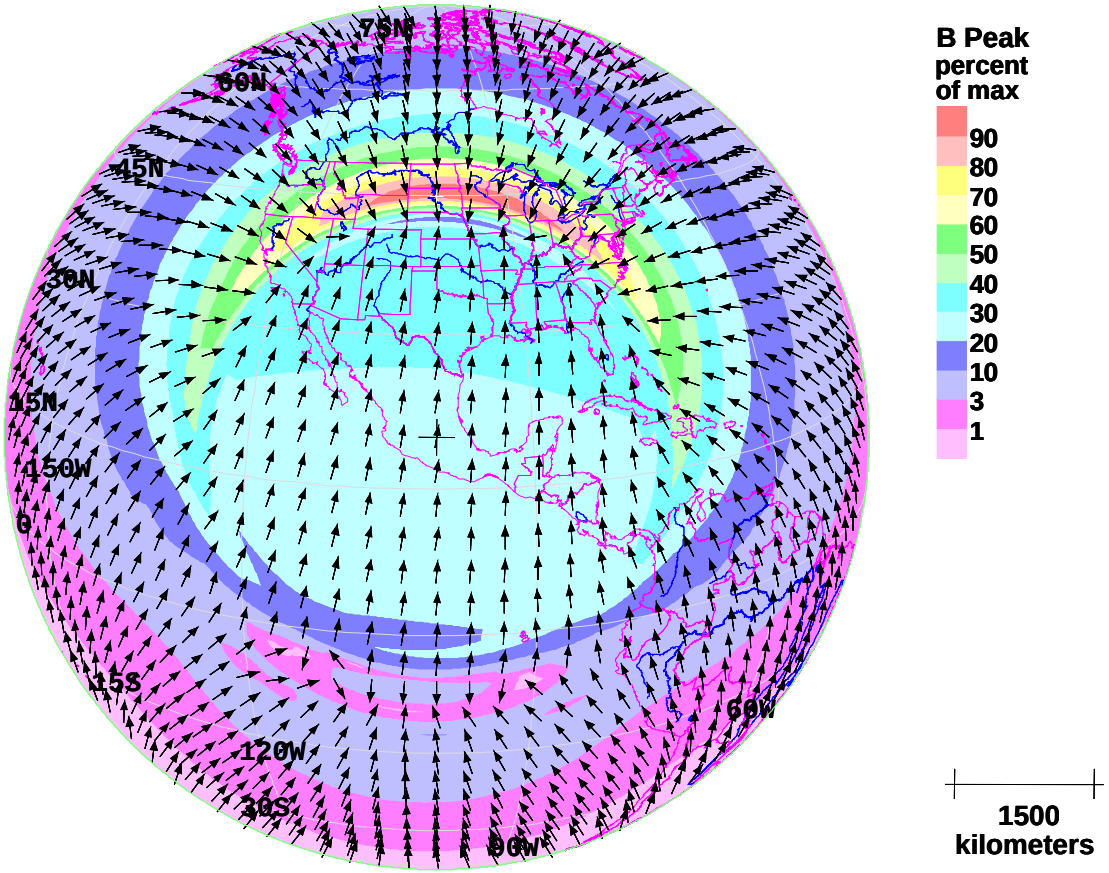

Figure 2-3. Direction of the horizontal component of the perturbed magnetic field for E3A Blast Wave.

The electric field in (volts per meter) associated with the magnetic perturbations can be calculated over a uniformly conducting ground by taking a convolution

$$E(t) = \frac{1}{\sqrt{\pi \mu_0 \sigma}} \int_0^t \frac{d\tau}{\sqrt{t-\tau}} \frac{\partial B(\tau)}{\partial \tau}$$

where the ground conductivity is σ, μ_0 is $4\pi \times 10^{-7}$ H/m, the magnetic permeability of free space, and B is the magnetic perturbation in Teslas. For specifications of E3A, the horizontal electric field is often given in volts per kilometer for a uniform ground conductivity of 10^{-3} or 10^{-4} Siemens per meter (Siemens are the unit of conductivity that are inverse ohms, and were archaically known as "mhos"), however the vertical stratification of the ground conductivity is very important and tends to emphasize the higher frequencies, as will be shown in Section 1.2.

Since the rise of the perturbed magnetic field is much more rapid than the decay for both E3A Blast Wave and E3B Heave, the peak electric field is related to the peak magnetic field for uniformly conducting soils approximately by

$$E_{pk} \approx \frac{0.9 B_{pk}}{\sqrt{\mu_0 \sigma t_t}}$$

where t_r is the rise time of the perturbed magnetic field, defined as the difference in time between 10% to 90% of the peak amplitude.

The horizontal component of the electric field is perpendicular to the horizontal component of the magnetic field and is shown in Figure 2-4 for a uniform ground conductivity of 10^{-3} (applied everywhere, including the oceans). Note the relative uniformity of the east-west field direction under the patch, contrasted with the rapid variation of both direction and magnitude outside the patch. For low latitude bursts in the northern hemisphere, the strongest fields are just north of the x-ray patch.

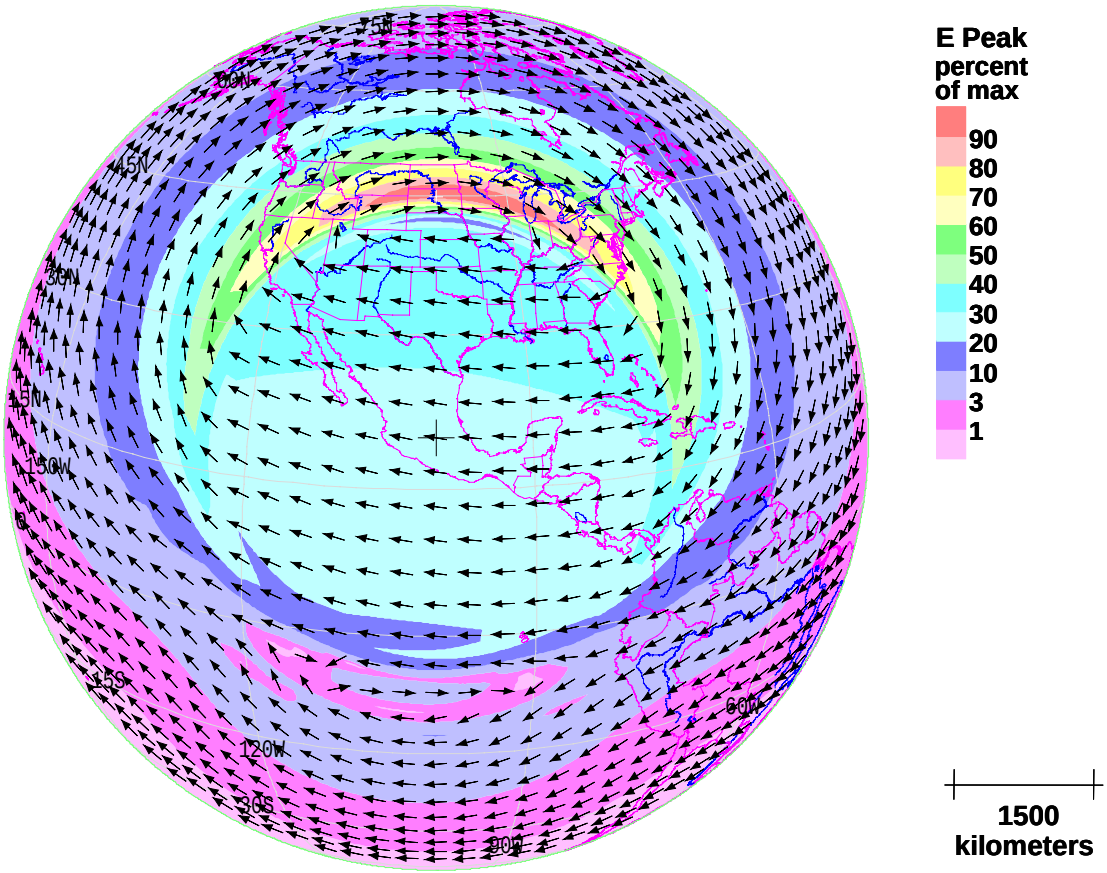

Figure 2-4. Direction of the horizontal component of the electric field for E3A Blast Wave.

2.1.2 Burst height, atmosphere and yield scaling for E3A Blast Wave

As mentioned earlier, the state of the ionosphere at the time of detonation strongly influences the magnitude of the peak electric field. Figure 2-5 shows this variation as well as the variation in burst height for a moderate yield device. The altitude dependence results from the balance between opposing effects – at higher burst altitudes, the conducting region can expand to a greater radius before being halted and then compressed by the geomagnetic field, giving a greater dipole moment, but the perturbed magnetic field on the ground is smaller for a given dipole moment because the field falls as $1/r^3$. The notation for the density of the atmosphere refers to its state of ionization, with "low density" referring to nighttime at the minimum of the solar cycle, "medium density" referring to daytime at solar minimum or nighttime at solar maximum and "high density" referring to daytime at solar maximum.

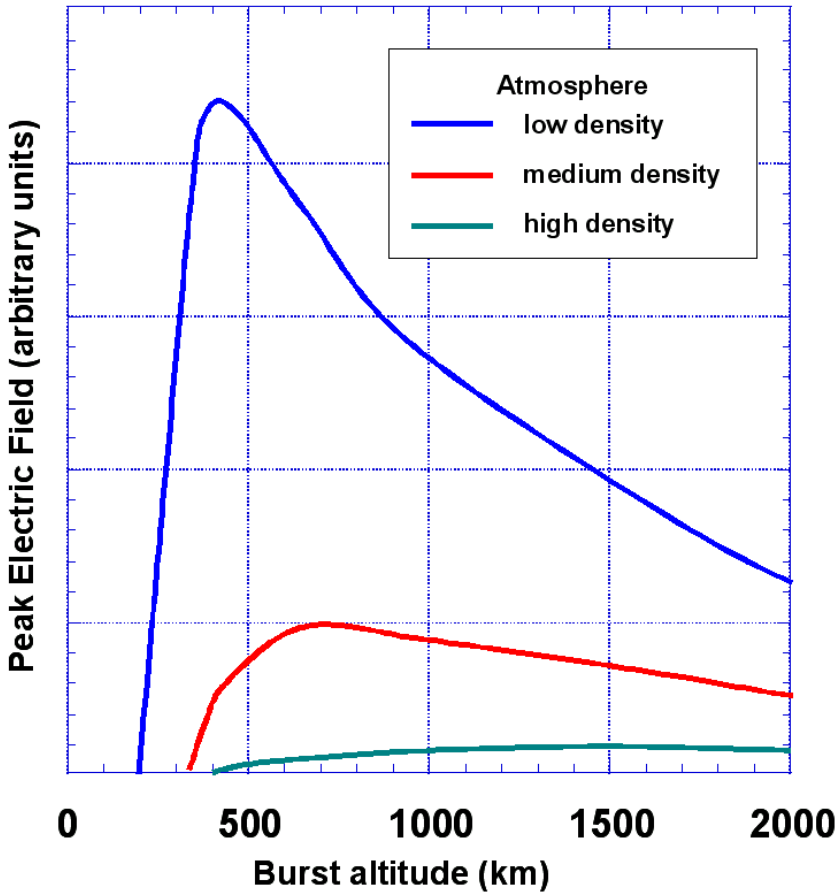

Figure 2-5. Burst height and atmosphere scaling for peak E3A electric field.

Figure 2-6 shows the scaling of the peak electric field as a function of device yield for a nighttime solar minimum burst at 400 km altitude. There are scaling relations that show that the maximum radius of the conducting region scales as the cube root of the burst

yield. Since the magnetic perturbation goes as the cube of the radius of the conducting region, the peak electric field scales nearly linearly with yield over a wide yield range.

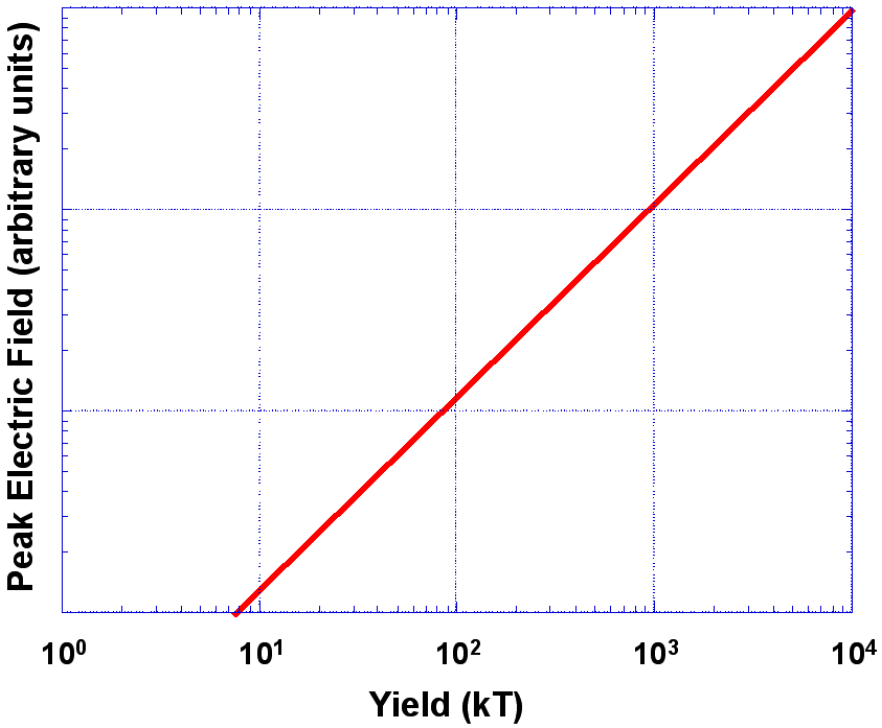

Figure 2-6. Yield scaling for peak E3A electric field.

2.1.3 E3B Heave

The second part of the E3 MHD EMP for bursts above 100 km altitude is the E3B or Heave effect. The basic phenomenology of the heave generation is shown in Figure 2-7. For bursts higher than 130 km altitude, bomb debris and shock heated air ions stream downward along geomagnetic field lines until they deposit their energy at altitudes near 130 km. These two processes contribute to both the heating and additional ionization of the E-layer of the ionosphere. There is also heating of this region by UV radiation from the burst, and this heating is centered beneath the burst. After an initial brief period of expansion of the heated air, it buoyantly rises. In the figure, we have shown the region with enhanced conductivity as a reddish "hat" with the heated center rising more rapidly than the brim. As this conducting layer rises across the geomagnetic field, a current is induced by the dynamo effect, as indicated by the solid arrow on the hat in the figure. The dynamo current flowing to the west is accompanied by northern and southern return currents in regions where the heating and buoyant rise is smaller, so that the overall current flow in the E-layer looks like a figure eight. This induces a current in the ground in the opposite direction, and the finite conductivity of the ground means that the current in the ground is accompanied by an electric field in the same direction, as shown by the blue pattern.

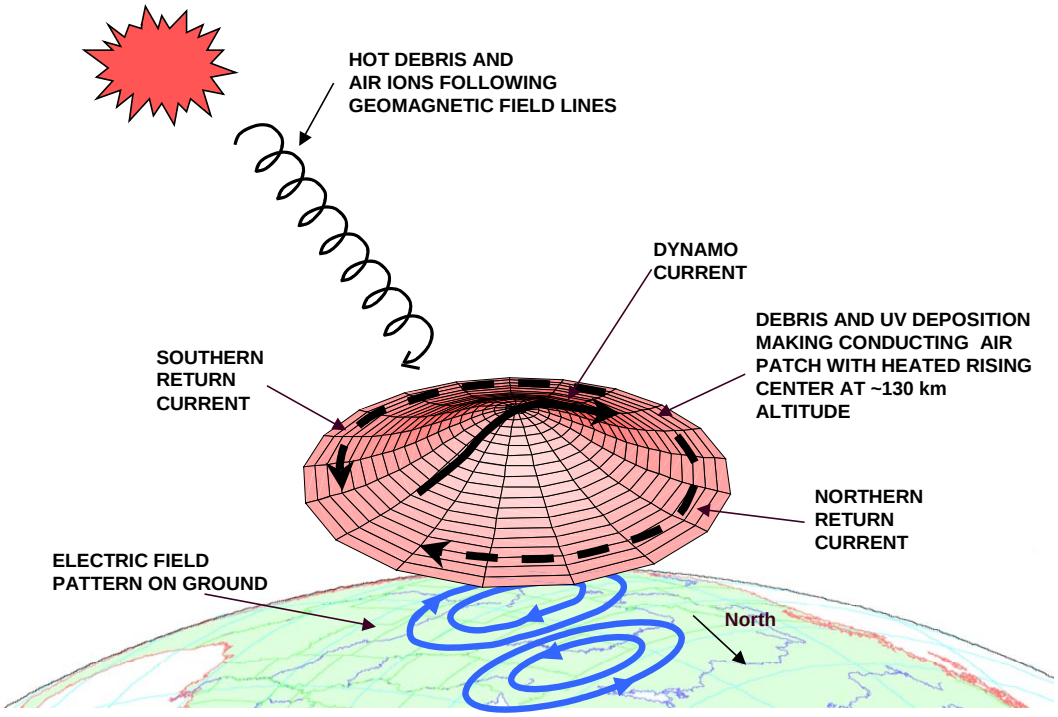

Figure 2-7. Schematic of E3B Heave phenomenology.

Several of the points in the preceding description deserve further explanation.

1. The relative importance of the debris and UV processes depends on altitude. For very high-altitude bursts, where debris expansion is largely magnetically contained, some portion of the downward directed debris expansion does nonetheless impinge upon and is contained by the earth atmosphere and ionosphere. This debris-air interaction results in the creation of shock heated air ions, which escape the burst region and, guided downward by the ambient magnetic field lines, deposit energy in the atmosphere away from the burst point towards the magnetic conjugate region. As the height of the burst is lowered, the amount of shock heated air ions and the attendant energy deposition in the neutral atmosphere is dramatically increased. For bursts below about 200 kilometers, UV processes increasingly contribute to heating of the neutral atmosphere. The region of peak heating for UV processes is centered directly below the burst.

2. This energy deposition process occurs during the first few seconds following the burst. Because of its increased buoyancy, the energy-deposition heated atmosphere then begins to rise. As this heaving region traverses the air above it,

including the ionospheric E region, it pushes the E-region along in its upward motion, which by 10 - 20 seconds has reached supersonic velocities.

3. On the heave time scale, the prompt shield x-ray ionization has decayed to the point where it is ineffective as an electromagnetic shield. However, the atomic ions that comprise the upper E region of the ionosphere and contribute to the electrical conductivity are long lived. Moreover, their densities are sufficiently high that the enhanced conductivity layer behaves as essentially a perfect conductor out to several hundred kilometers horizontally. This behavior persists for times out to the order of 60 seconds. As a result, the horizontal component of the geomagnetic field is trapped between this effectively perfectly conducting atomic ionization layer and the earth, so that as the heave region rises to a height H(t), the spacing of the geomagnetic field lines beneath the heaving layer is stretched out and the horizontal component of the earth's geomagnetic field B(t) decreases so as to preserve total flux. This magnetic field transport produces transverse currents in the heave region to preserve total flux. This process continues until the ionization in the heave region falls to a value where it ceases to behave as a perfect conductor. Magnetic flux then begins to slip through this region, and the geomagnetic field between the layer and the earth relaxes to its ambient state as the currents in the heave layer decay away.

As with the magnetic dipole model for E3A Blast Wave, a simple model can be made of the heave that illustrates the essential behavior. This model is made combining magnetic flux conservation with a ballistic rise for the conducting region. We assume that the region at 130 km is perfectly conducting and it rises ballistically, that is with the acceleration of gravity, upward. If the horizontal geomagnetic field is B_0, the acceleration of gravity is a and the original height of the rising region is h_0, then the perturbed magnetic field is

$$\Delta B = B_0 \left(\frac{h_0}{h_0 + at^2/2} - 1 \right)$$

Using the maximum value of the horizontal geomagnetic field, 0.4 Gauss (4×10^{-5} Teslas), and performing the convolution to obtain the horizontal electric field for a uniform 10^{-3} S/m soil, we obtain the time history shown in Figure 2-8.

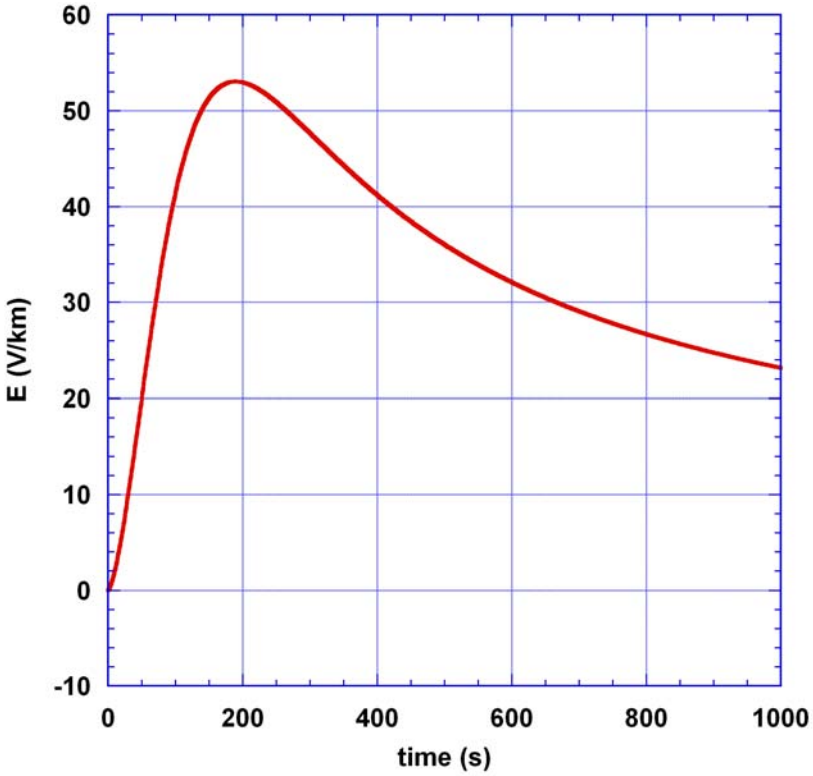

Figure 2-8. Simple Heave model horizontal electric field as a function of time.

This simple model gives reasonable values for the peak electric field, but many aspects of the model should not be taken too seriously. In detailed calculations, the horizontal electric field falls more rapidly as the heave region becomes deionized, and the transverse extent of the heave region is finite, allowing the geomagnetic field to "leak in sideways."

Returning to Figure 2-7, the maximum field strength is in the region beneath the most highly heated portion of the atmosphere. Because the heating of the atmosphere is relatively localized (i.e., spanning several hundred kilometers), one would expect a much smaller field coverage pattern than the E3A blast wave. Both expectations are borne out in numerical simulations of the E3B heave. The electric field pattern mirrors the current flow in the conducting heave region. For example, in the center of the pattern corresponding to the region of maximum energy deposition, one can see the large EW currents required to preserve total magnetic flux (the so-called "dynamo" effect), while away from the heave driven currents, one can see the return currents which must flow to conserve total current. These current flows result in a typical double bulls-eye pattern for heave E3 fields. The bulls-eye regions themselves are null field regions, where there is large cancellation between dynamo current flow and the return current flow. Because of the time and spatial dependence of the conductivity, as well as that of the heave, the point where the primary and return currents exactly cancel is not fixed but rather varies during the course of time. It is now known that the Fishbowl test series E3A Heave magnetic field data were unfortunately all recorded in the bulls-eye regions.

Figure 2-9 shows the spatial variation of the relative magnitude of the magnetic perturbations associated with the heave for a burst at an altitude of 130 km over central CONUS and Figure 2-10 shows the same figure with arrows showing the direction of the horizontal component of the perturbed magnetic field.

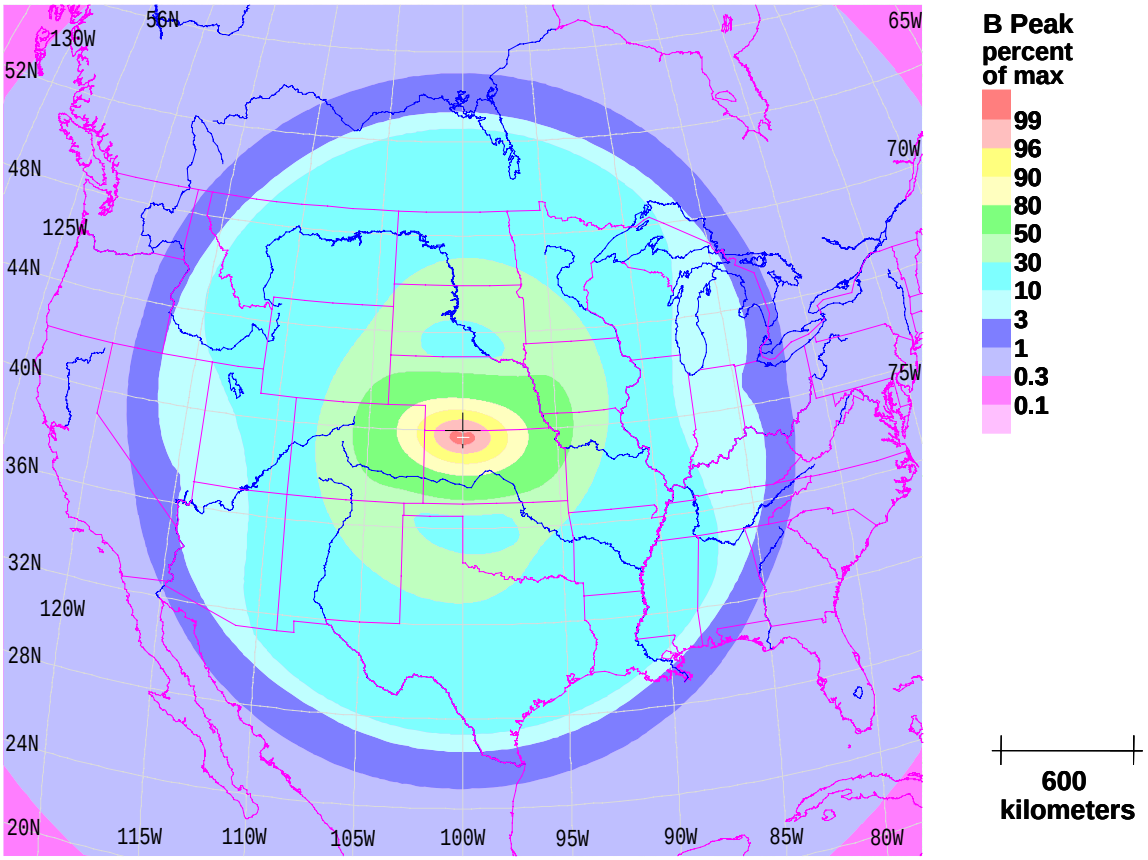

Figure 2-9. Spatial distribution of the perturbed magnetic field for E3B Heave.

In Figure 2-9, the bulls-eye regions lie about 500 km to the magnetic north and south of the sub-burst point. The peak magnetic field does not fall to zero in the bulls-eyes because the behavior of the magnetic field pattern is dynamic, and the bulls-eyes move outward as the heave patch rises and expands laterally, so that the point where there is no perturbed horizontal magnetic field at one time is not where there is no field at another time. There is a large region where the perturbed magnetic field is greater than 90 percent of its peak value, the location of which is indicated by a small white cross.

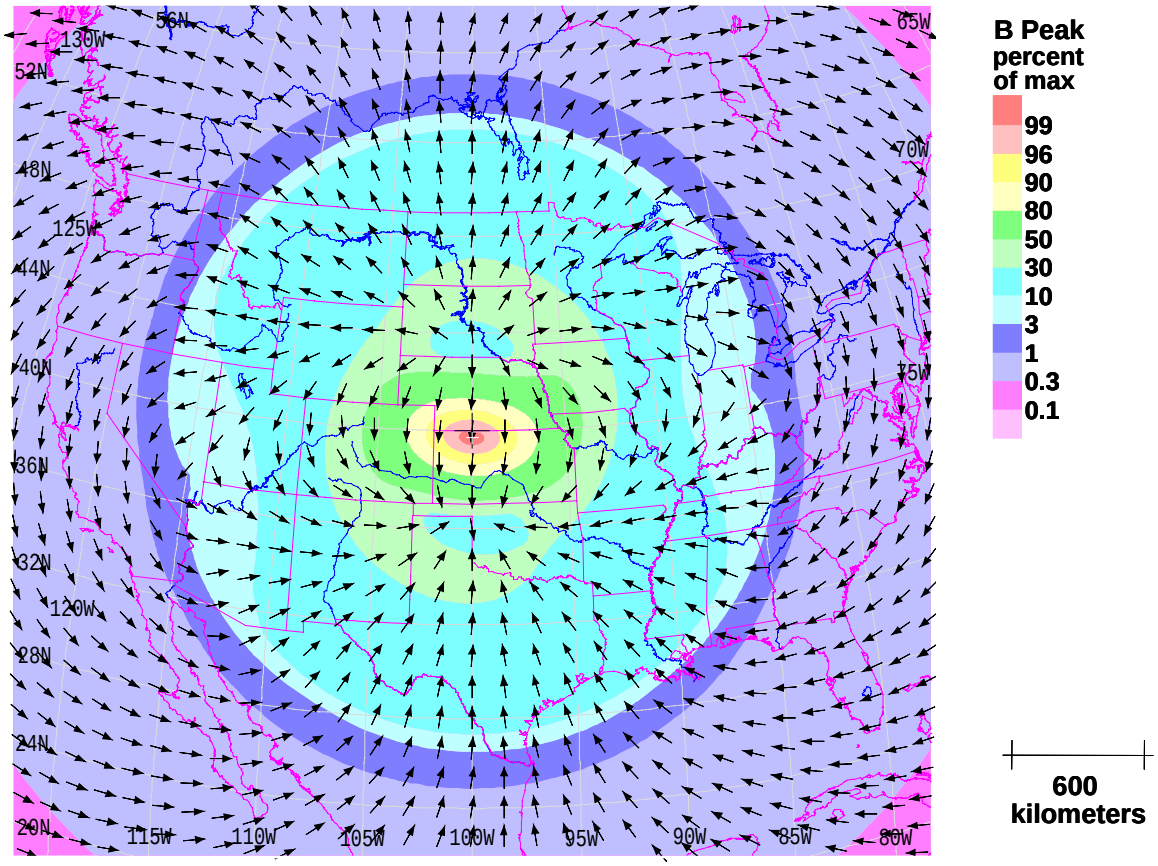

Figure 2-10. Direction of the horizontal component of the perturbed magnetic field for E3B Heave.

In Figure 2-10, the direction of the perturbed magnetic field beneath the burst is southward, so this indicates a reduction in the geomagnetic field. On the other side of the bulls-eyes, the northward perturbation is an increase in the geomagnetic field, although the increase is much smaller than the decrease beneath the heave patch.

The horizontal component of the electric field is again perpendicular to the horizontal component of the magnetic field and is shown in Figure 2-11 for a uniform ground conductivity of 10^{-3} (applied everywhere including the oceans). The electric field arrows circulate in the direction indicated in the schematic of Figure 2-7.

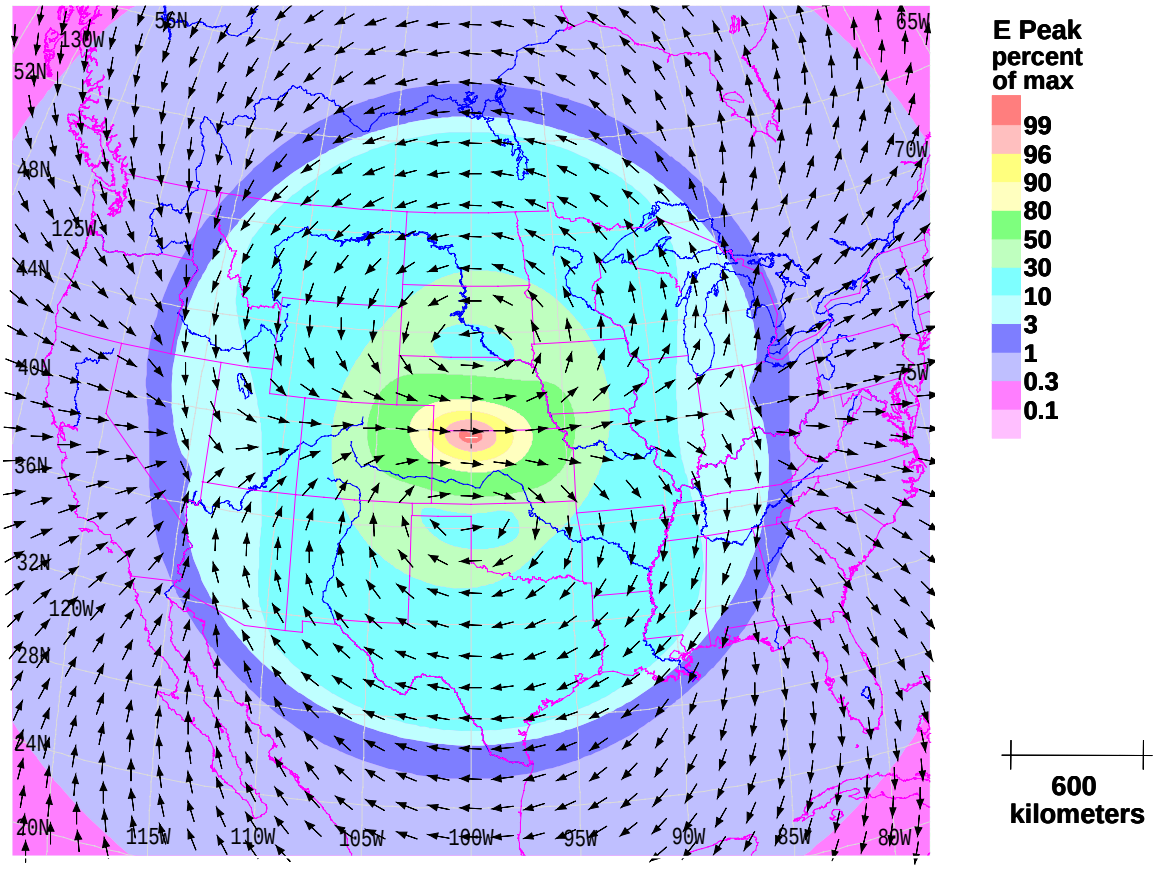

Figure 2-11. Direction of the horizontal component of the electric field for E3B Heave.

2.1.4 Burst height and yield scaling for E3B Heave

In contrast to the blast wave, which is maximized for bursts at about 400 km, the worst case heave occurs for much lower burst altitudes. Figure 2-12 shows the behavior of the peak electric field with burst altitude. Below about 200 km, the heating of the heave region is dominated by the UV deposition, and for higher burst altitudes it is dominated by the debris and heated air ions flowing down along the magnetic field lines, so it is not surprising that the peak electric field as a function of burst altitude changes slope near that altitude.

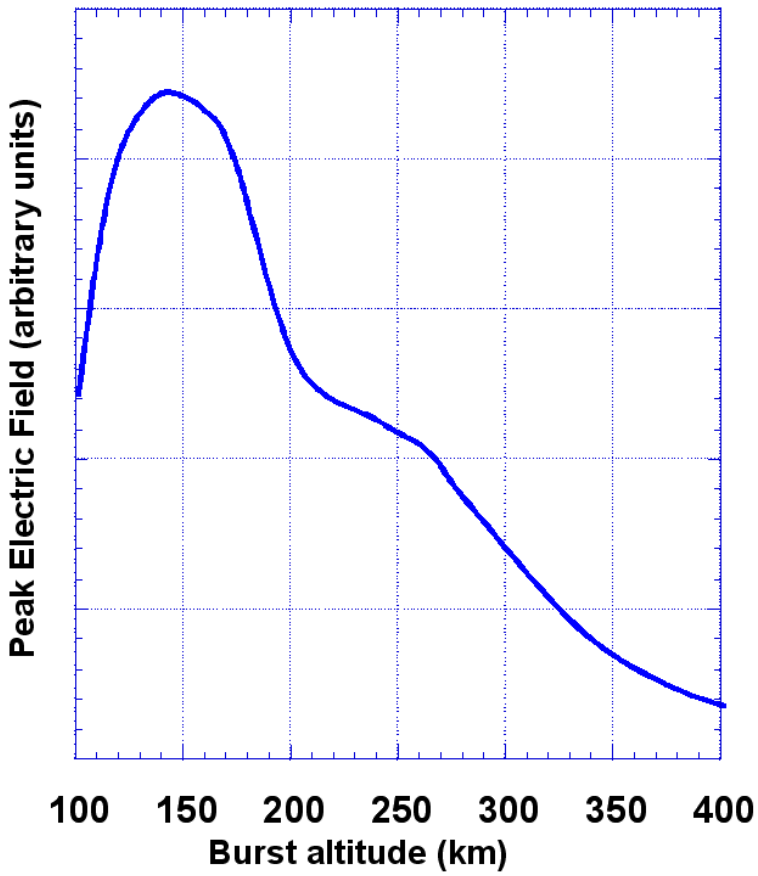

Figure 2-12. Burst height scaling for peak E3B electric field.

The behavior of the peak electric field as a function of burst yield for bursts at 130 km altitude is shown in Figure 2-13. Unlike the behavior in the Blast Wave, the peak electric field saturates below 100 kT yield, and larger devices do not produce a higher field. However, the pattern enlarges for larger yields, so that there is a larger region on the ground where the horizontal electric field is near its peak value.

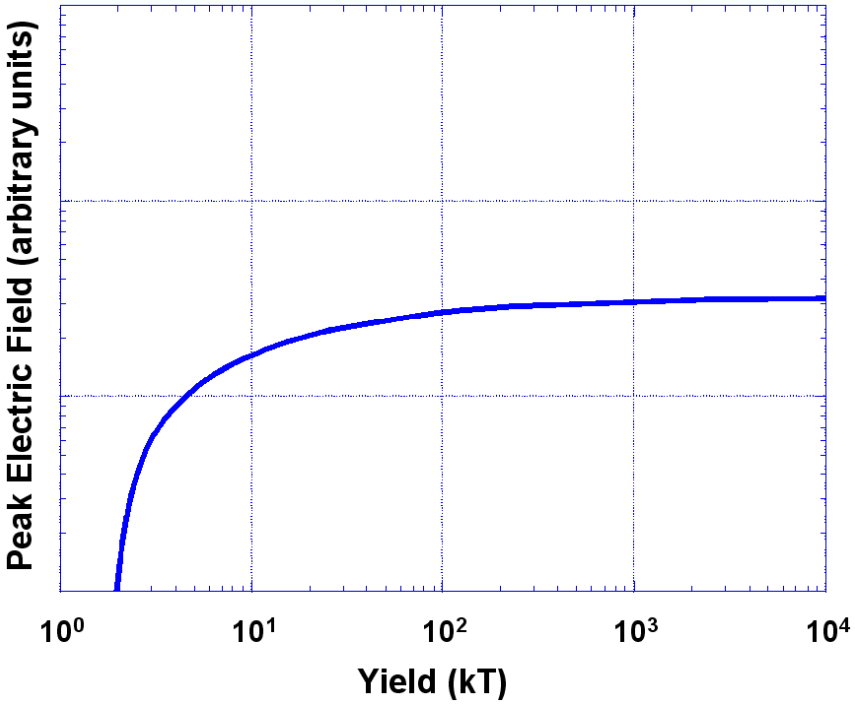

Figure 2-13. Yield scaling for peak E3B electric field.

2.1.5 Low Altitude Bursts

When the detonation occurs below 100 km, the blast wave E3 is replaced by another effect, the dipole E3. This effect is similar to the blast wave in that the expulsion of the geomagnetic field from the fireball drives the magnetic perturbations on the ground. The primary difference is that the geomagnetic field has little effect controlling the fireball expansion - this expansion is limited by the atmospheric pressure instead of the geomagnetic pressure that limits the fireball expansion at high altitudes. The final size of the region from which the geomagnetic field is expelled is much smaller, so the magnetic dipole moment is much less. This is partially compensated for by the closer proximity to observers on the ground and the lack of an intervening region of x-ray ionization that produces the characteristic pattern for the blast wave for bursts above 100 km, where both the electric and magnetic fields are greatest outside the x-ray patch. The dipole E3 has a much smaller ground electric field than either the blast wave or heave for bursts above 100 km and is rarely considered for system survivability.

2.1.6 Numerical Methods Used for E3 Calculations

Before the interest arose in the survivability of systems with long lines to MHD EMP, there was considerable development of numerical techniques to calculate the propagation of electromagnetic waves through an upper atmosphere disturbed by a nuclear explosion. This development resulted from interest in radar and radio communication, and was primarily driven by concern over the radar operation in antiballistic missile systems in a nuclear environment, where an adversary could detonate nuclear weapons above the

atmosphere to blind the radar with ionization and thus permit succeeding re-entry vehicles to reach lower altitudes without interception. The interest in the nuclear driven ionization affecting radio communications had to do with concern over loss of ability to communicate Emergency Action Messages with nuclear missile equipped submarines, bombers and missile silos. In addition to the loss of signal strength of radio communications, the complex geometry of the ionized region, including striations, meant that radio messages could become unintelligible even when sufficient signal strength was available on a given path, and accurate models of the time development of the conductivity were needed to simulate the effects of different modulation schemes and data rates. This led to the development of 2D and 3D simulations of the magnetic bubble, its collapse in the magnetic field, and the deposition of ionized weapons debris and shocked air in the E-region or the ionosphere.

The multidimensional simulations in the 1970s and 1980s, primarily done at Mission Research Corporation, used enormous quantities of supercomputer time (the Cray 1s of ~1980 had a floating point speed of 140 MFlops, modern PCs are two orders of magnitude faster), and this only permitted a small number of cases to be run – most of the runs were either validation runs of the U.S. Starfish test of 1962, or of a few hypothetical large yield Soviet devices. The codes could not be used directly to calculate the E3A Blast Wave HEMP because the full set of MHD equations would result in unacceptable time step requirements for the desired spatial steps, particularly at the lower altitudes where the ionization was small. The growth of the fireball could be taken from these simulations, and used to drive subsidiary electromagnetics codes, which did not include the plasma motion, to calculate how the magnetic perturbations reached the ground, and this was done to reach an acceptable degree of agreement with the Starfish Blast Wave. The rate of neutral heave could also be calculated with the multidimensional codes, and this led to the modeling of the E3B Heave signal for the limited number of cases for which the simulations were available.

The next step was the development of physical approximations codes by Austin Research Associates. These codes used models of the fireball and E-region heave dynamics instead of first-principles models, and these models were “tuned” to agree with the multidimensional calculations. The electromagnetics model used the thin-layer approximation where the conducting regions of the ionosphere were collapsed into sheets in those regions where the Hall conductivity and Pedersen Conductivity dominated. The use of physical models for the dynamics and the thin-layer models permitted the construction of a substantial database of U.S., Soviet and primitive devices E3 MHD environments as a function of magnetic latitude and burst altitude, and these have been automated into the Metatech HEMPTAPS code that automatically performs the needed interpolations and allows the user to calculate the MHD environments. These were used to perform the calculations in the study for the EMP Commission that are included in this report.

2.1.7 E3 Comparison with Soviet Data

In October of 1962, the Soviets performed a series of high altitude nuclear weapons tests to evaluate the capabilities of their design for an anti-ballistic missile system. During these tests, measurements of magnetic fields associated with the Heave signal were made, and several power outages were observed that were attributed to E1 and E3 HEMP. (The Blast Wave was small for these tests as they occurred during daylight hours.) In recent years, details of the tests have been openly reported and the magnetometer data was made available. These data were compared with the numerical modeling, and we will show some of the comparisons with the Soviet 150 km altitude burst of October 28 that has been stated to have a yield of 300 kilotons (personal communications with M. L. Sloan and J. R. Thompson).

The burst altitude of 150 kilometers is close to the altitude producing the worst case heave magnetic fields, and for this altitude the UV from the device is the most important contribution to the Heave. The comparisons that we can make are not in the high field region because the sites from which the magnetometer data were taken are too far away from the sub-burst point – the "bulls-eyes" of the pattern are predicted to lie about 110 km north and south of the sub-burst point, and the ground range of the observations varies from 227 to 371 km.

The first comparison, shown in Figure 2-14, is for a point well to the north of the sub-burst point. The magnitude and angle of the perturbed magnetic field are in good agreement, though the calculated rise rate is faster (1 gamma=10^{-9} Tesla).

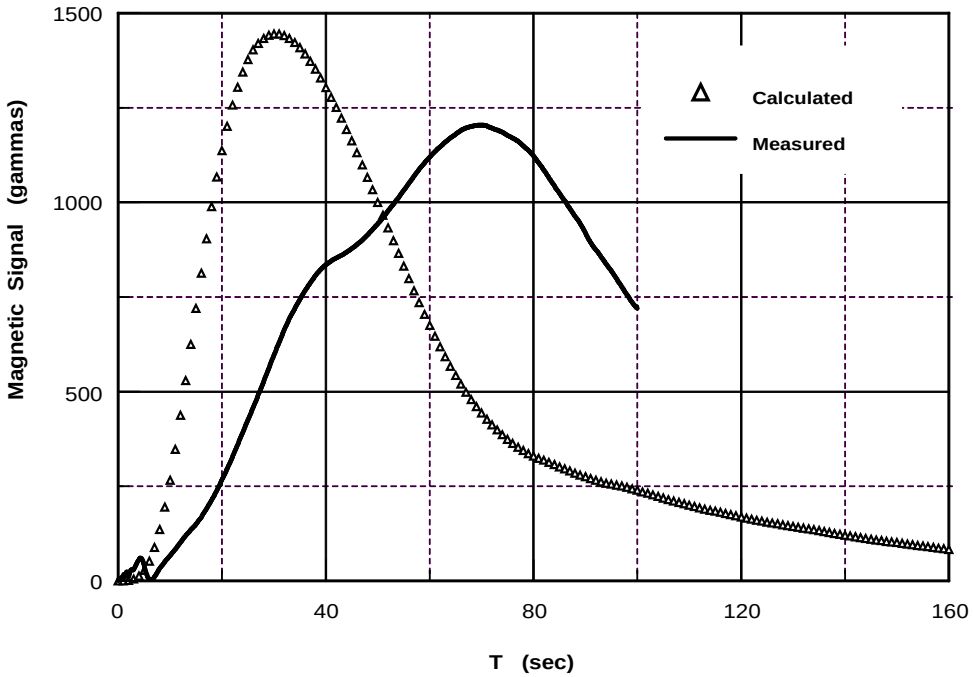

Figure 2-14. Comparison of measured vs. calculated magnetic signal field strength at an observation point 227 kilometers north of the burst location. The peak measured field had an orientation 41 degrees from the peak predicted field.

At locations further to the east, and more related to the sub-burst point, the rise rates are much closer to the observed data. This is shown in Figures 2-15 and 2-16. There is a short precursor seen in the data that has opposite polarity, and is believed to result from the initial expansion of the heave layer, which pushed geomagnetic field down into the earth – the later heave pulls the geomagnetic field out of the earth and has opposite magnetic and electric fields.

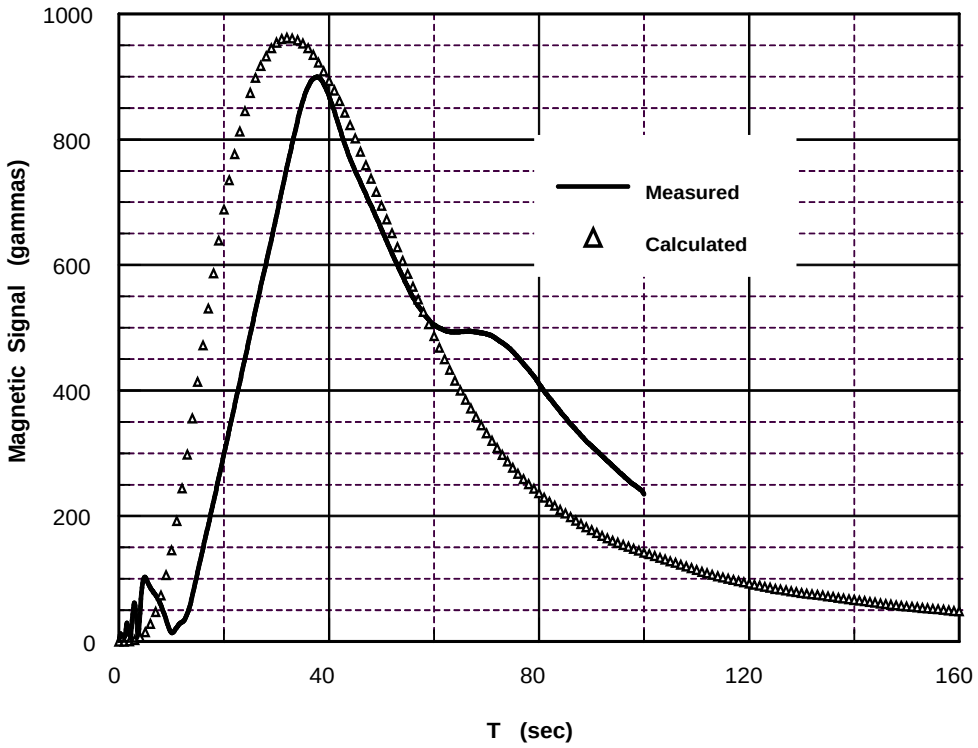

Figure 2-15. Comparison of measured vs. calculated magnetic signal field strength at an observation point 362 km east of the burst location. The peak measured field had an orientation 31 degrees from the peak predicted field.

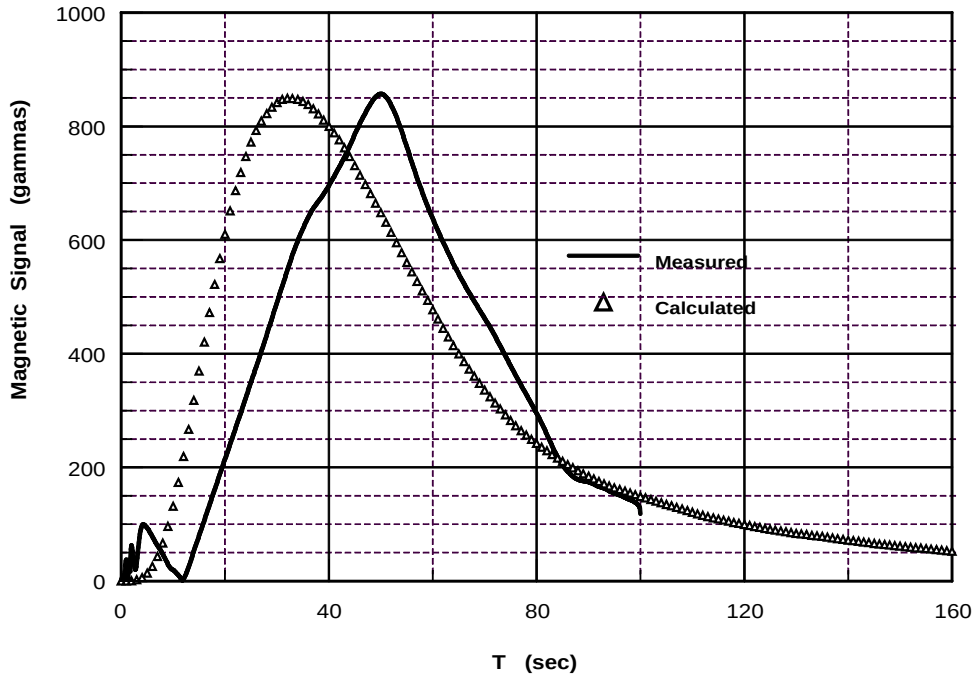

Figure 2-16. Comparison of measured vs. calculated magnetic signal field strength at an observation point 371 km east of the burst location. The peak measured field had an orientation 15 degrees from the peak predicted field.

2.1.8 The IEC E3 Specification

A standard for E3 HEMP was developed by the IEC and is available for unclassified use. This specification provides a composite waveform instead of separating the individual Blast Wave and Heave components, and does not provide guidance on the spatial extent of the field or the orientation. The specified horizontal electric field is shown in Figure 2-17, and is to be used with a uniform ground conductivity of 10^{-4} S/m. For other ground conductivities, the electric field is to be scaled as

$$E_3 \sim \sigma_g^{-1/2}$$

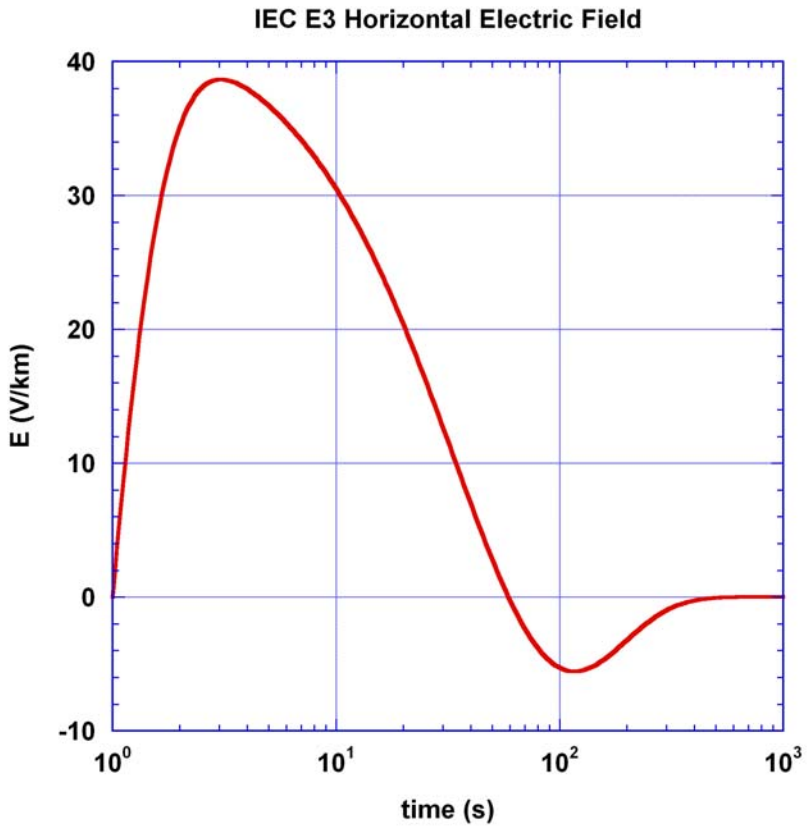

Figure 2-17. E3 standard from IEC-1000-2-9.

A horizontal magnetic can be extracted from this by taking the inverse of the convolution formula for the electric field shown in Section 2.1.1

$$B(t) = \sqrt{\frac{\mu_0 \sigma}{\pi}} \int_0^t \frac{d\tau}{\sqrt{t-\tau}} E(\tau)$$

The resulting magnetic field is shown in Figure 2-18.

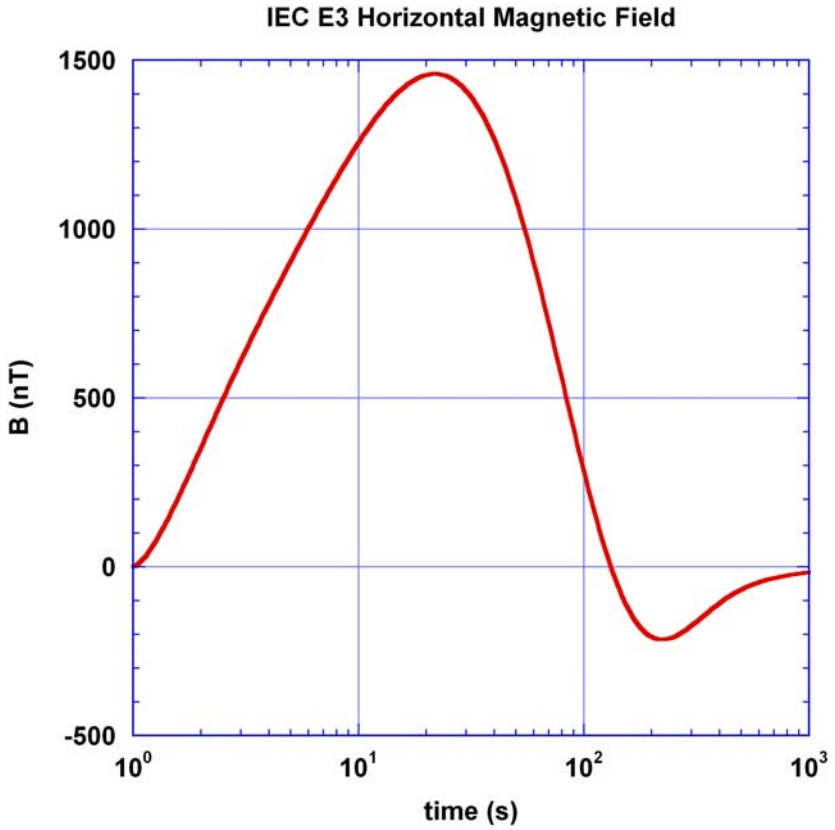

Figure 2-18. Magnetic field obtained from electric field.

2.2 Ground Models and Electric Field Calculation

The environment models discussed in Section 2.1 give the perturbed magnetic field at the surface of the ground assuming a perfectly conducting ground. In this section, we will discuss the technique used to calculate the horizontal electric field given that magnetic field. The conductivity of the first few hundred kilometers in depth of the earth depends strongly on the depth and the geographic location. For calculating the Geomagnetically Induced Current (GIC) arising from either natural phenomena or from E3 HEMP, it is necessary to account for the spatial variation. We start by examining how the stratification affects the horizontal electric field.

For a uniformly conducting ground of conductivity σ, assuming that there is no horizontal variation of the incident magnetic field, the horizontal electric field may be found by assuming that electric and magnetic fields vary as $\exp(j\omega t)$ and solving Maxwell's equations with only downward diffusion, neglecting the displacement current. The result, in MKS units, is

$$E(\omega) = \sqrt{\frac{j\omega}{\mu_0 \sigma}}\, B(\omega)$$

This equation can be Fourier transformed to the time domain to yield the result quoted in Section 2.1.

$$E(t) = \sqrt{\frac{1}{\pi \mu_0 \sigma}} \int_0^t \frac{dt'}{\sqrt{t-t'}} \frac{dB(t')}{dt'}$$

The frequency domain expression allows us to define the electric field response function, which we denote as R

$$R(\omega) = \frac{E(\omega)}{B(\omega)} = \sqrt{\frac{j\omega}{\mu_0 \sigma}}$$

(R is related to the surface impedance Z by $Z=\mu_0 R$.) When there is a purely vertical variation of the conductivity, the impedance has different behavior as a function of frequency. For a soil of two layers, with an upper layer of thickness d with a conductivity σ_u above a semi-infinite ground with conductivity σ_l, the surface impedance is given by

$$R(\omega) = \sqrt{\frac{j\omega}{\mu_0 \sigma_u}}\, \frac{\sqrt{\sigma_u} + \sqrt{\sigma_l}\, \tanh(d\sqrt{j\omega\mu_0\sigma_u})}{\sqrt{\sigma_l} + \sqrt{\sigma_u}\, \tanh(d\sqrt{j\omega\mu_0\sigma_u})}$$

as can be seen by solving Maxwell's equations for upward and downward diffusion within the upper region and downward diffusion only in the lower region, then matching the horizontal electric and magnetic fields at the boundary. The expression equates to the

uniform conductivity response with $\sigma=\sigma_u$ when, at high frequencies, $d\sqrt{j\omega\mu_0\sigma_u} >> 1$, and with $\sigma=\sigma_l$ when, at low frequencies, $d\sqrt{j\omega\mu_0\sigma_u} << 1$.

We will look at three cases. The first case has a 50 km thick upper layer with a conductivity of 10^{-3} S/m over a lower layer of 10^{-1} S/m and we will denote this as Low/High. The second case has a 5 km thick upper layer with a conductivity of 10^{-1} S/m over a lower layer of 10^{-3} S/m and we will denote this as High/Low. The third case has a uniform conductivity of 10^{-3} S/m and we will call this Low/Low. The results are shown in Figure 2-19.

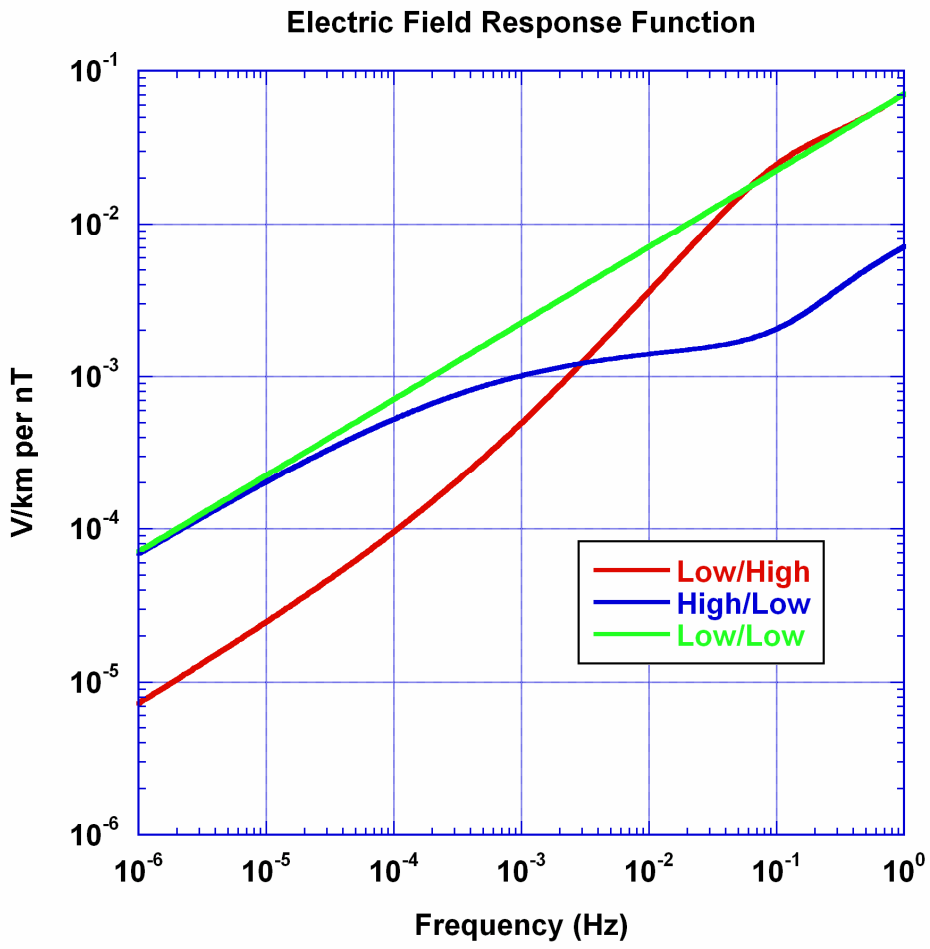

Figure 2-19. Magnitude of surface impedance for layered soils compared to uniformly conducting soil.

The response function for the uniformly conducting case (Low/Low) has a constant slope of ½ on the log-log plot, while the Low/High case response function shows a region with a slope of almost unity and the High/Low case response function shows a region where the slope is small. If we define the slope of the *E/B* curve in the log-log plot as γ, when γ

~1, characteristic of low conductivity layers over a high conductivity layer, we have inductive behavior and

$$E \sim K \frac{dB}{dt}$$

where K is an arbitrary constant. When γ~0, characteristic of high conductivity layers over low conductivity, we have resistive behavior and

$$E \sim KB$$

(The Kramers-Kroenig dispersion relation guarantees that the phase in the complex plane is correct for these limiting cases.) Since the deepest portions of the ground have high conductivity, at the lower frequencies encountered in geomagnetic storms, the ground will usually appear inductive.

Figure 2-20 shows the stratification of four soils (three of which are used in the CONUS power grid model, and one in Alaska) that cover the range of ground impedance that occur in the calculations that we will discuss. We have plotted the resistivity, which is the inverse of the conductivity. We can perform the same sort of analysis that was performed with the two-region soil within each of the layers of the stratified soil and the result is shown in Figure 2-21, which shows the electric field that results for a given E3 magnetic field as a function of frequency.

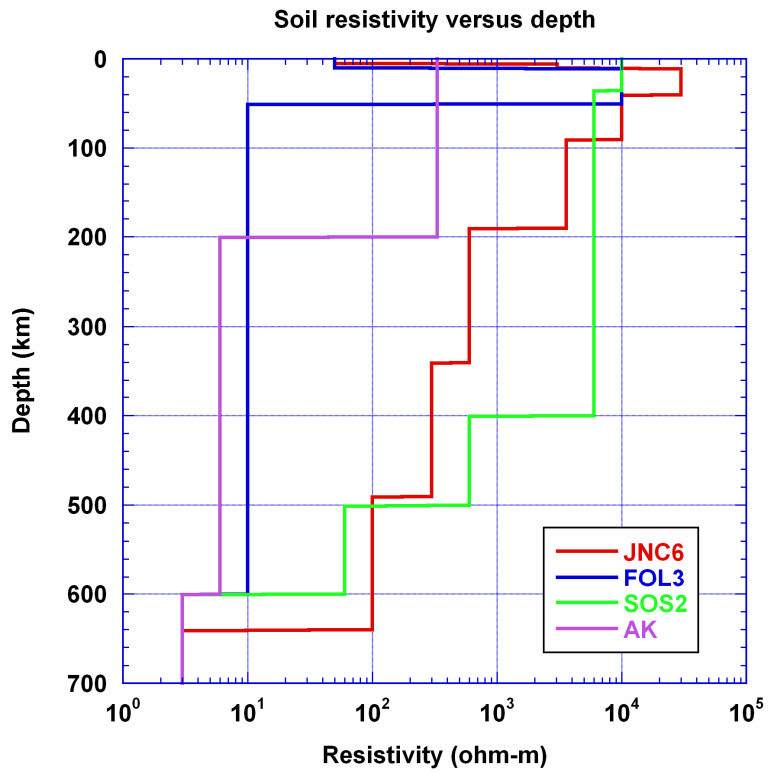

Figure 2-20. Soil resistivity as a function of depth for four ground models.

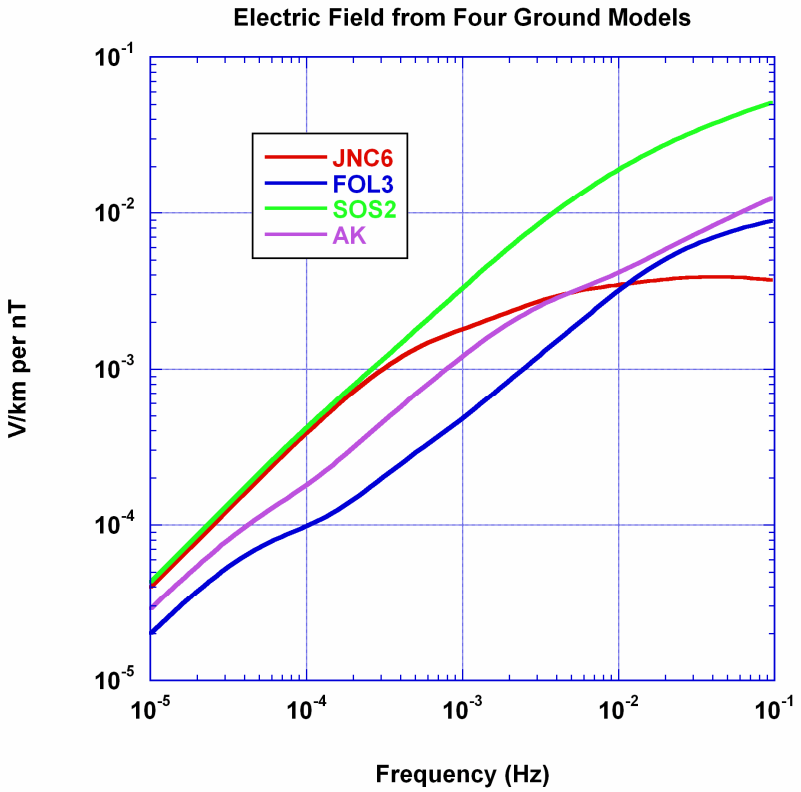

Figure 2-21. Resulting electric field as a function of frequency for four ground models.

At low frequencies all four models behave inductively, and are within a factor of a little over two. The greatest differences are seen near the surface where the difference is over a factor of twelve, and the JNC6 model is acting resistively, while the SOS2 model has just turned over from inductive behavior to look like a uniform conductivity with a slope of ½.

Four different techniques are used to develop the stratification of conductivity in ground models.

- Measurements of the conductivity vs. depth for the top 10s of km.
- Descriptions of the local geology, which can be used to infer an average conductivity vs. depth.
- Measurements of the deep conductivity for the region of interest (although continental data exists for most of the world).
- Measurements of geomagnetic and electric fields along with resultant geomagnetically-induced currents (GICs) at locations and frequencies of interest.

In general across the U.S., information is available in each category although the last technique is the most useful.

Figure 2-22 provides an overview map of the ground models selected for each color-coded region in the U.S. As shown, these models are applied in meso-scale dimensions throughout the U.S. The specific models were assigned based upon selecting a group of

ground conductivity models that were appropriate to the known geological profiles of the region. The geological profiles provided can narrow the search to several candidate ground models for various regions and further refinements to select the most appropriate ground model was done through a series of simulations where the best model was selected by validation against local observations through the use of monitored data from prior geomagnetic storms.

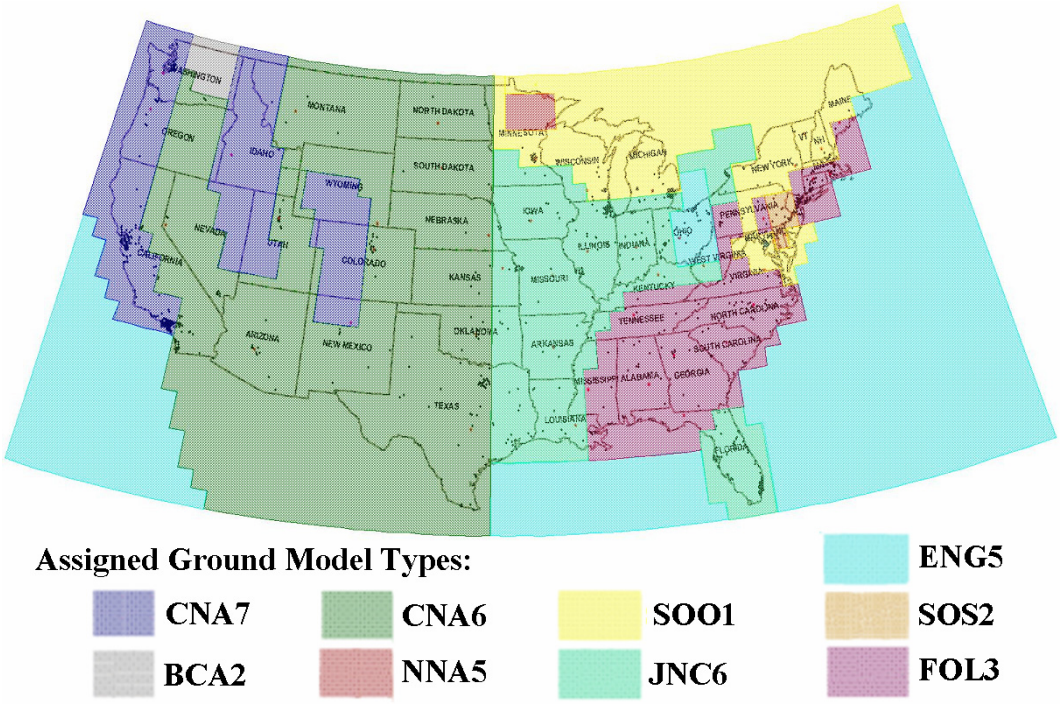

Figure 2-22. Multiple 1-D ground models for the U.S. grid.

As there has been no experience with late time HEMP over CONUS, we use geomagnetic field fluctuations to validate the ground modeling. Validation of the ground models against geomagnetic forensic data provides the best means to assure that appropriate responses are being observed and to provide assurance that correct responses will result when simulations of more severe disturbances are undertaken. Several examples are provided in this overview of model response versus actual observations.

Figure 2-23 provides an example of the validation of a ground model. This figure shows a comparison of the observed North-South and East-West geo-electric field during a minor geomagnetic storm on Nov 4, 1993 in northern Minnesota (from Kappenman, Zanetti, Radasky, *EOS Transactions of AGU*, Jan. 28, 1997, pg 37-45). Also provided are the results of the simulation, which indicate good agreement in magnitudes as well as wave shape. These observations and simulations were conducted using a 1-second data cadence. The ability to replicate over a broad frequency range provides for good overall fit between observed and simulated electric fields. This example illustrates the ability to validate the ground model separately.

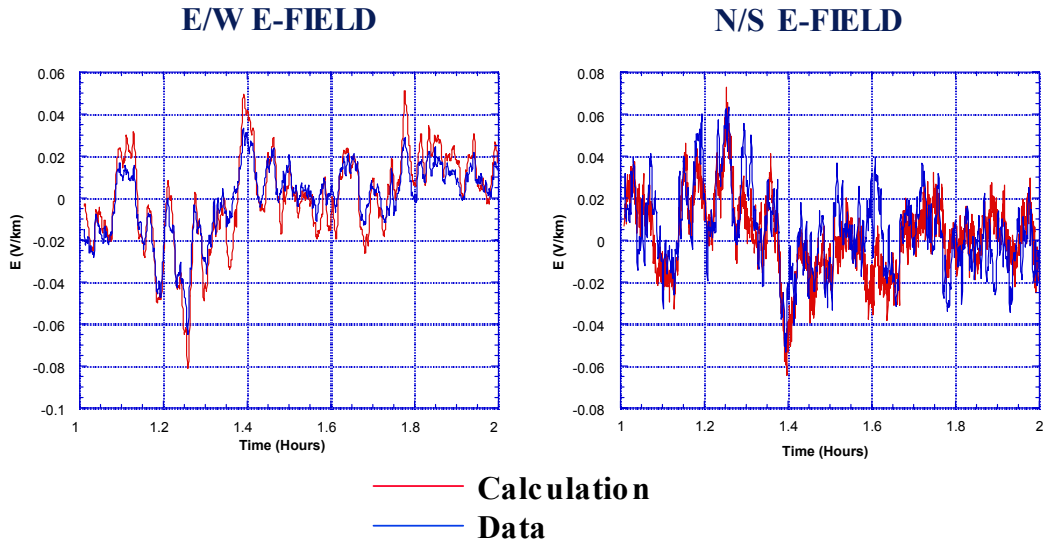

Figure 2-23. Comparison of calculated and measured electric fields for 4 Nov 1993.

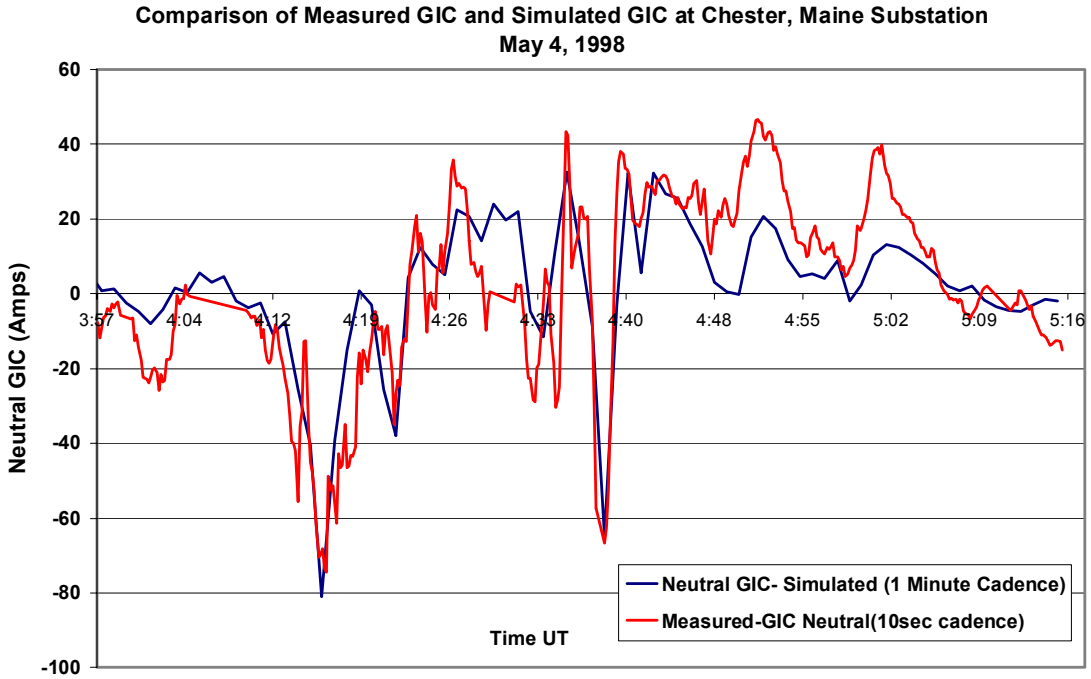

Figure 2-24. Comparison of measured and calculated GIC at Chester Maine.

It is also possible to demonstrate the validation using measurements of GIC with the combined ground model and power grid model. An example of this is provided in Figure 2-24 for GIC measurements made in northern Maine during a storm on May 4, 1998. In

this case, the measured data was observed at a 10 second cadence, while the calculation was limited to a one-minute cadence due to availability of regional geomagnetic field disturbance data. This will also limit the frequency response of the simulation and reduce some of the ability to replicate minor high frequency variations. In spite of the data limitation for simulations, the close agreement between observed GIC and calculated GIC indicates that both the ground model and the power grid model are accurately replicating the storm impacts.

The 1-D planar model is sufficient for most applications, but one situation where two-dimensional effects can be important is at the edge of the ocean, where the high conductivity of the seawater acts to short out the E3 electric field, and this can lead to substantial enhancement of the horizontal electric field perpendicular to the ocean boundary. This is most easily seen by considering the horizontal current flow - in the ocean the current flows within a skin depth of the surface. In the land, the current flows within the larger skin depth associated with the soil conductivity. There will be a transition region where the current spreads outward and downward from the ocean skin depth to the land skin depth, and in this region the electric field will be enhanced.

A detailed analysis of this effect shows that the integral of the electric field along a line running perpendicular to the interface has the same time history as the E3 magnetic field, instead of having the same time history as the horizontal electric field at the surface of the ground away from the interface. This can be visualized as an additional applied voltage of

$$\Delta V(t) = \frac{\Delta B(t)}{2\mu_0 \sigma(t)}$$

where $\Delta B(t)$ is the perturbed magnetic field, $\sigma(t)$ is the ground conductivity averaged to a skin depth and μ_0 is the magnetic permeability of free space. This is an additional voltage driver on lines running to locations near the sea. This has been taken into account in calculations of voltages on conductors powering fiber optic seafloor communications cables, and can be of importance to specific locations in the power grid, for example at nuclear power stations using sea water for cooling. It is not of importance in calculating the overall flow on the high voltage portion of the grid where the length of individual lines is long compared to the electromagnetic skin depth in the ground.

2.3 U.S. Electric Power Grid Circuit Model

As one of the four component models that are necessary to calculate GIC flows and the impacts on power system reliability due to GIC flows, the power grid model is important for two reasons in determining the simulation results. This portion of the model in particular defines the complex topology of the network circuit, as this topology couples with the equally complex electric field environment that occurs from E3 HEMP processes. The other important aspect of the power grid circuit model is contained in the resistive impedance of the network circuit elements (primarily the transmission lines,

transformers, and substation-to-ground resistance). The values of these circuit resistances combined with the resultant geo-electric fields across the network define the pattern and magnitude of E3 HEMP GIC flows.

Because of the mature nature of this data and the many years of power industry experience in modeling AC flows in the network, it is expected that this portion of the U.S. power grid model will be less uncertain that other portions of the overall model. The U.S. power grid model was assembled by using publicly available load flow model data and available transmission asset maps to define approximate locations. In order to calculate the flow of GIC, the model needs to define not only the impedance of all circuit elements, but also their locations. The definition of locations allows for proper determination of coupling with the complex 2D electric field patterns that will occur due to various threat conditions that are to be examined. In the estimation of substation position accuracy, in most cases, the position is accurate to within +/- 1 mile. This accuracy will be sufficient given the large-scale nature of the overall U.S. simulation model that is being developed. Due to the expedited nature of the investigation, the model for the CONUS region of the U.S. was limited to transmission network portions that are 345kV or higher in voltage. As will be shown in subsequent analysis, the majority of all GIC flows will occur in the highest voltage portions of the network, hence this limitation provides most of the GIC flows and resulting impacts from those flows.

Figure 2-25 provides a map of the overall transmission network included in the CONUS region model of the U.S. grid. The major transmission voltages are color highlighted by operating voltage with the three operating voltages of 345kV, 500kV and 765kV (there are also several lines in the Washington state region that are operated at 300kV which are included in the model). Figure 2-26 provides the mileage statistics for each of these three voltage classes that are represented in the U.S. model for the CONUS region. As shown, the most common transmission voltage is the 345kV that makes up about 64% of total transmission line miles. The highest operating voltage is the 765kV and is primarily located in the Illinois, Ohio, Indiana, West Virginia and upstate New York regions of the U.S. Both the 345kV and 500kV portions of the network are more widely distributed across the U.S.

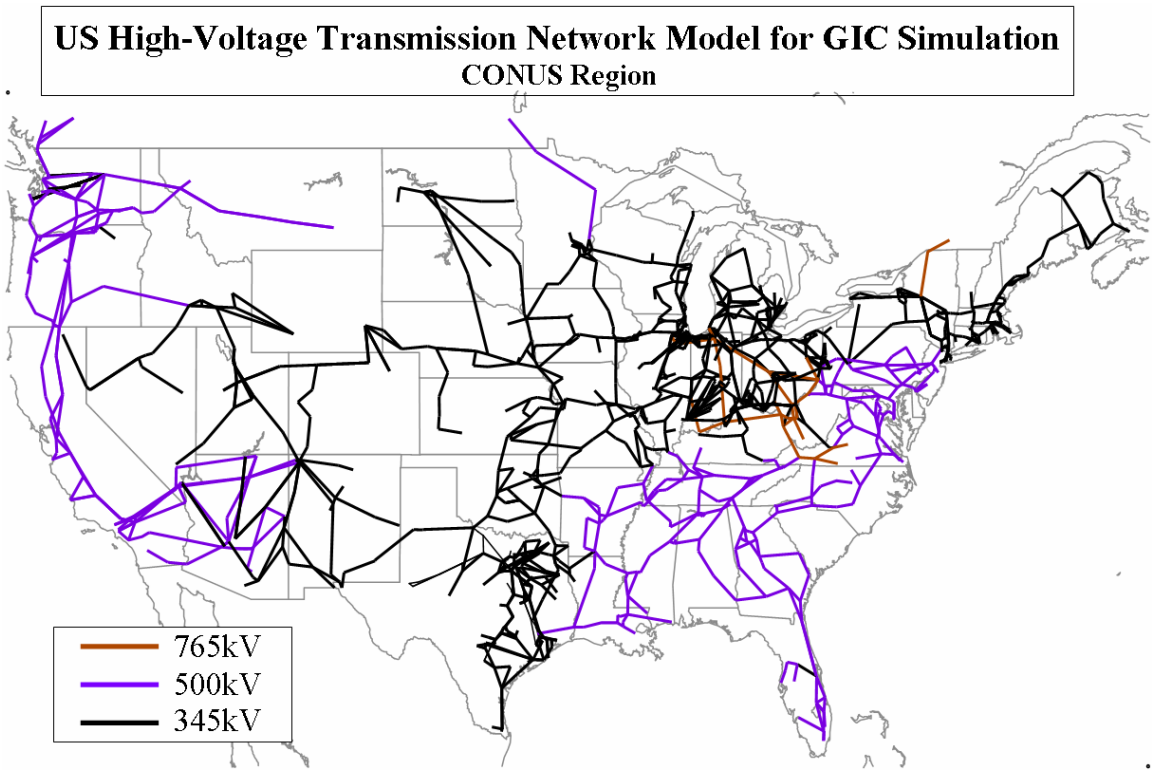

Figure 2-25. Map of 345kV, 500kV and 765kV substations and transmission network in U.S. grid model.

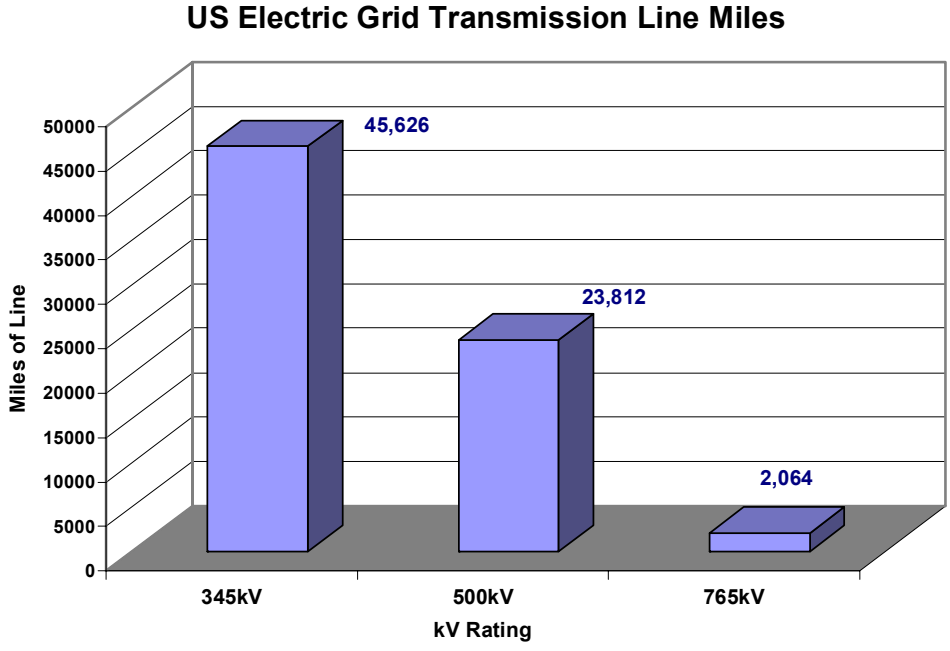

Figure 2-26. Miles of 345kV, 500kV and 765kV transmission lines in U.S. grid model.

A total of 2146 high-voltage transformers will be modeled in the CONUS region for the U.S. power grid model. The population of transformers by kV rating is shown in Figure 2-27. The population of transformers by kV rating generally follows the population of transmission line miles as previously shown. The simulation model will be able to calculate and estimate the flow of GIC in each of these transformers and provide estimates of the degree of half-cycle saturation and system impacts this saturation could cause to the operation of the U.S. power grid.

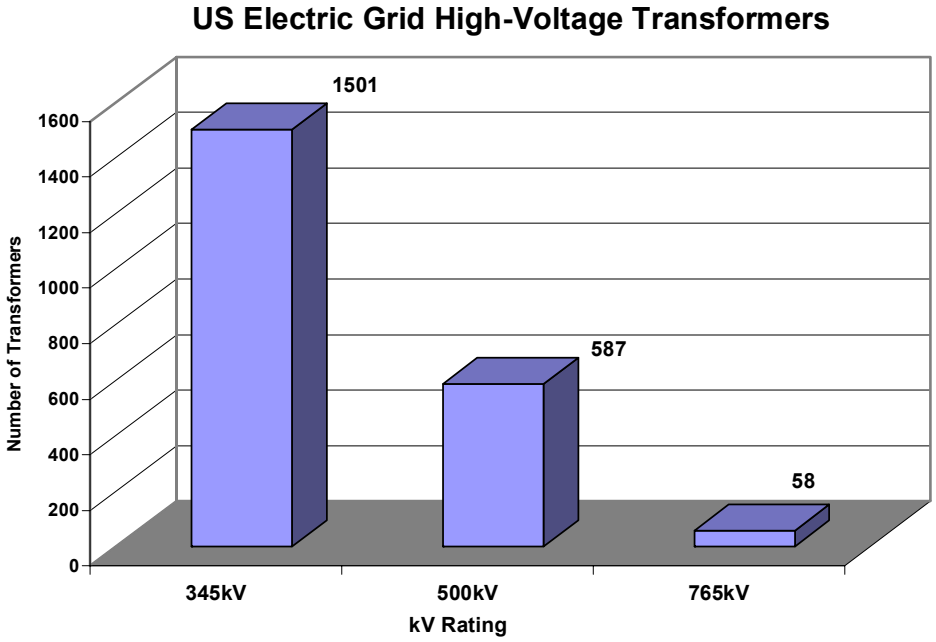

Figure 2-27. Number of 345kV, 500kV, and 765kV transformers in U.S. grid model.

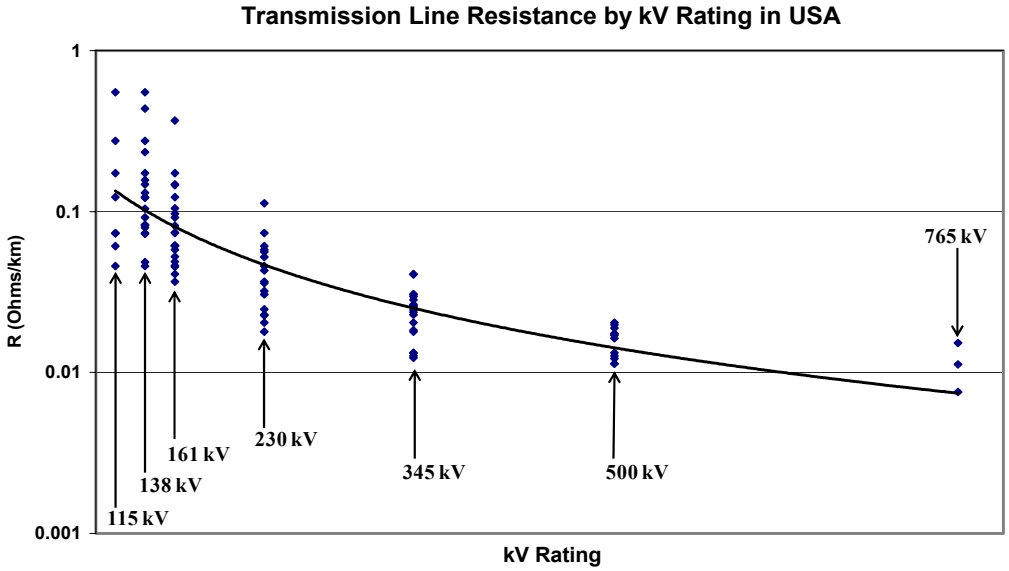

Figure 2-28. Range of transmission line resistance for the major kV-rating classes for transmission lines in the U.S. electric power grid infrastructure population. Also shown is a trend line of resistance weighted to population averages. The lower R for the higher voltage lines will also cause proportionately larger GIC flows in this portion of the power grid. (Derived from data in EHV Transmission Line Reference Book and from U.S. Dept of Energy-Energy Information Agency and FERC Form 1 Database.)

The operating voltage of the transmission network is an important factor in determining the level of E3 HEMP GIC flow that will occur on each part of the U.S. power grid. At the higher operating voltages, there is a pronounced trend that both the average circuit resistance decreases, but also the average length of each line increases. Both of these trends will result in larger GIC flows in the higher voltage portions of the network given the same geo-electric field conditions. To better illustrate the impact of kV rating and associated design factors that affect circuit resistance, a statistical analysis was performed on the network data that was available. This analysis also reviewed some of the lower voltage transmission elements as well. For example, when looking at the resistance per mile of transmission lines in the U.S., the resistance generally declines as larger and lower resistance conductors are generally used for the higher kV rates facilities. Figure 2-28 provides a summary of the average line resistance in the U.S. versus the kV rating of the transmission line. This summary extends from the 115kV to the 765kV transmission voltages. As shown in this figure, the per mile resistance decreases on average by approximately a factor of 10 as one progresses from the 115kV line to the 765kV line. It is also generally seen that, for operating voltages of 345kV and above, the resistances are generally very small (less than 0.1 ohms per mile). There is some diversity in the overall population due to variation in conductors that are used on specific transmission lines. The actual line resistance was used from the system model data that was available, reflecting actual conditions for each specific facility in the overall model.

Transformers also exhibit a general relationship of lower resistance as kV rating increases. However, the trend in transformer design is even more pronounced as a function of MVA or current rating of the transformer. It is generally consistent that the higher the MVA rating transformers are also the highest kV rated transformers, though there can be a few exceptions. Figure 2-29 provides a plot of the transformer winding resistance versus the kVA rating of the transformers in the U.S. population. The blue scatter plot points illustrate specific transformers from the data available, while the red line shows the general best-estimate trend of this data. As illustrated, there is also more than a factor of 10 reduction in transformer winding resistance as the current rating or MVA size of transformers increase. Since these very large transformers generally tend to be located on the higher kV rated portions of the network, this will again result in significantly larger GIC flows in these portions of the network given the same geo-electric field exposures. In the available transformer data, nearly 29% of all transformers modeled did not have available winding resistance data. Therefore in order to fill this missing data, estimated data was used that conformed with the trend line of the population statistics shown.

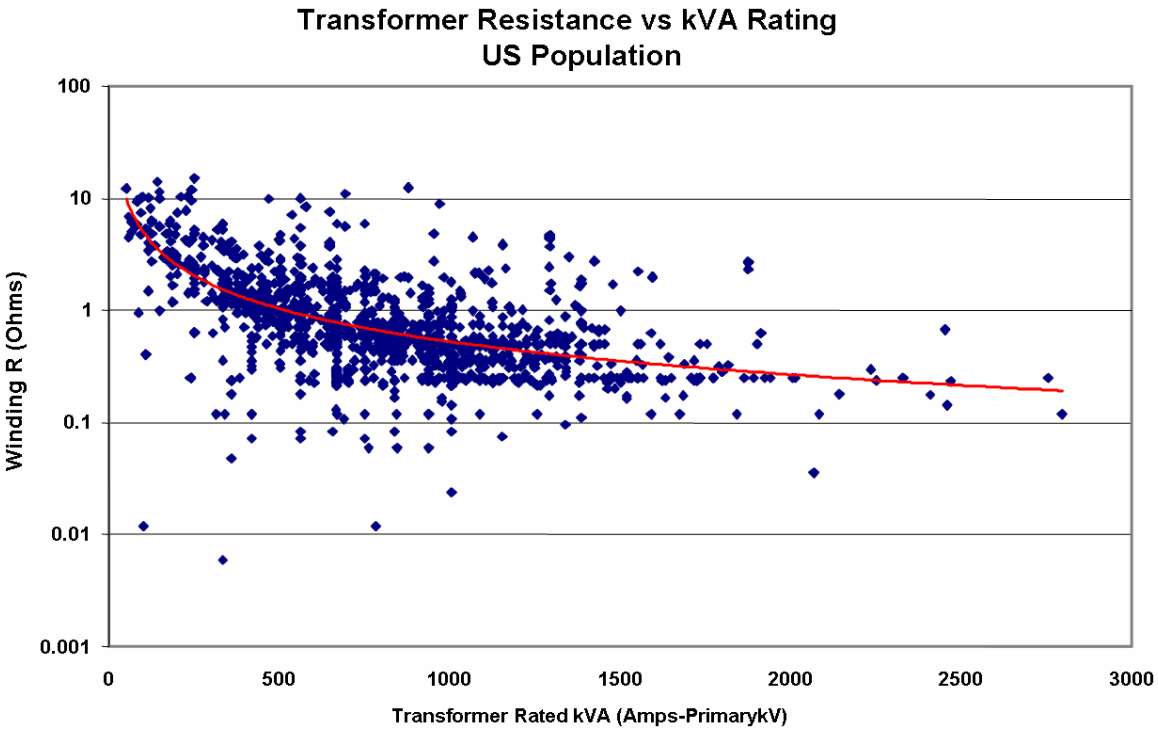

Figure 2-29. Decrease in transformer DC resistance versus kVA rating for transformers in U.S. grid model.

In addition to the lower resistances at the higher kV rating lines on the network, average length of these lines also introduces a higher overall risk of GIC flows as well. Figure 2-30 provides a summary of average transmission line lengths in the U.S. by kV rating. As illustrated, the average length of transmission line also increases significantly with increased kV ratings. The 765kV lines average over 60 miles in length while the 115kV lines are less than 15 miles in average length. While GIC flows need to take into consideration the network topology as a integrated whole, it is evident that on an individual line basis a combination of longer average length (and increased geo-electric potential between end points of the line) combined with lower average resistances will produce substantially larger GICs on average in the higher voltage portions of the power grid, all other risk factors being equal.

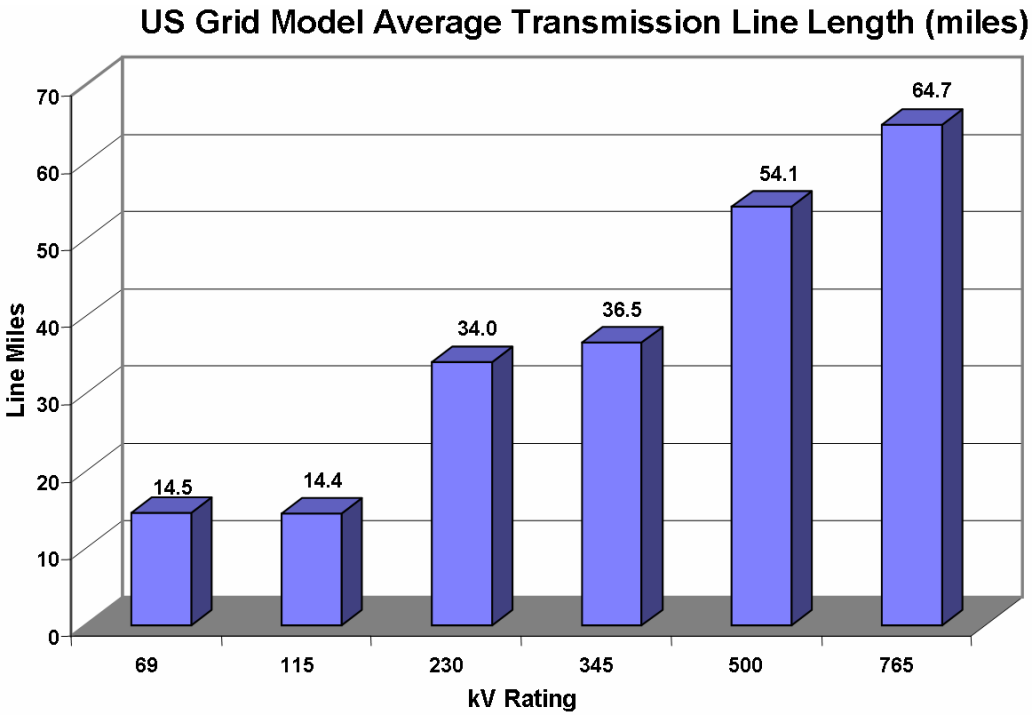

Figure 2-30. Average length of transmission lines in U.S. by kV-rating.

The application of series capacitors on transmission lines will block the flow of GIC. In the entire Eastern U.S. grid only two lines have series capacitors, however in the Western grid a significant number of the lines are series compensated. Figure 2-31 shows the extensive application of series capacitors on the transmission lines in the U.S. portion of the WECC pool. As shown in the chart in Figure 2-32, there are nearly equal total miles of 500kV and 345kV transmission in the WECC pool. Of the 500kV transmission, approximately 55% of these lines have series capacitors, while for the 345kV only ~25% of these lines are series compensated.

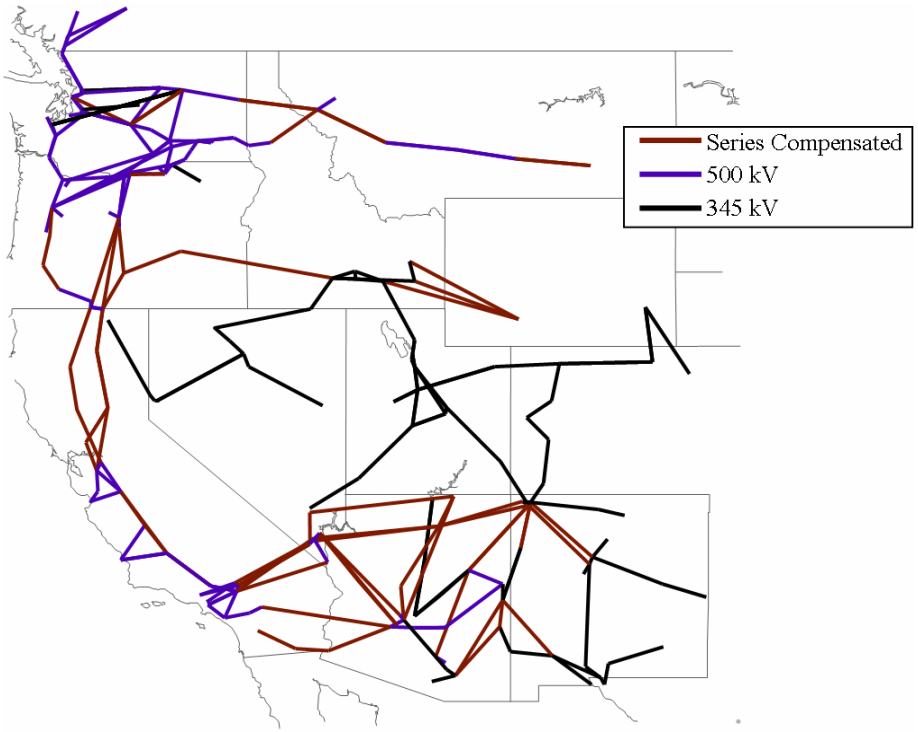

Figure 2-31. WECC 345kV and 500kV transmission lines that are uncompensated and series compensated.

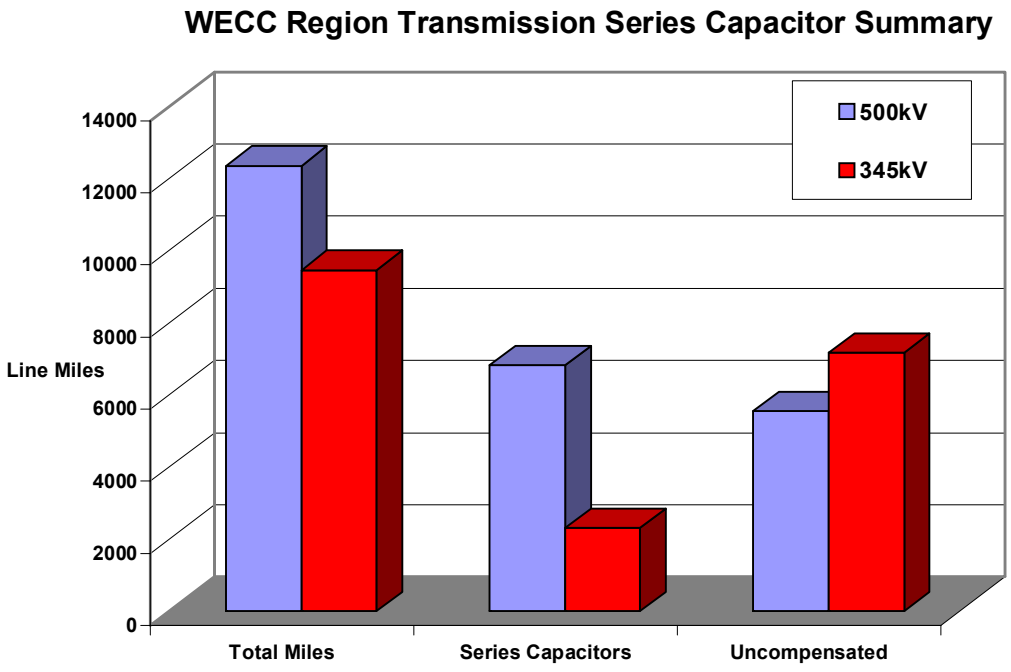

Figure 2-32. Miles of 345kV and 500kV series compensated and uncompensated transmission lines in WECC.

2.4 Transformer and AC Power Grid Performance Model

The flow of the E3 HEMP Geomagnetically Induced Current (GIC) in transformers is the root cause of all power system problems as the GIC causes half-cycle saturation to occur in the exposed transformers. While the extremes of the threat environment, the conductivity of the deep-earth ground and the kV rating and topology of the power grid can cause significant enhancements of the total GIC flows, the most significant enhancement of impacts due to GIC is how that GIC interacts within the transformer. Only a few Amps of GIC can result in an amplification of impacts in the operation of AC current flows in the transformer. In some cases the amplification effect can cause normal AC excitation current in a transformer to increase from less than 1 Ampere to nearly 300 Amperes, due to the flow of only 25 Amps/phase of GIC.

Transformer design is an important consideration, in particular single-phase core design transformers are much more responsive to influence from GIC than most standard 3 phase designs. Also, the higher the kV rating of the transformer, the higher the total reactive power increase that will occur due to GIC. Figure 2-33 provides a comparison plot of the reactive demand increase that occurs in both a single-phase and three-phase 500 kV transformer for various levels of GIC per phase. As shown, the simple difference between three-phase design and single-phase design causes a factor of four increase in total reactive power demand over the range of GIC flow levels.

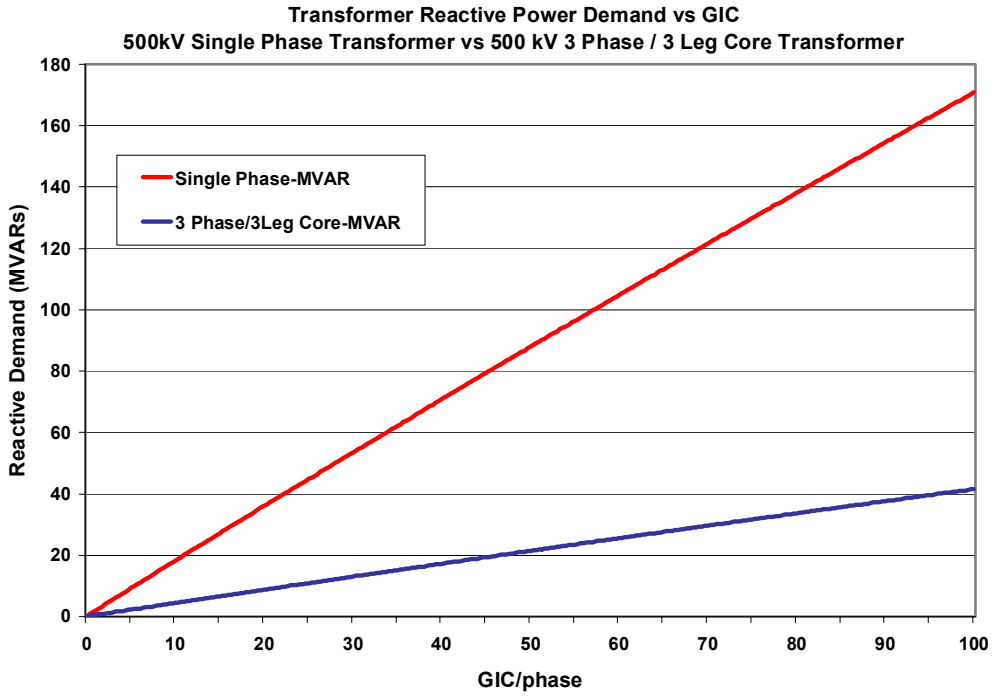

Figure 2-33. Transformer MVAR increase versus GIC for 500kV single phase and 3 phase, 3 legged core form.

A similar increase in the impacts of GIC flows on transformer reactive power demands occurs for increases in transformer kV rating. Figure 2-34 provides a comparison for a single-phase 345kV, 500kV and 765kV transformer. As shown in this comparison, for the same level of GIC flow, the 765kV transformer will have nearly two times higher reactive power demands than the 345kV transformer. A similar ratio of reactive power demand versus kV rating would also occur for three-phase transformers, though total reactive power levels will be smaller than those in comparable single-phase design transformers.

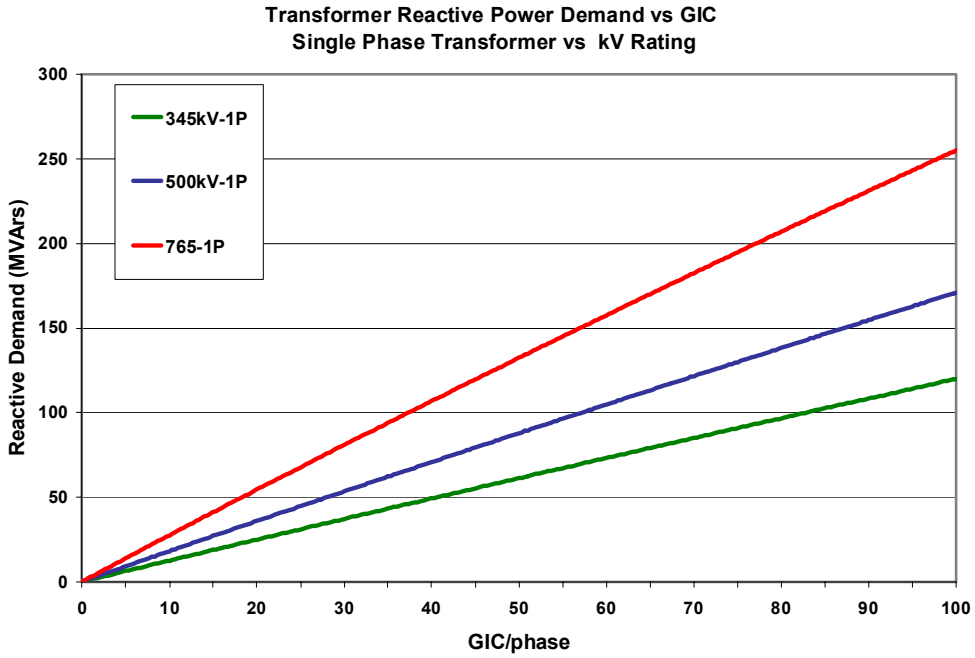

Figure 2-34. Transformer MVAR increase versus GIC for 345kV, 500kV and 765kV transformers.

As evident from these behavior characteristics, transformer design factors can be an important determinant in system behavior. While transformer kV rating is fully defined for all transformers included in the U.S. power grid model, there is some uncertainty about the context of the ratio of single phase and three-phase transformers in the overall transformer population. Because the design of transformers were not readily available in all cases, estimates of single-phase/three-phase populations were therefore based upon MVA rating, in that transformers of 600MVA or larger in size were assumed to be single-phase design. Based upon these estimates, it is estimated that 85% of the 345kV transformers will be three-phase (Figure 2-35). For the 500kV population, only 34% of these transformers are three-phase (Figure 2-36) while the bulk of the population is the more susceptible single-phase design. At the 765kV level, nearly all of these transformers are expected to be of single-phase design (Figure 2-37).

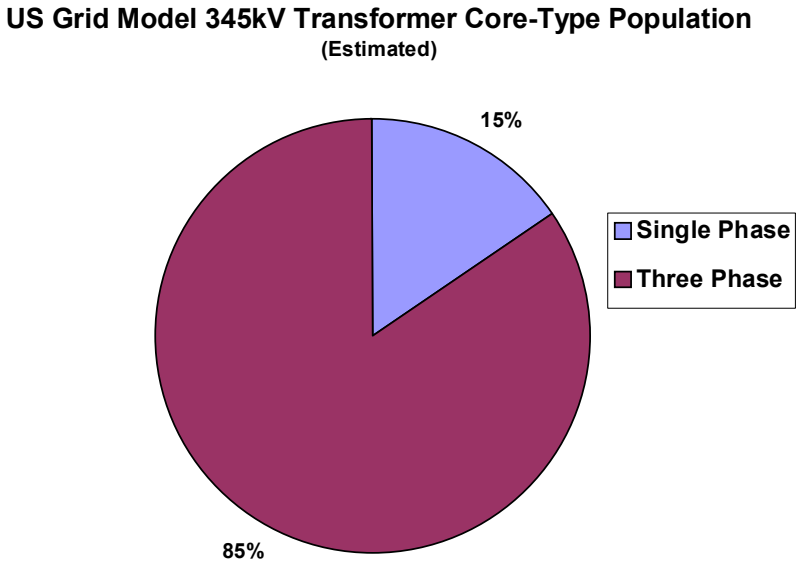

Figure 2-35. Demographic estimates of 345kV transformers – single phase vs. 3 phase.

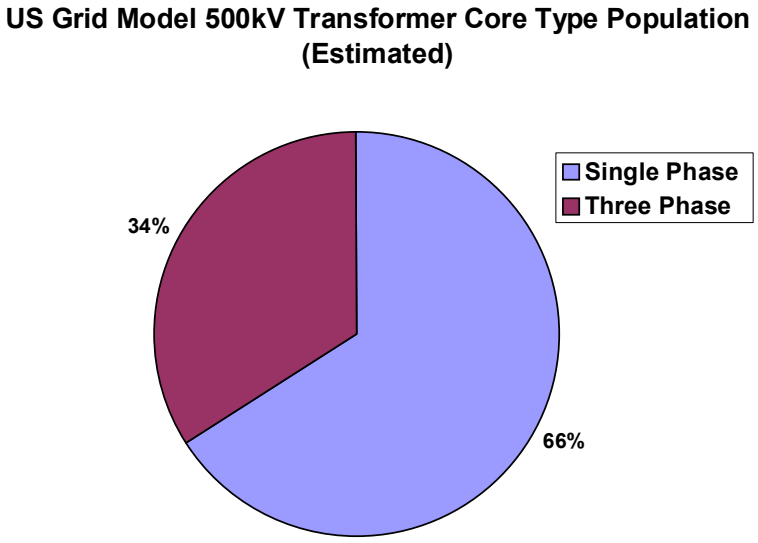

Figure 2-36. Demographic estimates of 500kV transformers – single phase vs. 3 phase.

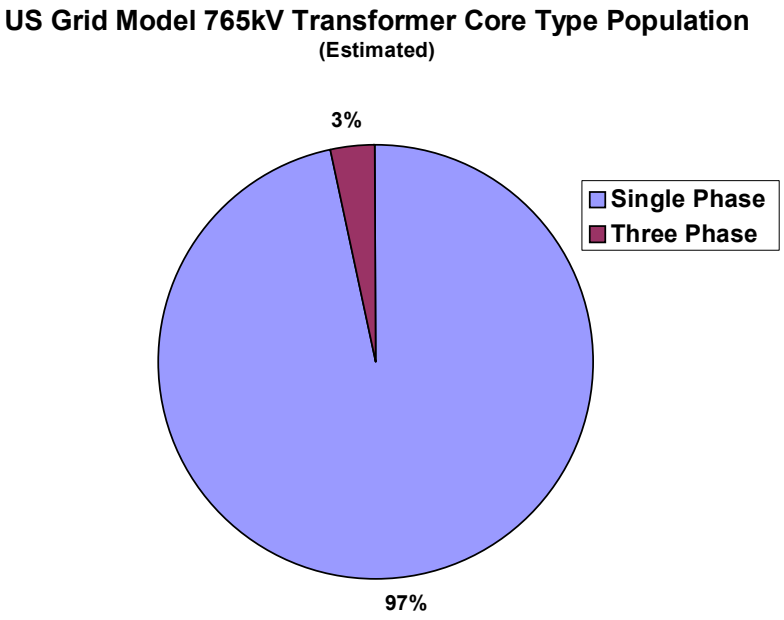

Figure 2-37. Demographic estimates of 765kV transformers – single phase vs. 3 phase.

Using this method of allocating transformer design is a possible source of uncertainty and the desire for this analysis is to not produce overly pessimistic results, which might occur if population estimates of single-phase transformer design in the U.S. grid are over-estimated. In order to test the assumptions applied to the U.S. grid as a whole regarding the transformer design population, a comparison was made with available transformer data from the BPA power grid in the Pacific Northwest region. The BPA system is predominantly a 500kV and 230kV transmission system, and also a small number of 345kV facilities. BPA has ~6% of the U.S. ownership of all 500kV transformers included in the power grid model. The population statistics on single-phase and three-phase design for their 500kV transformers are shown in Figure 2-38. The transformer nameplate data confirms that the population is indeed heavily single-phase design, with 97% of all 500kV transformers in this region being single-phase units. This population ratio is actually much higher than the U.S. 500kV population as a whole estimate, which is modeled as being only 66% single-phase design. BPA also has a large population of 230kV transformers, therefore population ratios of these transformers can be a somewhat relevant comparison for the estimated populations for the 345kV transformers estimated for the U.S. model. As shown in Figure 2-39, the ratio of single-phase design in the BPA 230kv transformers is 25%; this is also a higher ratio of single-phase units than assumed for the entire U.S. 345kV population, which is estimated to be only 15%. This comparison suggests that the 345kV population of single-phase design transformers may actually be larger than currently represented in the U.S. model.

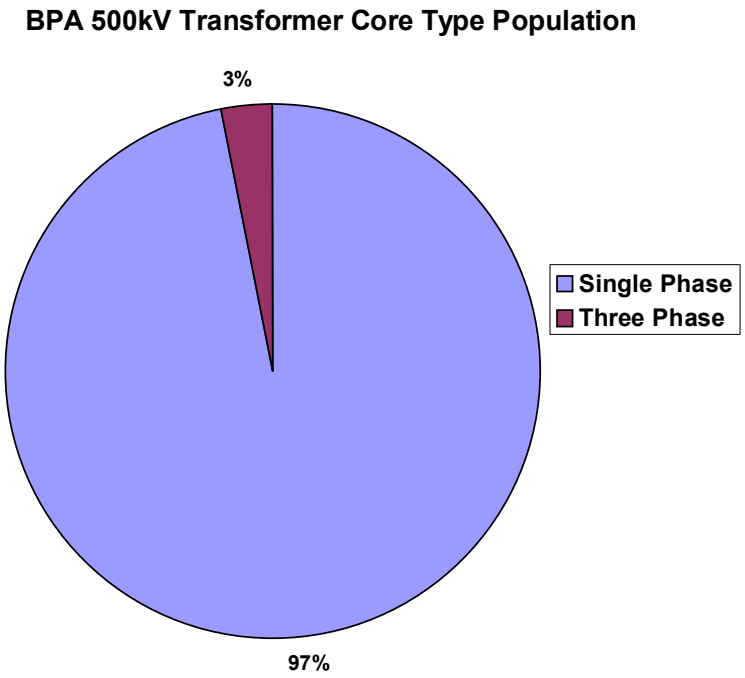

Figure 2-38. BPA 500kV transformer demographics – single phase vs. 3 phase.

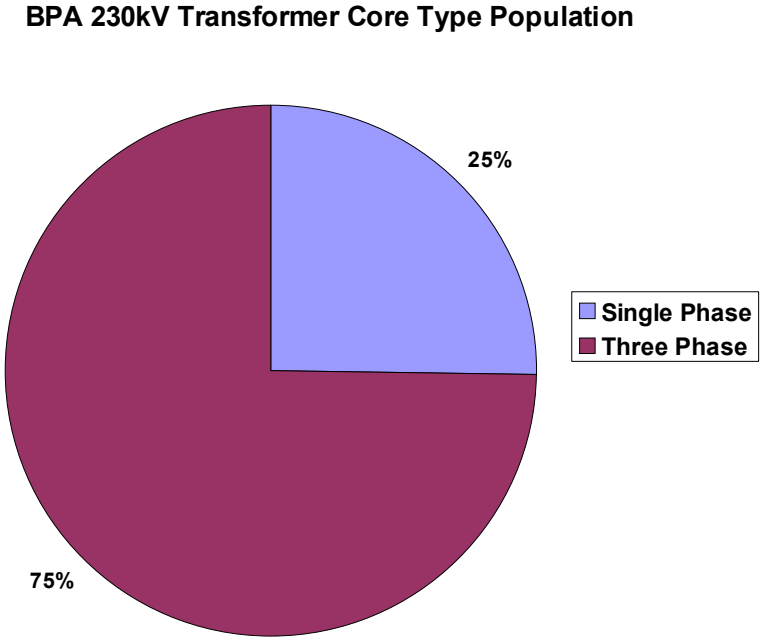

Figure 2-39. BPA 230kV transformer demographics – single phase vs. 3 phase.

Publicly available data from the ECAR pool was also used to confirm the very high population of 765kv single-phase design transformers. The ECAR power pool contains nearly all the 765kV transformers in the U.S., with the exception of a handful of 765kV transformers operating in upstate New York. These verifications provide a level of confidence that simulation results, which are in part based upon population estimates of transformer design, will generally not be overly pessimistic and may in actuality be somewhat optimistic for this expedited review.

Transformers under half-cycle saturation pose a dual threat to system reliability: system-wide voltage collapse by increase in reactive power in each exposed transformer and the disruptive effects of harmonics and AC waveform distortion on relay and protective systems. Accurate estimates of both reactive power demand and AC waveform distortions are therefore necessary in models of transformer behavior. Figures 2-33 and 2-34 (previously discussed) provided an overview of reactive power demand behavior of transformers. The AC waveform distortions are more difficult to estimate and need to be considered on a case-by-case basis. Some general examples can be provided to illustrate the nature of impacts that can occur on a wide-scale during disturbance threats. Figure 2-40 provides a plot of the normal AC excitation current that would be observed in the high-side of a 500kV transformer, while figures 2-41, 2-42, and 2-43 show the significant increases and distortion of transformer excitation current for 5 Amps/phase of GIC (Figure 2-41) and also for 25 Amp (Figure 2-42) and 100 Amp GIC events (Figure 2-43). These examples illustrate that AC peak excitation currents drawn from the power system by a transformer under various levels of GIC excitation can increase from less than 1 Amp to over 800 Amps. These increased transformer excitation currents are highly distorted and rich in both even and odd harmonics and they combine with the normal load current on the transformer and propagate distortions throughout the power grid. To illustrate the potential impact of these distortions, the primary current (including load of 300 Amps under normal conditions) can be synthesized during several severe GIC exposures. Figure 2-44 shows the normal AC load current for a 500kV transformer (blue waveform) and the resulting AC currents under three different GIC conditions. It is evident that not only are large distortions occurring, but also a significant peak of over-current will result. Total waveform distortions of over 200% are expected to occur; also these simulations do not take into account additional waveform distortions that could occur due to simultaneous saturation of adjacent transformers and local resonances, which could increase distortions further.

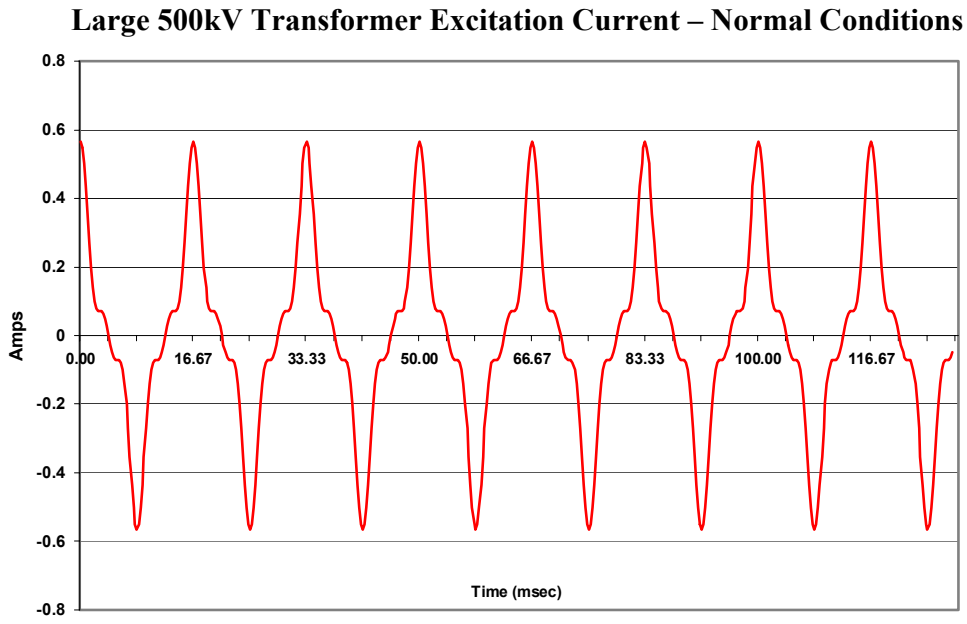

Figure 2-40. Normal excitation current in 500kV transformer.

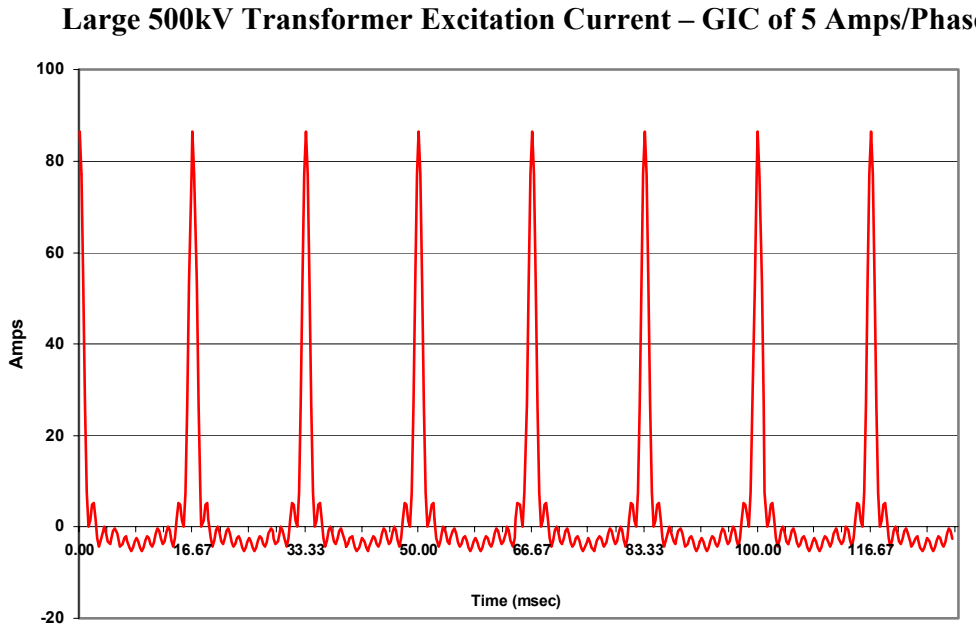

Figure 2-41. Distorted excitation Current with 5 Amps/phase of GIC.

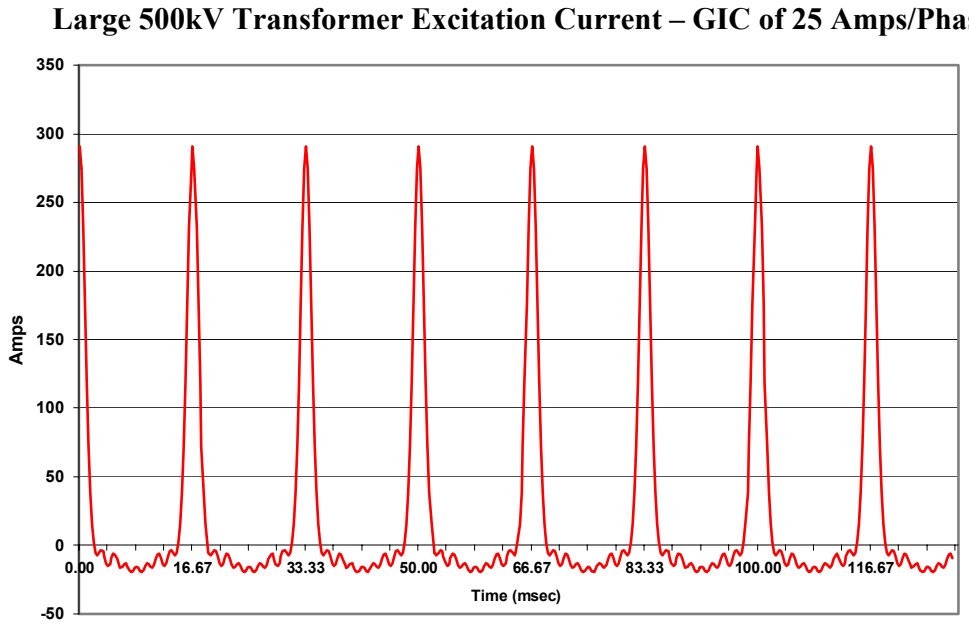

Figure 2-42. Distorted excitation current with 25 Amps/phase of GIC.

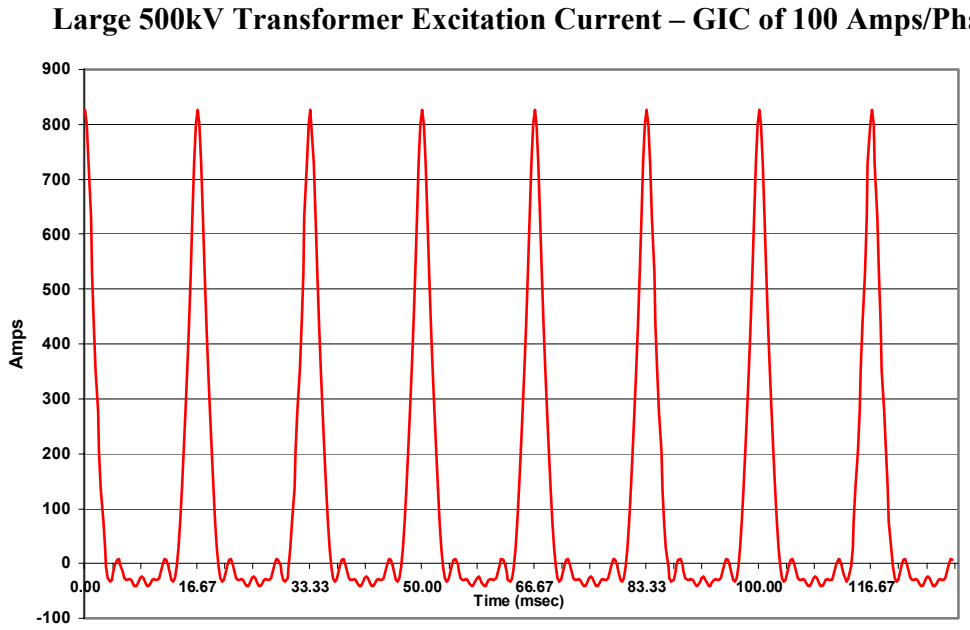

Figure 2-43. Distorted excitation current with 100 Amps/phase of GIC.

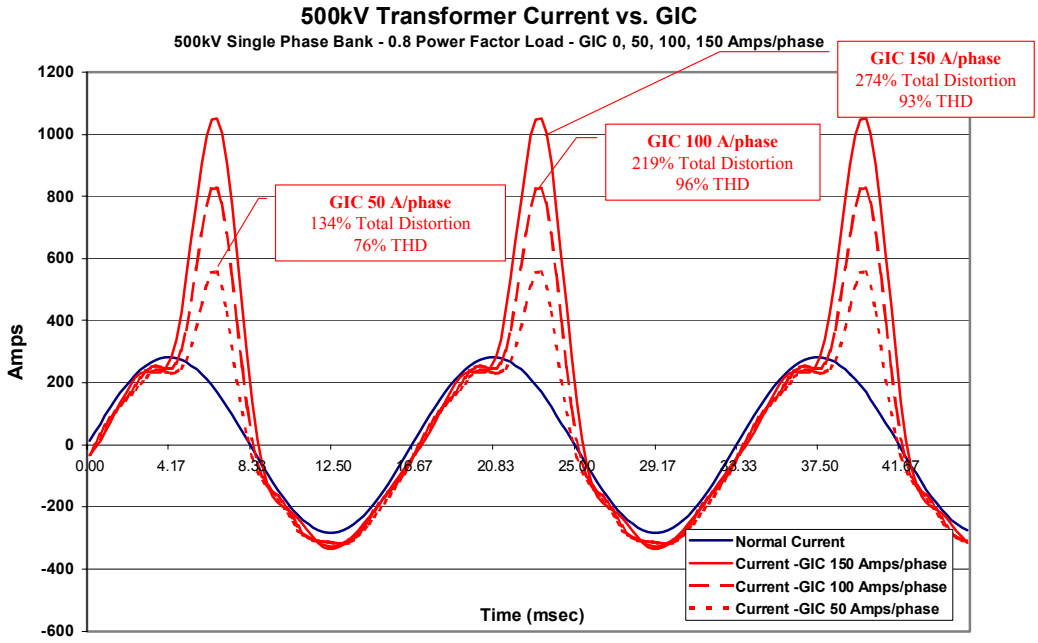

Figure 2-44. Transformer total load current – normal conditions and with 50, 100 and 150 Amps/phase of GIC.

2.5 The Evolving Vulnerability of Electric Power Grids

A simple way to summarize much of the discussion in this overview of the power grid model is that today's sprawling, high-voltage power grids are more susceptible to GICs, whether arising from E3 HEMP or space weather impacts, than ever before. While almost all research into space weather impacts on technology systems has focused upon the dynamics of the space environment, the role of the design and operation of the technology system in introducing or enhancing vulnerabilities to space weather is often overlooked. In the case of electric power grids, both the manner in which systems are operated and the accumulated design decisions engineered into present-day networks around the world have tended to significantly increase GIC impacts. The result is to increase the vulnerability of this critical infrastructure to space weather disturbances.

The space weather community, which has historically been interested in effects on power systems, and the power industry have not fully understood these operation and design implications. The application of detailed simulation models has provided tools for forensic analysis of recent storm activity and, when adequately validated, can be readily applied to examine impacts due to historically large storms, as will be described in subsequent sections of this report. However, even simple empirical extrapolations provide some perspective on the level of threat and the possible consequences of storms on present day infrastructures.

Historic records of geomagnetic disturbance conditions and, more importantly, geo-electric field measurements, provide a perspective on the level of driving forces that can produce large GIC flows in power grids. Because horizontal electric fields and resulting GIC are caused by the rate of change of the geomagnetic field, whether driven by E3 HEMP or by space weather effects, one of the most meaningful methods to measure the severity of impulsive geomagnetic field disturbances is by the magnitude of the geomagnetic field change per minute, measured in nanoteslas per minute (nT/min). For example, the regional disturbance intensity that triggered the Hydro Quebec collapse during the 13 March 1989 storm only reached an intensity of ~480 nT/min. Large numbers of power system impacts in the United States were also observed for intensities that ranged from 300 to 600 nT/min during this storm. However, the most severe rate of change in the geomagnetic field observed during this storm reached a level of ~2000 nT/min over the lower Baltic. The last such disturbance with an intensity of ~2000 nT/min over North America was observed during a storm on 4 August 1972, when the power grid infrastructure was less than half its current size.

An analysis of the AT&T telecom cable (L4) failure in northern Illinois showed that a region of ~800 nT/min disturbance intensity caused a geo-electric field of at least 7 V/km. A dB/dt disturbance of >2000 nT/min was observed over central and southern Sweden on 13-14 July 1982. A coincident peak geo-electric field of 9.1 V/km was observed in central Sweden during this storm, on railroad communication circuits. Similar observations from that region of 20 V/km occurred for a storm in May 1921, suggest that a peak rate of change of ~5000 nT/min is possible. This disturbance level is nearly 10 times larger than the levels that precipitated the North American power system impacts of 13 March 1989. While the magnetospheric drivers and deep-Earth conductivities that shape the geo-electric field response have not changed significantly over this period of time, power system infrastructures have experienced dramatic changes in size and complexity. E3 HEMP, which drives much larger values of dB/dt, could have disastrous effects on the power grid, as we will show in Sections 3 and 4.

For any natural or man-made hazard, prudence requires that design and operational adjustments be made to mitigate such risks to infrastructures. Power system designers and operators expect these systems to be challenged by the elements, and where those challenges were fully understood in the past, the system design has worked extraordinarily well. Most of these challenges have been terrestrial weather related. In cases of understood threats, system designers usually applied design and operational standards to harden or mitigate the consequences of these environments on the reliability of the power system. Indeed, investments in arresters and transmission line shield wires to mitigate against lightning alone can be measured in the several billion-dollar range. This has generally confined problems and usually limited the spread of outages that do occur to small regions at any one time. In contrast, the awareness of the geomagnetic storm and E3 HEMP environments and their potential impacts are much less understood and have aspects that are inherently more threatening than more familiar hazards such as earthquakes and extreme terrestrial weather events (including hurricanes). Geomagnetic storm and E3 HEMP environments can develop almost instantaneously over large geographic footprints, which have the ability to essentially blanket the continent with an

intense threat environment and have the capability to produce significant collateral damage to critical infrastructures. Power networks are operated using what is termed an "N-1" operation criterion. That is, the system must always be operated to withstand the next credible disturbance contingency without causing a cascading collapse of the system as a whole. This criterion normally works very well for the well-understood terrestrial environment challenges, which usually propagate more slowly and are more geographically confined. When a routine weather-related single-point failure occurs, the power system needs to be rapidly adjusted (10 minutes being the allowed time limit) and positioned to survive the next possible contingency. Both E3 HEMP and space weather disturbances, however, can have a sudden onset and cover large geographic regions. They therefore cause near-simultaneous, correlated, multipoint failures in power system infrastructures, allowing little or no time for meaningful human interventions. In contrast to well-conceived design standards that have been successfully applied for more conventional threats, no comprehensive design criteria have ever been considered to check the impact of the geomagnetic storm environments. Further, as this analysis demonstrates, the design actions that have occurred over many decades have greatly escalated the dangers posed by these storm threats for this critical infrastructure.

Section 3
Analysis of U.S. Power System Impacts from the Nuclear Late-Time HEMP Threat Environment

In this section we will describe a subset of calculations performed for the EMP Commission to quantify the effects of E3 HEMP on the U.S. power grid. Here we will only describe the results from a single high-yield device.

3.1 Description of the HEMP Scenarios Considered in this Study

For the Heave E3B HEMP threat, the burst locations are identified as directly over 8 specific locations, and the burst height is chosen to be 170 km. The worst case electric fields arise form a burst at 130 km, but a range of heights were calculated and it was found that the greater extent of the heave region produced higher reactive demand for the 170 km burst altitude.

For the Blast Wave threat, the maximum E3A field levels are centered over particular regions of the U.S.; to achieve this, the burst locations are typically south of 25 degrees North latitude. The optimum burst altitude, which was used in this report, for the Blast Wave E3A HEMP was 500 km. All the results shown are for solar minimum nighttime. As discussed in Section 2, daytime or non-solar minimum E3A is substantially smaller.

3.2 Simulation Results and Power Grid Impact Assessments for the Heave Scenarios

The EMP environment imposes a geographically widespread electromagnetic threat to large infrastructures, such as electric power grids. The electromagnetic threat environment has two important facets: the E1 and the E3. E1 is a high-intensity, rapid rise-time (10's of nanoseconds) threat, which is very widespread and more severe in intensity than the electric fields caused by natural events, such as lightning. E3 is slower (lasting 10's of seconds) and produces induced current flows in the exposed power grid, similar to the manner in which GIC is produced during a geomagnetic storm. Therefore, for convenience, here we will refer to all induced currents as geomagnetically induced currents (GIC). While this phase of the investigation is focused on the role of the E3 environment and its potential impacts on the reliable operation of the power grid, both the E3 and E1 environments might combine in important ways, to the detriment of the reliable operation of, and potential long-term damage to, this important infrastructure. However, due to the complexity of the E1 and E3 interactions by themselves, these threats are considered separately in two documents. In the E3 studies summarized in this section of the report, there are numerous threat scenarios in which the E3 threat environment by itself is severe enough to trigger the widespread collapse of portions of the U.S. power grid.

In addition to the reliability threats caused by the E1 and E3 EMP threat environments, the potential for damage to the power grid can be compounded further by the stresses that could occur due to extreme weather conditions that could be coincident with any EMP

attack on the infrastructure. For example, an attack during a severe cold snap would mean loss of auxiliary heaters that are needed on SF6 circuit breakers to prevent condensation of the interrupting gas. Similarly, storage batteries at substations and other important facilities would experience added drain and loss of storage capacities, resulting in added system restoration difficulties. Fuel and boiler systems for power plants could also be compromised for extended power outages. Extreme hot or cold weather conditions would also increase concerns for the possibility of consequential impacts to end-users dependent on electricity for heating and cooling systems.

3.2.1 The E3 Threat and Estimates of Power System Impacts from these Threat Environments

Because of the similarity of the E3 Environment to that associated with geomagnetic storms, and their potential interactions with power systems, the extensive experiences from these events can be used to estimate the potential impacts that a E3 threat could pose. By all means of measurement, the threat potential posed by either an E3 environment or a severe geomagnetic field disturbance exceeds the intended stress limit that a power network is designed and tested to withstand. For example, all power systems are designed for an N-1 criteria, where the system as a whole should remain intact after sustaining the next worst contingency disturbance event on the network.

Credible disturbance events considered usually involve three-phase faults that persist for approximately 70 msec or single phase faults where some relay malfunction delays successful clearing of the disturbance up to time delays of 180-200 msec. These events are also geographically confined to a specific location and only involve the removal of limited assets to isolate the disturbance. E3 and geomagnetic disturbance threats are geographically very widespread, causing the impact to operations to the grid to be realized at lower levels over many points in the network under attack. Though the impact of GIC at a particular location such as a substation or transformer will be smaller than that caused by a three-phase fault, the cumulative stress placed upon the system by the E3 and geomagnetic disturbance can be much larger in total than a single three-phase fault event. Further, E3 and geomagnetic storm events will have durations of cumulative stress that will persist for 10's of seconds, compared to the "msec" duration of discrete fault events. When looking at the disturbance energy of a 765kV 3 phase fault (assuming the largest practical fault current of 60kA fault current), the total disturbance energy of this event is ~5300 MVA-sec. A severe geomagnetic disturbance (whether from E3 or natural causes) can cumulatively produce a response in the power grid of disturbance energy (increased transformer reactive demands) that are many times higher in total than that caused by a 3 phase fault.

In addition, GIC events are likely to trigger the loss of key assets from harmonic interactions with relay and protective systems. This, in-effect, pulls the legs out from under the system and rapidly erodes the ability of the system to remain intact. In order to be conservative as possible, the criteria for equivalent disturbance energy used for the E3 threat impacts is 7.5 times larger (i.e. equivalent to a 30 cycle 3 phase fault applied

separately to each region of the power grid). Further, only a 15 second portion of the E3 threat event is used in the calculation of equivalent disturbance energy. Therefore, the determinations that have been made about the geographic extent of power system collapse caused by the E3B threat are likely to be best-case projections, and, under less-favorable power grid operating scenarios at the time of attack, the geographic boundaries of collapse could easily be much greater.

This disturbance criteria also does not take into account the experience gained from other recent power system collapses (August 2003). This experience has shown that disturbance events in one region can also trigger collapse through cascading outages from one region where the disturbance has occurred into neighboring interconnected grids that are un-affected by the initiating disturbance. These inter-relationships can therefore magnify the geographic extent of the disturbance beyond the estimates provided in this summary.

3.2.2 E3B Heave Threat Scenarios

The first class of disturbance scenarios is associated with the Heave portion of the E3 threat; the other threat scenario is the Blast Wave environment from an EMP attack, which will be considered separately. For these scenarios, a burst is specified to be located over a number of critical locations throughout the U.S. These locations have been selected because of the extensive complexity of the exposed power grid infrastructure that would be influenced by the E3B Threat environment. Table 3-1 provides a summary of the various E3B threat simulations that are discussed for the CONUS region of the United States. The table provides the assigned Case designations that were used and the location of the burst for each threat scenario, which will be used in the next section. The results will be provided for each location and provide a comparison of the impact of each weapon on the U.S. grid for each location. For the CONUS region, eight different locations were selected at important locations of the power grid infrastructure. Detailed analysis of each threat and regions of probable power system collapse will be provided in this section. Because of location differences and the differences of the underlying power grid at each location, the level of impact to operation of the U.S. grid can vary substantially. By looking at one of the important power system impacts, the increase in reactive demand from GIC flows, it is possible to provide a summary overview of the level of impacts that are estimated to occur. Figure 3-1 provides a summary of estimated reactive power demands on the U.S. power grid for the eight different locations.

Table 3-1. Scenario designations for E3B Heave cases.

Centered on	Case #
Columbus, Ohio	16D
Huntsville, Alabama	16E
Gary, Indiana	16F
Indiana/Ohio/Kentucky Border	16G
Dallas/Fort Worth, Texas	17A
Seattle, Washington	15A
Portland Oregon	15B
Las Vegas, Nevada	15C

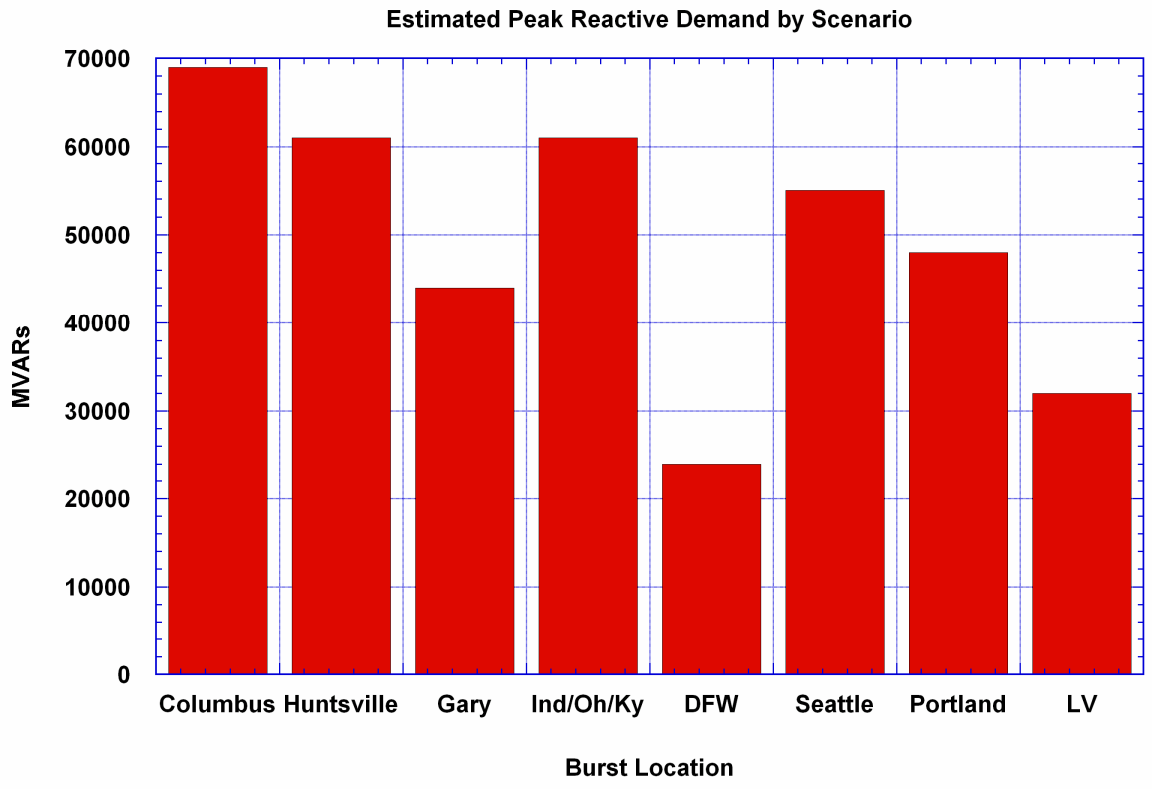

Figure 3-1. Estimated reactive demand for E3B Heave locations.

3.2.3 Heave Case 16d – Columbus Ohio

The above referenced case name relates to a burst event centered over Columbus, Ohio, which produces some of the most severe power system impacts observed for the Eastern U.S. interconnected power grid. The outlined region shown in Figure 3-2 would be expected to experience collapse from this E3B threat scenario. In addition, it is possible that wider regions beyond these boundaries could also experience cascading outages (particularly Maine, Florida and eastern Minnesota) if the threat occurs during a period of adverse system operating conditions. In this and succeeding plots, the area of circles is proportional to the current flow into or out of the ground at each site, with green indicating current flow into the ground and red indicating current flow out of the ground.

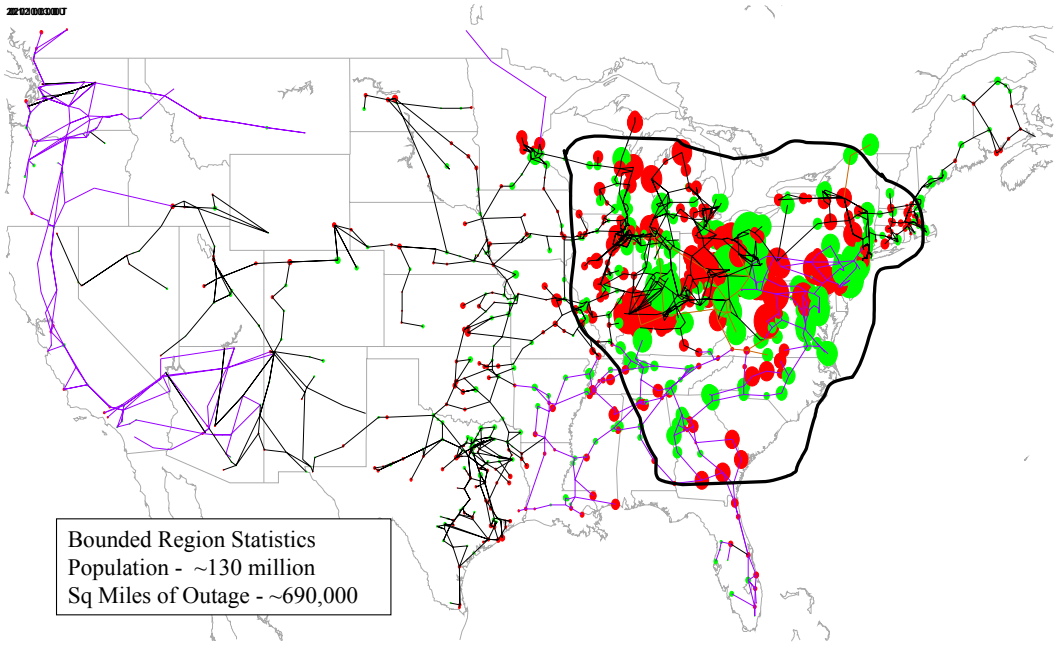

Figure 3-2. Summary of GIC flows in U.S. power grid for E3B from burst centered on Columbus, Ohio.

3.2.4 Heave Case 16e, Huntsville, Alabama

The outlined region shown in Figure 3-3 would be expected to experience collapse from this E3B threat scenario. In addition, it is possible that wider regions beyond these boundaries could also experience cascading outages (particularly the adjoining regions of New York, New England and central Wisconsin and Minnesota) if the threat occurs during a period of adverse system operating conditions.

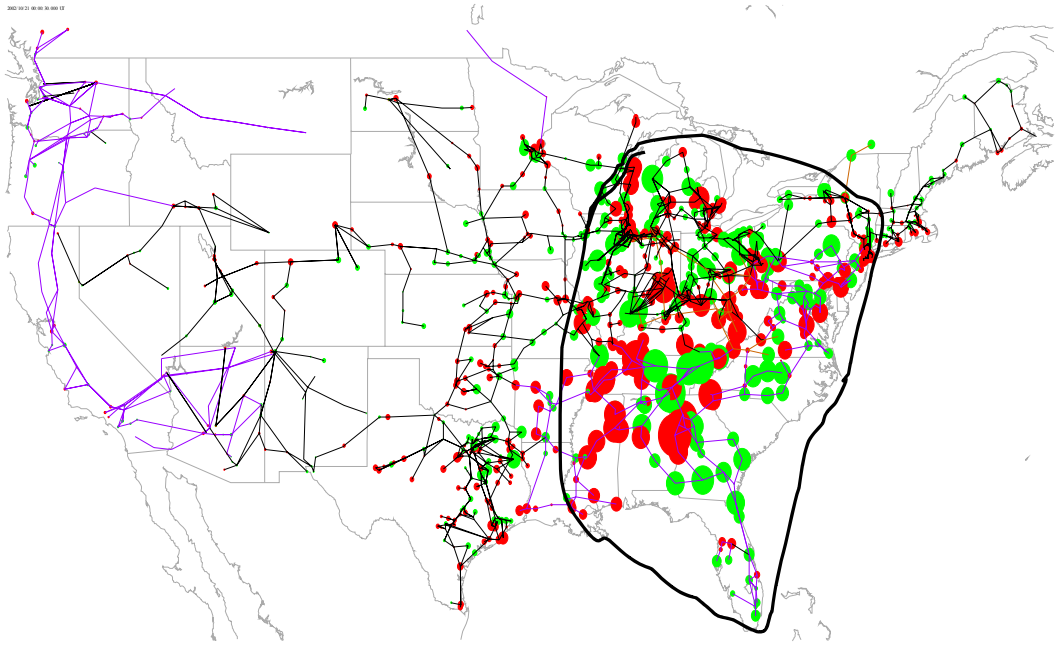

Figure 3-3. Summary of GIC flows in U.S. power grid for E3B from burst centered on Huntsville, Alabama.

3.2.5 Heave Case 16f, Gary, Indiana

The outlined region shown in Figure 3-4 would be expected to experience collapse from this E3B threat scenario. In addition, it is possible that wider regions beyond these boundaries could also experience cascading outages (particularly the adjoining regions of New York, New England and western Tennessee, Alabama and Mississippi) if the threat occurs during a period of adverse system operating conditions.

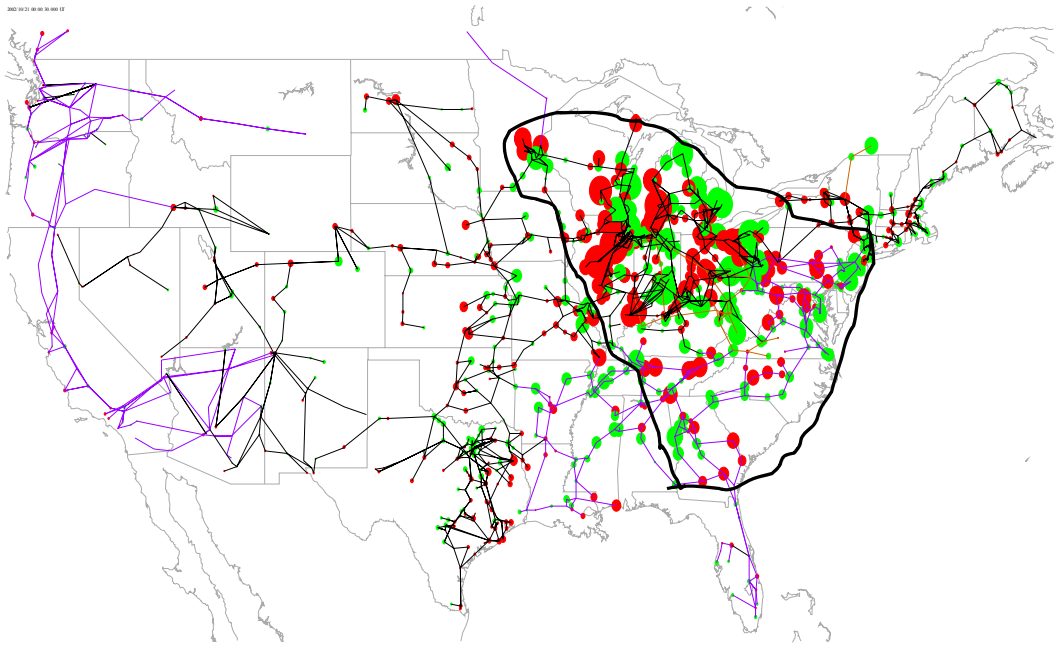

Figure 3-4. Summary of GIC flows in U.S. power grid for E3B from burst centered on Gary, Indiana.

3.2.6 Heave Case 16g, Indiana, Ohio and Kentucky Border

The outlined region shown in Figure 3-5 would be expected to experience collapse from this E3B threat scenario. In addition, it is possible that wider regions beyond these boundaries could also experience cascading outages (particularly adjoining regions of New England and west of the Mississippi River) if the threat occurs during a period of adverse system operating conditions.

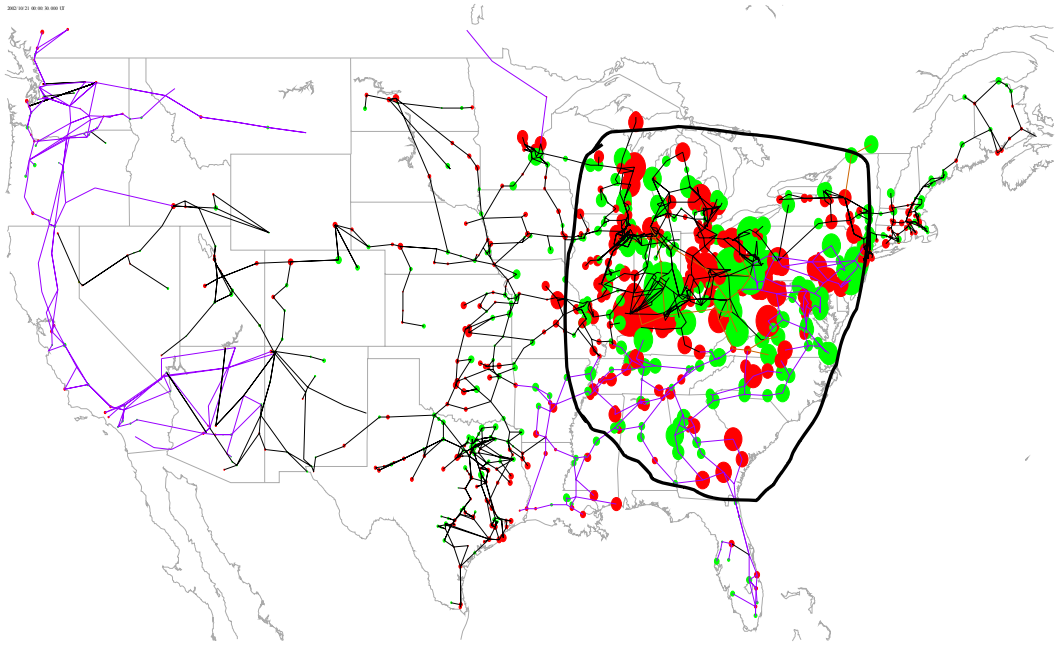

Figure 3-5. Summary of GIC flows in U.S. power grid for E3B from burst centered on the Indiana, Ohio and Kentucky border.

3.2.7 Heave Case 17a, Dallas/Ft. Worth

The outlined region shown in Figure 3-6 would be expected to experience collapse from this E3B threat scenario. In addition, it is possible that wider regions beyond these boundaries could also experience cascading outages (particularly adjoining regions north and east of Texas) if the threat occurs during a period of adverse system operating conditions.

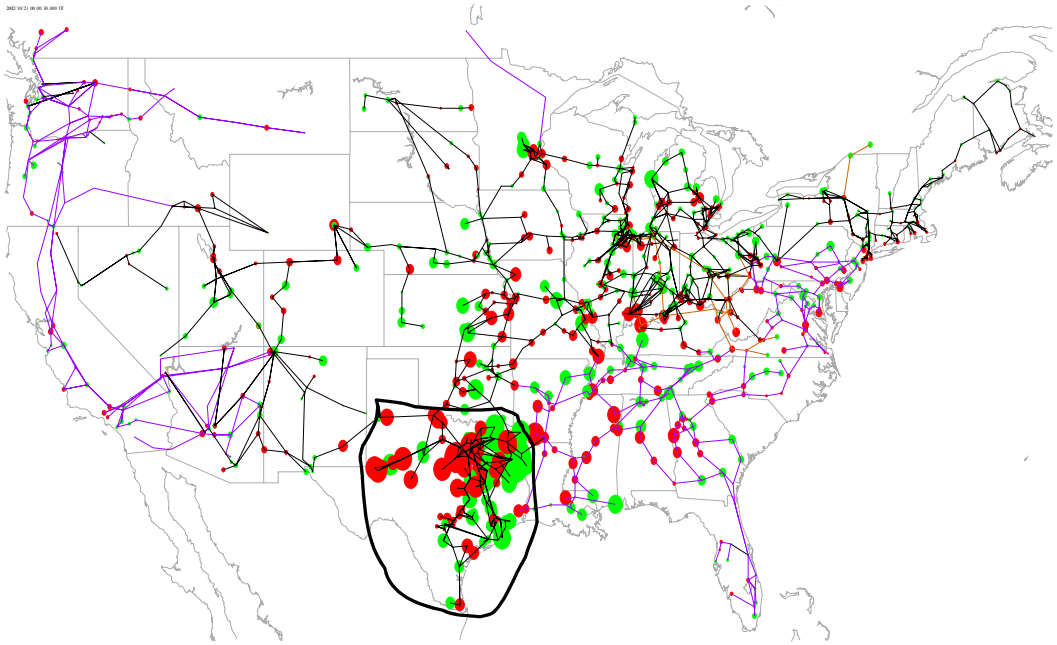

Figure 3-6. Summary of GIC flows in U.S. power grid for E3B from burst centered on Dallas/Ft. Worth, Texas.

3.2.8 Heave Case 15a, Seattle, Washington

The outlined region shown in Figure 3-7 would be expected to experience collapse from this E3B threat scenario. In addition, it is possible that wider regions beyond these boundaries could also experience cascading outages (particularly adjoining regions of California, Utah and Colorado) if the threat occurs during a period of adverse system operating conditions.

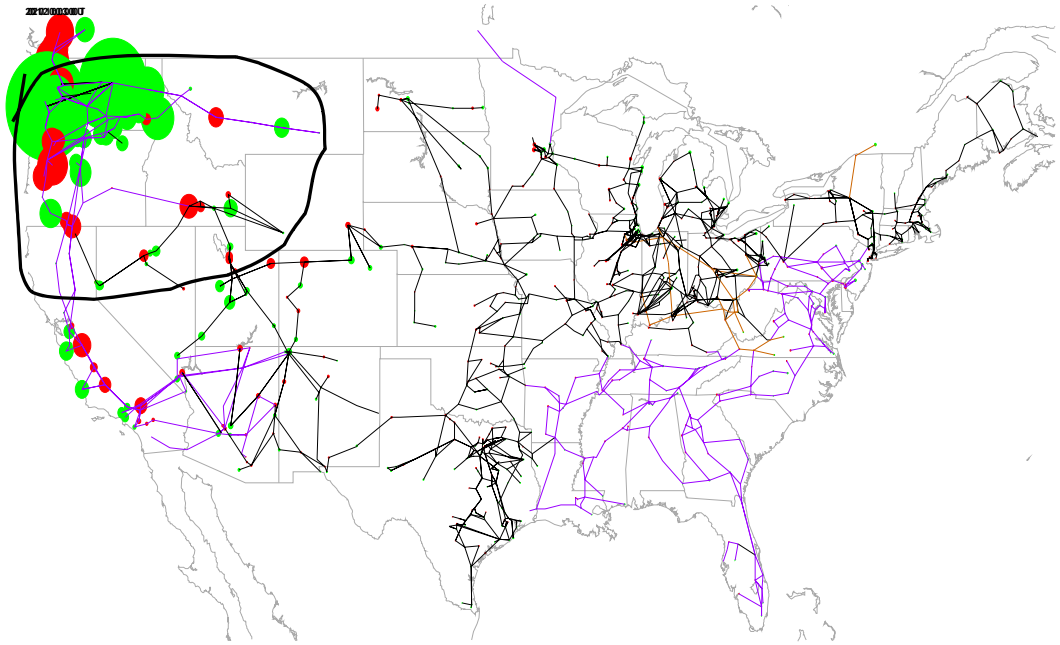

Figure 3-7. Summary of GIC flows in U.S. power grid for E3B from burst centered on Seattle, Washington.

3.2.9 Heave Case 15b, Portland, Oregon

The outlined region shown in Figure 3-8 would be expected to experience collapse from this E3B threat scenario. In addition, it is possible that wider regions beyond these boundaries could also experience cascading outages (particularly adjoining regions of Utah and Colorado) if the threat occurs during a period of adverse system operating conditions.

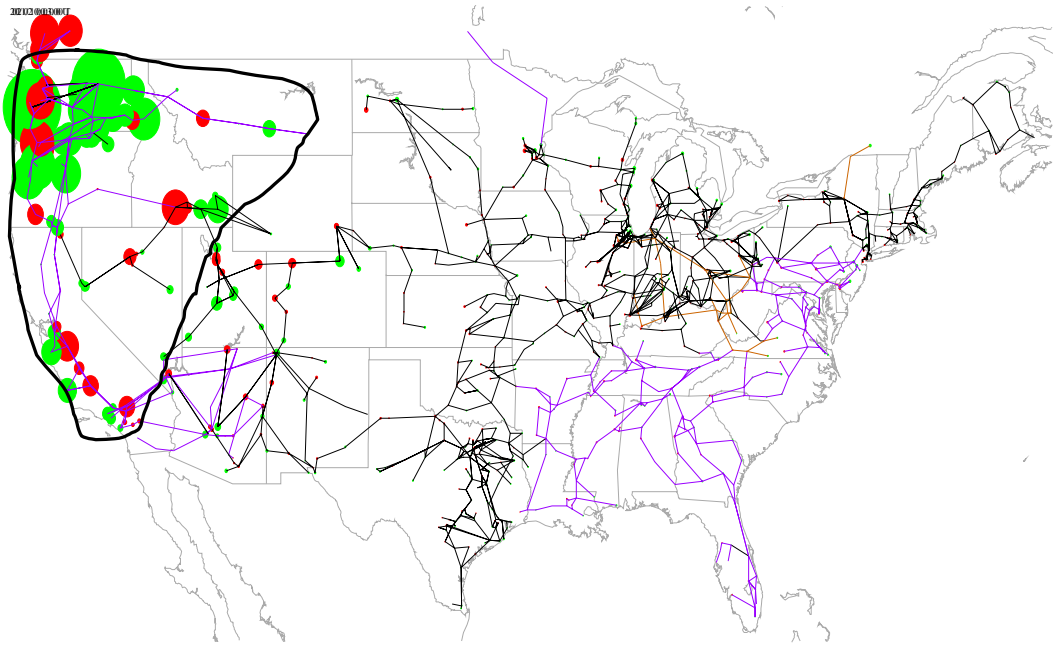

Figure 3-8. Summary of GIC flows in U.S. power grid for E3B from burst centered on Portland, Oregon.

3.2.10 Heave Case 15c, Las Vegas, Nevada

The outlined region shown in Figure 3-9 would be expected to experience collapse from this E3B threat scenario. In addition, it is possible that wider regions beyond these boundaries could also experience cascading outages (in particular Colorado, Wyoming and Montana) if the threat occurs during a period of adverse system operating conditions.

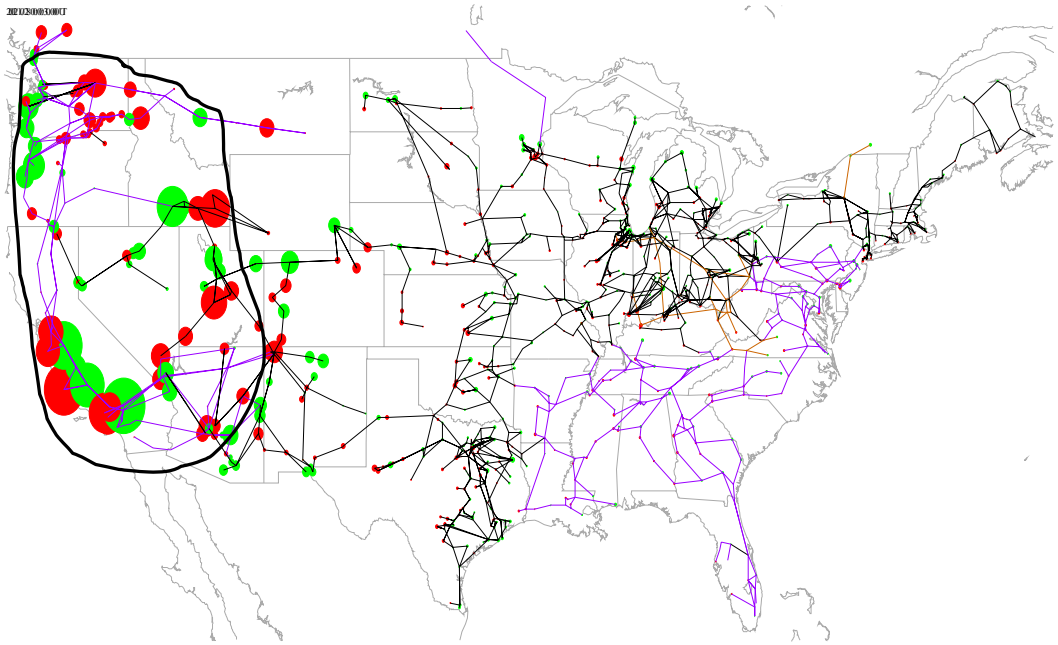

Figure 3-9. Summary of GIC flows in U.S. power grid for E3B from burst centered on Las Vegas, Nevada.

3.3 Simulation Results and Power Grid Impact Assessments for E3A Blast Wave Scenarios

The prior EMP summaries have focused on the Heave E3B disturbance generated by a nuclear detonation. The Heave disturbance produces a disturbance footprint that is generally within the immediate vicinity of the high altitude detonation event. However, a separate geomagnetic field disturbance condition can be generated over North America by a high altitude disturbance that can produce a more intense geomagnetic field disturbance and with a larger geographic footprint, but of much shorter duration. This E3 disturbance is the Blast Wave. Figure 2-2 of Section 2 showed the geographic footprint for a Blast Wave disturbance over a large portion of CONUS from a detonation located over Mexico. Because the worst case electric fields are located beyond the horizon from the burst, this disturbance does not pose a combined E1 and E3 threat like the Heave scenarios that are shown in Section 3.2.

The E3A Blast Wave cases used in this report are given in Table 3-2. All of the cases assume the worst case ionosphere, which exists at nighttime near the solar minimum. Daytime bursts, or those occurring at other times in the solar cycle, yield substantially smaller perturbed magnetic fields, and smaller GICs.

Table 3-2. E3A Blast Wave cases.

Peak fields	Case	Burst Location	
		Lat, deg.min	Long, deg.min
New York	B16A	15.00°N	76.00°W
Chicago	B16B	16.00°N	90.00°W
Dallas/Ft. Worth	B17A	8.30°N	103.00°W
Portland	B15A	21.00°N	132.00°W
Las Vegas	B15B	11.10°N	122.30°W

The Blast Wave threat poses a different threat potential than traditionally imagined due to GIC flows in electric power grids. While the duration of the disturbance event is much briefer (approximately 10 seconds) than that posed by a Heave disturbance scenario, the level of GIC flows caused by the Blast Wave can be many times larger in a number of locations than that caused by the Heave disturbances.

Because of the unusually large GIC flows, a new and previously unanticipated aspect or dimension of system failure has to now be considered. In some cases, the level of GIC (or DC current flow) can substantially exceed the pre-disturbance AC current flow through lines and transformers, and therefore also on the circuit breaker interrupting devices that could be required to operate and attempt to interrupt the combined AC & DC current during these disturbances. Operating circuit breakers under these circumstances raises the concern that widespread and long-duration failure and damage may result to critical high voltage breakers and other nearby apparatus that are exposed to extremely abnormal switching events that could generate high over-voltages during these operations.

While Blast Waves produce significantly larger GIC flows, an equally important factor is that the time duration is much shorter. The interaction of GIC and the onset of transformer saturation is complex and governed by various factors of transformer design and the magnitude and duration of GIC in the transformer. Therefore, it is plausible that a number of transformers will only partially exhibit the full degree of half-cycle saturation behaviors during the initial intense GIC spike that occurs during the first second of the Blast Wave disturbance. Due to this uncertainty, the level of impacts on the system can vary substantially. In the determinations of disturbance energy that the system would be exposed to during half-cycle saturation of transformers, calculations are made after the peak of the initial GIC onset, starting at 2 seconds after the Blast Wave disturbance. This primarily captures the disturbance energy contained in the second minor peak and tail of the event.

3.3.1 E3A Blast Wave Threat Scenarios

For these Blast Wave scenarios, the footprint of the intense disturbance region is specified to be located over a number of critical locations throughout the U.S. These locations have been selected because of the extensive complexity of the exposed power grid infrastructure that would be influenced by this E3A threat environment. Table 3-2 provides a summary of the various Blast Wave E3A threat simulations that are included in this report. The table provides the assigned Case designations that were used and the location of the burst. Five different locations were selected at important locations of the power grid infrastructure. Detailed analysis of each threat and regions of probable power system collapse will be provided in this section. Because of location differences and the differences of the underlying power grid at each location, the level of impact to operation of the U.S. grid can vary substantially. By looking at one of the important power system impacts, the increase in reactive demand from GIC flows, it is possible to provide a summary overview of the level of impacts that are estimated to occur. Figure 3-10 provides a summary of estimated reactive power demands for the five different locations. The detonation at the burst location placing high fields over Chicago produces a disturbance peak reactive demand of approximately one quarter of the total U.S. peak demand.

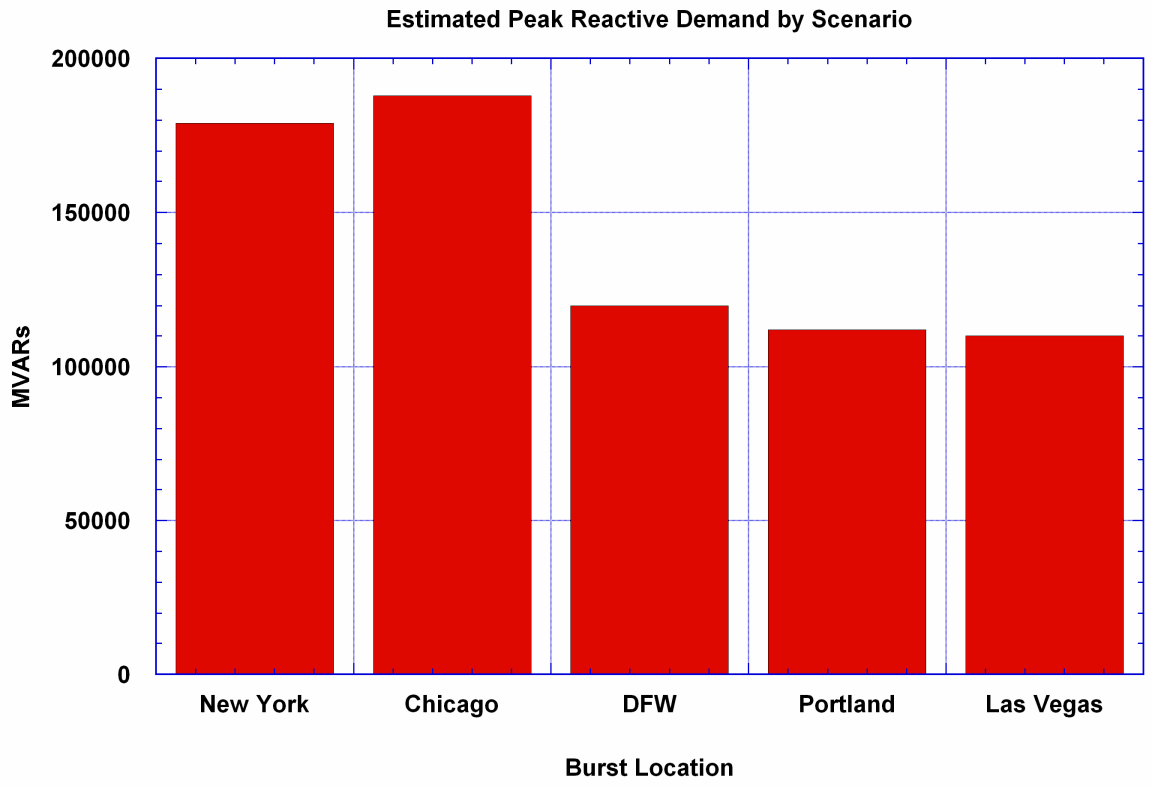

Figure 3-10. Estimated reactive demand for E3A Blast Wave locations

3.3.2 Blast Wave Case B16a – New York

This case refers to a Blast Wave event whose peak electric fields are centered over the New York region; this location will spread a large footprint of the disturbance, particular over much of the eastern U.S.

Every major state from the East Coast to the west coast states of Washington, Oregon and California, and from Maine to Florida and Texas, accumulated sufficient disturbance energy from this scenario to threaten collapse of the entire U.S. Power Grid (Figure 3-11). The disturbance also generated very high levels of GIC in the Pennsylvania/New York/New Jersey and neighboring regions. These levels could be large enough to exceed the normal AC current loads, and, as a result, could have consequential impacts that may lead to permanent damage to circuit breakers and other apparatus on the high voltage networks in these regions, due to attempts to operate under these unusual conditions. Possible widespread failures of this type could lead to significant delays in power system restoration in these regions.

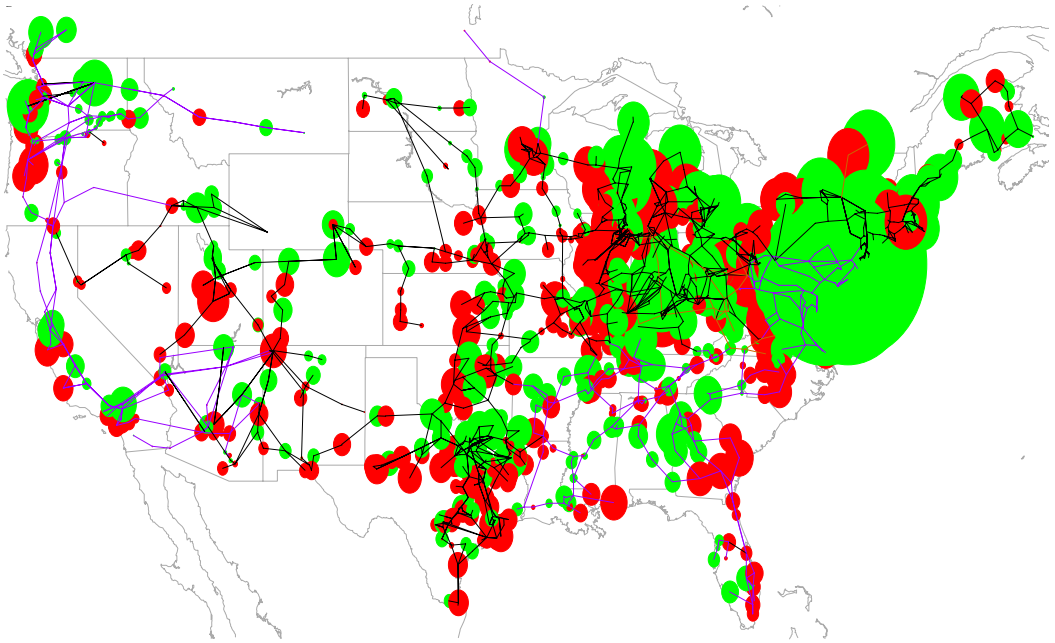

Figure 3-11. Summary of GIC flows in U.S. power grid for E3A Blast Wave Case B16a. The entire U.S. Power Grid is expected to collapse.

3.3.3 Blast Wave Case B16b - Chicago

This case refers to a Blast Wave whose peak electric fields are centered over the Chicago region; this location will spread a large footprint of the disturbance over much of the U.S.

This disturbance is even more severe in total impacts than Case B16a, which was previously described. The same impact concerns described for that event are even more of a concern for this larger disturbance scenario. As in Case B16a, every major state from the East Coast to the west coast states of Washington, Oregon and California, and from Maine to Florida and Texas, accumulated sufficient disturbance energy from this scenario to threaten collapse of the entire U.S. Power Grid (Figure 3-12). The disturbance also generated very high levels of GIC from Chicago to New Jersey and neighboring regions. These levels could be large enough to exceed the normal AC current loads, and, as a result, could have consequential impacts that may lead to permanent damage to circuit breakers and other apparatus on the high voltage networks in these regions. Possible widespread failures of this type could lead to significant delays in power system restoration in these regions.

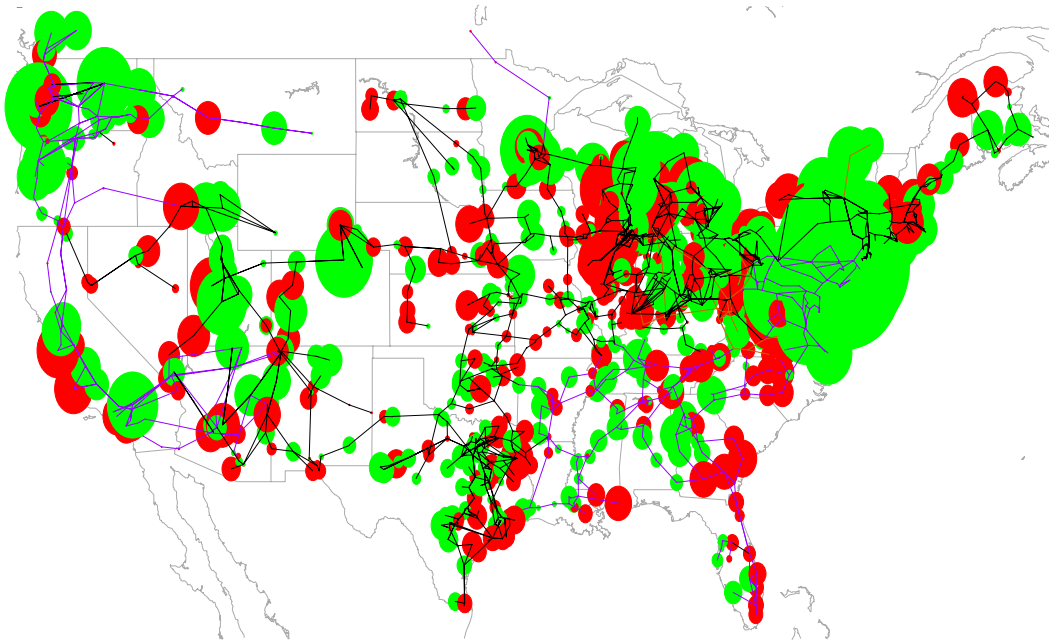

Figure 3-12. Summary of GIC flows in U.S. power grid for E3A Blast Wave Case B16b. The entire U.S. Power Grid is expected to collapse.

3.3.4 Blast Wave Case B17a – Dallas / Ft. Worth

This case refers to a Blast Wave whose peak electric fields are centered over the Dallas/Ft Worth region; this location will spread a large footprint of the disturbance over much of the U.S.

This disturbance is, in total, slightly less severe than Case B16a, which was previously described, however the same impact concerns described for that event are also of concern for this slightly smaller disturbance scenario. As in Case B16a, every major state from the East Coast to the west coast states of Washington, Oregon and California, and from Maine to Florida and Texas, accumulated sufficient disturbance energy from this scenario to threaten collapse of the entire U.S. Power Grid (Figure 3-13). The disturbance also generated very high levels of GIC in much more widely scattered regions than Case B16a. These levels could be large enough to exceed the normal AC current loads, and, as a result, could have consequential impacts that may lead to permanent damage to circuit breakers and other apparatus on the high voltage networks in these regions. Possible widespread failures of this type could lead to significant delays in power system restoration in these regions.

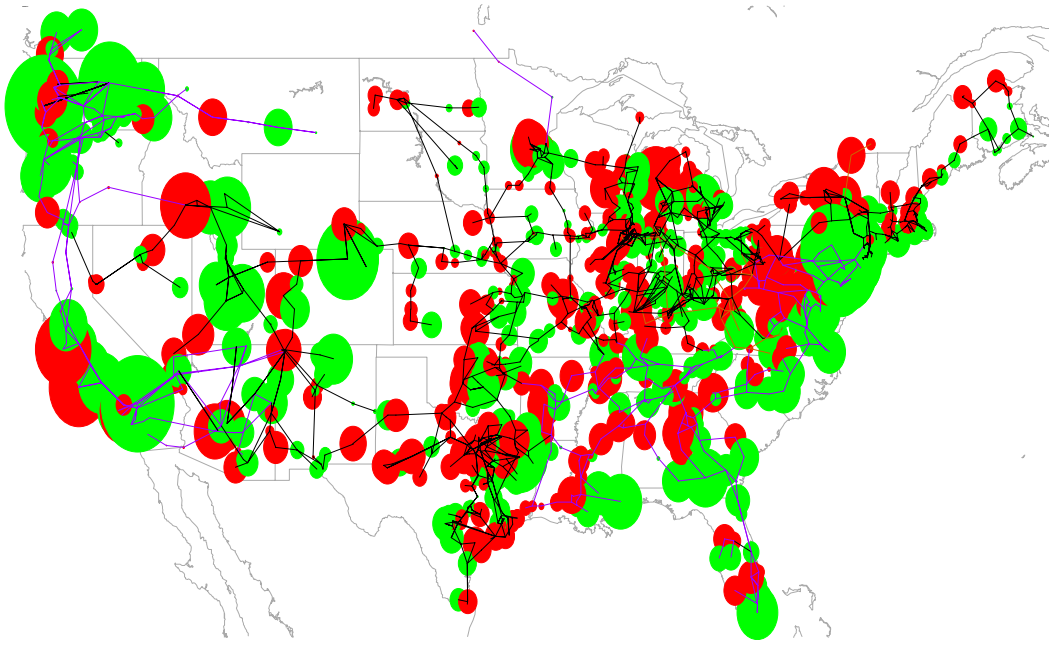

Figure 3-13. Summary of GIC flows in U.S. power grid for E3A Blast Wave Case B17a. The entire U.S. Power Grid is expected to collapse.

3.3.5 Blast Wave Case B15a – Portland, Oregon

This case refers to a Blast Wave whose peak electric fields are centered over the Portland, Oregon region; this location will spread a large footprint of the disturbance over much of the U.S.

This disturbance is, in total, 35% less severe than Case B16a, which was previously described. As a result, the estimated extent of power system collapse is not as extensive as in B16a. In Case B15a, the highest impact portions of the U.S. are the entire western grid and Texas grid, along with the portions of the Eastern grid from Minnesota to New York through Georgia (Figure 3-14). Considering the extent of the disturbance, it is conceivable that neighboring system may also collapse through a cascading process. The disturbance also generated very high levels of GIC in much of the western U.S. These levels could be large enough to exceed the normal AC current loads, and, as a result, could have consequential impacts that may lead to permanent damage to circuit breakers and other apparatus on the high voltage networks in these regions. Possible widespread failures of this type could lead to significant delays in power system restoration in these regions.

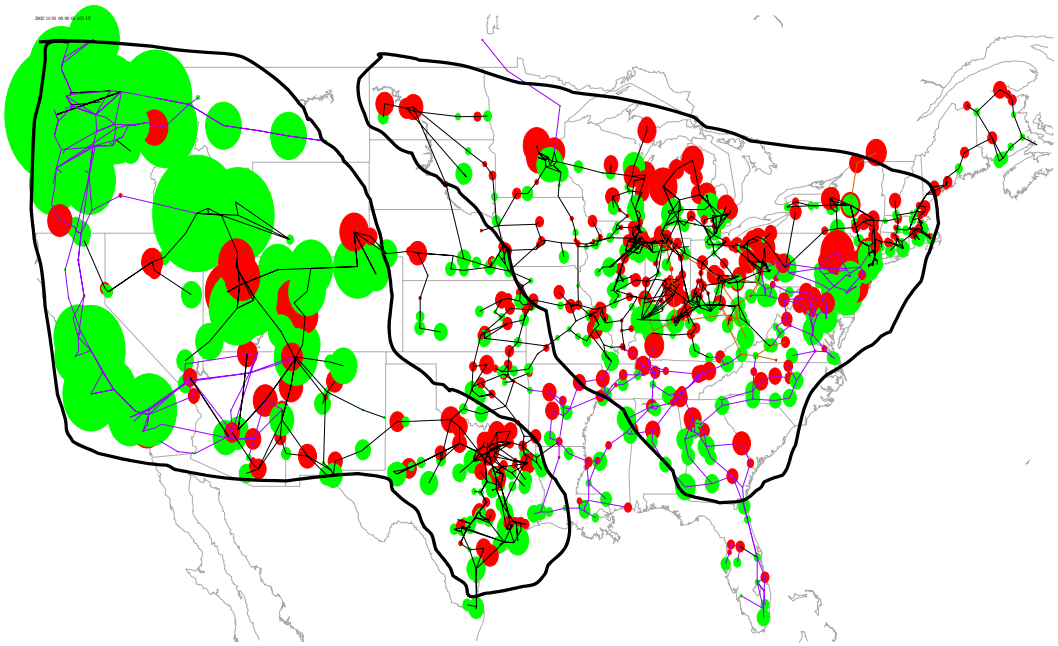

Figure 3-14. Summary of GIC flows in U.S. power grid for E3A Blast Wave Case B15a.

3.3.6 Blast Wave Case B15b – Las Vegas, Nevada

This case refers to a Blast Wave whose peak electric fields are centered over the Las Vegas, Nevada region; this location will spread a large footprint of the disturbance over much of the U.S.

This disturbance is, in total, 20% less severe than Case B16a, which was previously described. As a result the estimated extent of power system collapse is not as extensive as in B16a. In Case B15b, the highest impact portions of the U.S. are the entire Western grid and Texas grid, along with the portions of the Eastern grid from Minnesota to New York through Florida (Figure 3-15). Considering the extent of the disturbance, it is conceivable that neighboring system may also collapse through a cascading process. The disturbance also generated very high levels of GIC in much of the western U.S. These levels could be large enough to exceed the normal AC current loads, and, as a result, could have consequential impacts that may lead to permanent damage to circuit breakers and other apparatus on the high voltage networks in these regions. Possible widespread failures of this type could lead to significant delays in power system restoration in these regions.

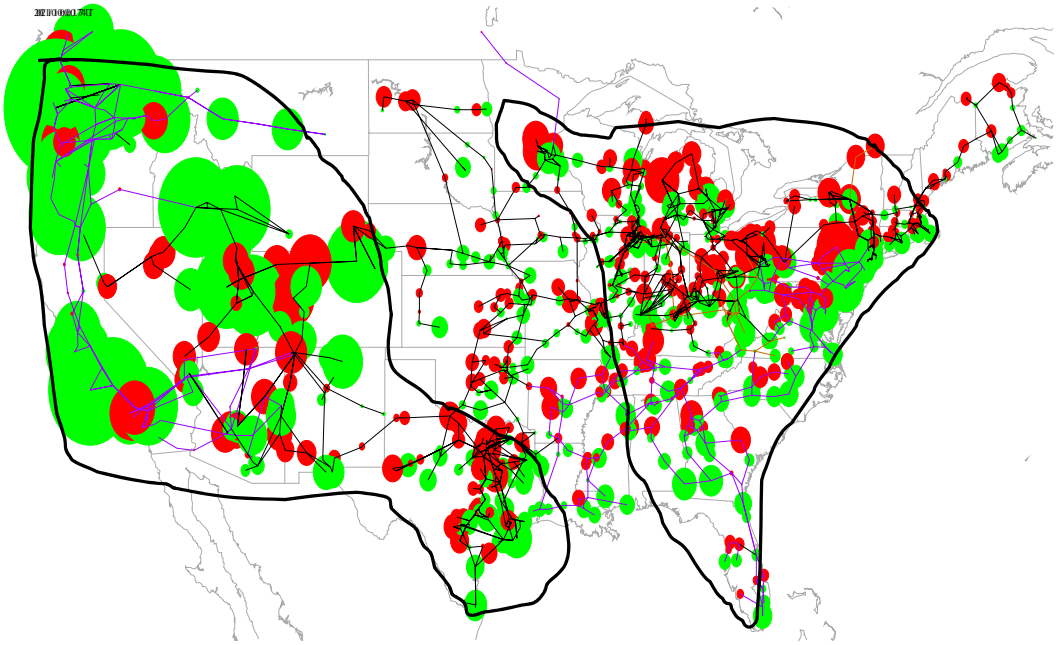

Figure 3-15. Summary of GIC flows in U.S. power grid for E3A Blast Wave Case B15b.

Section 4
Effects on Circuit Breakers

4.1 High Voltage Circuit Breakers and Current Interruption Process

Most technological progress and innovation follow a path from basic research to applied science and engineering innovations to develop specific product applications. A case-in-point is the example of the development of the transistor, which would not have been possible without first having understood the basic sciences of quantum mechanics, an understanding that ultimately opened the door to engineering innovations of solid-state electronics that followed. However, this process of basic scientific understanding to engineering application is not always the path for development. In particular, the development of high-voltage switchgear (circuit breakers) actually followed the opposite development path. The first high-power circuit breakers were designed and successfully operated at a time when very little was known about the physics of electric arcs. Intuitive design approaches were largely utilized because even steady-state models of the arcing process were not feasible. Even today, theoretical understanding is still insufficient to fully understand the complexities of the arc interruption process and present models only give a crude approximation of the dynamic conditions. Despite these limitations, designers have been able to develop successive generations of switchgear designs capable of interrupting several GVA per chamber. However, these intuitive development processes have still largely depended upon current interrupting device designs that follow from AC current flows that allow interruption to occur during the natural current zeros. Only general theoretical understandings of large DC current interruption is available and switches for HVDC transmission lines have needed to develop artificial methods to produce a current zero at the time of desired DC current interruption.

Successful current interruption requires both low dI/dt prior to current interruption and low dV/dt conditions immediately after interruption. Both these conditions are dependent upon, and at times even interdependent with, a number of factors. These factors include the level of current, the system design and circuit parameters, the kind of interrupting technology or gas used, the gas pressure and the electrode nozzle design. In addition to interruption of the current itself and its kinetic energy content, the large inductances of power circuit elements and high kV operating voltages of the system have the ability to store and release large amounts of energy during and immediately after the interruption process, and this acts to re-establish the current flow.

Large AC circuit breakers have the capability to interrupt currents that are as much as 40kA and for special applications as much as ~60kA in magnitude. The level of interrupting current generally defines the dI/dt rate during the AC current zero crossing that the device will experience. This has presented a limiting threshold in the design of these devices. Greenwood and other investigators provide some information on efforts that they undertook in the development of DC current interrupting devices specifically for application on HVDC transmission systems. Even with the objective of limiting DC current interruption to very low levels, such as 5kA, they had to develop methods that

would artificially produce current zeros for the DC interruption process. This process created large dI/dt's that were ~70 times larger than the dI/dt posed by 40kA AC currents. Their research found that vacuum interrupters provided the most robust capabilities for this application, but this interrupter approach is not used at high voltage, high power applications common on the existing AC transmission system.

4.2 Description of U.S. Circuit Breaker Population

Public data on the entire population of high voltage circuit breakers in the U.S. is not available. At present there are more than 100 utility entities that own and operate portions of the integrated high voltage power grid across the U.S. In only one case, that of the ECAR pool, has there been an attempt to define and assess the state of the population of these critical devices. In 1999, the ECAR Electric Equipment Panel published a report on the aging of major equipment that contained data on over 1000 high voltage circuit breakers at 345kV, 500kV and 765kV within their system. The ECAR pool is the largest in the U.S. and roughly accounts for 20% of the entire U.S. transmission system. The ECAR pool also provides an ideal cross-section of all three major operating voltages in the U.S. power grid infrastructure of interest to this particular investigation.

In total across the U.S. power grid model that has been developed, there are estimated to be ~1800 major transmission lines of 345kV or higher operating voltage. In the case of the ECAR region, the application of circuit breakers is typically one or more operating devices at each end of the network (i.e. ring-bus or breaker and a half substation configuration). This practice is also commonly applied throughout the remainder of the U.S. power grid as well. Therefore using the population information from the ECAR region, it is plausible to extrapolate that there is likely ~5000 circuit breakers of 345kV or higher operating voltage across the contiguous U.S.

The development of the present higher operating voltages also followed a time progression in the U.S. 345kV lines were first introduced in 1953. The development of 500kV and 765kV lines followed in 1964 and 1969 as experience gained from lower voltages was adapted and applied towards development of these higher voltages. Much of this initial development took place within the ECAR pool. As a result many of the vintage or initial attempts at switchgear technology at these voltage levels are still in place in the systems today. Figure 4-1 provides a plot of the year of manufacture (also installation) of all the 345kV and higher circuit breakers in the ECAR pool. Figures 4-2, 4-3, and 4-4 provide the age, based upon the 1998 survey date (note all breakers still in-service from this survey will all be ~10 years older) for each of the 345kV, 500kV, and 765kV breakers in the ECAR system. These statistics indicate a very old and potentially brittle population compared to the 25-35 year operating life that ECAR estimates for breakers in these operating voltage classes.

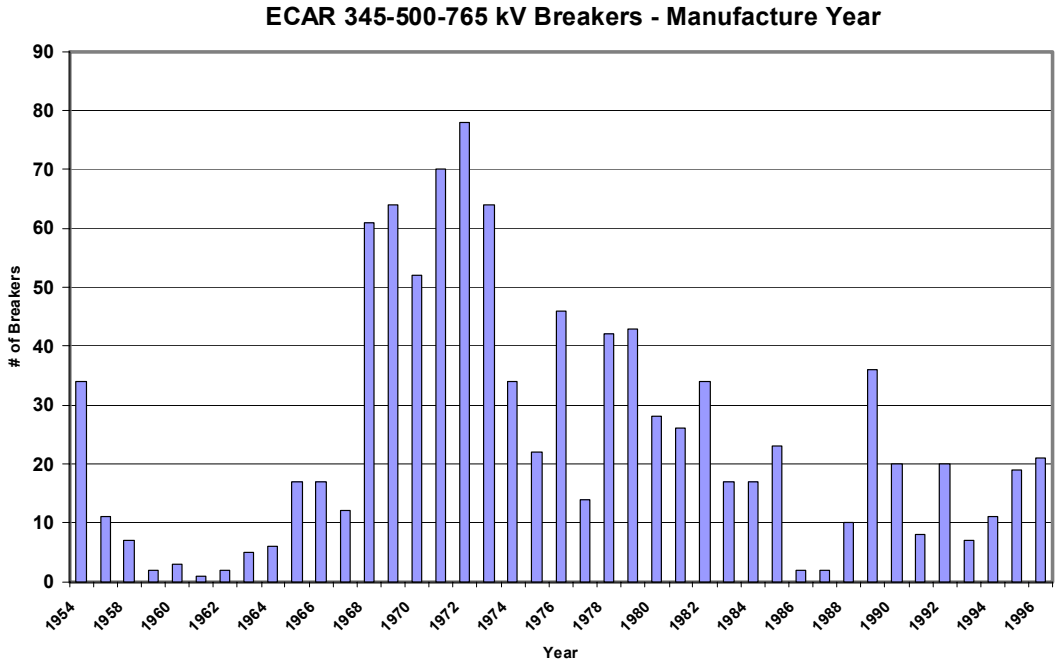

Figure 4-1. Manufacture dates of all 345kV and higher circuit breakers in the ECAR pool.

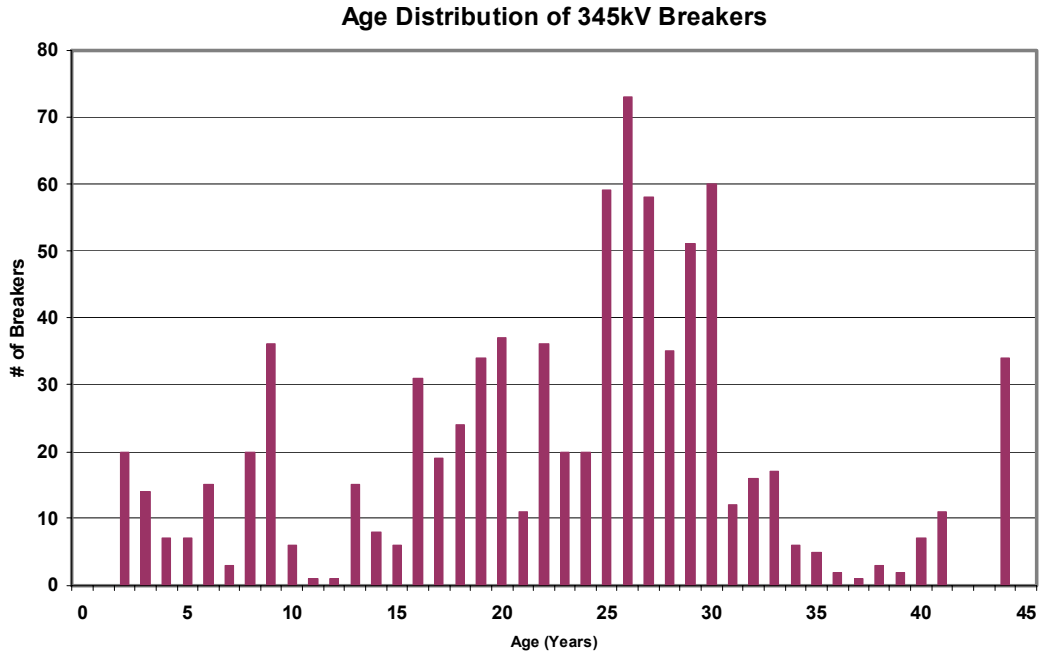

Figure 4-2. Age distribution of 345kV circuit breakers in ECAR pool, circa 1998 survey date.

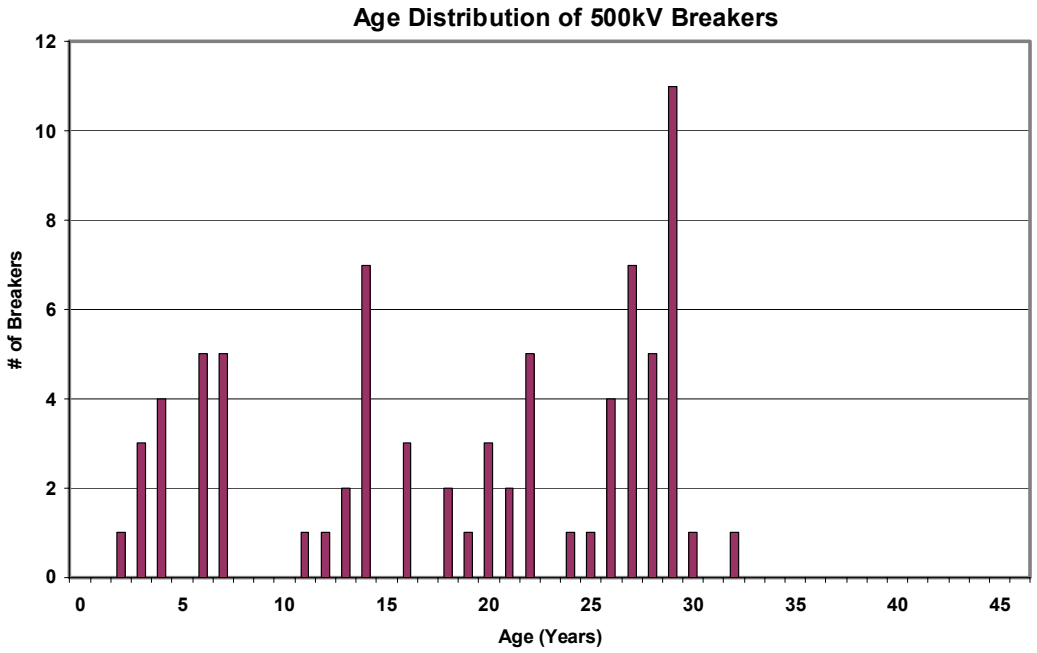

Figure 4-3. Age distribution of 500kV circuit breakers in ECAR pool, circa 1998 survey date.

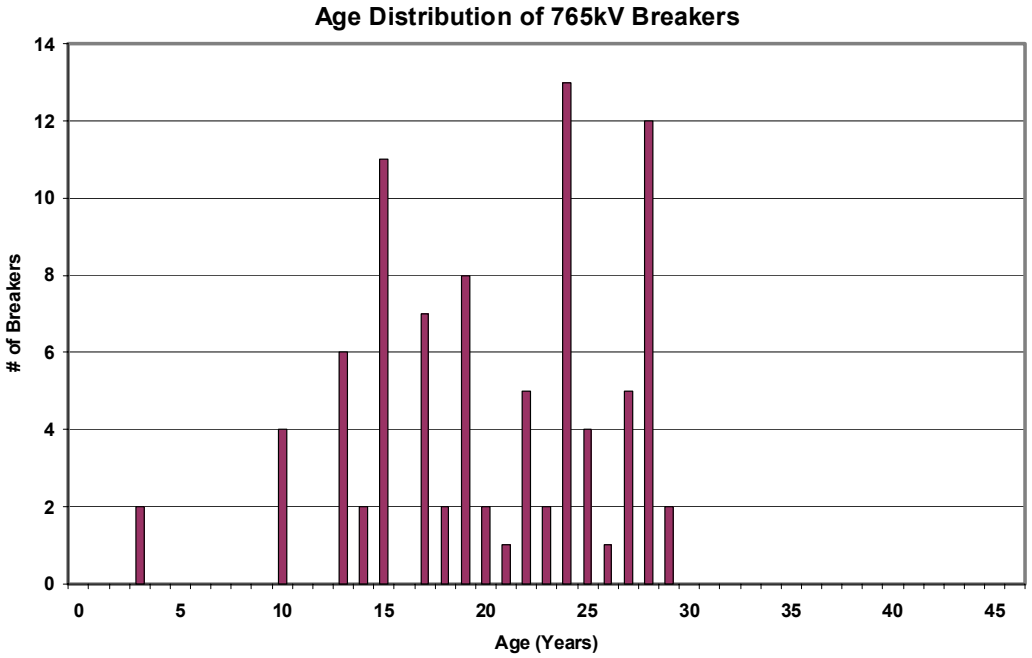

Figure 4-4. Age distribution of 765kV circuit breakers in ECAR pool, circa 1998 survey date.

4.3 GIC vs AC Flow Conditions

As previously discussed, the Blast Wave disturbance scenario in particular can cause very large GIC flows in the power grid. Figure 4-5 provides an example of the estimated GIC flow per phase in a 500kV transmission line between Waugh Chapel and Calvert Cliffs in the Baltimore/Washington DC area for the B16a Blast Wave disturbance scenario. Of particular concern is the large initial impulse of GIC that reaches a peak around 200 msec and then more slowly decays. Current interruption where the DC component exceeds the AC current component would be of particular concern. Figure 4-6 provides a plot of the normal AC current for this line (as provided from a PJM region power flow case) and the superimposed AC and DC current components that would occur for this Blast wave disturbance condition. As shown, for these conditions the peak DC is nearly a factor of two times higher than the normal AC current peak and as illustrated, the superimposed conditions could retard normal AC current zero crossing by ~700 msec.

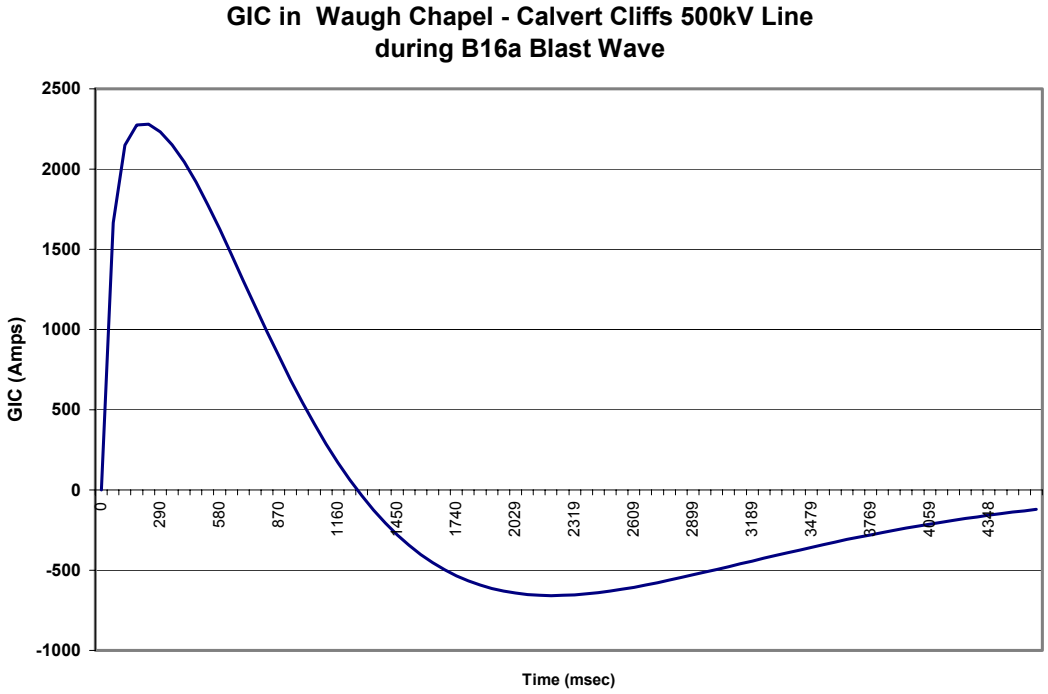

Figure 4-5. Waugh Chapel – Calvert Cliffs 500kV line GIC flow per phase during Blast Wave Case B16a.

The length of this absence of normal current zero crossing would be extended slightly due to either larger GIC flows or lower normal AC current flow conditions. For conditions where there is either sufficiently large AC current levels present or low GIC present, then normal breaker operation would be expected due to presence of AC current zero crossings. A key parameter for measuring this risk is likely to be the ratio of GIC flow to AC current. Any ratio greater than 1 is likely to cause at least some period of time of no current zero crossing. As will be discussed in more detail, there is considerable diversity of both normal AC and GIC flows in the network.

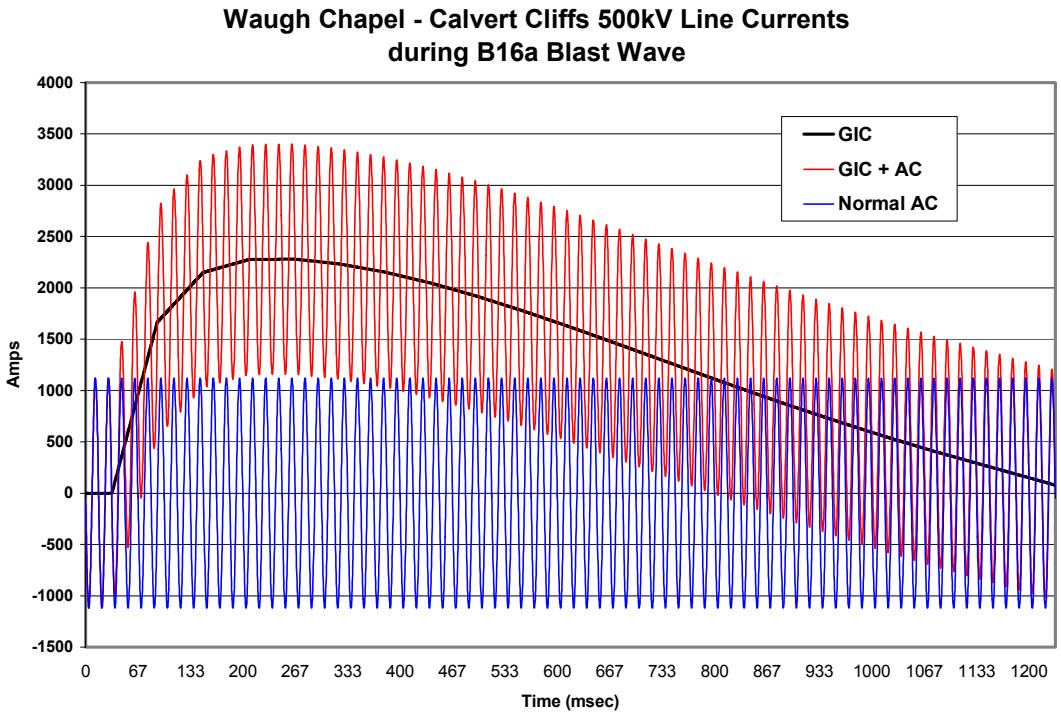

Figure 4-6. Normal AC current and superimposed GIC and AC current for Waugh Chapel – Calvert Cliffs 500kV line during Blast Wave Case B16a.

Since AC current flow conditions are one of the key factors in determining exposure risks due to E3 threats, only an approximation is possible of total risk due to large natural variations that can occur in transmission line AC current flows. Figure 4-7 provides an illustrative example of total transmission system load from the BPA power system over a 9 year period from 1993 to 2001. As shown, there are large scale network flow changes that can occur over daily, seasonal, and long term secular changes in flow patterns. From a system basis as illustrated in this example, greater than a factor of 2 change in total network flow demand can occur over short time periods. In addition to the bulk network flow changes, flows on specific lines can exhibit even greater diversity changes due to minor network configuration adjustments and/or any of a large number of other local operation factors.

In order to assess possible AC flow conditions, a diversity of U.S. regional power flow cases were examined to establish estimated AC flow conditions for all 345kV and higher transmission lines in the power grid. However, there are important limitations even in this level of rigorous review, in that power flow cases are usually only developed for a limited set of snapshot estimates of grid conditions (usually at or near peak load conditions). Therefore, they do not provide a reliable cross-section of the extremes of low AC system flow conditions that are also possible.

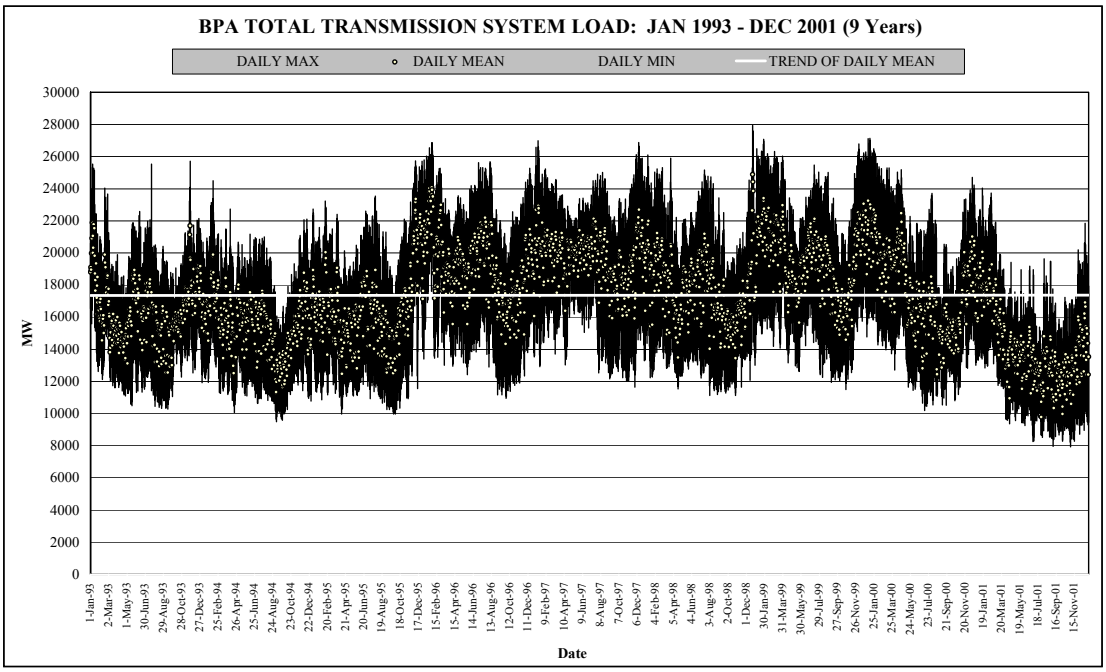

Figure 4-7. Plot of BPA transmission system load variations over 9 year period from 1993 to 2001.

4.4 U.S. Power Grid Assessment for Severe Blast Wave Disturbance Scenarios

Using the limited knowledge available of possible AC loadings of transmission lines, a comparison of simultaneous AC and GIC current flow conditions were calculated for the two most severe Blast Wave disturbance scenarios. As previously discussed, a series of Blast Wave disturbances were simulated and variations in the positioning of the largest region of disturbance impacts. Blast Wave disturbance scenarios B16a and B16b were the two disturbances that produced the largest cumulative impacts on the U.S. power grid.

Figures 4-8 and 4-9 provide a summary of the pattern of GIC flows in the U.S. power grid respectively for Blast Wave disturbances B16a and B16b. As illustrated, both disturbances produced very large and very widespread GIC flows. Case B16a, which has the largest disturbance impact centered over the New York region, produced a large pattern of GIC flows in the eastern portions of the U.S., while the GIC flows were lower in the western portions of the U.S. Case B16b, which had the disturbance impacts centered towards the Chicago area, produced generally consistently large GIC flows in both the eastern and western portions of the U.S. grid, though in this case the GIC flows in the east are noticeably reduced compared to Case B16a. Both cases present large widespread threats of power system collapse to the U.S. grid, as previously discussed. This assessment will attempt to determine the possible threat of large scale circuit breaker failure posed by such large scale disturbance threats.

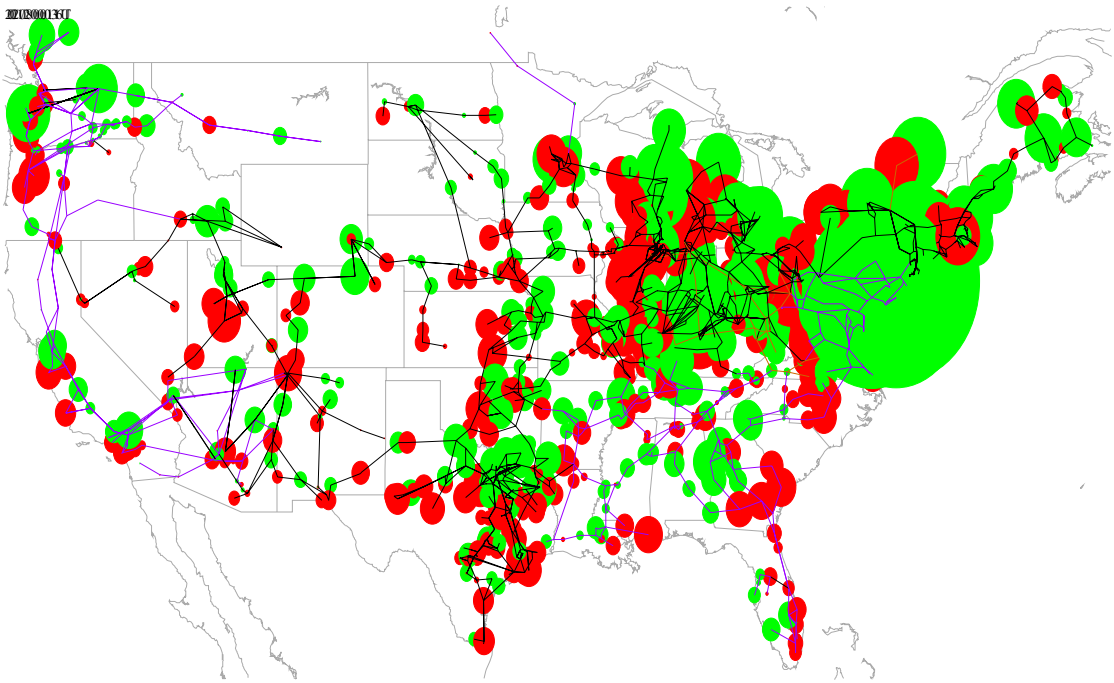

Figure 4-8. Pattern of GIC flows in U.S. power grid for Blast Wave Case B16a.

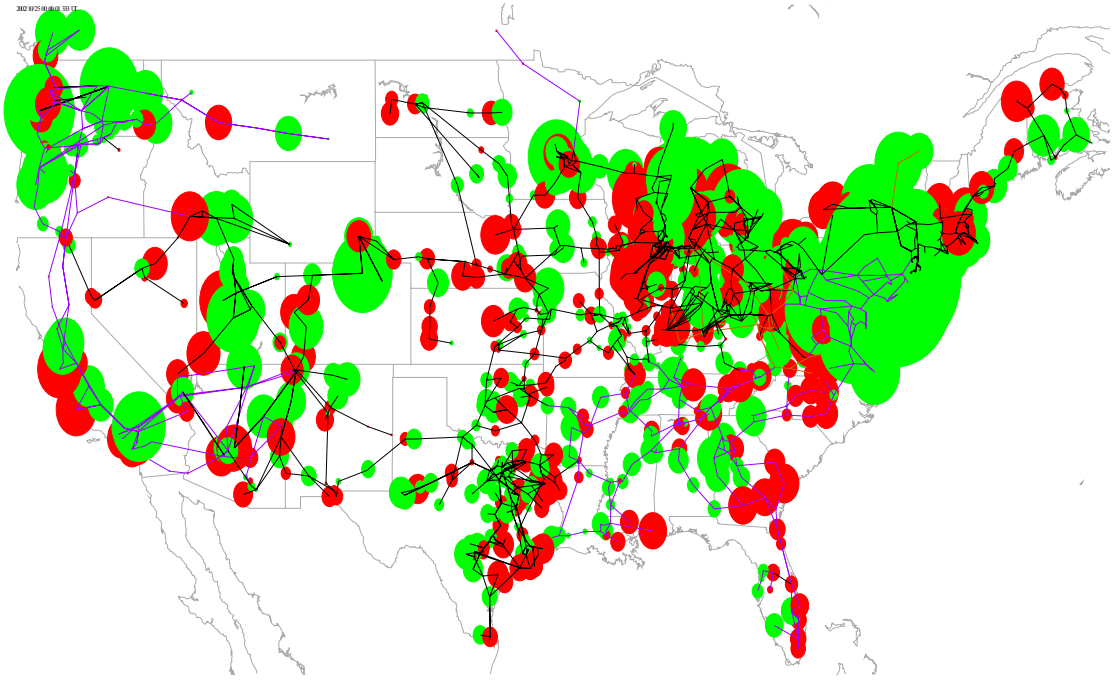

Figure 4-9. Pattern of GIC flows in U.S. power grid for Blast Wave Case B16b.

Because there are three asynchronously operated grids in the U.S., an analysis of combined AC and GIC flow conditions on these grids has to be done separately. In the case of the Eastern U.S. grid, the powerflow cases assessed were provided by the MAPP, SERC, PJM and IMO power pools. These cases generally indicated uniform agreement on the overall pattern of AC loading on each of the 345kV and higher operating voltage

transmission lines, with the caution as previously noted that large variations are possible due to changing system and local configuration conditions on any of these lines. Figure 4-10 provides a summary of combined AC and GIC flow conditions on transmission lines in the Eastern U.S. grid for the B16a Blast Wave case. The AC current loading was as provided by the MAPP power flow model for the Eastern U.S. grid. Note that the data has been ordered by increasing AC load and that corresponding GIC load does not follow a similar consistent pattern with respect to AC current load. Figure 4-11 provides the same AC/GIC comparison for the Eastern U.S. transmission network using a powerflow case provided by the SERC pool. These two independent models provide very similar results. As shown in these two comparisons, there are a large number of lines where the estimated GIC flow will be larger than the expected AC line currents. In some extreme cases, the levels of GIC will even exceed 10,000 Amperes.

Figure 4-12 provides a similar summary of AC and GIC current load conditions for the Eastern U.S. grid for Blast Wave Case B16b. As expected, the B16b case produced a large number of situations in which the GIC exceeded the AC currents, however, some of the largest GIC peaks are also reduced from those observed for Case B16b.

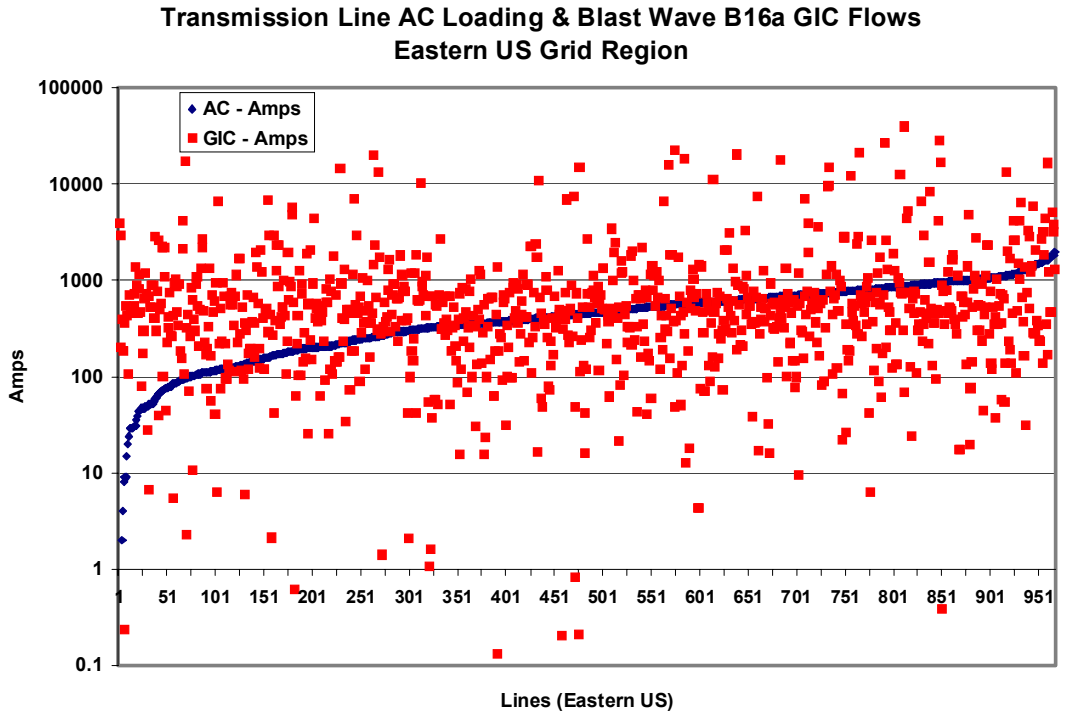

Figure 4-10. Summary of combined Eastern U.S. transmission line simultaneous AC and GIC current loadings for Case B16a, using MAPP powerflow model.

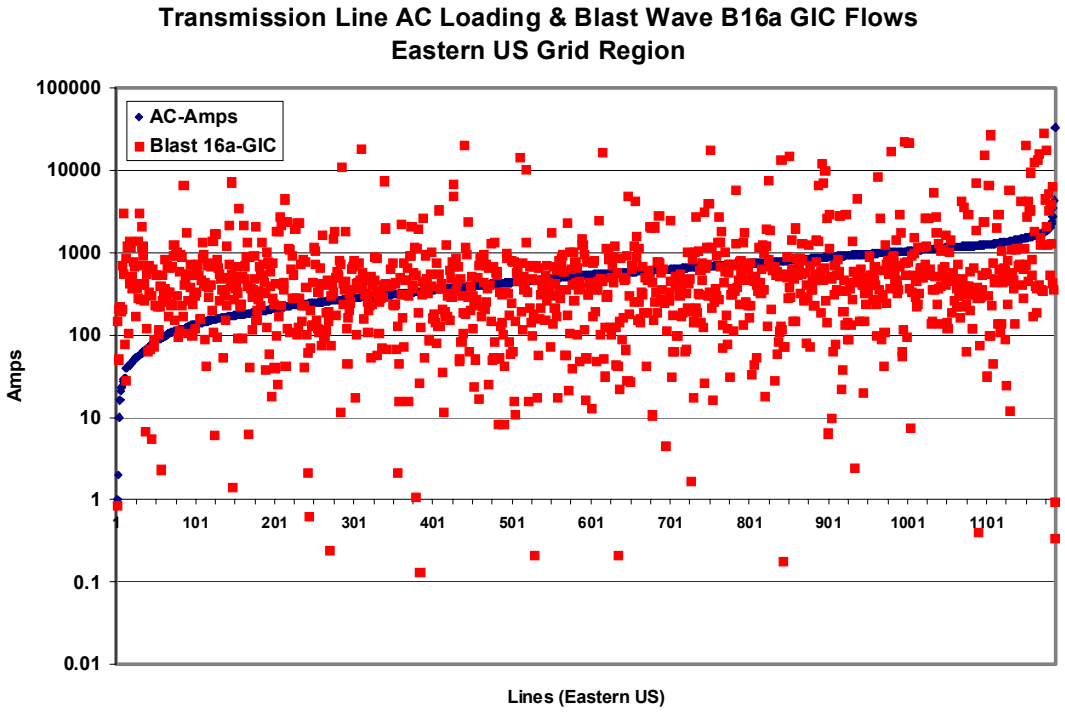

Figure 4-11. Summary of combined Eastern U.S. transmission line simultaneous AC and GIC current loadings for Case B16a, using SERC powerflow model.

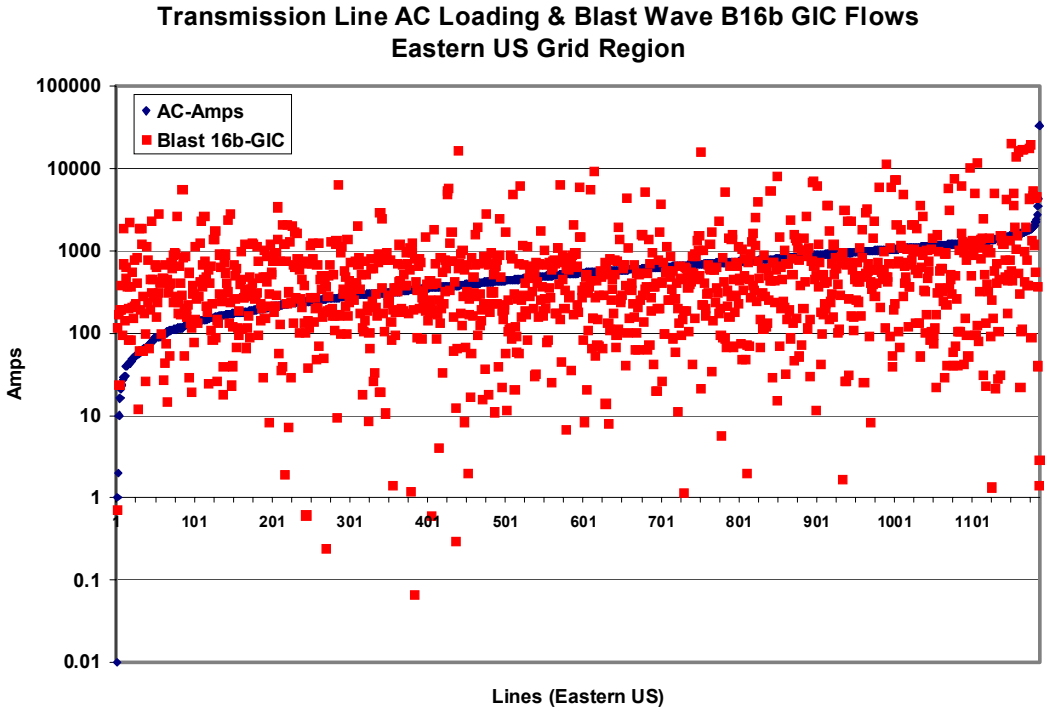

Figure 4-12. Summary of combined Eastern U.S. transmission line simultaneous AC and GIC current loadings for Case B16b, using SERC powerflow model.

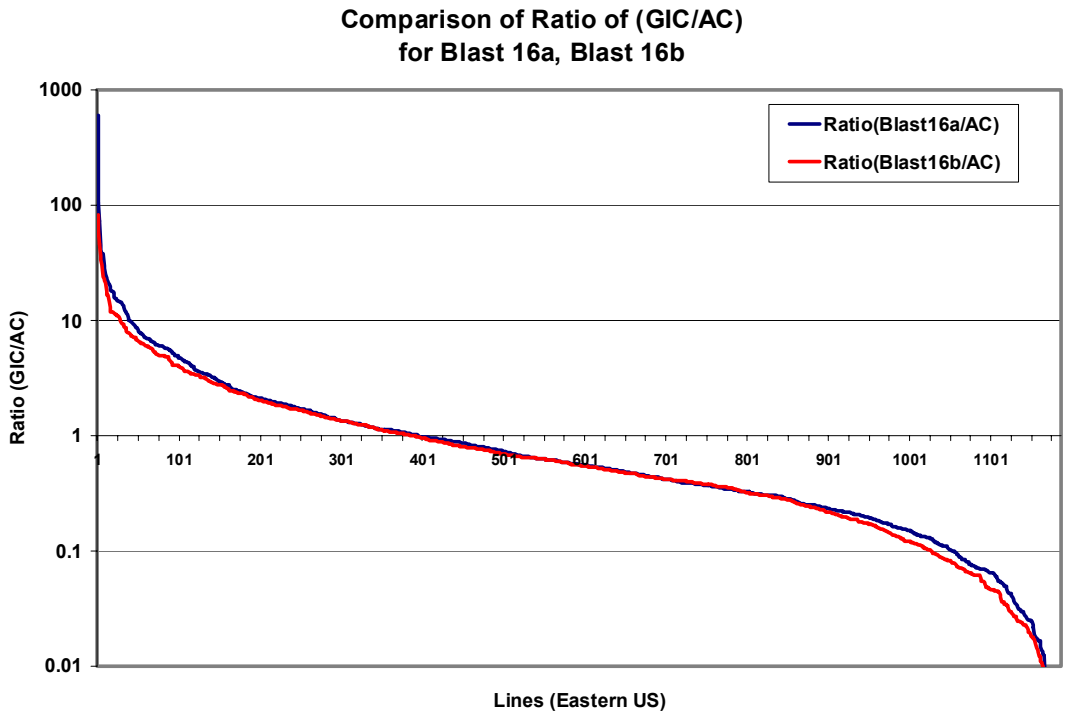

Figure 4-13. Summary of ratio of (GIC/AC) current flows for Eastern U.S. transmission lines for Blast Wave Cases B16a and B16b.

In all cases, it is important to note that as the level of AC current load increases on the transmission line, the probability decreases that the GIC will be larger than the AC current. As previously discussed, the ratio of GIC to the level of AC current flow conditions provides the best indicator of possible circuit breaker current interruption concerns. A workable estimate can be developed by calculating the population distribution from this analysis of all lines with GIC/AC current ratios that exceed one. Figure 4-13 provides this ratio summary for both the Case B16a and B16b disturbances. With the exception of a few large GIC/AC ratios, the population distribution for both cases is very similar. As shown by this comparison, both cases indicate ~400 transmission lines where the GIC will exceed the AC current flows. Using an extrapolation that most lines have ring or breaker and a half configurations at each line end, each line may require up to four breakers to operate to clear the line. This implies as many as ~1600 breakers are potentially at risk due to large GIC flows. A similar analysis was also conducted for the ERCOT grid (i.e. Texas). Figure 4-14 provides a summary of AC and GIC current loads for the ERCOT grid for Blast Wave Case B16a, while Figure 4-15 provides the similar comparison for Blast Wave Case B16b. It is important to note that, with respect to ERCOT, neither of these two cases would be a worst-case scenario for this region. However, the Blast cases that were centered over the Dallas region were not cumulatively as large for the U.S. as these two scenarios. Figure 4-16 provides a summary plot of the ratios of GIC/AC for this region for both Cases B16a and B16b. As indicated, Case B16a is slightly more severe in that approximately 40 lines have ratios exceeding 1, while for Case B16b, only ~20 lines have ratios in excess of 1.

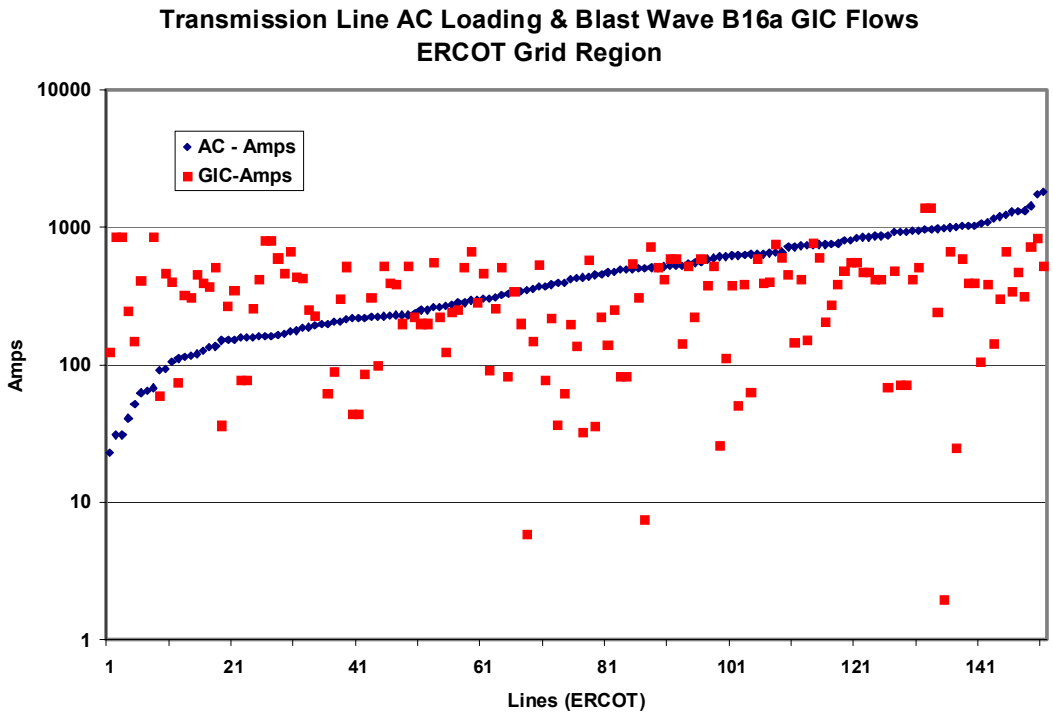

Figure 4-14. Summary of combined ERCOT transmission line simultaneous AC and GIC current loadings for Case B16a.

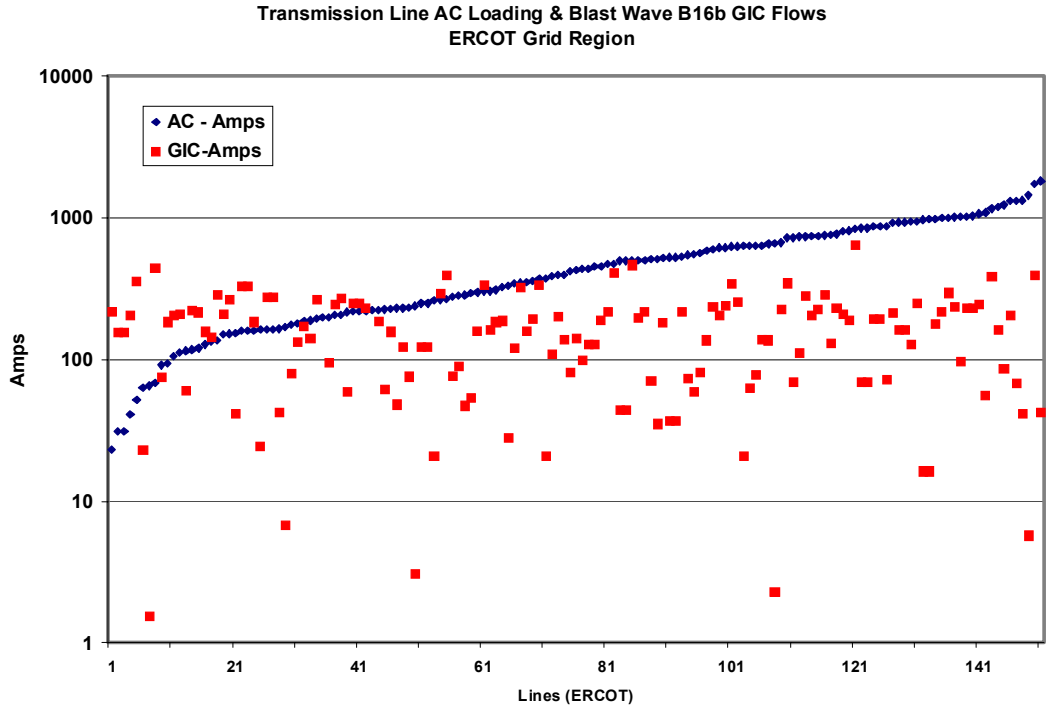

Figure 4-15. Summary of combined ERCOT transmission line simultaneous AC and GIC current loadings for Case B16b.

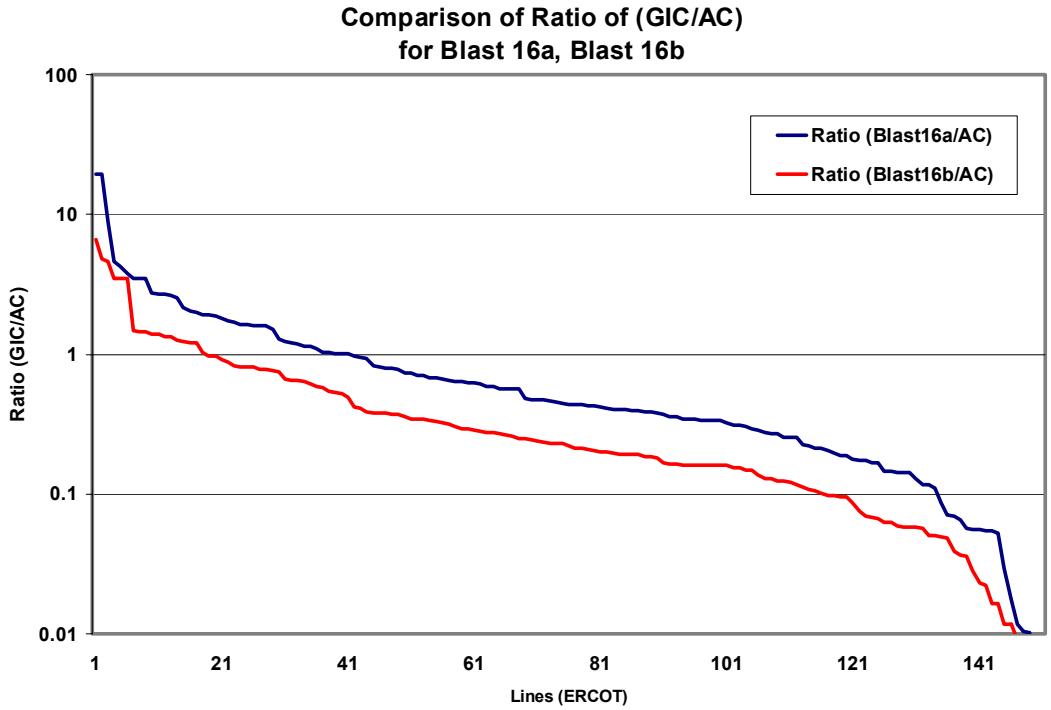

Figure 4-16. Summary of ratio of (GIC/AC) current flows for ERCOT transmission lines for Blast Wave Cases B16a and B16b.

A similar analysis of Blast Wave Cases B16a and B16b was also conducted for the WECC system covering the western U.S. The WECC, unlike the rest of the U.S., has a large number of transmission lines that are series compensated so that no GIC flows would occur. Approximately a third of all WECC lines at 345kV and higher that were modeled have series compensation. In spite of this, there are large GIC flows that will still occur in this region through the uncompensated transmission lines. Figures 4-17 and 4-18 provide summary plots of the simultaneous AC and GIC flows for Cases B16a and B16b. As shown, Case B16b is more severe in this region, as the blast center for this case has a more pronounced impact on the western grid than that for the B16a scenario. Figure 4-19 provides a summary of the ratios of GIC/AC for the two cases for the WECC region. As expected, Case B16b will produce a larger number of transmission lines and associated breakers with ratios of GIC exceeding the AC currents. For Case B16b, the number of lines at risk is ~60 while for Case B16a the number of at risk lines is ~20. As with the case for ERCOT, neither B16a nor B16b represented the worst case scenario when looking at impacts for the WECC region in isolation.

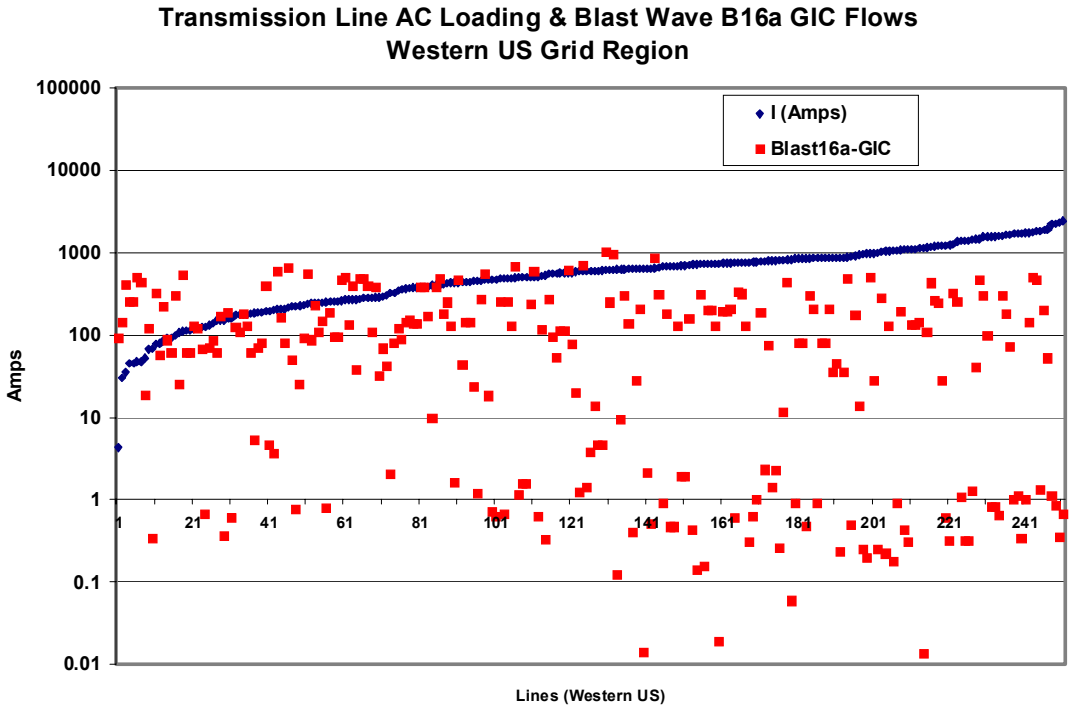

Figure 4-17. Summary of combined WECC transmission line simultaneous AC and GIC current loadings for Case B16a.

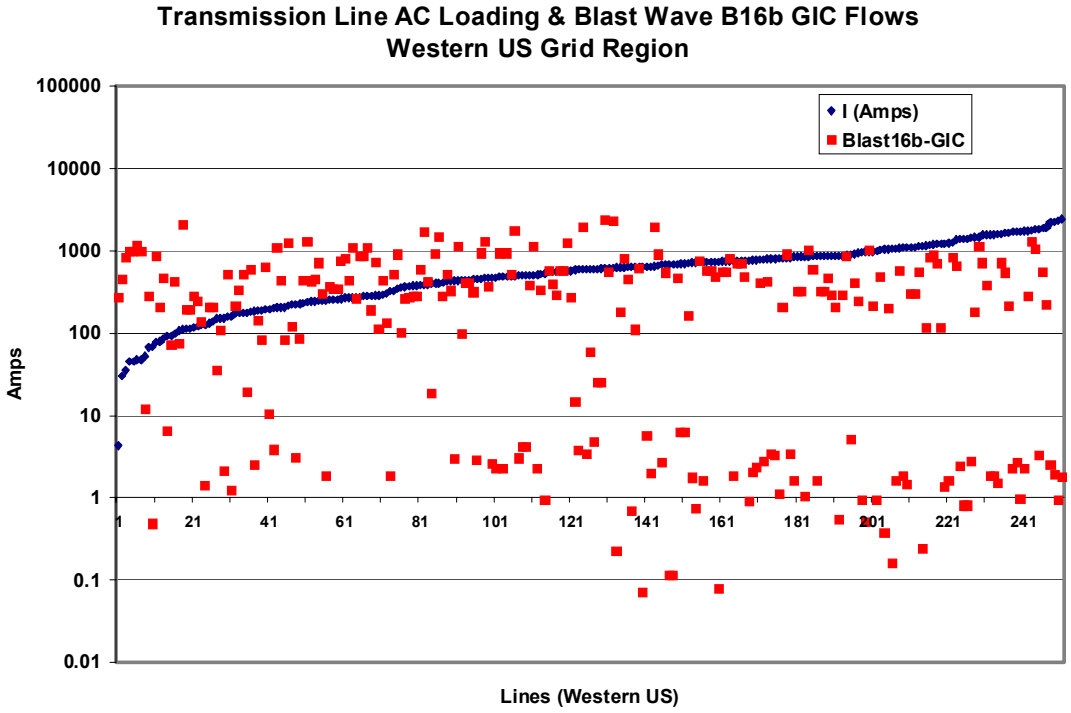

Figure 4-18. Summary of combined WECC transmission line simultaneous AC and GIC current loadings for Case B16b.

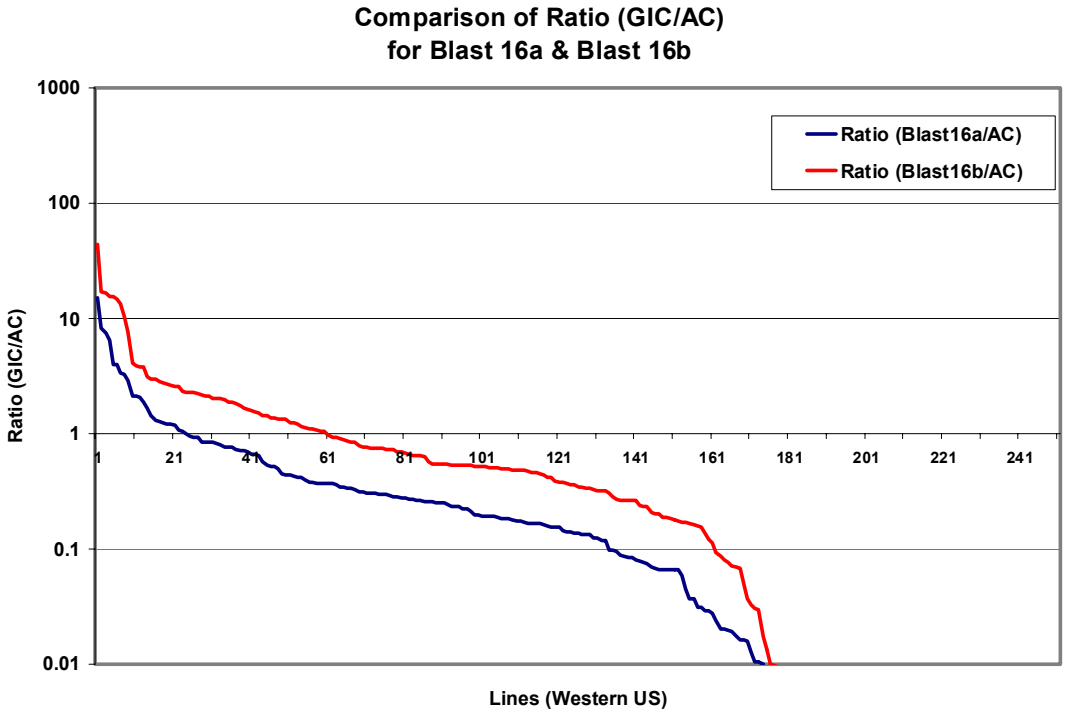

Figure 4-19. Summary of ratio of (GIC/AC) current flows for WECC transmission lines for Blast Wave Cases B16a and B16b.

In looking at the total impacts across the U.S. for each of these two Blast Wave cases, the ratio of GIC/AC summaries provide the best guidance. Each of these two cases had very similar total impacts, in that for Case B16a, ~460 lines had GIC exceeding AC flows, while for case B16b, approximately 480 lines had GIC flows exceeding AC currents. When either of these sets of at risk lines is extrapolated to include circuit breakers on the 345kV and higher transmission infrastructure, one finds ~1500 to 2000 circuit breakers at-risk, a level that is approximately 1/3rd of the entire U.S. population of circuit breakers. The widespread distribution of these at-risk assets across the U.S. is also important. Figures 4-20 and 4-21 provide maps of the locations of line terminals for all of the at-risk lines with a ratio of GIC/AC of 1.5 or greater for Blast Wave Cases B16a and B16b. These locations are the line terminals for each end of the line above the 1.5 ratio and would therefore also provide the location of the substation with the associated at-risk circuit breakers for these lines. Blast Wave Case B16a produces a weighting of potential circuit breaker impacts that is more easterly dominated than for Case B16b due to the differences in where the maximum disturbance impacts were centered. In both cases, the potential is present for large scale debilitating impacts to the integrity and restoration of the U.S. grid should permanent damage occur to the circuit breakers in these regions. Especially noteworthy is the clustering of impacts around major population centers.

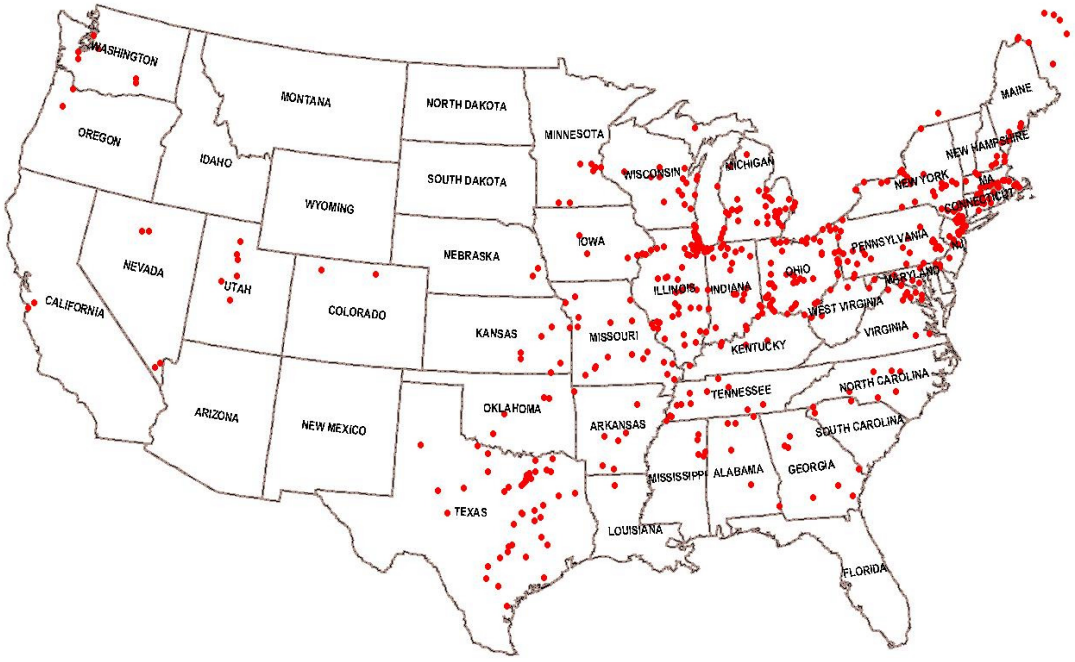

Figure 4-20. Location of at-risk circuit breakers for Blast Wave Case B16a.

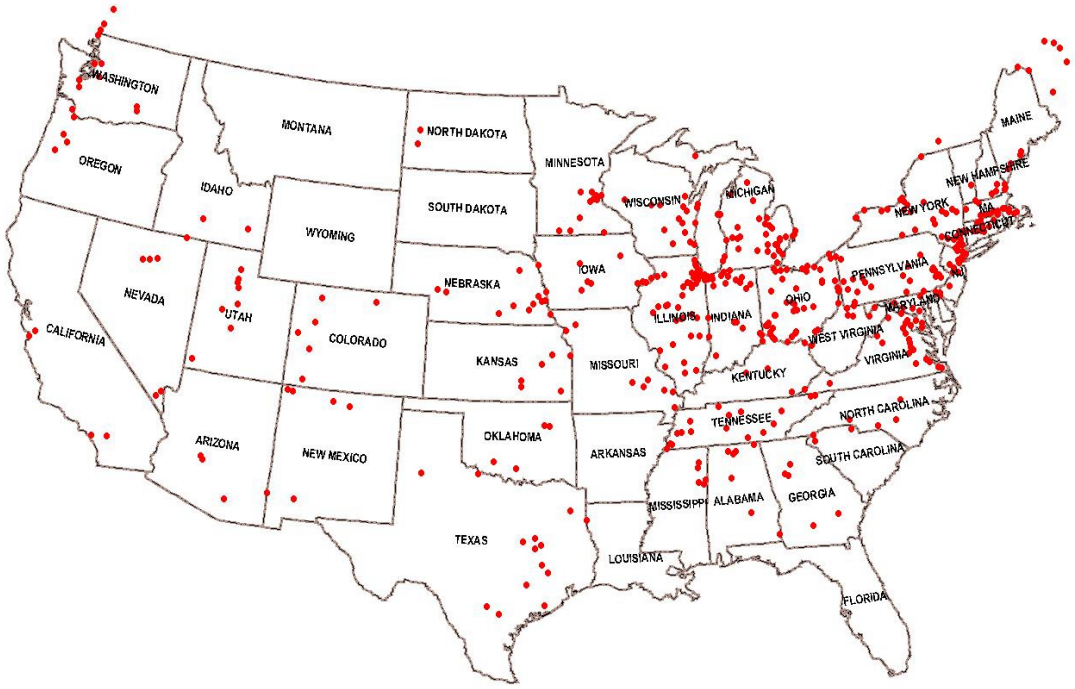

Figure 4-21. Location of at-risk circuit breakers for Blast Wave Case B16b.

4.5 U.S. Power Grid Assessment for Severe E3B Heave Disturbance Scenarios

The prior assessment provided a summary of potential circuit breaker impacts due to the two most severe Blast Wave scenarios. As previously discussed, the Heave disturbance scenarios will not produce as widespread or as large magnitude GIC flows as those caused by the Blast Wave disturbances. However, even the regional level of GIC flows could raise the concern of circuit breakers being faced with the duty of attempting to interrupt large GICs that may be in excess of AC current flows. The two largest E3B Heave disturbance scenarios were Cases 16d and 16e, which were high altitude devices positioned over eastern U.S. locations. The pattern of GIC flows for these two cases are as shown in Figures 4-22 and 4-23.

As shown, both of these cases produce large GIC flows in the eastern U.S. portions of the power grid. Figures 4-24 and 4-25 provide a summary of simultaneous AC and GIC flows in transmission lines in the eastern portion of the U.S. power grid. In comparison to the Blast Wave results for the eastern portions of the U.S. as summarized in Figure 4-10, the levels of large GIC flows are reduced nearly an order of magnitude. However, there still remain a number of examples where the GIC is larger than the AC current and therefore could pose a hazard to circuit breaker operation. Of these two specific Heave disturbance scenarios, Case 16d has ~100 lines at-risk, while Case 16e has ~70 lines at-risk due to large GIC flows. Figures 4-26 and 4-27 provide maps of the locations of line terminals for all lines with a GIC/AC ratio of 1.5 or greater. These results also indicate that debilitating impacts on a regional basis could also occur to these portions of the U.S. grid, or by extension into other regions that are in the footprint of these Heave disturbance environments.

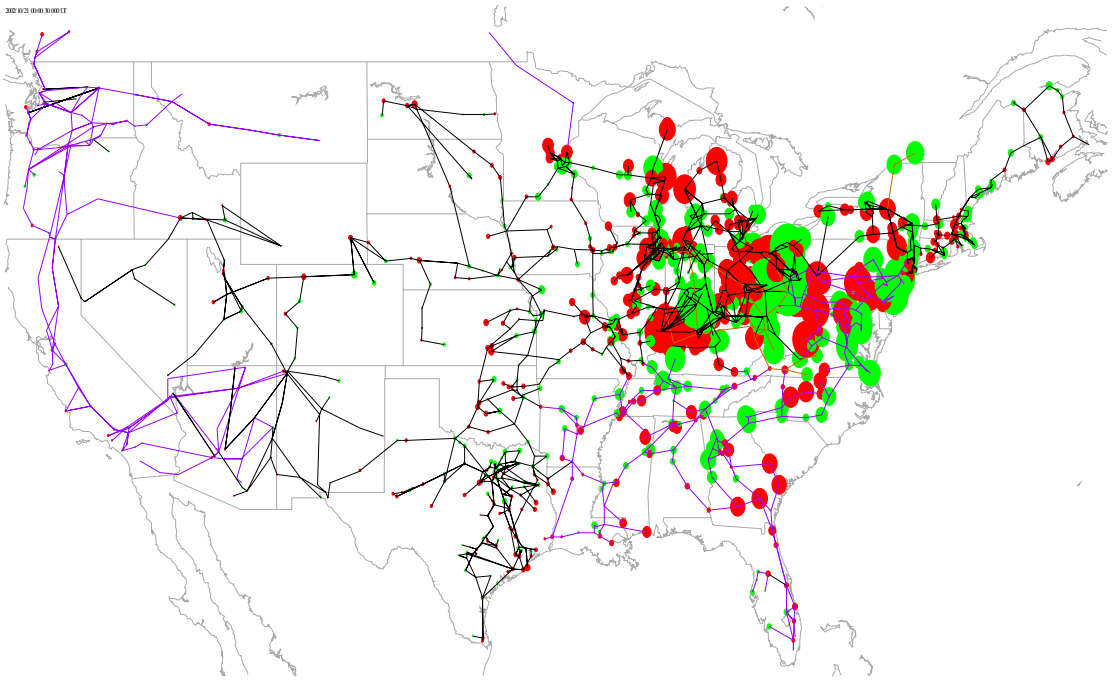

Figure 4-22. Pattern of GIC flows in U.S. power grid for Heave Case 16d.

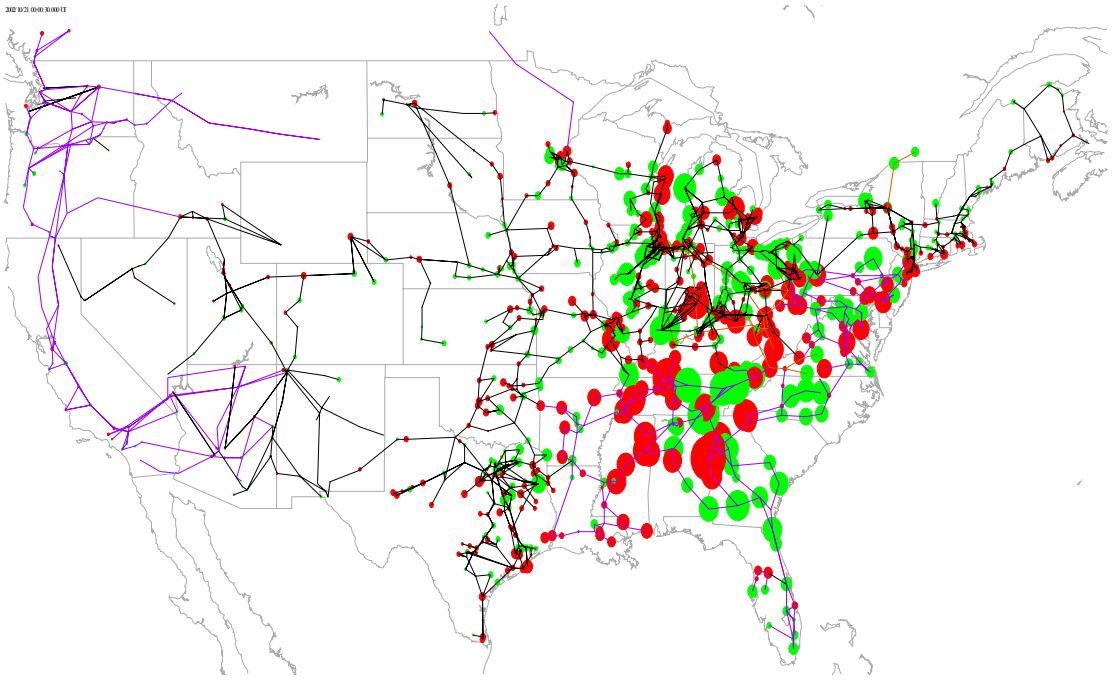

Figure 4-23. Pattern of GIC flows in U.S. power grid for Heave Case 16e.

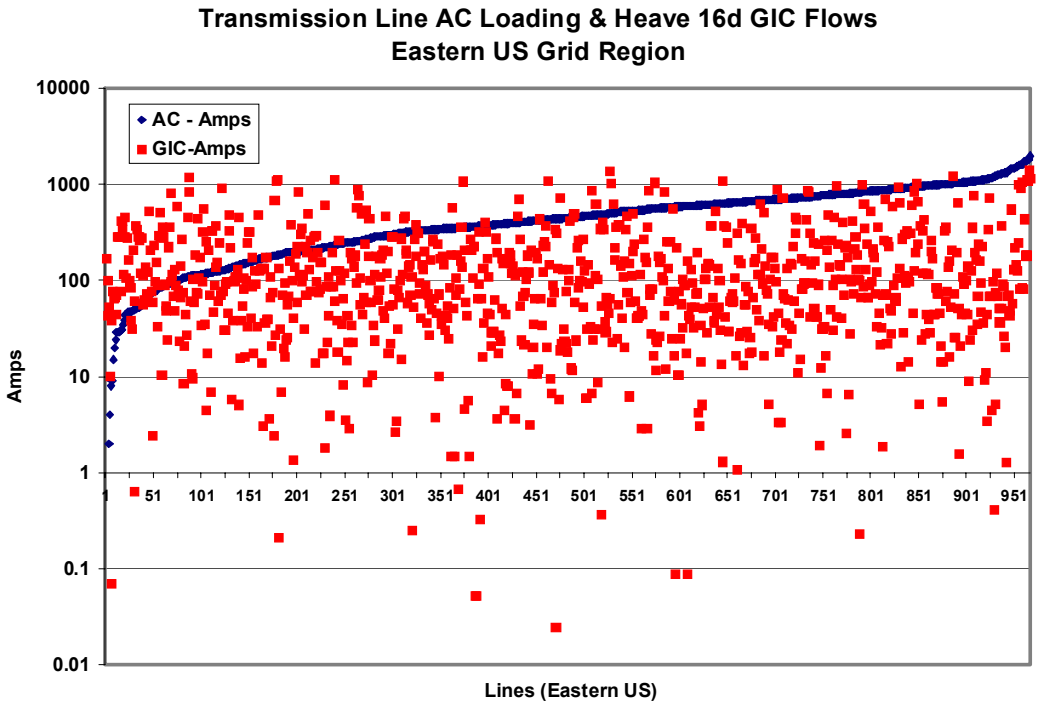

Figure 4-24. Summary of combined Eastern U.S. Grid transmission line simultaneous AC and GIC current loadings for Heave Case 16d.

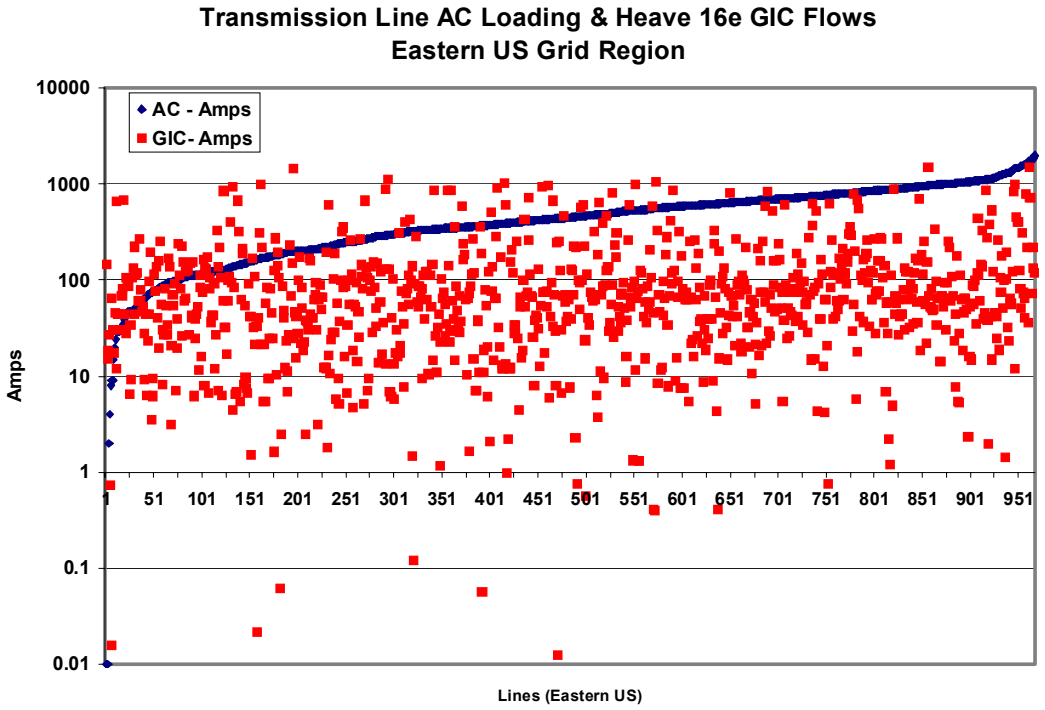

Figure 4-25. Summary of combined Eastern U.S. Grid transmission line simultaneous AC and GIC current loadings for Heave Case 16e.

Figure 4-26. Location of at-risk circuit breakers for Heave Case 16d.

Figure 4-27. Location of at-risk circuit breakers for Heave Case 16e.

Section 5
Power Grid Damage and Restoration Concerns Due to Large E3-Initiated Power Grid Collapses

5.1 Overview

As summarized in prior sections of this report, disturbance scenarios have been performed to examine the potential for E3 environment impacts on the Electric Power Grid infrastructures in regions of the U.S. While the full analysis of these scenarios will require the consideration of combined E1 and E3 impacts, this initial analysis will consider only the impact due to the large E3 currents that will occur to the electric power infrastructure. Several additional cases were simulated, the three cases that are used in this analysis were high altitude detonations centered over the New York region, the Los Angeles region and near Columbus, Ohio. The New York and Los Angeles cases were selected specifically to examine the possible damage-causing and restoration potential for such attacks over large population regions.

In examining large power grid blackout experiences, it is important to emphasize that there will be important differences in the events that have occurred due to relatively benign initiating causes and the events that could unfold due to either severe geomagnetic storm activity or the E3 environment of an intentional EMP attack. These scenarios also have a footprint that can simultaneously threaten large geographic regions and can plausibly trigger even larger regions of grid collapse than that which occurred on August 14, 2003. Therefore, depending on the morphology of the disturbance, it would be conceivable that a power blackout could readily impact areas and populations larger than those of the recent August 14, 2003 blackout. Further, the nature of these disturbances poses the added possibility of permanent and highly disruptive failures to key substation apparatus such as large capacity EHV transformers and EHV circuit breakers. These devices, when they have failed in the past, have a tendency to fail in a highly catastrophic fashion. Circuit breakers and their relatively fragile porcelain bushings and in some designs porcelain operating heads can become a source of shrapnel. This can pose a risk beyond the destruction of the breaker itself to personnel or other apparatus within the substation that are within range of the possible explosion. Catastrophic failures to large transformers have also resulted when these devices are caused to have internal faults due to heating. These apparatus, because they utilize many thousands of gallons of oil for cooling and high voltage insulation purposes, come with a ready made source of fuel for generating large fires. When the transformer tanks rupture due to the failure, the spreading oil becomes a fire accelerant that can rapidly engulf major portions of the substation and/or power plant facility where the apparatus is located. Unless there is a large deluge system as part of a fire suppression system already built into the facility, there are no practical means of intervening to control the fire-caused damage. Responders generally have to let the fire burn itself out first. Large GSU (generator stepup) transformers are designed with exceptionally low resistance and integrated into the low resistance EHV transmission grid. It is these transformers, in particular, that will carry very large GICs during severe geomagnetic storms or from the E3 environment and become the most likely transformers to fail disruptively. Because nuclear plants are also

of such large average size, the transformers at these facilities can be of particular concern and a resulting large transformer catastrophic failure at these locations can pose the possibility and complication of control and safety system failures for the nuclear facilities at these locations.

The nature of these scenarios will pose challenges that are well-beyond the power industries experience base for size of power grid collapse and the consequential concerns of collateral damage that may result from the source disturbance environment. The threats to large metropolitan regions may pose special challenges for restoration and there is some evidence in particular from the long-duration Auckland business district blackout (and to a much lesser extent the Chicago 1999 distribution substation outages). However, the potential size and complexity issues could be substantially larger for a metropolitan scenario involving either New York City or Los Angeles.

While the August 14, 2003 event provides a good case study, it may not provide the most reasonable expected outcome should either a severe geomagnetic storm or intentional EMP attack occur on the U.S. power grid infrastructure. The utilities and various municipal organizations should be commended for the rapid and orderly restoration efforts that occurred after August 14, 2003. However, it should also be acknowledged that in many respects this blackout occurred during highly optimal conditions that were somewhat taken for granted and should not be counted upon in future blackouts. For example, an outage on January 14 rather than August 14 could have meant coincident cold weather conditions. Particularly, if it is an intentional attack and the enemy is sophisticated enough to develop a high capacity EMP device, then they would also be sophisticated enough to subscribe to "The Weather Channel" and launch their attack under conditions which could greatly magnify the debilitating impacts of their assault on critical infrastructures. For example under very cold-weather conditions, breakers and equipment at substations and power plants can be enormously more difficult to re-energize when they become cold. This can translate into the possibility of significantly delayed restorations. Large GICs from the E3 or geomagnetic storms as previously discussed can also permanently damage key transformers on the grid, which further burdens the restoration process.

5.2 New York Scenario

Figure 5-1 denotes the area of power grid disturbance and collapse due to the large E3-related stress. Wider regions of collapse are likely, due to progressive collapse/cascade. The size of this collapse area in total would be of unprecedented scale. For restoration analysis purposes, it is assumed that adjoining areas to the regions outlined above would be able to achieve nearly complete restoration within approximately 24-72 hours, while the regions outlined in black border region may take substantially longer. E3 impacts to infrastructure and resultant impact on restoration will be focused on the outlined areas as shown. Unfavorable weather conditions (particularly cold-weather) should be assumed as an important complicating factor that would have potential to make restoration of all facilities and infrastructures more problematic. E1 impacts, when they are more fully detailed, will add further complicating factors to the restoration process.

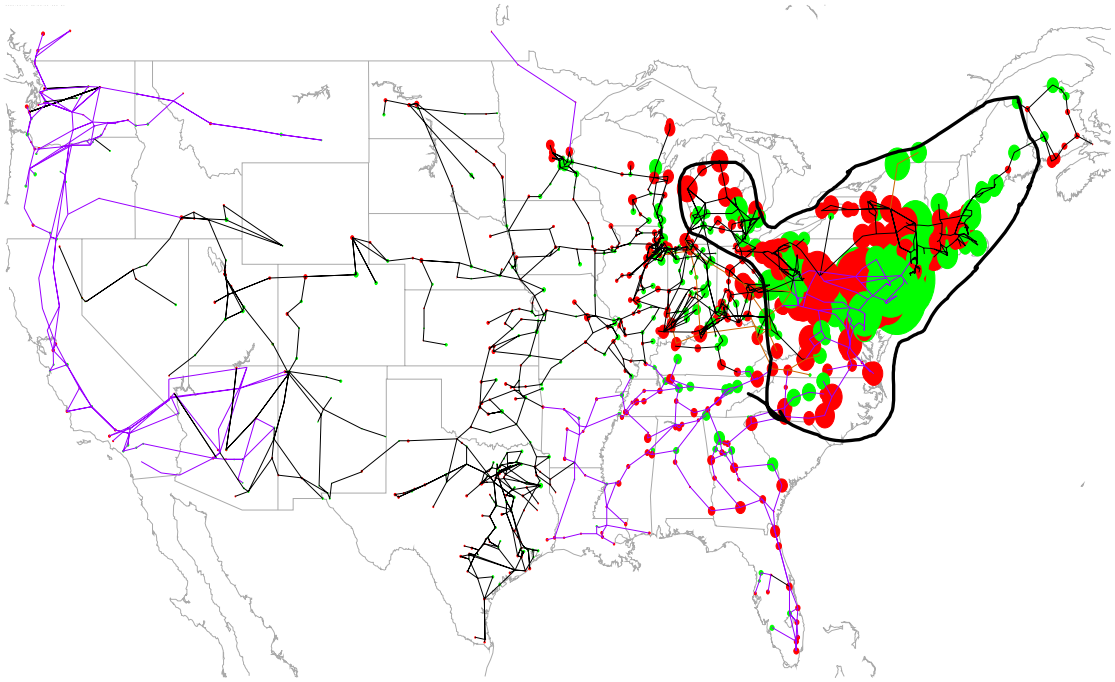

Figure 5-1. Heave over NY at time 30 Seconds.
Peak U.S. MVAR Demand – 95,366, Peak U.S. GIC-Eff – 88,026 Amps,
Grid Disturbance Energy Sum (sec 26-40) – 1,454,630. MVAR-sec.

5.2.1 Power Grid and Generation Plant Overview

Restoration will entail concerns about the ability to fully restore the function of needed power plants (especially those involved in blackstart) and the EHV power grid. Therefore, the impact of the disturbance on these portions of the infrastructure will be of most concern. Because the blackout region will encompass several pools and reliability regions, the ability to transfer power from neighboring regions will be of concern. In most respects, these interregional transfer capabilities are only a small fraction of the total load that needs to be served within a respective region. For example, the NY-ISO region has peak load demands that can approach ~30,000 MW, yet has transmission capabilities from outside the region that are less than 25% of these demand levels. In general, the same limitations will apply for all other regions, in that restoration will require the ability to restore normal operation of regional power plants to meet native load demands in the regions.

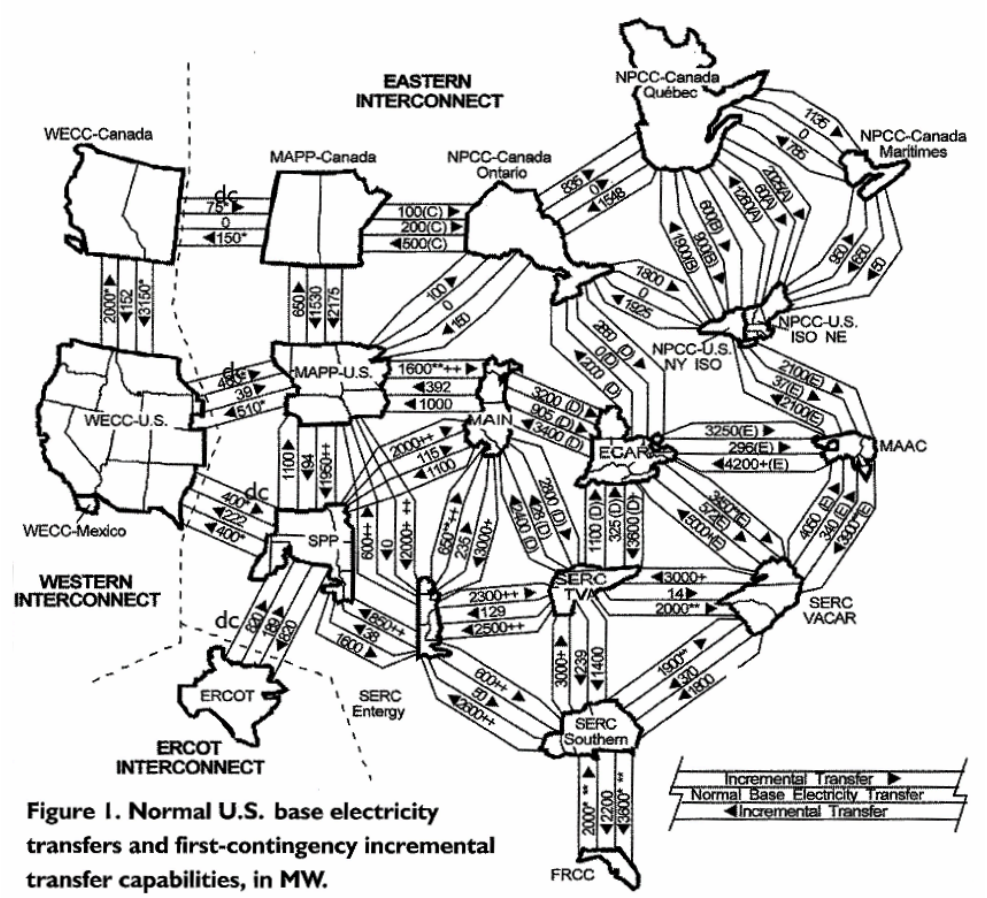

Figure 5-2. NERC map of interregional transmission network transfer capabilities.

In addition to age of plants, fuel type for generation will be an important consideration. Because of special restart issues, nuclear-fueled capacity would not be available for blackstart and largely unavailable for several days (best case assumption) and perhaps a significant chunk of this capacity would not be available for up to 12 months or longer. A worst-case assumption is to assume large GSU transformer failure occurs across this segment of the generation plant.

5.2.2 Power Plant Fuel and Capacity Overview

Hydro, coal and petrol fueled facilities may be the only ones that could be available for blackstart, natural gas may not be available for blackstart, if this infrastructure cascades into failure due to loss of electric power or from direct E1 impacts on control systems. Therefore, the availability of natural gas should be suspect due to the potential for interdependency issues with the operation of pipeline systems. Hydro may also be adversely affected due to time of year. Much of the petrol and hydro are small plant facilities and may not be available to run on a baseload basis at their nameplate capacity and may only be able to produce fractional amounts of power production (in MWH) over extended periods of time. Fuel reserves and storage onsite is only possible for coal and petrol units.

The following figures provide a concise summary of the size and diversity of power plants by nuclear, hydro and coal fuel type within the NY region. For general purposes, it would not be unreasonable to assume that most of the nuclear and natural gas fueled capacity in the region would not be readily available in the aftermath of a HEMP event.

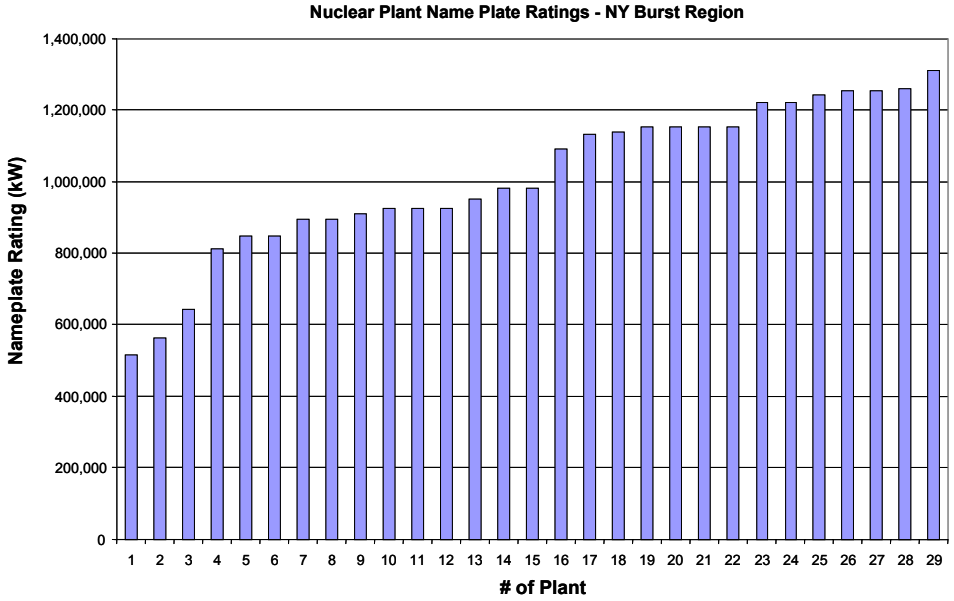

Figure 5-3. Average nuclear plant size is very large and would have large GSU transformers that could be readily exposed to large GICs.

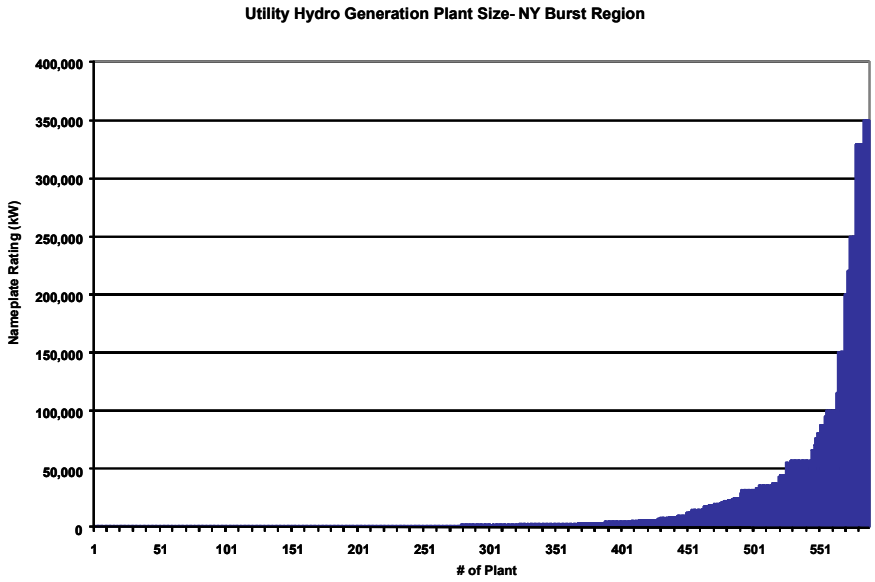

Figure 5-4. Average hydro plant size is very diverse, with an even larger number of small plant classes of generator plants. Many of the small to mid-sized plants are on small rivers, widely scattered and operate via "run-of-river" and would only be able to achieve full output for spring run-off. These would have limited reservoir or water storage available. It is likely that only generation along the Niagara Falls region would have sufficient water storage/cfm available for baseload operation.

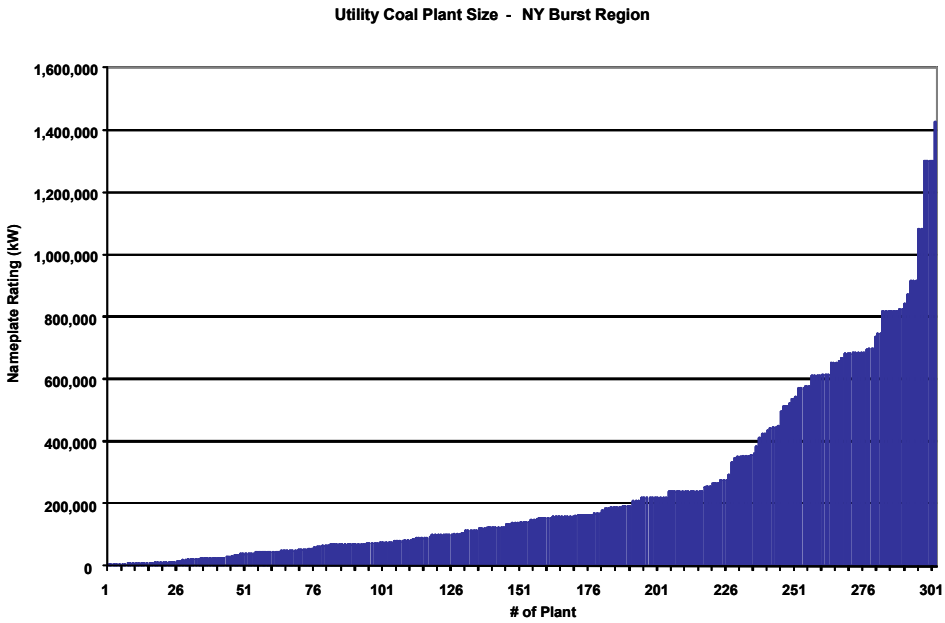

Figure 5-5. Average coal plant size is quite diverse, ranging from small to large plants that have capability to be run as significant baseload facilities. Most of the small plants have suspect ability to be run on a continuous basis. E1 impacts to control systems may be a very important concern. For example the furnace burns fuel energy at a rate ~equivalent to 1 Ton of dynamite per second. Major furnace/boiler explosions have been known to occur due to control system malfunctions and damage to these systems can be very catastrophic. E3 concerns and damage to large GSU transformers would also apply to the large size generation plants as well.

The blackstart capability and continuous power plant run capability will be heavily dependent upon the impact to power system and other interdependent infrastructures due to the E3 and E1 impacts of the HEMP attack scenarios. Only the E3 impacts are being considered in this report. For E3 events, the biggest impact concerns will arise from large EHV transformer failures and large EHV circuit breaker failures. Power plant generator heating and negative sequence concerns have also been attributed to geomagnetic storm conditions as well and those plants that are operating at the time of such an event may have the risk of damage due to the related E3 and GIC environments as well.

In assessing the blackstart capability, the assessment considers that nuclear-fueled generation and natural gas-fueled generating plants in the region will not be generally available due to interdependency issues that would cause these to be unavailable due to grid collapse across the region. Therefore, the ability to blackstart will heavily depend upon hydro, coal and petrol fueled generation capacity. These all have some limited fuel stockpiles or reserves that will generally provide the capability to operate for several days. Even a more moderate average demand in the NY region could be difficult to serve with the available nameplate capacity of these fuel types. The capacity shortage problems may become even more acute in some metropolitan regions, especially if there

are debilitating outages to key transmission network infrastructures. A more focused review of these concerns will be provided in the following subsections of the NY region analysis.

5.2.3 Overview of Potential Impacts to EHV Circuit Breakers due to High GIC Levels

As discussed in Section 3, one of the unique E3-caused risks to the U.S. EHV transmission network infrastructure could be posed by the extraordinarily high levels of GIC that could flow through EHV transmission system circuit breakers in the area of intense geo-electric field under the burst region. Circuit breakers are inherently incapable of DC current interruption and estimates provided by prior evaluations indicate that GIC levels in many cases could exceed the AC current levels causing a situation where there is no current zero crossing to accomplish normal circuit interruption in the circuit breaker. For the New York region scenario, Figure 5-6 provides a summary of the transmission lines and the expected AC current flows and expected GIC currents. As shown, a number of circuits will have the potential for GIC levels that could be substantially larger than the AC current flows.

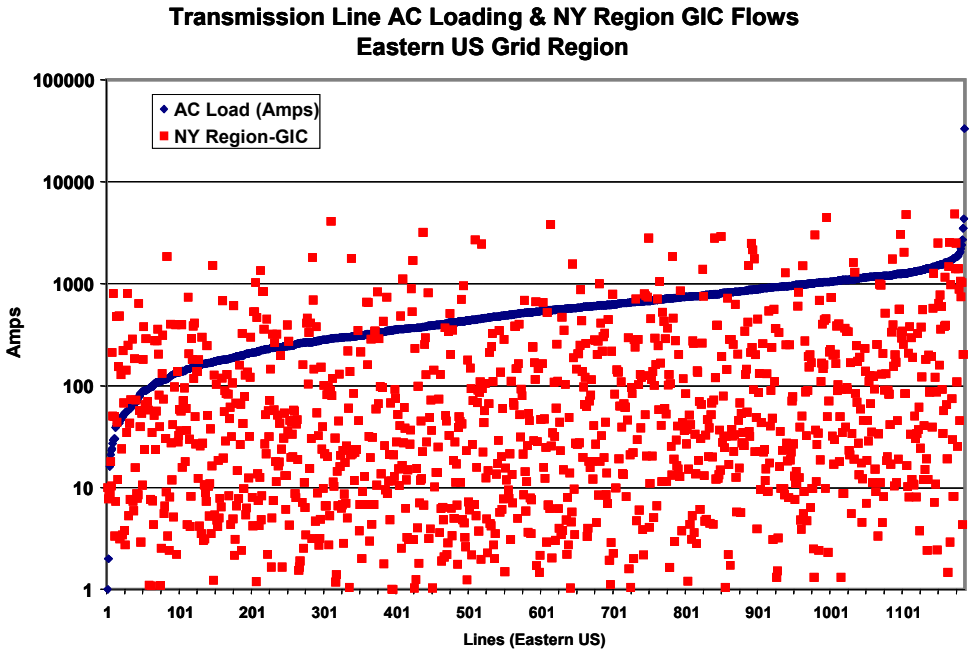

Figure 5-6. NY region and summary of AC current flows on various EHV transmission lines (blue dots) and simultaneous GIC current flows on the same lines (red dots). A number of lines have potential for GIC flows larger than AC currents, which leads to concerns about circuit breaker operation.

The large number of breakers at risk, as suggested by the comparison in Figure 5-6 is plotted as to their locations in Figure 5-7. In this map, the circuit breakers at each of the lines with large GIC flows would have circuit breakers that are exposed to potentially damaging levels of GIC. Figure 5-8 provides a map of the various EHV transmission lines in the region that could be rendered-out-of-service for long durations due to damage

at circuit breaker locations due to the high GIC levels. As shown, any of the colored lines (color difference denotes kV rating) is a line that may be unavailable due to circuit breaker problems. A large number of lines in Pennsylvania and New York state are at risk. If permanent damage to breakers at these locations occurs, restoration may take months for a large scale failure scenario such as this.

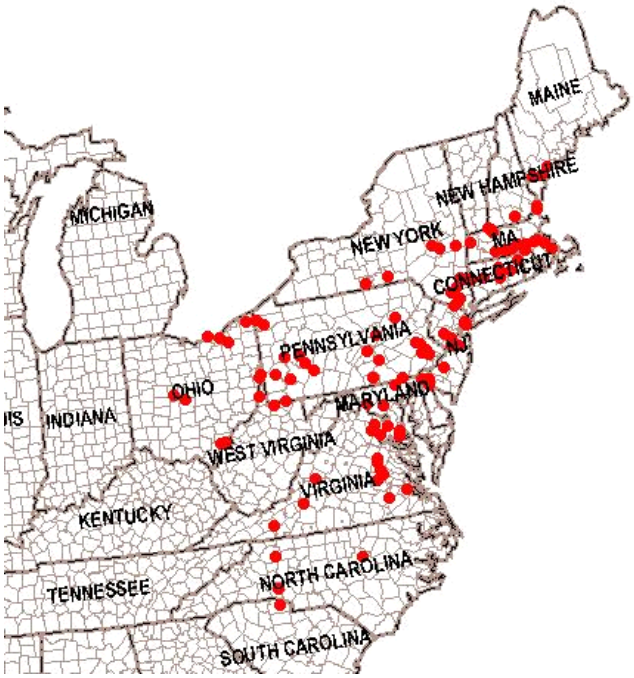

Figure 5-7. NY region - location of EHV circuit breakers at risk.

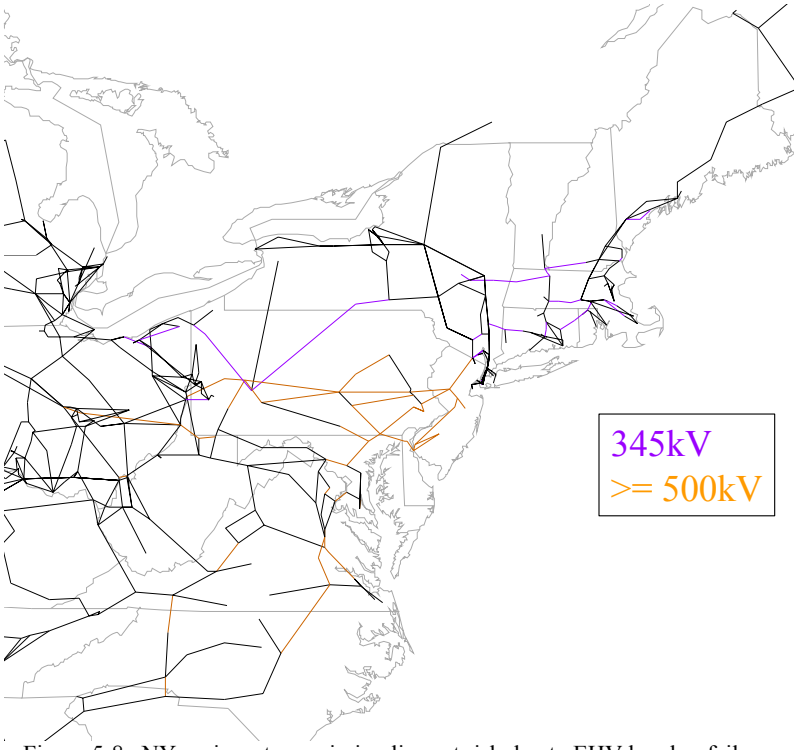

Figure 5-8. NY region - transmission lines at risk due to EHV breaker failure.

5.2.4 Overview of Potential Impacts to EHV Transformers due to High GIC Levels

Transformers failures and permanent damage are also of concern due to large GIC flows from either E3 threats or severe geomagnetic storms. Large EHV transformer failures have been well-documented due to GIC from naturally occurring and relatively low-intensity geomagnetic storm activity. Very large GICs from the E3 environment or extremely intense geomagnetic storms could pose the concern of large-scale and geographically widespread failures and permanent loss of EHV transformers on the network. If enough of these key assets are lost, the restoration of the EHV power grid could also be considerably delayed. Because there is considerable uncertainty as to the threshold level of GIC that will cause transformer failure, a minimum GIC level of 200 Amperes per phase has been selected as the screening level for possible transformer failure. This level of GIC would be at a level that is expected to be of unprecedented intensity, as transformer failures have generally been observed at much lower thresholds. Figure 5-9 provides a map of the location of all exposed EHV transformers with GIC of 200 amps per phase or greater. In addition to the geographically widespread distribution of the location of at-risk transformer, there is a large number of them. There are a total of 100 transformers in this at-risk category. If these all failed, it would constitute a resultant loss of ~73,000 MVA of EHV network transformation capacity at all voltages (typical of ~800 MVA per transformer).

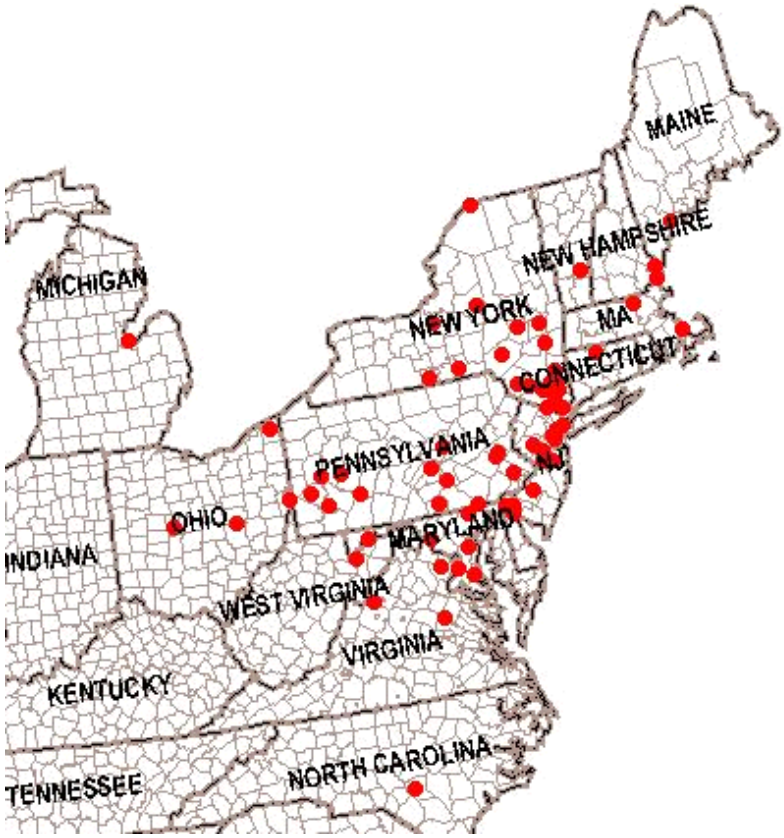

Figure 5-9. NY region - location of transformers at risk, GIC of 200 Amps or greater per phase.

These at-risk transformers also represent a diverse population of function as well as kV and MVA ratings. Figure 5-10 provides a population summary of the auto and non-auto transformer types, and their primary and secondary voltage ratings. This diversity underscores the problems of providing spare facilities for such large scale infrastructure failures. Normally, only a handful of transformers of this size are purchased for North American locations on an annual basis. The need for immediate replacement of such a large portion of the infrastructure would pose serious challenges and add considerable delays to the restoration process for the power grid.

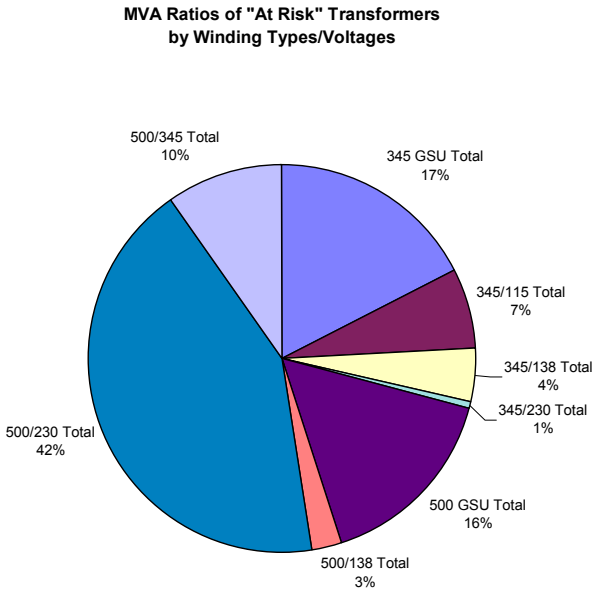

Figure 5-10. NY region - range of transformer sizes, and winding configurations that would be at risk.

Of particular concern would be the permanent loss of large GSU transformers at power plants in the region. The loss of these transformers causes a compounding of difficulties, in that the EHV transmission network is impaired along with the loss of output of vital and usually baseload generation resource for the power grid. If we assume that 200 Amps per phase would cause the loss of a GSU transformer, the combined loss of generation capacity in the NY region would be ~25,000 MW and the average size of each impacted power plant is ~1000 MW.

Even assuming a larger GIC threshold before assuming transformer failure would still cause extensive disruption of the grid. Figure 5-11 provides a map of the location of all transformers "at-risk" with levels of GIC of 500 Amps per phase or greater. Transformer failures would cause resultant loss of as many as 33 large EHV transformers with ~26,000 MVA of network transformation capacity at all voltages (typical size of ~1500 MVA per transformer). As indicated in this map and earlier maps, these failures would be clustered in and around major metropolitan regions in New York and Pennsylvania.

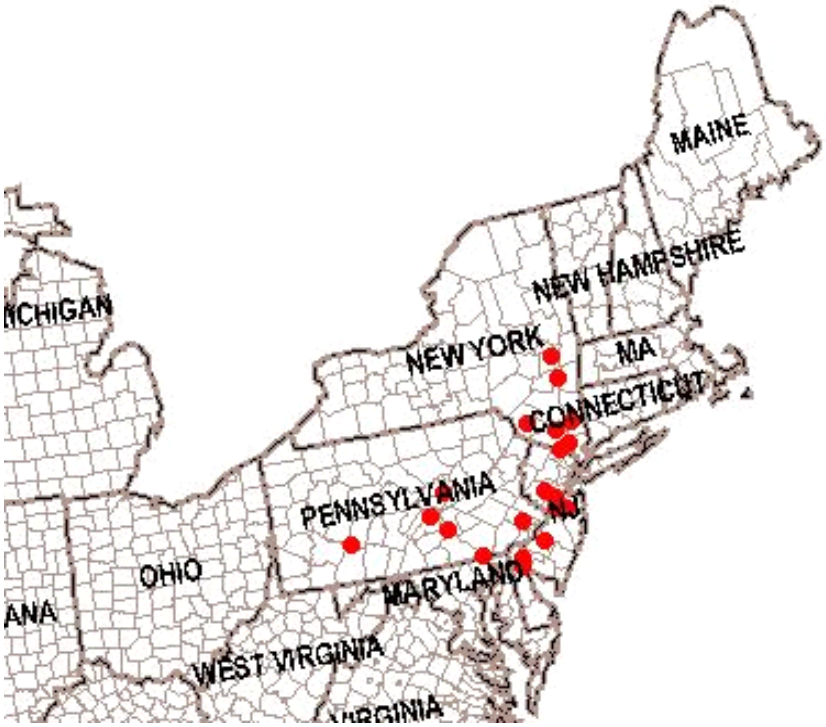

Figure 5-11. NY region - location of transformers at risk, GIC of 500 Amps or greater per phase.

5.2.5 Overview of Potential Impacts to Transmission Network Supply to New York City Regions

As evidenced from the prior analysis of possible E3-caused EHV circuit breaker failures (and resultant EHV transmission line outages) and E3-caused (or GIC-caused) transformer failures, many of the failures tend to cluster around the major metropolitan regions from Pennsylvania to New York. If enough failures or the right combination of failures occur, the possibility exists that a major metropolitan region, such as New York city could be isolated from the EHV Power Grid for an extended period of time and that very long duration power system outages could occur, or at least only very limited power system restoration could occur in the impacted region. This regional isolation scenario could come about due to combination EHV circuit breaker and EHV transformer failures in and around NY City that would physically isolate the region for an extended period of time. Since NY City has only a few geographic ties north and west (due to its nearly peninsular location), the region would be quite prone to transmission network isolation. The city is supplied by only a few 345kV transmission lines from the rest of the New York state power gird and via a few phase-shifter regulated and interties with New Jersey.

5.3 Los Angeles Scenario

Figure 5-12 denotes the area of power grid disturbance and collapse due to the large E3-related stress. Wider regions of collapse are likely, due to progressive collapse/cascade. The size of this collapse area in total would be of unprecedented scale. For restoration analysis purposes, it is assumed that adjoining areas to the regions outlined above would be able to achieve nearly complete restoration within approximately 24-72 hours, while the regions outlined in the black border region may take substantially longer. E3 impacts to infrastructure and resultant impact on restoration will be focused on the outlined areas as shown. Unfavorable weather conditions should be assumed as an important complicating factor that would have the potential to make restoration of all facilities and infrastructures more problematic. E1 impacts are also likely to add further complicating factors to the restoration process, but are not included in this analysis.

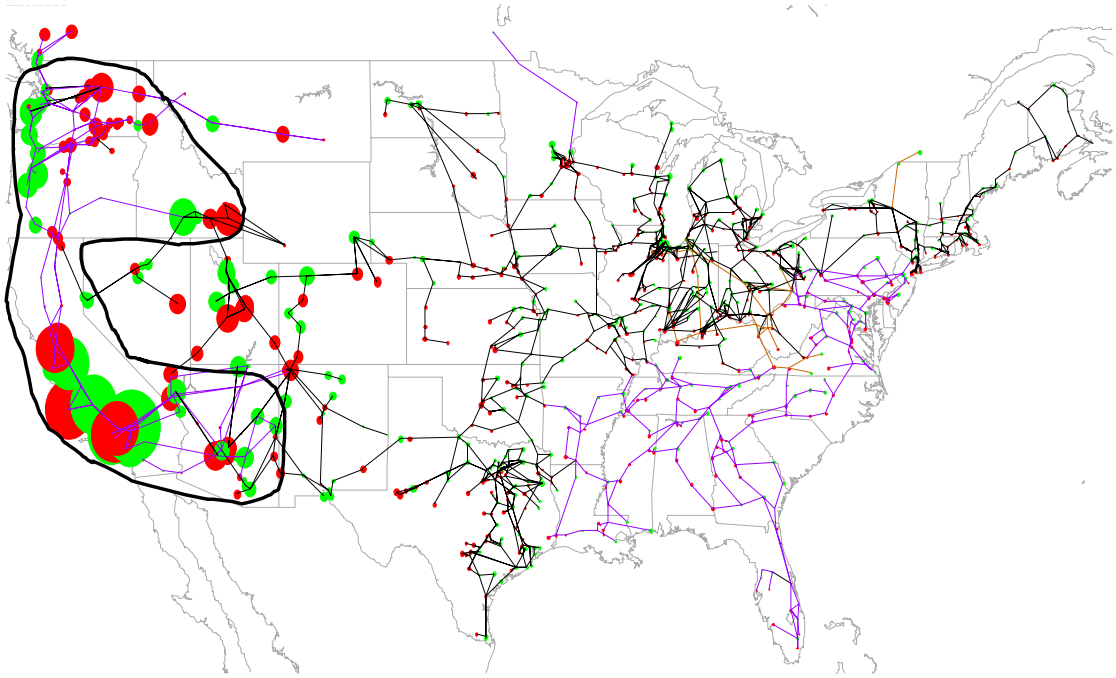

Figure 5-12. Heave over Los Angeles at time 30 Seconds.
Peak U.S. MVAR Demand – 42,722, Peak U.S. GIC-Eff – 34,568 Amps,
Grid Disturbance Energy Sum (sec 26-42) – 522,002. MVAR-sec.

5.3.1 Power Grid and Generation Plant Overview

Restoration will entail concerns about the ability to fully restore the function of needed power plants (especially those involved in blackstart) and the EHV power grid. Therefore, the impact of the disturbance on these portions of the infrastructure will be of most concern. Because the blackout region will encompass many states and all of the California-ISO reliability regions, the ability to transfer power from neighboring regions will be of concern, as previously discussed in Section 5.2.

As with the NY region scenario, age and condition of both transmission/substation assets and power plant assets will also be of concern. In addition to age of plant, fuel type for

generation will be an important consideration. Because of special restart issues, nuclear-fueled capacity would not be available for blackstart and largely unavailable for several days (best case assumption) and perhaps a significant portion of this capacity would not be available for a year or longer if damage to the EHV transformers occurs. A worst-case assumption would be to assume large GSU transformer failures occur.

5.3.2 Power Plant Fuel and Capacity Overview

Hydro, coal and petrol fueled facilities may be the only ones that could be available for blackstart. Natural gas may not be available for blackstart, if this infrastructure cascades into failure due to loss of electric power or from direct E1 impacts on control systems. Therefore, the availability of natural gas should be suspect due to the potential for interdependency issues with operation of pipeline systems. Hydro generation may also be adversely affected due to time of year. Much of the petrol and hydro are small plant facilities and may not be available to run on a baseload basis at their nameplate rating and may only be able to produce fractional amounts of power production (in MWH) over extended periods of time. Fuel reserves and storage onsite is only possible for coal and petrol units. Table 5-1 provides a summary of capacity by fuel type for utility-owned power plant facilities in the LA region. In contrast to the NY region, which had ~20% nuclear capacity, the percentage of nuclear capacity is only 11.8% in the LA region. For general purposes, it would not be unreasonable to assume that most of the nuclear and natural gas fueled capacity in the region would not be readily available in the aftermath of an HEMP attack. Figure 5-13 provides a map showing the location of all hydro electric generation plants in the western portion of the WECC region.

Table 5-1. Summary of utility-owned generation by fuel type within the LA region.

Gen Cap Summary	Nuclear	Coal	Hydro	Petrol/Distil
Total Capacity (kW)	9,964,150	22,684,546	36,993,256	987,352
% Capacity	11.8%	26.8%	43.7%	1.2%
# of Plants	8	61	1008	89
Ave Plant Size (kW)	1,245,519	371,878	36,700	11,094

5.3.3 Overview of Potential Impacts to EHV Circuit Breakers due to High GIC Levels

For the LA region scenario, Figure 5-14 provides a summary of the transmission lines and the expected AC current flows and expected GIC currents. The transmission network is less dense, with fewer terminations, and as a result there is a lower total number of circuit breakers at-risk compared to the NY scenario. An additional mitigating factor is the large number of lines in the WECC with series compensation and hence no path for GIC flow over those lines. On the other hand, this blocking effectively channels added GIC flows on available parallel paths and places these breaker assets at a potentially higher degree of risk. Many of the at-risk lines are some of the important short-distance connector lines in and around some of the major metropolitan regions of the WECC,

particularly in the greater LA region. And though they are fewer in number, the loss of any large EHV lines in the LA region would still have potential for consequential impacts. As shown, a number of circuits will have the potential for GIC levels that could be substantially larger than the AC current flows.

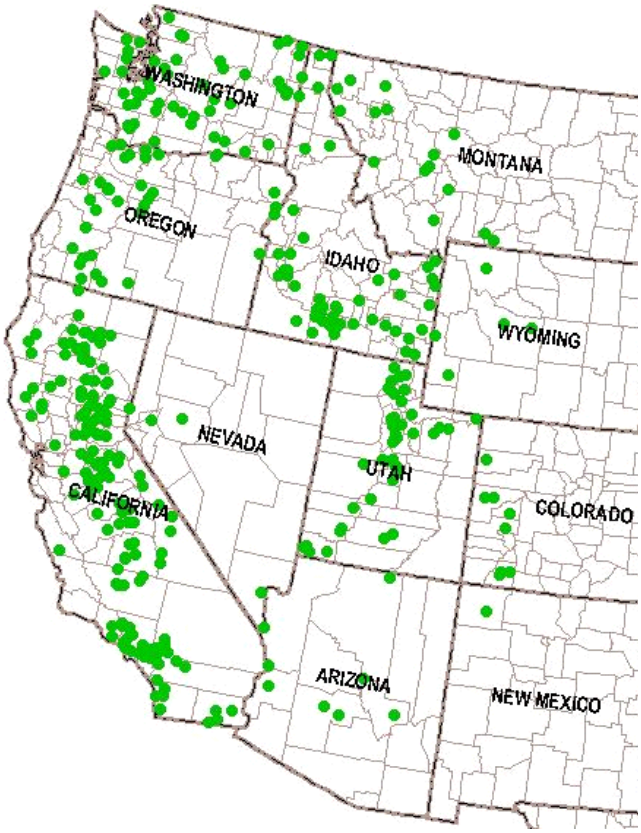

Figure 5-13. Location of all hydro electric plants in the LA region of blackout.

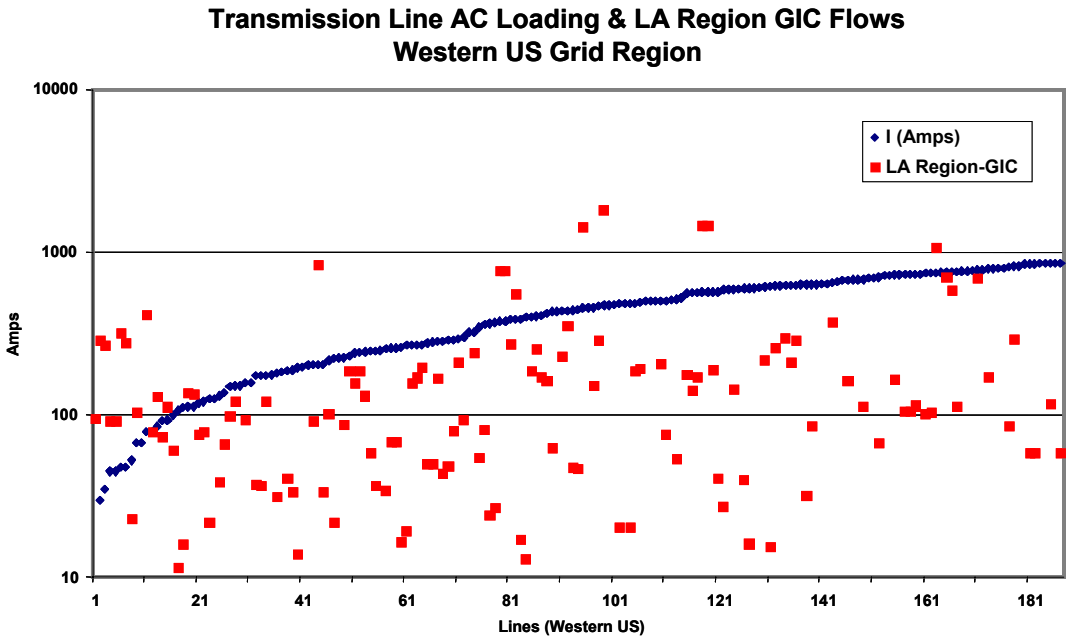

Figure 5-14. LA region and summary of AC current flows on various EHV transmission lines (blue dots) and simultaneous GIC current flows on the same lines (red dots). A number of lines have potential for GIC flows larger than the AC currents, and this leads to concerns about circuit breaker operation.

The large number of breakers at risk, as suggested by the comparison in Figure 5-14 is plotted as to their locations in Figure 5-15. In this map, the circuit breakers at each of the lines with large GIC flows would have circuit breakers that are exposed to potentially damaging levels of GIC. Table 5-2 provides a listing of the various EHV transmission lines in the region that could be rendered-out-of-service for long durations due to catastrophic circuit breaker locations as a result of the high GIC levels. This table in particular lists a number of important supply lines into the Los Angeles area that are at risk. If permanent damage to breakers at these locations occurs, restoration may take months for a large scale failure scenario such as this.

Table 5-2. LA region - transmission lines at risk due to EHV breaker failure.

To Name	From Name	kV
Marketplace WECC	Mead WECC	500
Oquirrh WECC	Camp Williams WECC	345
Sigurd WECC	Mona WECC	345
Sigurd WECC	Mona WECC	345
Moss Landing PP WECC	Metcalf WECC	500
Valley WECC	Serrano Place WECC	500
Vincent WECC	Lugo WECC	500
Vincent WECC	Lugo WECC	500
Midpoint WECC	Kinport WECC	345
Victorville WECC	Rinaldi WECC	500
Rinaldi 2 WECC	Adelanto WECC	500
Victorville WECC	Adelanto WECC	500
Victorville WECC	Adelanto WECC	500
Toluca WECC	Adelanto WECC	500

Figure 5-15. LA region - location of EHV circuit breakers at risk.

5.3.4 Overview of Potential Impacts to EHV Transformers due to High GIC Levels

Figure 5-16 provides a map of the location of all exposed EHV transformers with GIC of 200 Amps per phase or greater. There is a geographically widespread distribution of the location of at-risk transformers, and their number is also large. There are a total of 35 transformers in this at-risk category. If these all failed, it would constitute a resultant loss of ~35,000 MVA of EHV network transformation capacity at 345kV and 500kV voltages (typical size of ~1000 MVA per transformer).

Figure 5-16. LA region - location of transformers at risk, GIC of 200 Amps or greater per phase.

Even using a larger GIC threshold before assuming transformer failure will still have the potential to cause widespread disruptive impairment to the LA region power grid. Figure 5-17 provides a map of the location of all transformers "at-risk" with levels of GIC of 500 Amps per phase or greater. For this scenario, transformer failures would cause resultant loss of as many as 15 large EHV transformers with ~14,000 MVA of network transformation capacity at all voltages (typical size of ~900 MVA per transformer). As indicated in this map and earlier maps, these failures would be clustered in an around the major metropolitan regions of Los Angeles and San Francisco.

Figure 5-17. LA region - location of transformers at risk, GIC of 500 Amps or greater per phase.

5.3.5 Overview of Potential Impacts to Transmission Network Supply to Los Angeles Regions

The Los Angeles metropolitan region has coastal geographic constraints on EHV transmission supply similar to those discussed for the New York City region. As previously discussed, there appears to be a clustering of both EHV circuit breakers and EHV transformers "at-risk" in the Los Angeles metropolitan area and if large scale failures of these occur, this could hinder the rapid restoration.

Table 5-3. Population of counties and estimated peak demands for the LA metropolitan region.

LA City Region County	Population	Est Peak Demand
Riverside	1,170,413	2,488
Sam Bernardino	1,418,380	3,015
Los Angeles	8,863,164	18,840
Orange	2,410,556	5,124
Ventura	669,016	1,422
Total	14,531,529	30,891

Available generation capacity and the type of fuel supply that would be available are keys to the extent of the outage and degree of restoration that might be achievable in such an isolation scenario. As shown in Table 5-3, the estimated peak electrical demand for the LA metropolitan region is expected to be as much as ~30,000 MW, with a total population of over 14 million residents.

Table 5-4. Summary of LA metropolitan region generation capacity by fuel type.

Gen Cap Summary	Nuclear	Coal	Hydro	Petrol/Distil	Nat Gas	Other
Total Capacity (kW)	2,254,000	0	1,627,109	126,161	9,606,328	2,819,954
% Capacity	13.7%	0.0%	9.9%	0.8%	58.5%	17.2%
# of Plants	2	0	45	14	109	94
Ave Plant Size (kW)	1,127,000	0	36,158	9,012	88,131	30,000

Table 5-4 provides a summary by fuel type of the available nameplate capacity in this same geographic region, which is estimated to be only ~16,000 MW. Figure 5-18 provides a map of the power plant locations from Table 5-4 in the region. The large mismatch between estimated peak electrical demand and local generation capability in the region would suggest that significant shortages of electricity would occur under a scenario of large scale failures to EHV transmission infrastructure in the LA region.

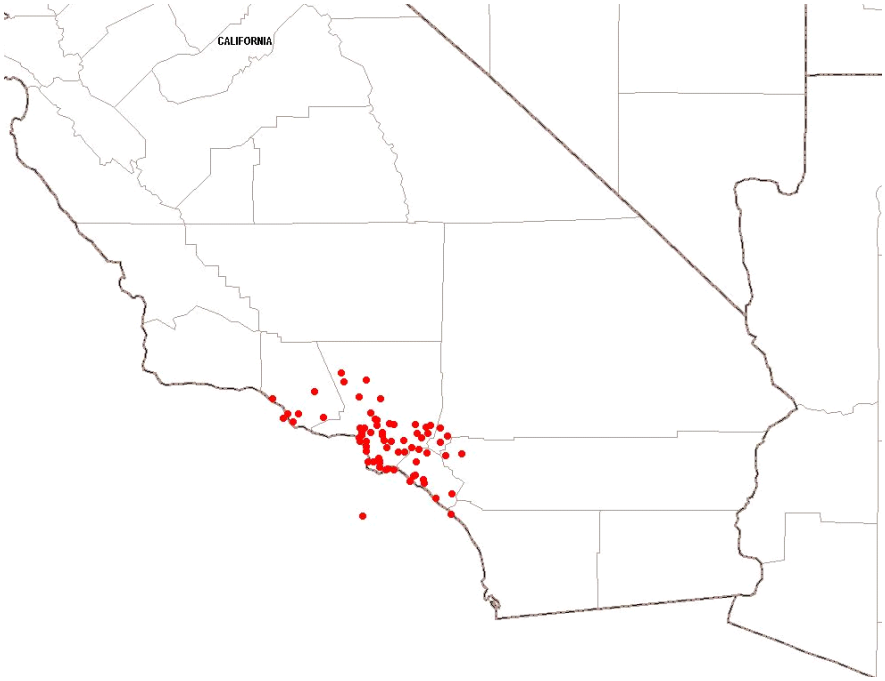

Figure 5-18. Los Angeles metropolitan region locations of power plants.

5.4 Ohio Region Scenario (Case 16d)

Figure 5-19 denotes the area of power grid disturbance and collapse due to the large E3-related stress. Wider regions of collapse are likely, due to progressive collapse/cascade. The size of this collapse area in total would be of unprecedented scale. For restoration analysis purposes, it is assumed that adjoining areas to the regions outlined above would be able to achieve nearly complete restoration within approximately 24-72 hours, while the regions outlined in black border region may take substantially longer. E3 impacts to infrastructure and resultant impact on restoration will be focused on the outlined areas as shown. Unfavorable weather conditions (particularly cold-weather) should be assumed as an important complicating factor that would have the potential to make restoration of all facilities and infrastructures more problematic. E1 impacts will add further complicating factors to the restoration process.

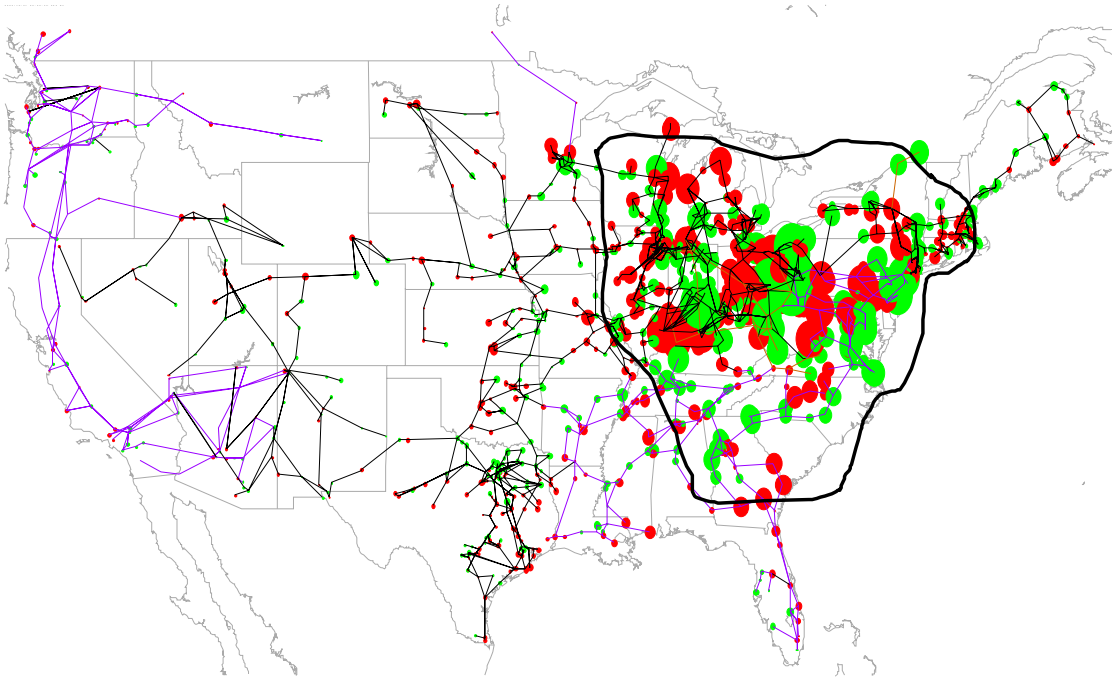

Figure 5-19. Case 16d positioned over Columbus OH at time 30 Seconds.
Peak U.S. MVAR Demand – 69,879, Peak U.S. GIC-Eff – 71,954 Amps,
Grid Disturbance Energy Sum (sec 26-40) – 931,693. MVAR-sec.

5.4.1 Power Plant Fuel and Capacity Overview

Hydro, coal and petrol fueled facilities may be the only ones that could be available for blackstart – natural gas may not be available for blackstart, if this infrastructure cascades into failure due to loss of electric power or from direct E1 impacts on control systems. Therefore, the availability of natural gas should be suspect due to the potential for interdependency issues with operation of pipeline systems. Hydro may also be adversely affected due to time of year. Much of the petrol and hydro are small plant facilities and may not be available to run on a baseload basis at their nameplate and may only be able to produce fractional amounts of power production (in MWH) over extended periods of time. Fuel reserves and storage onsite is only possible for coal and petrol units. Table 5-

5 provides a summary of capacity by fuel type for utility-owned power plant facilities in the Case16d region. Similar to the NY region, which had ~20% nuclear capacity, the percentage of nuclear capacity is also 20% in the Case 16d region.

Table 5-5. Summary of utility-owned generation by fuel type within the Case 16d region.

Gen Cap Summary	Nuclear	Coal	Hydro	Petrol/Distil
Total Capacity (kW)	61,301,293	165,279,016	27,282,544	22,784,887
% Capacity	20%	54.0%	8.9%	7.4%
# of Plants	61	646	1242	1010
Ave Plant Size (kW)	1,004,939	255,850	21,967	22,559

5.4.2 Overview of Potential Impacts to EHV Circuit Breakers due to High GIC Levels

For the Case 16d region scenario, Figure 5-20 provides a summary of the transmission lines and the expected AC current flows and expected GIC currents. The transmission network is less dense and with fewer terminations, as a result there is a similar total number of circuit breakers at-risk compared to the NY scenario. Therefore similar concerns are possible for large-scale loss of EHV circuit breakers and EHV transmission lines in the region and the overall ability to rapidly restore power to all impacted end-users.

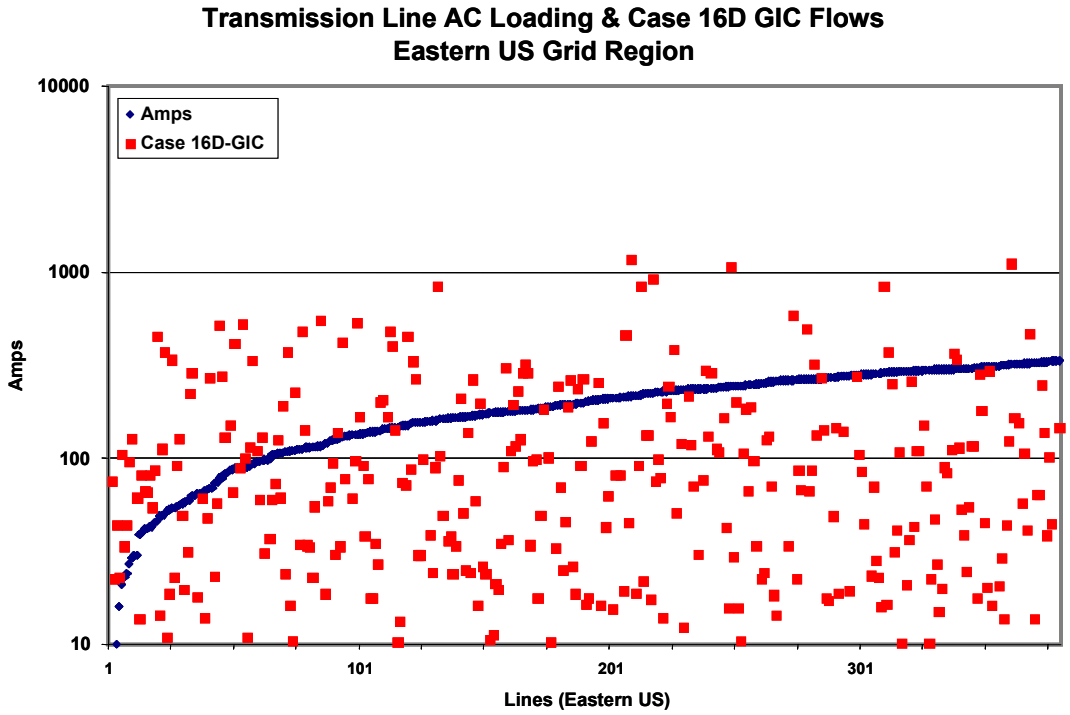

Figure 5-20. Case 16d region and summary of AC current flows on various EHV transmission lines (blue dots) and simultaneous GIC current flows on the same lines (red dots). A number of lines have potential for GIC flows larger than the AC currents and this leads to concerns about circuit breaker operation.

The breakers at risk shown in Figure 5-20 are mapped in Figure 5-21. In this map, the circuit breakers at each of the lines with large GIC flows would be exposed to potentially damaging levels of GIC. Figure 5-22 provides a map of the various EHV transmission lines in the region that could be rendered-out-of-service for long durations due to loss of circuit breaker locations as a result of the high GIC levels. As shown, any of the colored lines (color difference denotes kV rating) is a line that may be unavailable due to circuit breaker problems. If permanent damage to breakers at these locations occurs, restoration may take months for large scale failure scenarios such as this.

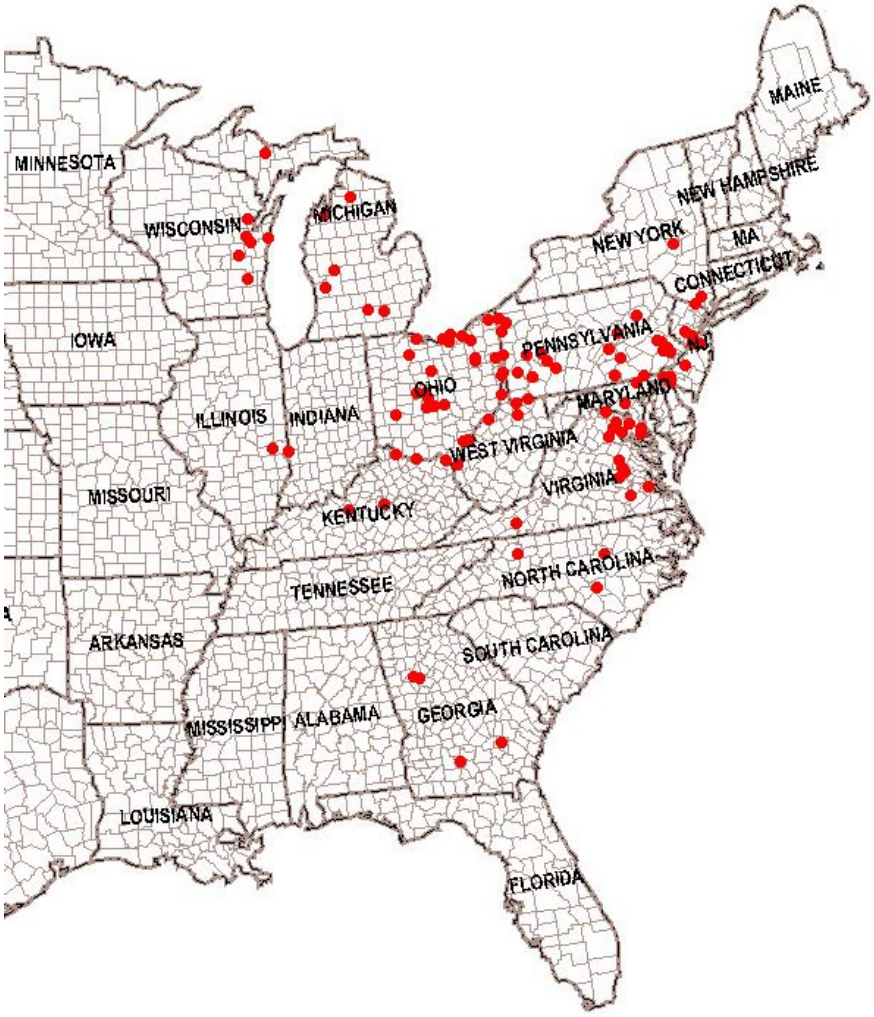

Figure 5-21. Case 16d region - location of EHV circuit breakers at risk from Figure 5-20.

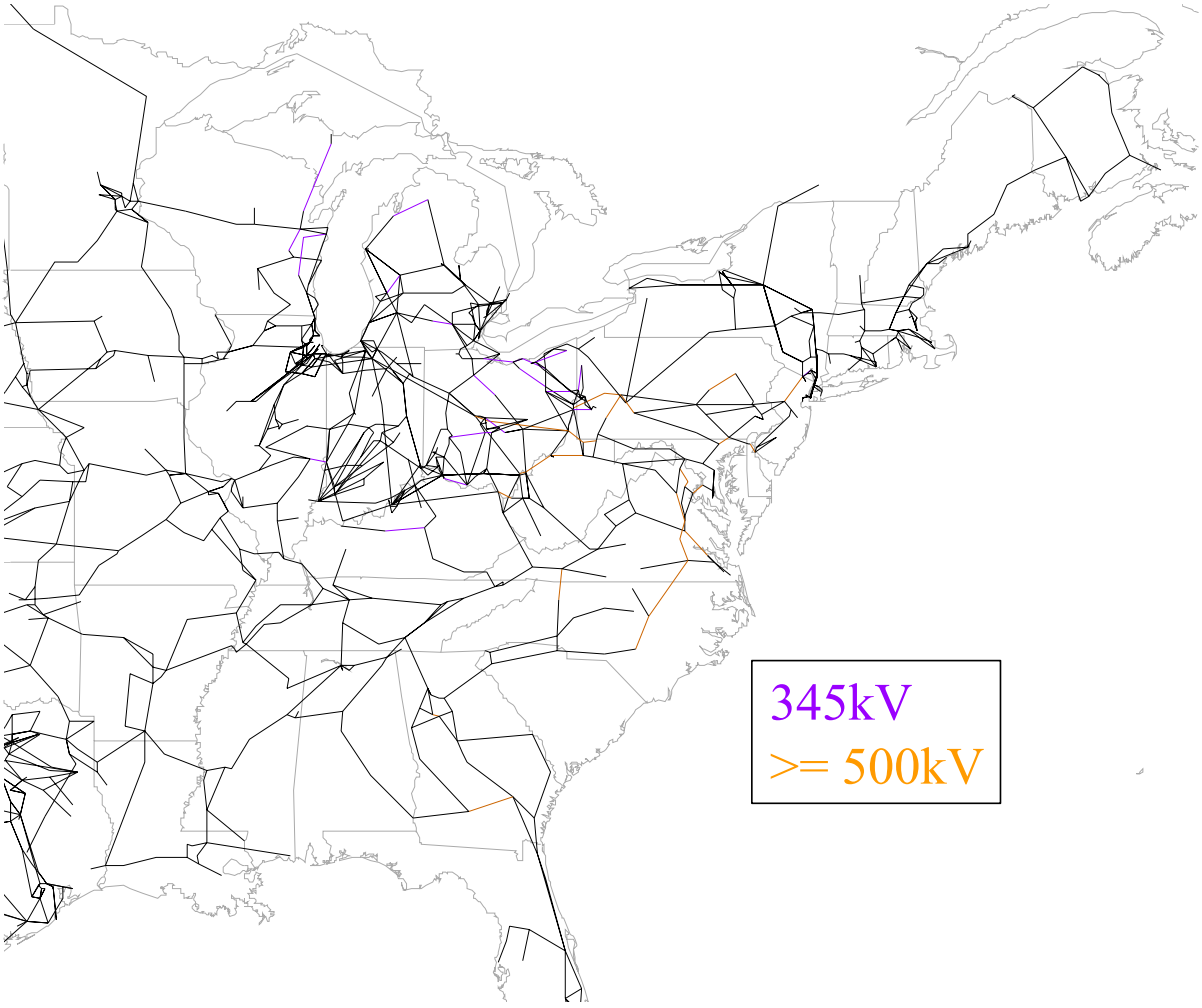

Figure 5-22. Case 16d region - transmission lines at risk due to EHV breaker failure.

5.4.3 Overview of Potential Impacts to EHV Transformers due to High GIC Levels

Figure 5-23 provides a map of the location of all exposed EHV transformers with GIC of 200 Amps per phase or greater. There is a geographically widespread distribution of a large number of at-risk transformers. There are a total of 58 transformers in this at-risk category. If these all failed, it would constitute a resultant loss of ~46,000 MVA of EHV network transformation capacity at 345kV, 500kV and 765kV voltages (typical size of ~800 MVA per transformer).

Figure 5-23. Case 16d region - location of transformers at risk, GIC of 200 Amps or greater per phase.

While this attack scenario involves a larger geographic area than the NY scenario, the resulting large GIC flows are reduced due to the ground conductivity conditions over the region of the most intense portion of the E3B Heave magnetic fields.

Section 6
Bibliography of E3 HEMP References

6.1 E3 HEMP References

Barnes, Paul R., Fred M. Tesche, Ben W. McConnell and Edward F. Vance, "MHD-EMP Analysis and Protection," September 1993, DNA-TR-92-101.

Barnes, P.R., F.M. Tesche and E.F. Vance, "Mitigation of Magnetohydrodynamic Electromagnetic Pulse (MHD-EMP) Effects from Commercial Electric Power Systems," March 1992, ORNL-6709.

Berthold, W.K., A.K. Harris and H.J. Hope, "World-Wide Effects of Hydromagnetic Waves Due to Argus," *Journal Geophysical Research* **65**, 2233 (1960).

Bomke, H.A., I.A. Balton, H.H. Grote and A.K. Harris, "Near and Distant Observations of the 1962 Johnston Island High Altitude Nuclear Tests," *Journal of Geophysical Research* **69**, 3125 (1964).

Bomke, H.A., A.K. Harris, J.W. Walker and W.J. Ramm, "The Nature of Worldwide Geomagnetic Disturbances Generated by the Starfish Explosion of July 9, 1962," *Journal of Geophysical Research* **71**, 2777 (1966).

Chavin, S., W.F. Crevier, R.W. Kilb and C.L. Longmire, "MHD-EMP Code Simulation of STARFISH," August 1979, DNA 5055F.

Fajen, F.E., "MICE: An Implicit Difference Scheme for MHD Calculations," March, 1973, DNA 2877Z.

Gilbert, J. L., "Modeling the effect to the ocean-land interface on induced electric fields during geomagnetic storms," *Space Weather*, **3**, S04A03, doi:10.1029/2004SW000120.

Gritsai, V.N. Kondratiev and E.L. Stupitsky, "Numerical Modelling of the Processes of High Altitude Nuclear Explosion MHD-EMP Formation and Propagation," *Proceedings of the International Symposium on Electromagnetic Compatibility EMC '96*, Rome, Italy, 769-771 (1996).

Gritsai, V.N., A.H. Kozlovsky, V.M. Kuvshinnikov, V.M. Loborov, Y.V. Parfenov, O.A. Tarasov and L. N. Zdoukhov, "Response of Long Lines to Nuclear High-Altitude Electromagnetic Pulse (HEMP)," *IEEE Trans EMC* **40**, 348-354 (1998).

Kondratiev, V.M., "High Altitude Nuclear Explosion EMP Effects on Communication Lines," *Proceedings of the International Symposium on EMC and EME*, St. Petersburg, Russia, 131-132, June 1995.

Kondratiev, V.M. and V.V. Sokovikh, “Re-Determination of MHD-EMP Amplitude Characteristics and Spatial Distribution on the Ground Surface,” *Proceedings of the EMC Conference*, Rome, Italy (1996).

Legro, J.R., N.C. Abi-Samra and F.M. Tesche, “Study to Assess the Effects of Magnetohydrodynamic Electromagnetic Pulse on Electric Power Systems Phase I (Final Report),” May 1985, ORNL/Sub-83/43374/1/V3.

McConnell, B.W., P.R. Barnes, P.R., F.M. Tesche and D.A. Schafer, “Impact of Quasi-DC Currents on Three-Phase Distribution Transformer Installations,” March 1992, ORNL/Sub—89-SE912/1.

MIL-STD-188-125-1, “Department of Defense Interface Standard. High-Altitude Electromagnetic Pulse (HEMP) Protection for Ground-Based C4I Facilities Performing Critical, Time-Urgent Missions, Part 1 Fixed Facilities”, 17 July 1998.

Tesche, F.M., P.R. Barnes and A.P. Sakis Meliopoulos, “Magnetohydrodynamic Electromagnetic Pulse (MHD-EMP) Interaction with Power Transmission and Distribution Systems,” February 1992, ORNL/Sub/90-SG828/1.

6.2 IEC HEMP References

IEC, “Electromagnetic compatibility (EMC) - Part 1-3: General - The effects of high-altitude EMP (HEMP) on civil equipment and systems”, IEC 61000-1-3, International Electrotechnical Commission, Geneva, Switzerland

IEC, “Electromagnetic compatibility (EMC) - Part 1-5: General - High power electromagnetic (HPEM) effects on civil systems”, IEC 61000-1-5, International Electrotechnical Commission, Geneva, Switzerland

IEC, “Electromagnetic compatibility (EMC) - Part 2: Environment - Section 3: Description of the environment - Radiated and non-network-frequency-related conducted phenomena”, IEC 61000-2-3, International Electrotechnical Commission, Geneva, Switzerland

IEC, “Electromagnetic compatibility (EMC) - Part 2: Environment - Section 5: Classification of electromagnetic environments. Basic EMC publication”, IEC 61000-2-5, International Electrotechnical Commission, Geneva, Switzerland

IEC, “Electromagnetic compatibility (EMC) - Part 2: Environment - Section 9: Description of HEMP environment - Radiated disturbance. Basic EMC publication”, IEC 61000-2-9, International Electrotechnical Commission, Geneva, Switzerland

IEC, “Electromagnetic compatibility (EMC) - Part 2-10: Environment - Description of HEMP environment - Conducted disturbance”, IEC 61000-2-10, International Electrotechnical Commission, Geneva, Switzerland

IEC, “Electromagnetic compatibility (EMC) - Part 2-11: Environment - Classification of HEMP environments”, IEC 61000-2-11, International Electrotechnical Commission, Geneva, Switzerland

IEC, “Electromagnetic compatibility (EMC) - Part 2-13: Environment - High-power electromagnetic (HPEM) environments - Radiated and conducted”, IEC 61000-2-13, International Electrotechnical Commission, Geneva, Switzerland

IEC, “Electromagnetic compatibility (EMC) - Part 4-1: Testing and measurement techniques - Overview of IEC 61000-4 series”, IEC 61000-4-1, International Electrotechnical Commission, Geneva, Switzerland

IEC, “Electromagnetic compatibility (EMC)- Part 4-2: Testing and measurement techniques - Electrostatic discharge immunity test”, IEC 61000-4-2, International Electrotechnical Commission, Geneva, Switzerland

IEC, “Electromagnetic compatibility (EMC) - Part 4-3 : Testing and measurement techniques - Radiated, radio-frequency, electromagnetic field immunity test”, IEC 61000-4-3, International Electrotechnical Commission, Geneva, Switzerland

IEC, “Electromagnetic compatibility (EMC) - Part 4-4: Testing and measurement techniques - Electrical fast transient/burst immunity test”, IEC 61000-4-4, International Electrotechnical Commission, Geneva, Switzerland

IEC, “Electromagnetic compatibility (EMC) - Part 4-5: Testing and measurement techniques - Surge immunity test”, IEC 61000-4-5, International Electrotechnical Commission, Geneva, Switzerland

IEC, “Electromagnetic compatibility (EMC) - Part 4-6: Testing and measurement techniques - Immunity to conducted disturbances, induced by radio-frequency fields”, IEC 61000-4-6, International Electrotechnical Commission, Geneva, Switzerland

IEC, “Electromagnetic compatibility (EMC) - Part 4-12: Testing and measurement techniques - Ring wave immunity test”, IEC 61000-4-12, International Electrotechnical Commission, Geneva, Switzerland

IEC, “Electromagnetic compatibility (EMC) - Part 4-18: Testing and measurement techniques - Damped oscillatory wave immunity test”, IEC 61000-4-18, International Electrotechnical Commission, Geneva, Switzerland

IEC, “Electromagnetic compatibility (EMC) - Part 4-20: Testing and measurement techniques - Emission and immunity testing in transverse electromagnetic (TEM) waveguides”, IEC 61000-4-20, International Electrotechnical Commission, Geneva, Switzerland

IEC, “Electromagnetic compatibility (EMC) - Part 4-21: Testing and measurement techniques - Reverberation chamber test methods”, IEC 61000-4-21, International Electrotechnical Commission, Geneva, Switzerland

IEC, “Electromagnetic compatibility (EMC) - Part 4-23: Testing and measurement techniques - Test methods for protective devices for HEMP and other radiated

disturbances", IEC 61000-4-23, International Electrotechnical Commission, Geneva, Switzerland

IEC, "Electromagnetic compatibility (EMC) - Part 4-24: Testing and measurement techniques - Section 24: Test methods for protective devices for HEMP conducted disturbance - Basic EMC Publication", IEC 61000-4-24, International Electrotechnical Commission, Geneva, Switzerland

IEC, "Electromagnetic compatibility (EMC) - Part 4-25: Testing and measurement techniques - HEMP immunity test methods for equipment and systems", IEC 61000-4-25, International Electrotechnical Commission, Geneva, Switzerland

IEC, "Electromagnetic compatibility (EMC) - Part 4-32: Testing and measurement techniques - High-altitude electromagnetic pulse (HEMP) simulator compendium", IEC 61000-4-32, International Electrotechnical Commission, Geneva, Switzerland

IEC, "Electromagnetic compatibility (EMC) - Part 4-33: Testing and measurement techniques - Measurement methods for high-power transient parameters", IEC 61000-4-33, International Electrotechnical Commission, Geneva, Switzerland

IEC, "Electromagnetic compatibility (EMC) - Part 4-35: Testing and measurement techniques - HPEM simulator compendium", IEC 61000-4-35, International Electrotechnical Commission, Geneva, Switzerland

IEC, "Electromagnetic compatibility (EMC) - Part 5: Installation and mitigation guidelines - Section 1: General considerations - Basic EMC publication", IEC 61000-5-1, International Electrotechnical Commission, Geneva, Switzerland

IEC, "Electromagnetic compatibility (EMC) - Part 5: Installation and mitigation guidelines - Section 2: Earthing and cabling", IEC 61000-5-2, International Electrotechnical Commission, Geneva, Switzerland

IEC, "Electromagnetic compatibility (EMC) - Part 5-3: Installation and mitigation guidelines - HEMP protection concepts", IEC 61000-5-3, International Electrotechnical Commission, Geneva, Switzerland

IEC, "Electromagnetic compatibility (EMC) - Part 5: Installation and mitigation guidelines - Section 4: Immunity to HEMP - Specifications for protective devices against HEMP radiated disturbance. Basic EMC Publication", IEC 61000-5-4, International Electrotechnical Commission, Geneva, Switzerland

IEC, "Electromagnetic compatibility (EMC) - Part 5: Installation and mitigation guidelines - Section 5: Specification of protective devices for HEMP conducted disturbance. Basic EMC Publication", IEC 61000-5-5, International Electrotechnical Commission, Geneva, Switzerland

IEC, "Electromagnetic compatibility (EMC) - Part 5-6: Installation and mitigation guidelines - Mitigation of external EM influences", IEC 61000-5-6, International Electrotechnical Commission, Geneva, Switzerland

IEC, “Electromagnetic compatibility (EMC) - Part 5-7: Installation and mitigation guidelines - Degrees of protection provided by enclosures against electromagnetic disturbances (EM code)”, IEC 61000-5-7, International Electrotechnical Commission, Geneva, Switzerland

IEC, “Electromagnetic compatibility (EMC) - Part 5-8: Installation and mitigation guidelines - HEMP protection methods for the distributed infrastructure”, IEC 61000-5-8, International Electrotechnical Commission, Geneva, Switzerland

IEC, “Electromagnetic compatibility (EMC) - Part 5-9: Installation and mitigation guidelines - System-level susceptibility assessments for HEMP and HPEM”, IEC 61000-5-9, International Electrotechnical Commission, Geneva, Switzerland

IEC, “Electromagnetic compatibility (EMC) - Part 6-1: Generic standards - Immunity for residential, commercial and light-industrial environments”, IEC 61000-6-1, International Electrotechnical Commission, Geneva, Switzerland

IEC, “Electromagnetic compatibility (EMC) - Part 6-2: Generic standards - Immunity for industrial environments”, IEC 61000-6-2, International Electrotechnical Commission, Geneva, Switzerland

IEC, “Electromagnetic compatibility (EMC) - Part 6-5: Generic standards - Immunity for power station and substation environments”, IEC 61000-6-5, International Electrotechnical Commission, Geneva, Switzerland

IEC, “Electromagnetic compatibility (EMC) - Part 6-6: Generic standards - HEMP immunity for indoor equipment”, IEC 61000-6-6, International Electrotechnical Commission, Geneva, Switzerland

6.3 EMP Commission and Related References

Dr. John S. Foster, Jr., et al., “Report of the Commission to Assess the Threat to the United States from Electromagnetic Pulse (EMP) Attack, Volume 1: Executive Report”, 2004.

Dr. John S. Foster, Jr., et al., “Report of the Commission to Assess the Threat to the United States from Electromagnetic Pulse (EMP) Attack, Critical National Infrastructures”, April 2008.

J.G. Kappenman, W.A. Radasky and J.L. Gilbert, “Evaluation of the Vulnerability of the NGC Power Transmission Grid to the Effects of Geomagnetic Storms”, May 8, 1998, Meta-R-144.

J.G. Kappenman, “Evaluation of the Vulnerability of the CEPCO Transmission Network to the Effects of Geomagnetic Storms”, March 2001, Meta-R-182.

J.G. Kappenman, J.J. Patrick, J.L. Gilbert, E.B. Savage and W. A. Radasky, “An Expedited Geomagnetic Storm and Late-Time HEMP Threat Analysis Study to Assess the Vulnerability of the U.S. Power Grid”, Prepared for the EMP Commission, December 31, 2002, Meta-R-208.

W.A. Radasky, J.L. Gilbert, E.B. Savage, J.G. Kappenman, J.J. Patrick, M.A. Messier and P.R. Barnes, “An Expedited early-Time HEMP Threat Analysis Study to Assess the Vulnerability of the U.S. Power Grid”, Prepared for the EMP Commission, December 31, 2002, Meta-R-209.

W.A. Radasky, J.L. Gilbert and E.B. Savage, “The Use of the Russian HEMP E3 Measurements for Model Verification”, Meta-R-218.

J.G. Kappenman, J.J. Patrick, J.L. Gilbert, W.A. Radasky and E.B. Savage, “Power Grid Restoration Report: Analysis of Power Grid Restoration Concerns Due to Large E3-Initiated Power Grid Collapses”, Prepared for the EMP Commission, November 2003, Meta-R-222.

E.B. Savage, W.A. Radasky, J.G. Kappenman, J.L. Gilbert, K.S. Smith and M.J. Madrid, “HEMP Impulse Injection Testing of Power System Electronics and Electrical Components”, Prepared for the EMP Commission, December 29, 2003, Meta-R-225.

W.A. Radasky, J.G. Kappenman, E.B. Savage and J.L. Gilbert, “Metatech Recommendations to the EMP Commission”, Prepared for the EMP Commission, December 31, 2003, Meta-R-226.

Gilbert J.L, W.A. Radasky, J.G. Kappenman, E.B. Savage, K.S. Smith and M.J. Madrid, “Final Report of Scenario Results Volume 2: E1 HEMP Effects”, Prepared for the EMP Commission, January 16, 2004, Meta-R-227.

J.G. Kappenman, J.J. Patrick, J.L. Gilbert, E.B. Savage and W.A. Radasky, “ Initial Report on Outage and Restoration Concerns for the U.S. Power Grid Due to HEMP Threats”, Prepared for the EMP Commission, June 1, 2003, Meta-R-229.

J.G. Kappenman, J.J. Patrick, J.L. Gilbert, E.B. Savage and W.A. Radasky, “Interim Report on Outage and Restoration Concerns for the U.S. Power Grid Due to Late-Time HEMP Threats (Deliverable 2)”, Prepared for the EMP Commission, July 15, 2003, Meta-R-230.

J.G. Kappenman, J.J. Patrick, W.A. Radasky and E.B. Savage, “Detailed Test Plan Including Ordered Equipment” Prepared for the EMP Commission, September 18, 2003, Meta-R-231.

J.G. Kappenman, J.J. Patrick, J.L. Gilbert, E.B. Savage and W.A. Radasky, “Final Outage and Restoration Results (Deliverable 3) An Overview of Major International Power System Blackouts and System Restorations”, Prepared for the EMP Commission, September 8, 2003, Meta-R-232.

W.A. Radasky, “Russian Research Activities Work Plan for Research”, Prepared for the EMP Commission, October 3, 2003, Meta-R-233.

E.B. Savage, J.L. Gilbert, K.S. Smith, M.J. Madrid and W.A. Radasky, “Preliminary Test Results: Fast Pulse Testing of Allen Bradley MicroLogix 1000 PLC (Programmable Logic Controller)”, Prepared for the EMP Commission, October 30, 2003, Meta-R-234.

W.A. Radasky, “Russian Research Activities Preliminary Results”, Prepared for the EMP Commission, January 16, 2004, Meta-R-235.

W.A. Radasky, “Russian Research Activities Summary of Washington, DC Meeting Held on 9 December 2003 at IDA”, Prepared for the EMP Commission, Meta-R-236.

J.G. Kappenman, J.J. Patrick, W.A. Radasky, E.B. Savage, J.L. Gilbert, K.S. Smith and M.J. Madrid “Draft Research Report: Metatech Work for the EMP Commission”, Prepared for the EMP Commission, January 30, 2004, Meta-R-237.

W.A. Radasky, J.G. Kappenman and P. Warner “Report on Evaluation of Harmonics Data from SARA Field Tests” October 1, 2006, Meta-R-271.

W.A. Radasky, “The Threat of High-Altitude Electromagnetic Pulse (HEMP) on the U.S. Power Infrastructure (Deliverable 4.2.1a) December 18, 2006, Meta-R-274.

W.A. Radasky and J.G. Kappenman, “The Threat of a 100 Year Geomagnetic Superstorm to the U.S. Power Infrastructure” 25 January 2007, Meta-R-280R2.

J.G. Kappenman, P. Warner and W.A. Radasky. “ TEST REPORT: Report on Task 2a Modeling Analysis to Support Additional SARA Field Tests”, May 11, 2007, Meta-R-284.

J.G. Kappenman, P. Warner and W.A. Radasky. “TEST REPORT: Report on Evaluation of UPS Performance, Complex Load Recommendations and Harmonic Propagation and Modeling Analysis to Support Additional SARA Field Tests” Meta-R-282, 26 March 2007, Meta-R-282.

F.M. Tesche, “HEMP Field Penetration into Poorly Shielded Enclosures and Coupling to Internal Conductors”, June 4, 2007, Meta-R-287.

W.A. Radasky, “The Threat of Non-Nuclear EMP on the U.S. Infrastructure (Deliverable 4.3)” September 30, 2007, Meta-R-294.

J.G. Kappenman, “An Assessment of the Threat Potential to the U.S. Electric Power Grids from Extreme Space Weather Storms – Analysis of U.S. Power System Impacts from Large Geomagnetic Storm Events (Task A-C)” October 1, 2007, Meta-R-295.

J.G. Kappenman and P. Warner, “An Assessment of the Threat Potential to the U.S. Electric Power Grids from Extreme Space Weather Storms – Analysis of U.S. Power System Impacts from Large Geomagnetic Storm Events (Deliverable 4.6 – Part 1 of 3)” October 24, 2007, Meta-R-297.

J.G. Kappenman and P. Warner, “An Assessment of the Threat Potential to the U.S. Electric Power Grids from Extreme Space Weather Storms – Analysis of U.S. Power System Impacts from Large Geomagnetic Storm Events (Deliverable 4.6 – Part 2 of 3)” October 24, 2007, Meta-R-298.

J.G. Kappenman and P. Warner, “An Assessment of the Threat Potential to the U.S. Electric Power Grids from Extreme Space Weather Storms – Analysis of U.S. Power

System Impacts from Large Geomagnetic Storm Events–U.S. West (Deliverable 4.6 – Part 3 of 3)" November 19, 2007, Meta-R-299.

J.G. Kappenman, P. Warner and W.A. Radasky. "Analysis of U.S. Power Grid Hardening Options Due to E3 HEMP" November 14, 2008, Meta-R-307.

W.A. Radasky, J.G. Kappenman, J.L. Gilbert and E.B. Savage, "Recommendations for the Protection of the Oahu High Voltage Power Network from High-Altitude Electromagnetic Pulse (HEMP)" July 13, 2009, Meta-R-314.

Appendix 1
Disturbance Impact Criteria for the U.S. Power Grid

Low voltage electric distribution systems are designed to operate radially and over geographically small subsystems. Unlike the distribution system, which is compartmentalized to protect from widespread risks, the transmission network is tightly interconnected and every station has redundant feeds from a geographically widespread grid. However, this design feature introduces new failure concerns in that a distinguishing characteristic of bulk transmission systems is that severe disturbances that occur in them can have a system-wide impact. Because the transmission networks in the U.S. are tightly interconnected, the concern also becomes failure modes that can cascade a failure or collapse from one region into neighboring interconnected and unaffected regions as well.

A1.1 Overview of U.S. Transmission Grid Design Criteria

Because these bulk transmission systems are geographically widespread and critical infrastructures, it is not possible to physically test the reliability of the power grid to the multitude of probable and severe disturbances that can occur. Rather, these networks have been designed by use of deterministic design criteria and, for the most part, tested through the application of large-scale network simulation models. The design and operating criteria are aimed at limiting the risk of widespread shutdowns and blackouts, and require grids to be operated in a manner in which they are prepared to survive the most severe contingency. The criteria are commonly called the N-1 design criteria and their application has generally required substantial redundancy in network design, to accommodate the loss of any single element under any probable operating condition. The N-1 design criteria applies to real and reactive power capacity sources, as well as the delivering transmission lines and transformers. The deterministic criteria for bulk power systems will typically include the following requirements:

- Severe Disturbances which include 3 Phase Normal Clearing Faults (~4-5 cycles) and Single Phase Delayed Clearing Fault (~10-12 cycles)
- System operated to withstand Generation Capacity Outage Contingency due to unanticipated loss of single largest generation plant in the pool or region, typically around 1000-1200 MW (Spinning Reserves).
- Withstand extreme contingencies such as simultaneous outage of two parallel lines or entire substation.

These contingencies are tested in simulation through the application of large network models.

This design approach has generally served the power industry very well and has in particular made the U.S. power grid highly reliable. The conventional stresses contemplated above are very localized in nature. This means there are limitations inherent in this design approach when stressed by simultaneous and geographically widespread disturbances, such as those associated with severe geomagnetic storms and HEMP E3 threats. These threats pose a common-mode stress to the network, as these threats can cause simultaneous stresses to occur at multiple locations, and multiple outage

events can arise from independent incident stresses. There are three important failure progressions that are commonly considered in design of the power system: 1) Thermal overload of elements, causing protective systems to interrupt the line or apparatus; 2) Transient instability due to angular accelerations from an initiating disturbance; 3) Voltage instability, where widespread progressive drops in system voltage occur, initiating a complete system collapse. Voltage instability is the most recent and most emergent of the three mechanisms for widespread system failures (Reference AP1-1). Several factors have contributed to this situation. The building of new transmission capacity is more difficult and often delayed, while network loads continue to increase unabated. NERC indicates that between 1990 and 2000 electric power demand in the U.S. increased by 29.4%, while the addition of transmission capacity (345kV and higher) has grown by only 4%.

The increasingly heavy use of the transmission network to accommodate higher power transfers causes burdens on voltage regulation capability, as these power transfers in and of themselves consume considerable reactive power through I^2X losses over the network lines and transformers. To counter some of the concerns of voltage instability, additional design criteria have been adopted, which essentially require that systems provide adequate voltage regulation resources locally. In response, the power industry has employed frequent use of shunt compensation to support voltage profiles on the network. This application of shunt compensation has had the effect of bringing the system instability point closer to normal voltage operating conditions. In many cases, the failure thresholds are so close to normal operating conditions that relatively minor disturbances can and have propagated widespread failures across portions of the U.S. power pools. Figure A1-1 best illustrates these operating concerns. In this figure is a plot of voltage versus power flow across an important transmission network interface between upstate and downstate New York on the New York power pool (Reference AP1-2). This shows the relative sensitivity in this region to increased power flows. Notice at certain transfer levels the voltage starts a steep decline. In essence, the system has been operated over the edge of the cliff and complete voltage collapse is now occurring. What is even more alarming is that this point of collapse is occurring at a network voltage of ~97% of normal, rather than the 70-80% levels that occurred in the past. This sudden transition can, at times, limit the operator's ability to fully recognize when the network has entered a precarious operating posture. Further, the two curves in this case are the system transfer capability, either with or without a 200 MVAR capacitor bank, at the EDIC station being in-service. This is a relatively small change in reactive supply and, as will be shown in the course of this study, sudden increases in system-wide reactive power demands across the state of New York can easily exceed 3000 MVARs due to GIC events, which essentially dwarfs the beneficial attributes of this single capacitor bank being analyzed.

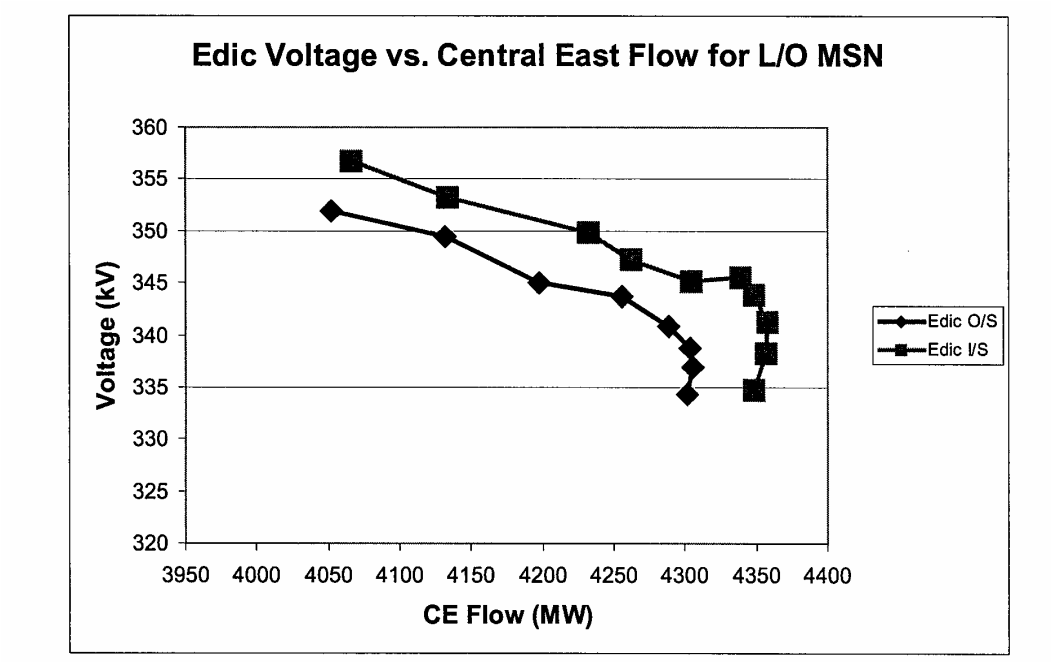

Figure A1-1. NY ISO voltage collapse threshold for system transfers

Restructuring is also raising concerns over the reliability of the nation's electricity grid, as evolution to a competitive market structure has created substantial new operating and planning challenges for reliability. In this environment, operators are faced with large volumes of transactions, larger areas to control, new players, changing operational responsibilities, movement of power over long distances in response to market signals, shrinking and changing definitions for reserve margins, unpredictable system behavior, and finally, in an environment of having to manage systems with operational tools that were designed for a centrally planned and controlled electric grid (Reference AP1-3). Reactive power management is one of the more pressing and yet unmet needs for the power industry. While existing and developing threats require precise knowledge of the available reactive power and voltage regulation reserves on the network, very limited knowledge, in practice, exists in most networks.

These limited disturbance/voltage stability margins and ability to control the system heighten the concern about the capability of the today's network to withstand future probable and severe geomagnetic storm threats, and also increases the likelihood of wider failure footprints for E3 threats to the grid. Until recent developments, power grid operators have generally not had a comprehensive understanding of the threat potentials that could be caused by probable and severe geomagnetic disturbances. Much work has been done on power grids in other world locations (Reference AP1-3), but has not, until this study, been undertaken in large scale for the U.S. (Reference AP1-4). For cases in which power grid operators have performed such analysis, the assessment of impact results indicate that a severe geomagnetic storm event may pose greater stress on the network than the conventional threats of the design criteria now in use (Reference AP1-5).

This expedited study of U.S. Power Grid infrastructure did not allow sufficient time and resources to perform the wide range of power flow and transient stability simulations of AC power system response due to impacts of storms threats. From a practical standpoint, comprehensive studies of power system behavior under GIC threat conditions are not able to replicate all risk factors. Load flow studies alone provide insights on the voltage regulation risks posed to the system by increased transformer reactive demands (Reference AP1-6). However geomagnetic storms have dual threat concerns: voltage collapse caused by increased MVARs combined with disruptive affects of harmonics/waveform distortions on relay and protective systems, and resulting possibility of widespread common-mode failures of critical system elements (i.e. tripping of capacitor banks, when that device is needed for voltage support, can rapidly escalate decay of system integrity). A comprehensive assessment of harmonic interactions would require, as a starting point, large-scale harmonic load flow calculations, which have not previously been performed on bulk transmission system models. Still, such studies would not take into account relay malfunction impacts, and a review of all possible relay malfunctions is also beyond the scope of this effort. As an appropriate screening guide for assessment of potential collapse, a disturbance energy function is derived from the deterministic design criteria and assessments of operational experience from prior storm threats. This provides a means to assess the accumulated impacts of prospective widely spread increases in reactive power demands, and evaluate against a set of thresholds based upon more conventional threats that are likely to precipitate widespread failures of the system. While this provides an estimated threshold for collapse in this study, it is conceivable that a collapse may actually initiate at lower levels because of the unusual nature of this common mode threat to the grid.

A1.2 Disturbance Intensity and Energy Thresholds for System Failure

An important aspect of assessing failure thresholds is having to take into consideration the ability of the system to meet an instantaneous large change in reactive demand. This level of failure threshold can readily take into consideration relevant operating experience examples. For instance, the Hydro Quebec collapse from the March 1989 geomagnetic storm has been estimated to have caused about a 1600 MVAR increase in reactive demand and related harmonic distortion impacts on the system. This demand increase is at a level that is ~7% of the Hydro Quebec system load. In a subsequent study and report to the NPCC, TransÉnergie (the new name for Hydro Quebec), estimates that they have typical reactive reserves of ~ 3000 MVARs (Reference AP1-7). While this network has gone to extraordinary efforts to develop fast response VAR resources, this capability is still only a level that is ~9% of 2002 peak load for the system. National Grid (England/Wales) estimates that geomagnetic storm collapse could occur for 2000-3000 MVARs for their system, a level that is 4 - 6% of peak system demand (Reference AP1-4). The DOE Power Outage Study Team Report and several other reports indicated a number of system events where extreme load demands and/or capacity shortages pushed systems very close to, or actually into, voltage collapse in regions such as the NEPOOL, PJM, SERC, and WECC power pools (References AP1-8, AP1-9, and AP1-10). Regional pools are also required to provide for a spinning reserve margin for contingency

loss of real power capacity. This reserve requirement generally falls in the range of 1000 to 1500 MW, and provides useful guidance as a surrogate bound for reactive power reserve margins as well, lacking any better information.

In combination with the instantaneous demand of reactive power increases, the duration of the impulsive event needs to be considered. A useful measure is a Disturbance Energy Estimate and Threshold, as adapted from Standard System Design Criteria. This design criterion requires all systems to withstand creditable fault events. Using this event criterion as a measurable threshold, a calculation of MVA-Seconds Disturbance Energy can be applied to the power grid in each state. For example, on a 500kV system with a 3-Phase /60kA fault (a very high magnitude fault current) lasting 4 cycles (66.6msec), the total disturbance energy applied to a power grid would be 3464 MVA-sec. Since all power grids of 500kV design would be expected to successfully survive this level of threat, a much larger disturbance needs to be set as the threshold for failure. Most power grids would be expected to fail for such a fault extended to 30 cycles accompanied by simultaneous loss of key elements, which is analogous to the dual threat of GIC disturbances. GIC from geomagnetic storms and E3 threats are not single-point disturbances, but widely scattered, causing smaller MVA increases at each affected transformer. However, when accumulatively considered these events can be cumulatively very large disturbances to the network. To allow for reasonable margins of uncertainty, a cumulative disturbance energy based upon a 3-Phase 30 cycle fault was used as a threshold applied to each state region as the basis to determine geographic boundaries and thresholds for likely power grid collapse. For states with a predominant 765kV infrastructure, the threshold disturbance energy would be 39749 MVA-sec. For regions with predominant 500kV or 345kV systems, the respective disturbance energy thresholds would be 25980 MVA-sec and 17926 MVA-sec. Because there are several states that have sparse infrastructure, it is likely these regions will not have cumulative energy to meet these levels. The criteria would then need to include evaluation of GIC levels at available locations and assessment of neighboring regions that would collapse. Under these conditions, it would be reasonable to expect a cascading collapse to these sparse regions. Further, in application, both the instantaneous demand and disturbance energy thresholds must be exceeded.

A1.3 System Operating State Considerations

Stress calculations can be made for GIC threats, but there is considerable uncertainty, as the measurement of stress caused by a disturbance has to be weighed against the ability of the network to survive the stress. System uncertainty primarily arises from the large variability that can occur in system loads or operating posture of the system as a whole. Figure A1-2 provides a comparison of the power demand on the NY-ISO pool on July 15, 2000, the day of one of the largest geomagnetic storms during Cycle 23, and the load demand on August 7, 2001, during an extreme heat wave. As shown, the power demand for the region was effectively twice as high on August 7. Adverse demand conditions on this day strained the capability of the system and every available resource and, public appeal to limit demand was employed. While a moderately severe geomagnetic storm occurred on July 15, 2000, the NY-ISO had considerable available capacity, due to the

much reduced network demand, and no important system upset events occurred. The same storm scenario coincident with the system conditions of August 7, 2000, could have had much more serious consequences.

Figure A1-3 provides a graphic illustration of these combined probability considerations. The red curve represents a distribution of GIC disturbance impacts from geomagnetic storm conditions. This curve shows a normal distribution of storm related stress to the power grid, such that a large number or probability of small storm events will produce limited amounts of stress to the exposed power grid. As storm related intensity increases dramatically, these extreme storm events are far less probable. The blue curve represents a distribution of power grid operating posture or reserves available to counter disturbance events. The further to the right the system operating posture is, the greater the ability to withstand a stress environment such as that posed by a geomagnetic storm. Both the previously illustrated conditions of adverse load demands, as well as the desire to maintain economic operations, prevent the system from being maintained continuously in a highly resistant operating posture, hence a gaussian type distribution is assumed for this example. Where the stress and capability curves overlap, then network stress exceeds the ability of the network operating posture to successfully absorb that imposed stress, which indicates that failure would be expected.

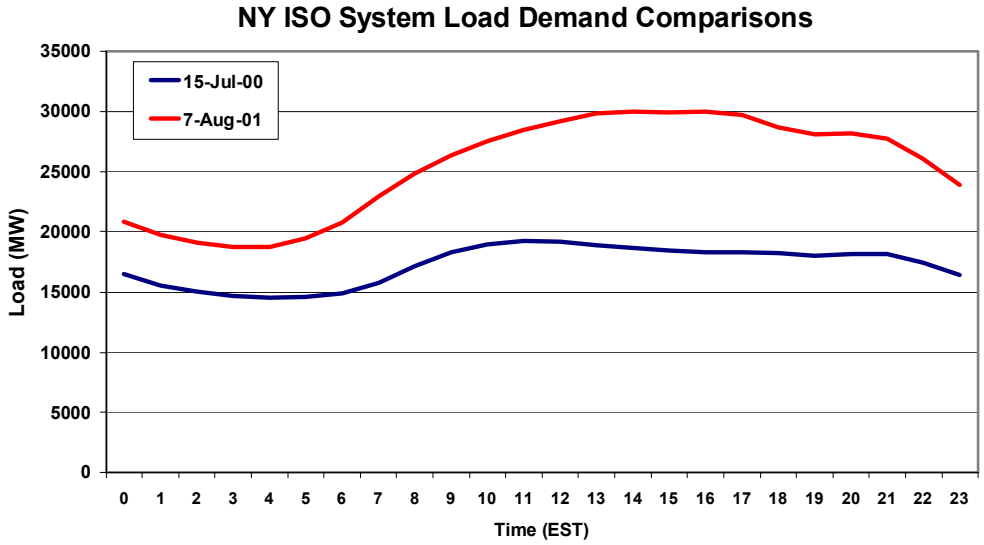

Figure A1-2. Comparison of NY ISO load for July 15, 2000 storm date and peak load conditions on August 7, 2001

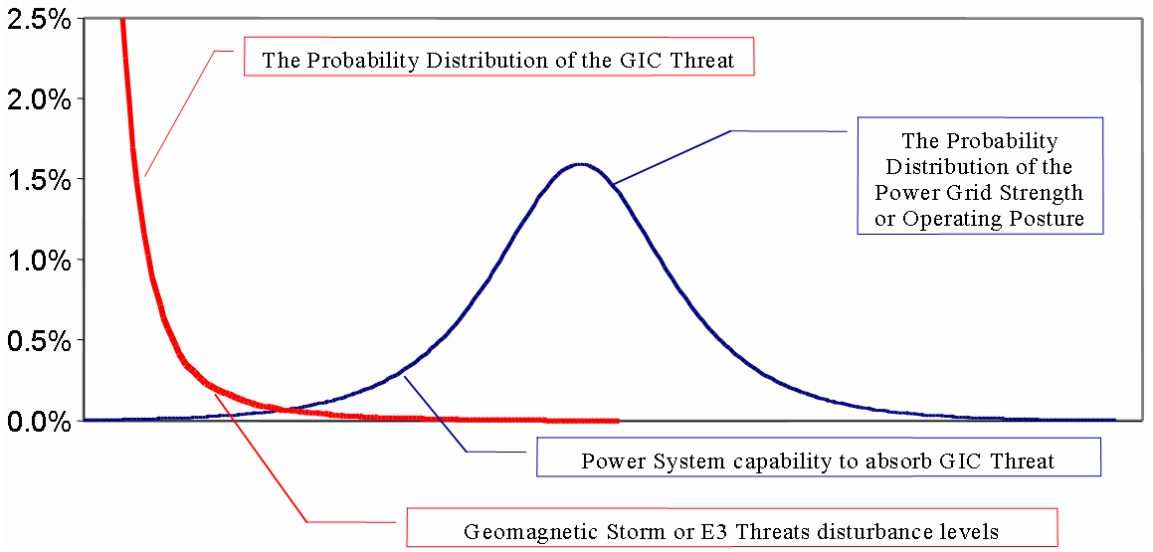

Figure A1-3. Power grid failure probability analysis from GIC threat scenario.

In this state-space depiction, Figure A1-4 illustrates how the system operating reserves can rapidly erode for sudden real or reactive demand changes on the grid, a scenario that is plausible under GIC threat events. Also as previously discussed, the consensus viewpoint has been that the electric industry restructuring that is occurring has produced a secular change in the overall reliability and operating capability of the U.S. Power Grid. This decline in capability can be represented by the shifted system capability distribution that is shown in Figure A1-5. While the operating state of the network is an important consideration in the assessment of network failure, there is also no practical means to assess the range of operating postures that could be present during severe GIC events, either from natural geomagnetic storm processes or from HEMP E3 threat scenarios. In the prior discussed disturbance energy assessments, the underlying assumption in the threshold levels that were developed is that the network condition is robust and not overly weakened at the time of the GIC event.

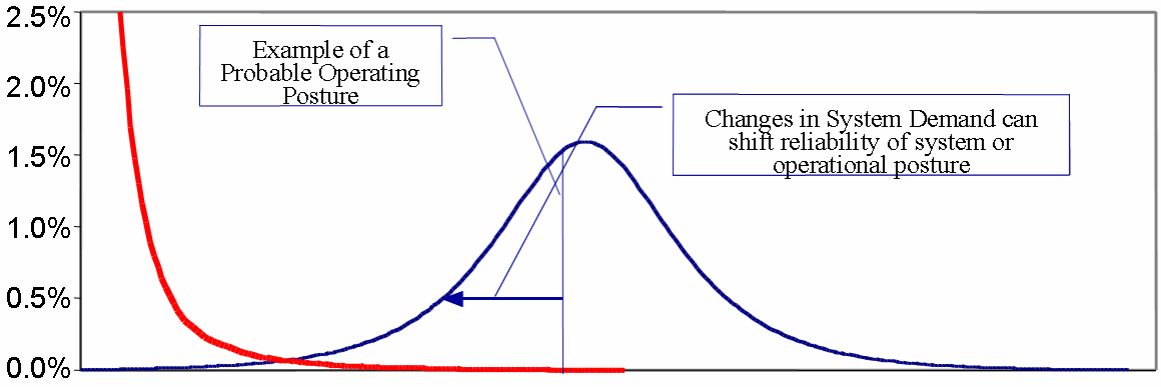

Figure A1-4. Power grid failure probability analysis from GIC threat scenario and cross section at a particular grid operating posture.

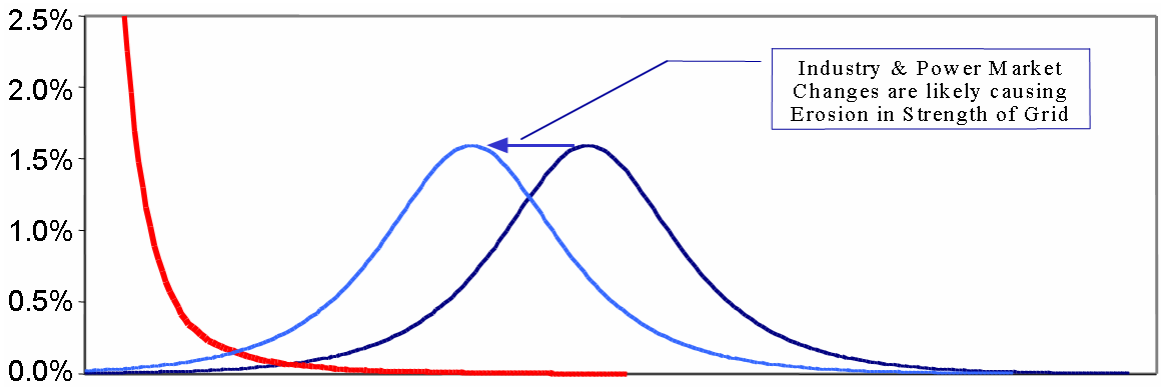

Figure A1-5. Power grid failure probability analysis from GIC threat scenario and impact of secular changes to power grid operating reliability.

In the estimate of power system impacts due to severe geomagnetic storms, the primary concern is increased reactive power, as measured by cumulative estimates of increases of reactive power losses at individual exposed transformers, which will be widely distributed around the network. There is the possibility of further AC power system responses that could act to compound the already large increase in reactive power demand. As reactive power demand increases in saturated transformers, the supply of the reactive power will result in an incremental increase in AC current flow in exposed portions of the power grid. This incremental current flow will also produce an incremental I^2X reactive power loss in the network, which adds to the increased reactive power loss due to this GIC event. In effect, this network response compounds the severity of the initial GIC event impacts even further. In order to estimate these impacts, it would be necessary to identify all base AC current flows on the exposed network and to perform a set of comprehensive load flow studies. Again, because of the limitations of this investigation, only a screening analysis can be considered, to establish creditable upper bounds on this impact adder.

An example of the WECC system (Western U.S.) will be used to illustrate the potential magnitude of this I^2X reactive demand adder. As will be shown in the course of this study, there are creditable geomagnetic storm and E3 threats that are likely to cause an increase of reactive demand in the WECC system by 11,000 MVARs or greater. Based upon the load and line flow conditions for the WECC Heavy Spring Load model, a calculation of I^2X increases can be made. The WECC load in this heavy spring model is 109,123 MW. Therefore, an 11,000 MVAR GIC caused reactive demand increase represents an approximate 10% increase in net system demand. While reactive load, in theory, needs to be supplied locally, in real systems substantial flows across the network will need to occur, as not all fast-response reactive sources are homogeneously distributed. Given the uncertainty and lack of detailed information to compute all possible exact increases, a reasonable approximation can be made by assuming that all transmission line AC currents will increase by an average 10% from base conditions in response to the GIC event. Using this assumption, it can be calculated for the WECC region that the GIC caused 11,000 MVAR increase will also result in an added I^2X loss on transmission lines of an additional ~5800 MVARs, a 52% adder to increased MVARs. If AC current flows also increase in network transformers, this would add even further to

incremental I^2X losses. For GIC threats of even larger magnitude as a percentage of system load, the percentage adder due to I^2X response of the network could be even larger.

While the I^2X response adder is not specifically calculated in the GIC threat scenarios, due to lack of sufficient AC line flow data, it is reasonable to assume that a significant percentage increase will occur and that estimates of disturbance energy functions described previously are conservative estimates of grid failure, and that wider spread disturbances than estimated could actually result for any of the studied scenarios.

A1.4 An Overview of GIC Threats and Relay Misoperation Concerns

Relay malfunctions during GIC events are a primary source of system reliability threats as well. This threat is usually caused by harmonic interactions with protective systems, but can also occur due to other causes, such as transformer current saturation or other secondary interactions (Reference AP1-11). While a comprehensive review of this threat is beyond the scope of this investigation, a brief overview of some potential areas of concern can be provided. In the U.S. it is estimated that there are ~40,000 transmission and distribution substations. Of the very largest and most important substations, which operate at voltage levels of 345kV and above, there are over 2000 stations. Figure A1-6 provides a schematic of a typical 500/230/138kV substation. At this substation there are 3 - 500kV lines entering, and 2 - 230kV lines and 2 - 138kV lines exiting. There are also 4 large power transformers, 4 busses, and 11 large circuit breakers. In addition, there is considerable other associated equipment, such as Current Transformers and Potential Transformers (CTs and PTs). In general, each piece of apparatus, line exit and bus zone in this substation has redundant levels of protection to sense fault events and remove the faulted device from the network as soon as possible. For a substation of this caliber, relay times are as fast as 70 msec for Primary Schemes (1-2 cycles to sense fault, 2-3 cycles for breaker to operate). The Secondary Protection is in case of relay failure, breaker failure, CT failure, etc. and is generally set to operate and sense at lower thresholds than primary, with a delay in time in the range of 100-150 msec. In cases of additional relay system malfunction, a more rudimentary backup protection is set to be very sensitive, but delayed a very long time, typically 0.5 seconds (30 cycles). When called upon to operate, these backup schemes usually result in tripping of an entire station or portion of a network. Relative to other conventional threats that relay systems are designed to address, GIC events last a very long time, many times longer than the slowest backup time delay for protection schemes. Because of this, and harmonic interactions, GIC events have been shown to adversely effect nearly every type of relay system. In this example substation, there could be over 45 different relays, up to 3 relays to protect each line, bus, and transformer at this one station alone, and with overlapping protection as well. Any of these relays could malfunction due to GIC, and precipitate wider-spread system reliability problems in the process.

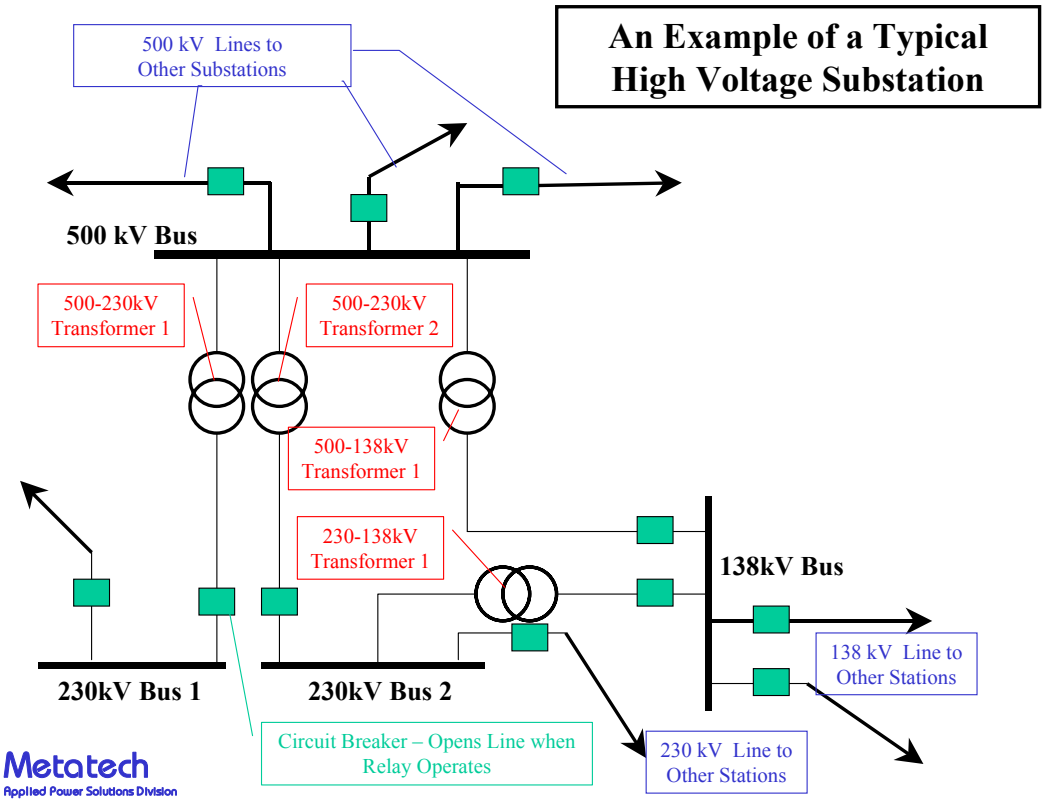

Figure A1-6. One line diagram of example 500kV, 230kV, 138kV substation

A1.5 Capacitor Banks, General Relay and Overload Protection Concerns due to GIC

For a Shunt Capacitor or SVC (simple schematic as shown in Figure A1-7), the primary protection of the capacitor is based on over-current sensing. Since a capacitor is a high-pass filter, harmonics from nearby GIC saturated transformers will inrush to the device and cause large increases in total current flow. Some relays do not distinguish between fundamental and harmonic frequencies and can false-trip due to even a modest increase in harmonics current. These systems in particular were the primary culprits of failure in storms during Solar Cycle 22. Failure of these key fast response reactive sources is a significant loss to the system as a whole, as these capacitive devices are the key response to compensate for the increased reactive power demand from the GIC event itself. Rapid erosion of power network integrity or voltage collapse can occur when compounded by these device failures. More modern relays have the ability to differentiate between fundamental frequency and harmonics and, as a result, are less likely to malfunction. However, under extreme GIC events, the current rating of the capacitor can be exceeded. Figure A1-8 shows several cycles of AC current in a 500kV capacitor bank at the Three Mile Island station in Pennsylvania for a 1-in-30 geomagnetic storm threat scenario. Shown is both a normal capacitor bank current (blue curve), while the red curve shows the harmonic distorted capacitor bank current due to saturation of a nearby transformer from a GIC of 400 Amps/phase. This simulation result indicates that the substantial

harmonic flow will cause a nearly 400% overload condition in total current flow in the capacitor bank, sufficient to initiate bank trip for any properly designed relay system.

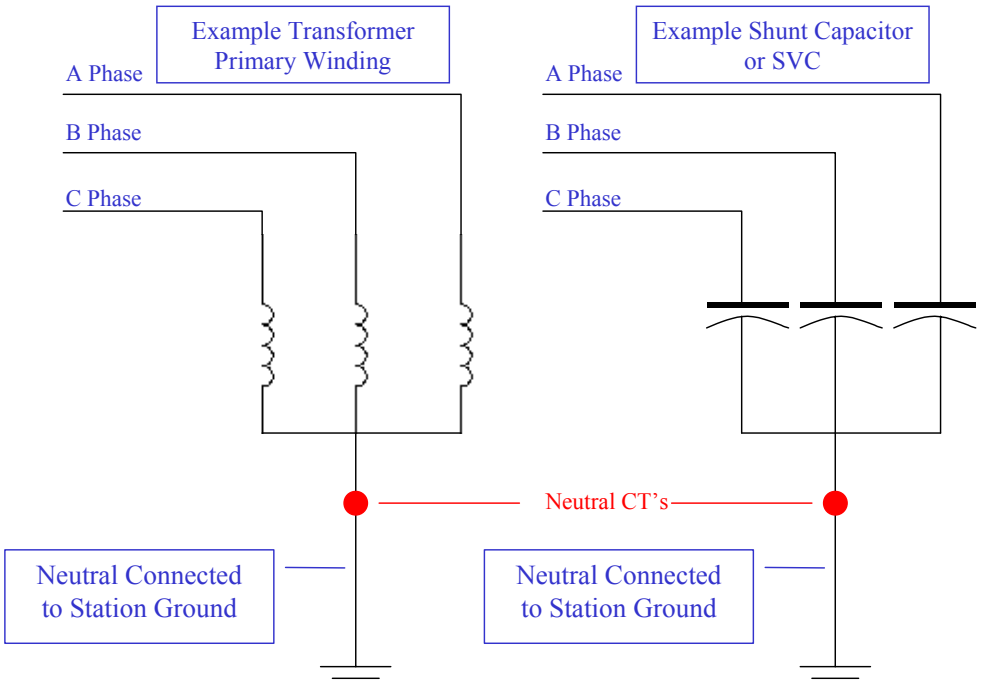

Figure A1-7. Schematic of shunt reactor and shunt capacitor

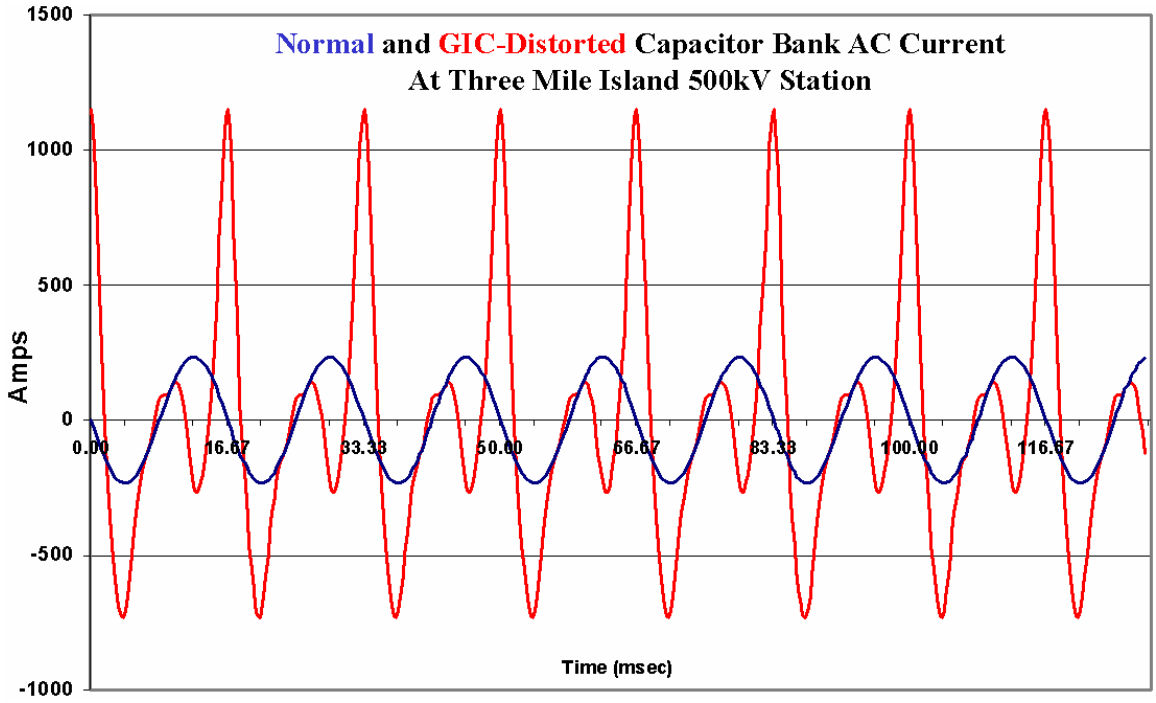

Figure A1-8. Normal and GIC-distorted 500kV capacitor bank current at Three Mile Island for severe geomagnetic storm threat

Another example of relay operation due to GIC is presented in Figure A1-9. The two curves represent the GIC threat over a 40 second duration in the top graph. The bottom graph is the envelope of the AC waveform of the exposed transformer as it is experiencing harmonic distortion from half-cycle saturation. The transformer's normal ~600 Amp peak AC waveform rapidly increases to a peak AC of ~2400 Amps (a ~300% increase in current level). This current will also flow from each transformer into the system and through each line, breaker, and the CTs that sense these large currents. Since these over-currents last for many 10s of seconds, it is highly likely that either primary, secondary, or back-up protection systems on transmission lines, busses, transformers, and cap banks will sense the disturbance and likely initiate a trip of some kind during this event. Instantaneous relay trips will occur if current levels exceed trip settings. But because of long duration, secondary and back-up systems are more likely to trip even if primary systems do not operate, as these back-up protection systems, while delayed by 100 milliseconds to 0.5 seconds, are set to trip at much lower over-current levels. Extreme levels of harmonic distortion are likely to cause relay malfunctions, as well as lead to scenarios of large-scale simultaneous tripping of devices outside of the high current overload zones. If numerous transformers are exposed and begin operation simultaneously in this manner, widespread tripping of key assets across the transmission network will occur. If these trips of key apparatus are sufficient in number or location, this can readily result in cascading collapse of the network as a whole.

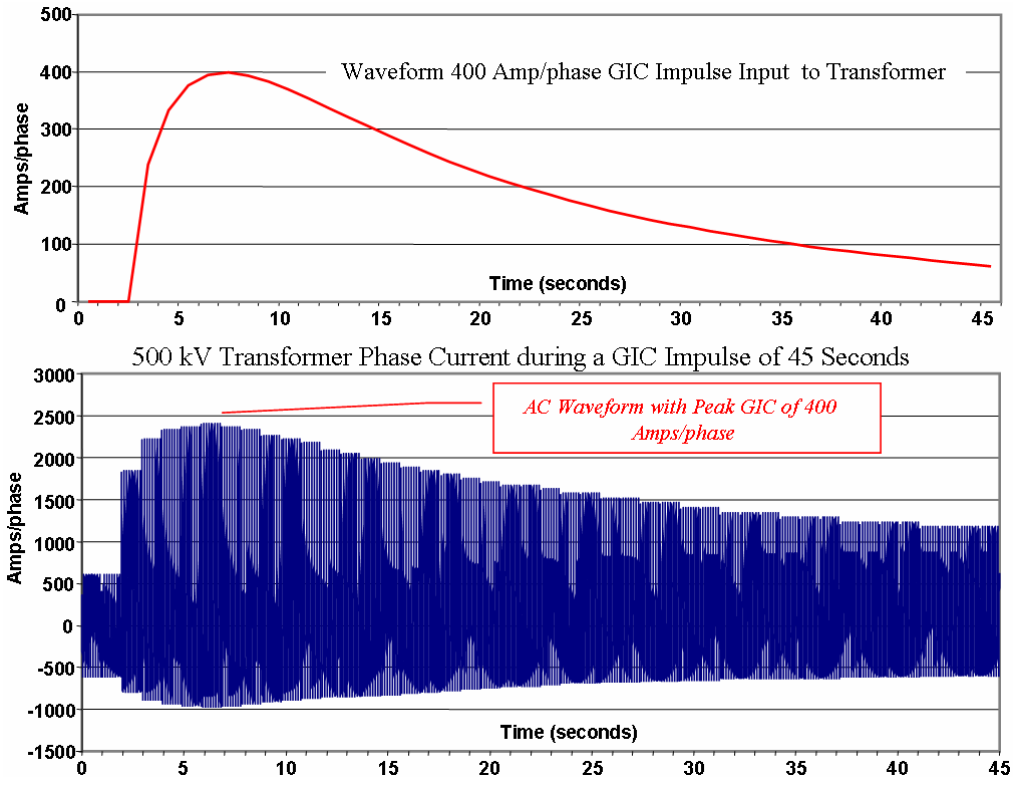

Figure A1-9. Top plot – GIC current versus time in 500kV transformer, bottom plot – AC current versus time of saturated 500kV transformer

Appendix 1 References

AP1-1 Thierry Van Cutsem, Voltage Instability: Phenomena, Countermeasures, and Analysis Methods, Proceedings of IEEE, Vol 88. No. 2, Feb 2000, pg 208-227.

AP1-2 "Central East Voltage Analysis – For Addition of 200MVAr Capacitor Bank at the Eidc 345kV Substation," NYISO Operations Engineering, March 2002.

AP1-3 J. Eto, C. Martinez. et. al., "Grid Management Tools," IEEE Winter Power Meeting, January 28-31, 2001.

AP1-4 J. G. Kappenman, et. al., "Application of Modeling Techniques to Assess Geomagnetically Induced Current Risks on the NGC Transmission System," CIGRE, Session 2002, paper 39-304.

AP1-5 J.G. Kappenman, Chapter 13 - "An Introduction to Power Grid Impacts and Vulnerabilities from Space Weather," NATO-ASI Book on Space Storms and Space Weather Hazards, edited by I.A. Daglis, Kluwer Academic Publishers, II Mathematics, Physics and Chemistry, Vol. 38, pg 335-361.

AP1-6 V. D. Albertson, J. G. Kappenman, N. Mohan, G. A. Skarbakka, "Load-Flow Studies in the Presence of Geomagnetically-Induced Currents," IEEE PAS Transactions, Vol. PAS-100, February 1981, pp. 594-607.

AP1-7 Antonio Dutil, "Impact of Geomagnetic Storms on TransÉnergie Transmission System- Situation at the Dawn of Year 2000," Report to NPCC, January 2000.

AP1-8 DOE, "Consortium for Electric Reliability Technology Solutions – Grid of the Future White Paper on Review of Recent Reliability Issues and System Events."

AP1-9 "The Electric Power Outages in the Western United States, July 2-3, 1996," Report to the President, U.S. Department of Energy, August 1996.

AP1-10 Interim Report of the U.S. Department of Energy's Power Outage Study Team, Findings from the Summer of 1999, January 2000.

AP1-11 J. G. Kappenman, V. D. Albertson, N. Mohan, "Current Transformer and Relay Performance in the Presence of Geomagnetically-Induced Currents," IEEE PAS Transactions, Vol. PAS-100, March 1981, pp. 1078-1088.

Appendix 2
Transformer Internal Heating

A2.1 Transformer Internal Heating – Empirical and Analytical Data

While there is some uncertainty as to the threshold level of GIC that will cause transformer failure, there is both empirical evidence and engineering analysis that provide basic guidance as to overall trends and vulnerability issues. The Eskom network of South Africa experienced a large number of GIC-caused transformer failures due to storms in late October and early November of 2003 (Reference AP2-1). These failures are suspected by them to have occurred at relatively low levels of GIC exposure. Their analysis also indicated that even 3-legged core form transformers were susceptible to half-cycle saturation at levels as low as 2 Amps/phase. Price in his analysis of transformer saturation had determined that tank shunting is important in three legged core form transformers and that local heating is affected by the construction details (Reference AP2-2). As both of these analysis efforts note, without adequate control of the flux under saturation conditions, local heating in parts of the transformer may not be cooled effectively. In turn, this leads to rapid temperature increase in some cases in small but sensitive areas. The intensity of overheating depends on the level of GIC but is also a function of various design parameters of the transformer itself. These include the saturation flux paths, cooling flow and the thermal condition or loading of the transformer. When overheating occurs, it causes the breakdown of oil and paper insulation in the hot spot regions.

Observations from monitoring and field tests also empirically illustrate the concerns about internal heating and damage potential this could cause. Figure A2-1 shows the rise of monitored external tank hotspot on the Meadowbrook transformer during a minor storm on May 10, 1992. As measured, there is a very fast response (on order of 2-4 minutes) between the onset of a large GIC spike and also the sudden and sharp temperature rise at the known hotspot on this transformer tank wall. Since this transformer is located very close to the Fredericksburg magnetic observatory, the corresponding rate of change (dB/dt) of the regional geomagnetic field can also be described. Figure A2-2 provides a plot of the observed dB/dt in UT time (4 hour difference between local time used in Figure A2-1). The dB/dt responsible for the ~60 Amp neutral GIC observed in the Pennsylvania transformer in Figure 4-3 reached a peak dB/dt of only ~55 nT/min. Extreme storm scenarios can produce up to 5000 nT/min disturbance levels. This would be a level ~100 times larger. It is expected that this could also produce ~100 times larger GIC levels in this same transformer.

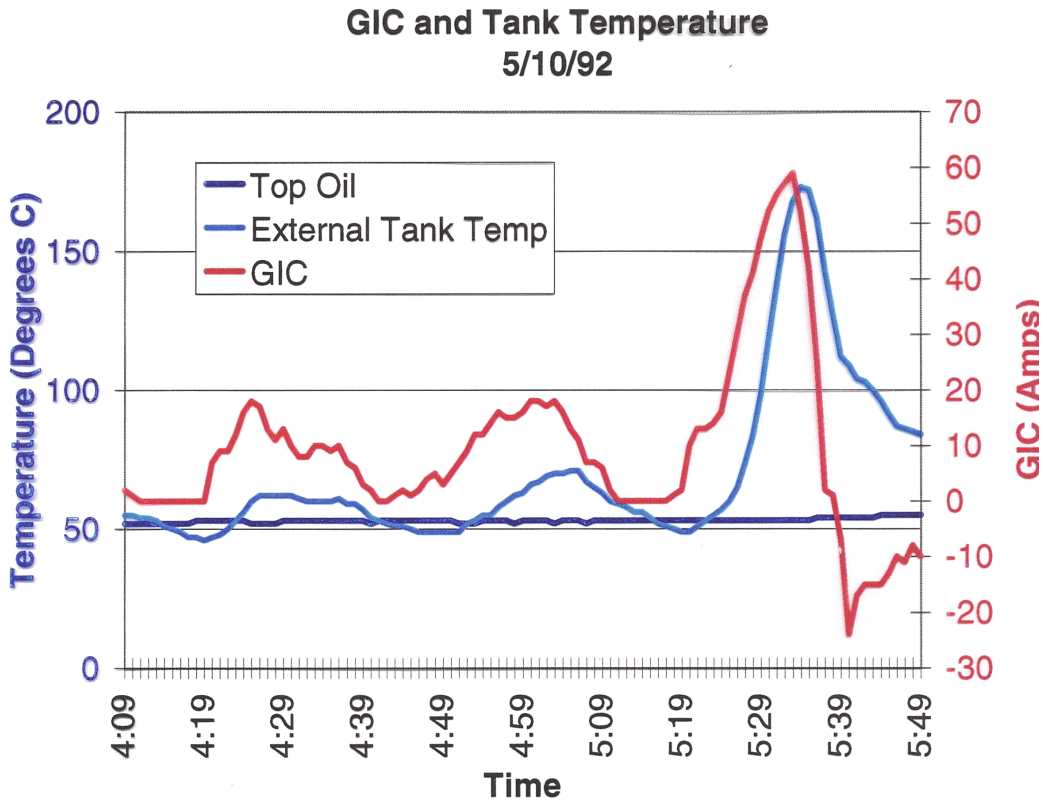

Figure A2-1. GIC and transformer tank temperature for May 10, 1992 geomagnetic storm.

Figure A2-3 shows the results of measured temperature rises for DC testing of a transformer. As clearly demonstrated by these tests (Reference AP2-3), the intensity of the GIC plays an important role in both the level of internal heating but also in the rate of rise of this heating. Note that when the DC injection is suddenly increased from 12 Amps to 75 Amps, the temperature (top of tie plate) experiences a sudden increase over a time span of only three minutes.

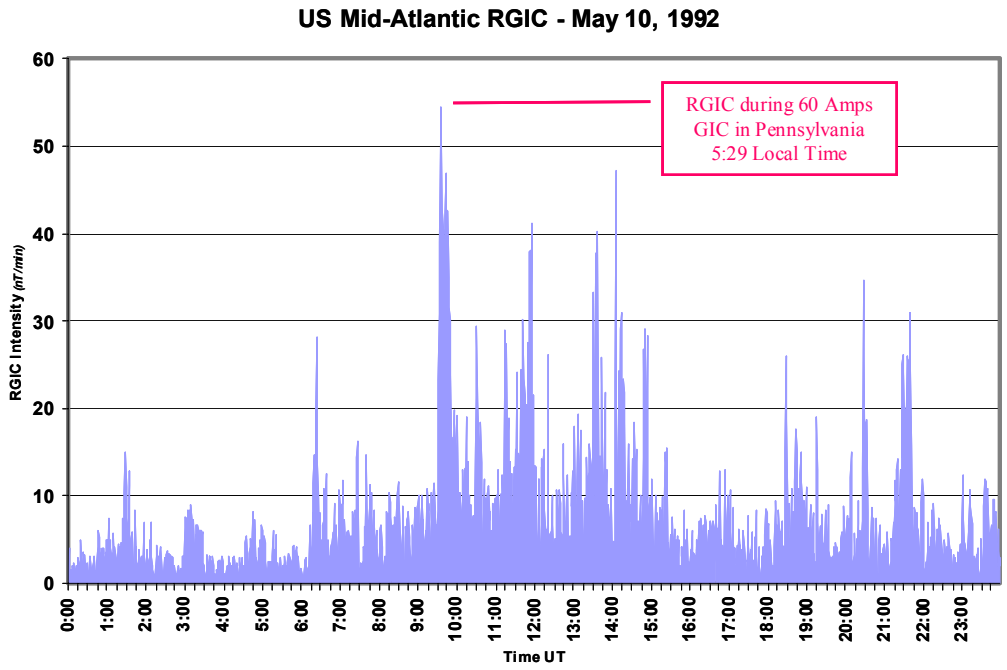

Figure A2-2. Observed dB/dt near Meadowbrook for May 10, 1992 geomagnetic storm.

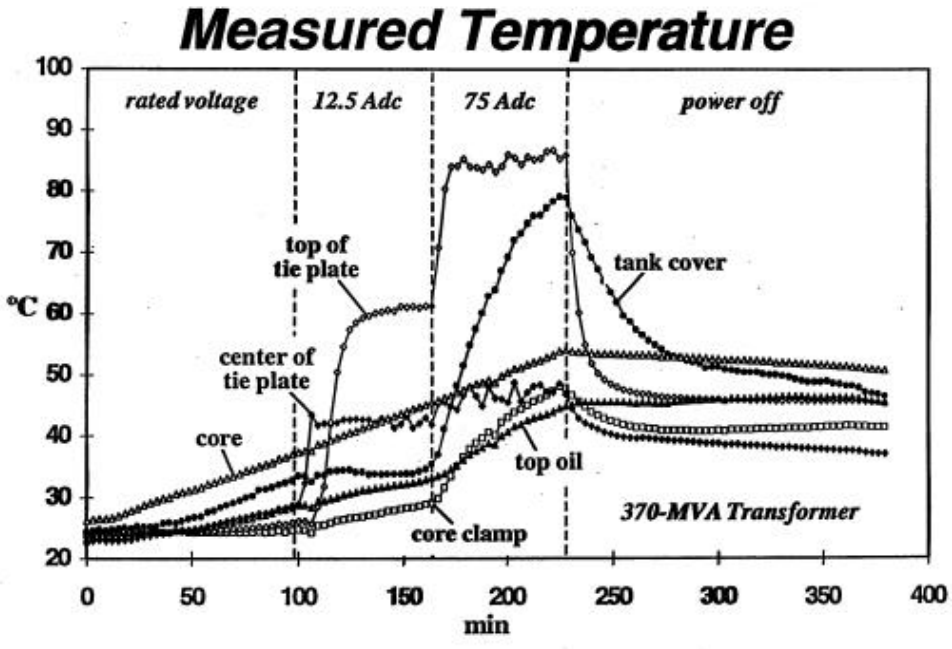

Figure A2-3. Observed temperature From Hydro Quebec tests showing response between two levels of neutral GIC (12.5 A & 75 A) and measured temperatures in the transformer in easy to access spots.

Further reports also correlate sudden storm commencement (SSC) geomagnetic disturbances with incidents of transformer failures. Figure A2-4 provides a plot from a paper noting observations of sudden onset of a geomagnetic storm with a transformer

failure in New Zealand which occurred on Nov. 6, 2001 (Reference AP2-4). The SSC has an onset and rise time very similar (though much smaller in GIC intensity) to that posed by a E3 HEMP threat scenario. This indicates that even brief duration GIC events can lead to transformer failures.

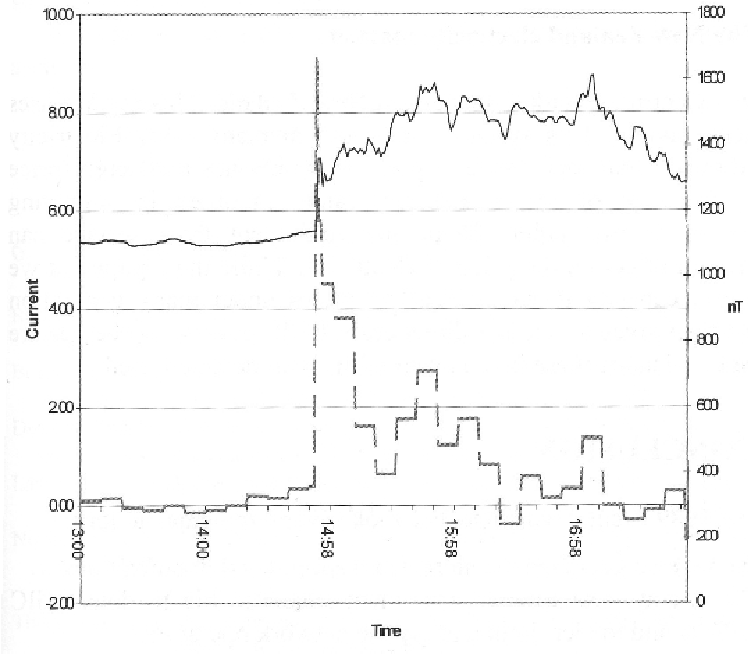

Figure A2-4. Observed SSC and sudden failure of New Zealand transformer, Nov 6, 2001.

Further analysis of the failure of the Salem Nuclear Plant GSU transformer also provides insights on possible large intensity but short duration GIC events and the potential for transformer failure. Figure A2-5 provides a plot of the dB/dt observed at Fredericksburg (FRD) which is near the Salem plant. As noted, several of the most energetic substorm intervals were simulated on the U.S. power grid model to estimate GIC levels. It is also shown that the peak dB/dt of ~470nT/min was observed at 21:44UT. The GIC in the Salem transformer also peaked at this time, reaching a peak of ~90 Amps/phase near the 21:44UT peak dB/dt. Figure A2-6 provides a more expanded scale plot of the Salem GIC for the substorm time interval from 21:20 to 22:30 UT. As shown in this plot, the duration of the peak GIC levels are very brief (less than 2 minutes), yet were able to cause permanent and extensive damage to this large GSU transformer.

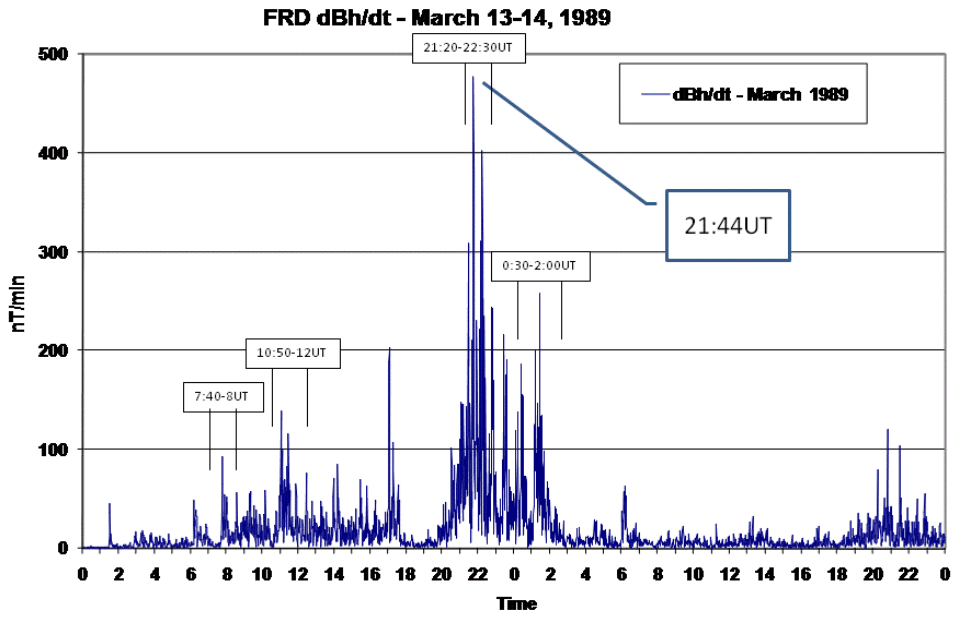

Figure A2-5. Specific storm intervals on March 13-14, 1989 selected for forensic analysis using FRD observatory.

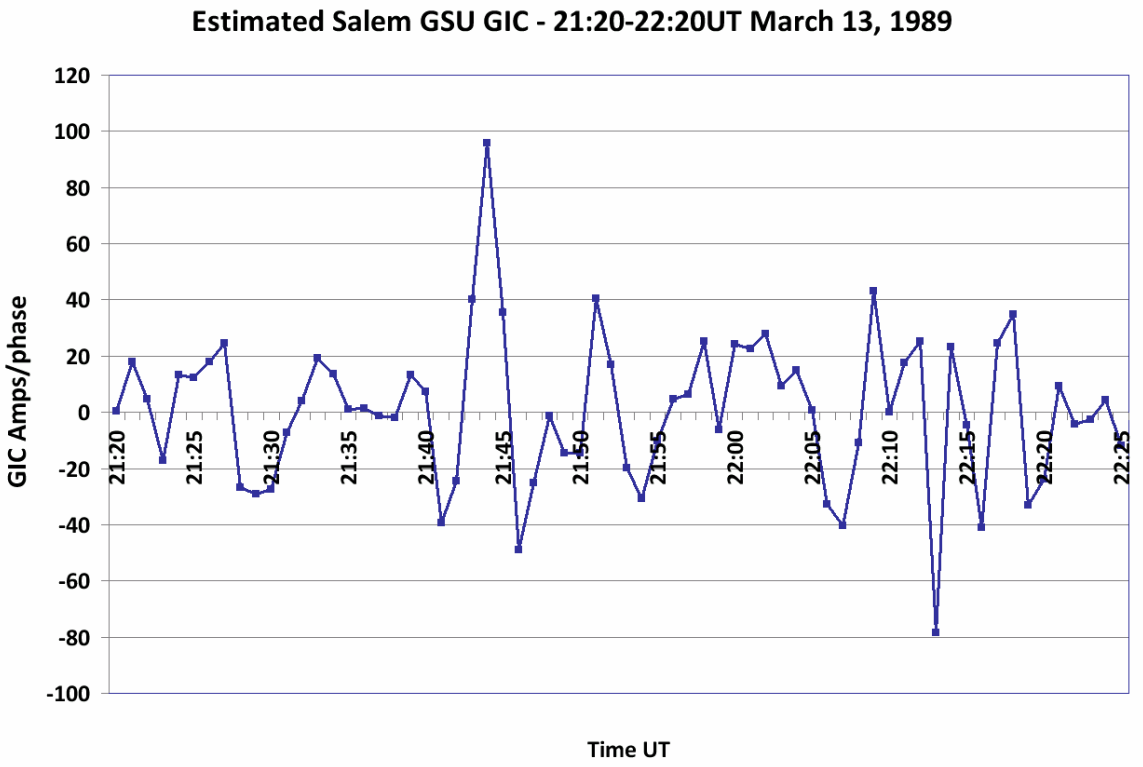

Figure A2-6. Estimated GIC in Salem GSU on March 13, 1989.

Subsequent analysis undertaken by Girgis (Reference AP2-5) provides analytical examinations of a transformer of this design as well as another transformer which has design features that make it somewhat more tolerant of GIC exposure. Figure A2-7 provides a plot of the GIC level and load level that can be tolerated on a transformer of design like that at Salem. It should be noted that for a neutral GIC of as little as 90 Amps (or equivalent to 30 Amps/phase), the transformer can no longer have any load or there is risk of permanent damage. This situation would be particularly problematic for large baseload GSU transformers, as loading on these apparatus are nearly always operated at nameplate MVA rating.

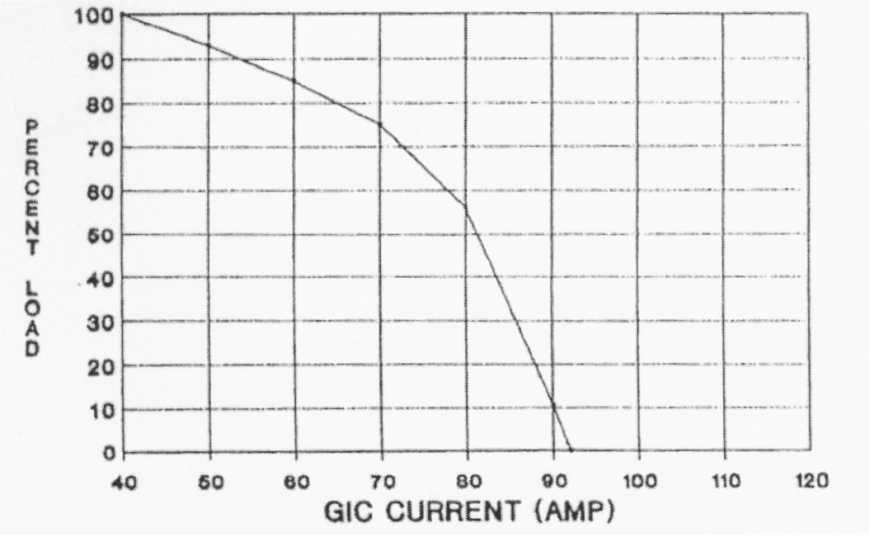

Figure A2-7. Decrease in load level as a function of GIC current.

Other analytical examinations of GIC thresholds come to similar conclusions (Reference AP2-6). In this analysis, the authors provide an equivalent of short-time emergency overload guide to determine the amount of time that a transformer can withstand GIC. This overload guide has DC current exposure limit results for the un-optimized transformer design similar to that noted by Girgis, *et al.* The work by Hurlet also indicates that even optimized designs have limited time durations of GIC exposure, though with higher thresholds. Therefore, if a storm occurs that produces 10 to 100 times higher GIC levels, then damage potential is plausible for these more robust transformer designs as well. It should further be noted that this work covers only a few of the multiple design variations that exist for these transformers and that this work also contains other limitations in the analysis on the scope of the problem. However, the summary of both empirical experience and various analytical determinations provides a basis for estimating potential at risk transformers for large and severe storm events that are yet to occur on today's power grid infrastructure.

A2.2 Transformer Internal Heating – Data Related to the Special Case of E3 and other Natural Fast GIC Transients

As noted in Figure A2-4, transformer failure has been observed due to fast transient geomagnetic field disturbances associated with Sudden Storm Commencements or Sudden Impulses. These naturally occurring transients have a rise and decay time that mimics (at much smaller magnitudes) the E3 transient behavior. Previous analysis carried out by ORNL raised the question of whether the GIC from an E3 event would last long enough to cause transformer saturation (Reference AP2-8). This time-to-saturation question has subsequently been answered by a variety of tests, observations and also analysis. Kappenman, in field tests performed in the early 1990s, injected DC current into 500kV and 230 kV transformers. While the pulse of DC was not as fast rising as from an E3 pulse, data from these tests indicated that saturation response was prompt (Reference AP2-9). Kappenman also provided examples of other observations of rapid half-cycle transformer saturation is response to Sudden Storm Commencements, these were observations from Meadowbrook, Limerick and Pleasant Valley all during a SSC event on March 24, 1991 (Reference AP2-10).

Several comparisons can be provided to examine the similarity of the SSC with the IEC E3 HEMP specification pulse described in Section 2. Figure A2-8 provides a time plot of a more typical 2400nT/min impulse associated with a large electrojet-driven geomagnetic disturbance along with the IEC E3 pulse waveform and the waveform observed at Kakioka (Japan) during the March 24, 1991 SSC. The SSC and E3 waveforms, while different in magnitude, have similar time characteristics. Figure A2-9 provides a Fourier analysis comparison of the three waveforms. The spectral content of both the E3 and SSC are very similar, with the exception of magnitude.

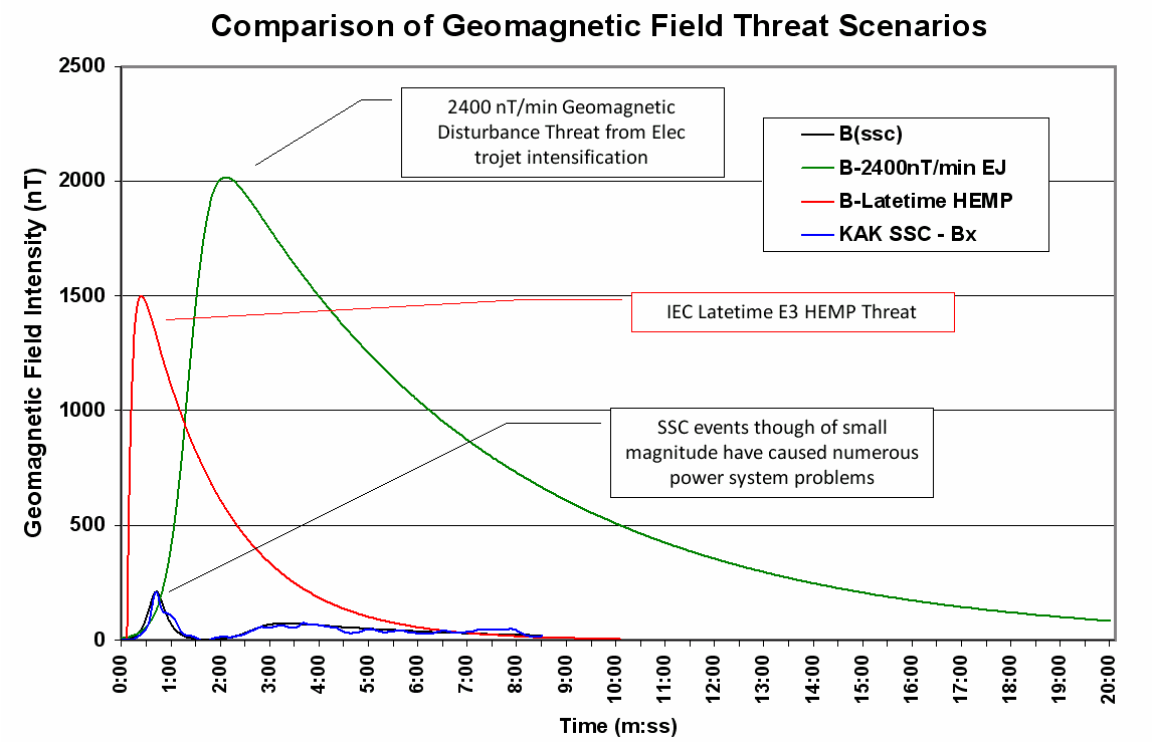

Figure A2-8. Comparison of geomagnetic disturbance waveforms due to electrojet intensification, the IEC E3 HEMP specification and SSC (Sudden Storm Commencement).

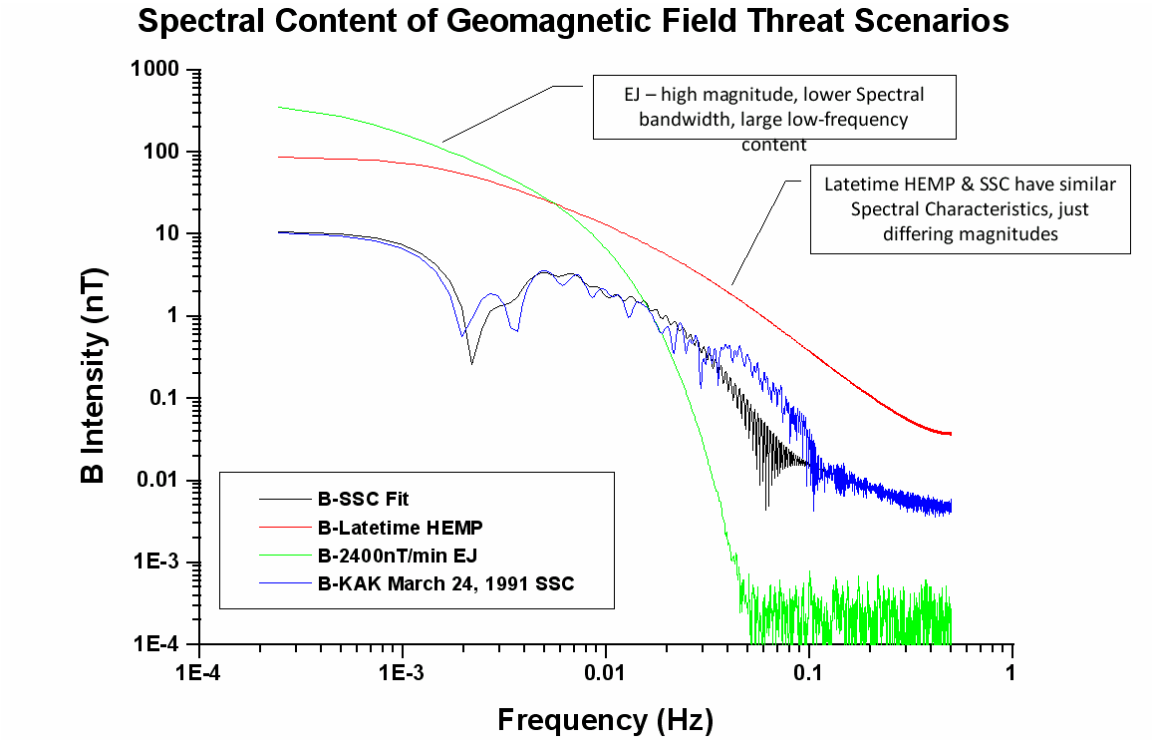

Figure A2-9. Spectral comparison of geomagnetic disturbance waveforms due to electrojet intensification, the IEC E3 HEMP specification and SSC (Sudden Storm Commencement).

Observations also provide insights into the role of GIC magnitude and the time to saturation. Observations taken at the Chester Maine 345kV transformer during a storm on May 4, 1998 (Figure A2-10) provide a comparison of observed GIC and observed 2nd Harmonic in the same transformer (even harmonics are only caused by DC half-cycle saturation). This data was all sampled at a 10 second cadence, at the lower levels of GIC (less than 10 Amps), there appears to be some short time lags. As GIC increases in levels, virtually no time lag is evident between GIC and harmonic current response.

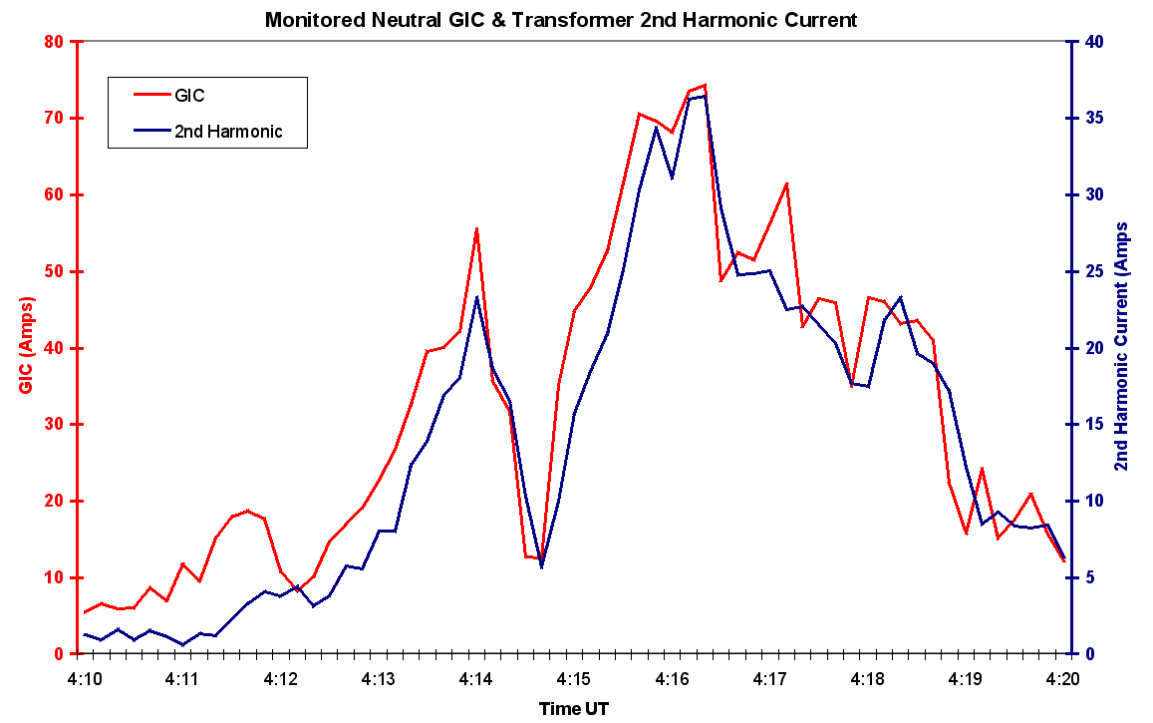

Figure A2-10. Observations of GIC and 2nd Harmonic current at Chester Maine, May 4, 1998. As GIC levels increase, time to saturation appears to decrease.

Price in his analytical modeling provides further insights in that increasing levels of GIC (or DC current) will cause increasing fast half-cycle saturation response of the transformer (Reference AP2-2). Figures A2-11 and A2-12 provide model responses for two different levels of sudden DC excitation to a 240MVA 400/132kV transformer with a tertiary winding. Figure A2-11 is for a step DC input of only 10 Amperes - in this case, the delay in saturation is ~10 seconds. In Figure A2-12, the same transformer is now subjected to 100 Ampere step DC input. The higher current has reduced the delay time for transformer saturation to begin by a factor of ~10. This indicates that for the large GIC levels that will typically be produced due to the severe E3 threat environment, transformer saturation and other related impacts such as internal heating will all be of concern just as they have been observed for more frequent, but lower level, naturally occurring geomagnetic storms.

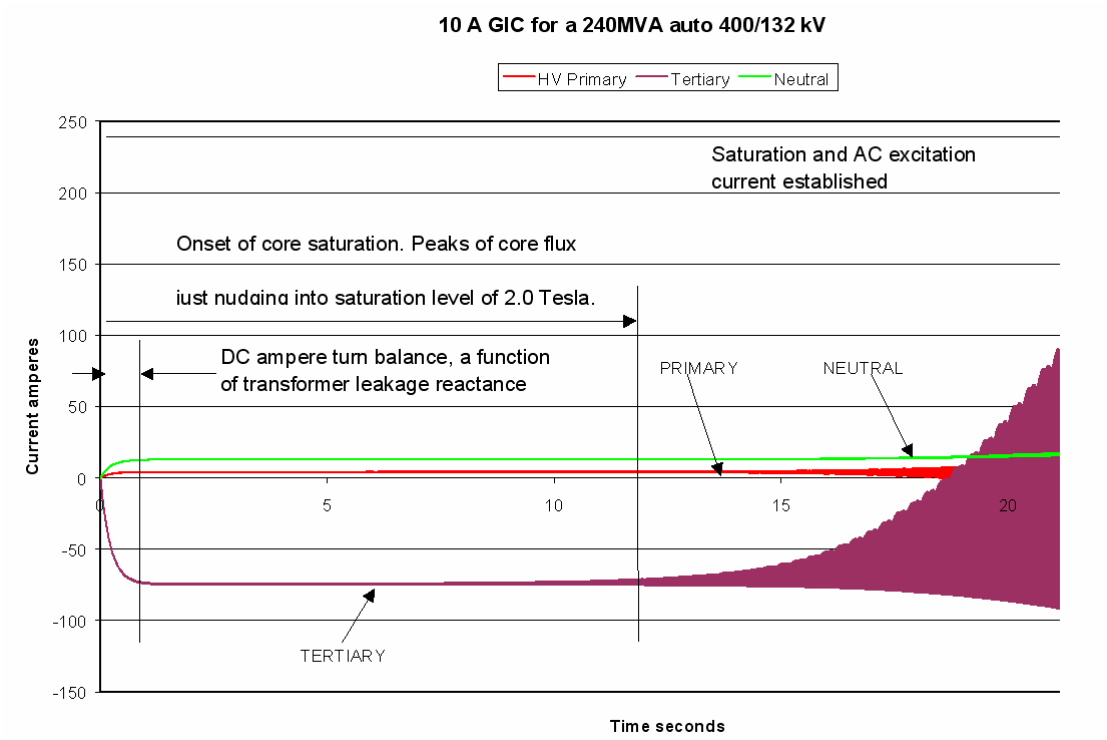

Figure A2-11. Analysis of saturation delay for 240MVA 400/132kV auto transformer with 10 Amperes of step DC input.

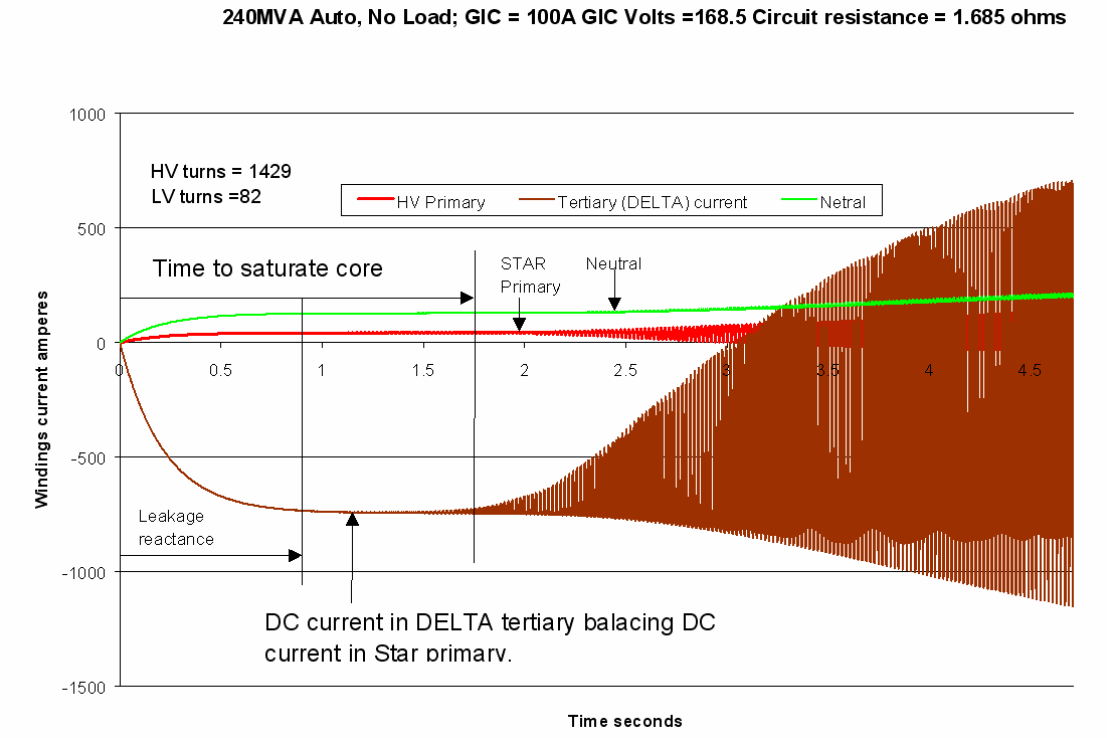

Figure A2-12. Analysis of saturation delay for 240MVA 400/132kV auto transformer with 100 Amperes of step DC input.

Appendix 2 References

AP2-1 C. T Gaunt, G. Coetzee, "Transformer failures in regions incorrectly considered to have low GIC-risk," IEEE Power Tech 2007, 1-5 July 2007, Lausanne, Switzerland, Paper 445.

AP2-2 P. R. Price: Geomagnetically induced current effects on transformers. IEEE Trans on Power Delivery, vol 17, no 4, October 2002, p1002-1008.

AP2-3 P. Picher, et.al., Discussion to Paper "Study of the Acceptable DC Current Limit in Core-Form Power Transformers," IEEE Winter Power Meeting, Baltimore MD.

AP2-4 J. Beland, K. Small, "Chapter 15: Space Weather Effects on Power Transmission," Effects of Space Weather on Technology Infrastructure, edited by I. A. Daglis, Kluwer Acad., Norwell, Mass., pages 287-300, vol. 176, 2004.

AP2-5 R.S. Girgis, C.D Ko, "Calculation Techniques and Results of Effects of GIC Currents as Applied to Two Large Power Transformers," IEEE Transactions on Power Delivery, Vol. 7, No. 2, April 1992.

AP2-6 P. Hurlet , F. Berthereau, "Impact of geomagnetic induced currents on power transformer design," IEEE Conference MATPOST'07 - LYON (France), JST Transformateurs, France.

AP2-7 Craig L. Stiegemeier, Ramsis Girgis, Rapidly Deployable recovery Transformers, IEEE Power & Energy, Vol 4, Number 2, March /April 2006, pp. 38-45.

AP2-8 P.R. Barnes, D.T. Rizy, B.W. McConnell, F.E. Tesche, E.R. Taylor, Jr., "Electric Utility Experience with Geomagnetic Disturbances" Oak Ridge National Laboratory, Sept. 1991.

AP2-9 J. G. Kappenman, S. R. Norr, G. A. Sweezy, D. L. Carlson, V. D. Albertson, J. E. Harder, B. L. Damsky, "GIC Mitigation: A Neutral Blocking/Bypass Device to Prevent the Flow of GIC in Power Systems, IEEE PES Special Publication 90TH0357-4-PWR, Special Panel Session July 17, 1990, pages 45-52.

AP2-10 Kappenman, J. G., Storm sudden commencement events and the associated geomagnetically induced current risks to ground-based systems at low-latitude and midlatitude locations, Space Weather, 1(3), 1016, doi:10.1029/2003SW000009, 2003.